

The functional roles of Rac1b in mammary gland development and breast tumourigenesis

A thesis submitted to the University of Manchester for the degree of Doctor of
Philosophy in the Faculty of Faculty of Biology, Medicine and Health

2022

Fuhui Chen

Division of Cancer Sciences

Table of Contents

ABBREVIATIONS	5
ABSTRACT	7
DECLARATION	8
COPYRIGHT STATEMENT	9
ACKNOWLEDGEMENTS	10
CHAPTER 1. General Introduction	12
1.1 Ras homologous (Rho) GTPases and their functions as molecular switches	12
1.2 The functional roles of RhoGTPases in mammary gland development.....	13
1.3 The functional roles of RhoGTPases in breast tumourigenesis and metastasis	15
1.4 Rac1 and Rac1b functions in various tumours.....	17
CHAPTER 2. Materials and methods	24
2.1 Molecular Biology	24
2.1.1 PCR (Polymerase Chain Reaction) for High-fidelity cloning.....	24
2.1.2 Digestion, Purification and Ligation	26
2.1.3 Bacterial Heat-shock transformation and plasmid DNA extraction.....	26
2.1.4 Sequencing	27
2.1.5 Genomic DNA isolation.....	27
2.1.6 RNA isolation	27
2.1.7 Reverse Transcription (RT) - cDNA synthesis	27
2.1.8 DNA gel electrophoresis	28
2.1.9 Protein isolation	28
2.1.10 Western blotting.....	28
2.2 Cellular Biology.....	30
2.2.1 Cell culture and passaging for cell line	30
2.2.2 CRISPR/Cas9 double nickase transfection	30
2.2.3 Primary monolayer cell culture and passaging for mouse tumour cells	30
2.2.4 Mammospheres Assay	31
2.2.5 Doxorubicin treatment	31
2.2.6 Immunofluorescence for cytopinned cells.....	32
2.2.7 Immunofluorescence for 3D spheres derived from mammosphere assay.....	32
2.3 Mice studies	33
2.3.1 Mouse experiments	33
2.3.2 PCR for genotyping mice.....	33
2.3.3 Whole-mount Carmine-Alum staining.....	34
2.3.4 Hematoxylin & Eosin staining.....	35

2.3.5 Immunohistochemistry.....	35
2.3.6 Primary cell isolation	37
2.3.7 FACS (Fluorescence-activated cell sorting) sorting	38
2.4 Statistical analysis.....	39
CHAPTER 3. Results Part I - Rac1b, the splice variant of Rac1, is dispensable for normal mammary gland development	40
3.1 Introduction.....	40
3.1.1 Mammary Gland Development: insights from mouse models.....	40
3.1.1.1 Embryonic development of mammary gland	40
3.1.1.2 Puberty	42
3.1.1.3 Pregnancy and Lactation.....	44
3.1.1.4 Involution.....	44
3.1.2 Mammary Epithelial Cell ontogeny	45
3.1.3 The surface markers used for isolating distinct mammary epithelial subsets	47
3.1.4 The evidence supporting the existence of MaSCs	51
3.1.5 Rac1 function during mammary gland development	54
3.2 Results - The deletion of Rac1b does not alter normal mammary gland development.....	57
3.2.1 Loss of Rac1b function does not lead to obvious defects during mammary gland development at a macroscopic level	57
3.2.1.1 Rac1b-null mammary ductal tree is able to elongate and branch normally similar as in wild-type mammary glands.....	57
3.2.1.2 Loss of Rac1b function does not alter mammary gland development during pregnancy and lactation stages	59
3.2.1.3 The Rac1b deficiency has no effect on the involution stage of mammary gland development.....	61
3.2.1.4 Rac1b deficiency does not affect mammary glands even after multiple rounds of pregnancy	62
3.2.2 The loss of Rac1b function does not hamper mammary gland involution.....	64
3.2.3 The loss of Rac1b function does not alter mammary epithelial cell lineage distribution or MaSC frequency	67
3.2.4 Rac1b is dispensable for the maintenance of mammary epithelial stem cells	70
3.3 Results - The generation of Rac1b ^{T2A-RFP} -knockin mouse model by using CRISPR technology	79
3.3.1 The optimization of CRISPR/Cas9 Double Nickase strategy by using Eph4 cells.....	79
3.3.2 The optimization of HDR templates for the knock-in of 'T2A-RFP' cassettes into the Exon3b sequence	86
3.3.3 The generation of Rac1b ^{T2A-RFP} -knockin mouse line	91
3.4 Results - The verification of surrogate reporter ability of RFP for Rac1b expression.....	93
3.5 Results - Characterisation of Rac1b-expressing mammary cells.....	98

3.5.1 Rac1b-expressing cells consists of both CD24 ⁺ and CD24 ⁻ mammary cells	98
3.5.2 Rac1b-expressing cells consists of both epithelial and non-epithelial cells.....	100
3.6 Results - Rac1b is expressed by a substantial subset of sphere-forming mammary cells.....	103
3.6.1 Rac1b expression marks a large subset of sphere-forming cells in the mammary gland...	103
3.6.2 Characterisation of the Rac1b-expressing sphere-forming cells.....	106
3.6.3 Loss of Rac1b function does not alter the stem cell frequency in neither the RFP ⁺ nor the RFP ⁻ cell fractions	108
3.7 Discussion	110
3.7.1 Rac1b function is dispensable for mammary gland development.....	110
3.7.2 The generation of Rac1bT2ARFP knock-in transgenic mouse model.....	113
3.7.3 The characterization of Rac1b-expressing RFP ⁺ cells in nulliparous mammary glands...	115
CHAPTER 4. Results Part II Rac1b is required for maintaining BCSCs and chemoresistance of breast tumour cells.....	117
4.1 Introduction	117
4.1.1 The subtypes of breast cancer and their conventional treatments	117
4.1.2 BCSC plasticity	122
4.1.3 The BCSC plasticity is presumed to play crucial roles in tumour metastasis, tumour recurrence and therapeutic resistance in breast cancer.....	124
4.1.4 Comparison of Rac1 and Rac1b functions in various cancers	126
4.2 Results.....	130
4.2.1 Rac1b-expressing cells consists of various cell subtypes in Her2 ⁺ tumours	130
4.2.2 Rac1b is expressed by a substantial fraction of mammosphere-forming BCSCs	133
4.2.3 Characterisation of RFP ⁺ tumour cell driven spheres	135
4.2.4 Rac1b is required for the maintainance of Rac1b-expressing BCSCs	137
4.2.5 Loss-of Rac1b function does not alter MMTV-Neu tumour latency	139
4.2.6 Rac1b deficiency results in decreased BCSC frequency in MMTV-Neu tumours	142
4.2.7 Rac1b deficiency sensitises primary breast tumour cells to chemotherapy	144
4.3 Discussion	150
4.4.1 Characterization of Rac1b-expressing cells in breast tumour.....	150
4.4.2 Rac1b is expressed by a substantial subpopulation of BCSCs.....	150
4.4.3 Loss of Rac1b function does not alter tumour latency and morphology in the MMTV-Neu model of breast cancer	151
4.4.4 Loss of Rac1b function increases the chemosensitivity of breast tumour cells	153
CHAPTER 5. General Discussion	155
CHAPTER 6. Conclusion.....	158
REFERENCES.....	159

ABBREVIATIONS

ALDH1 Aldehyde Dehydrogenase 1

BCSC Breast Cancer Stem Cell

BER Base Excision Repair

Cas9n Cas9 nickase

Cdc42 Cell division cycle 42

CK14 Cytokeratin 14

CK18 Cytokeratin 18

CSC Cancer Stem Cell

DN Double Negative

DP Double Positive

EMT Epithelial Mesenchymal Transition

ER Estrogen Receptor

FACS Fluorescence-Activated Cell Sorting

FSC Forward Scatter

GAP GTPase-Activating Protein

GDI GDP Dissociation Inhibitor

GEF Guanine nucleotide Exchange Factor

GH Growth Hormone

GTP Guanosine Triphosphate

H&E Hematoxylin & Eosin

HDR Homolog-Directed Repair

InDel Insertions and/or Deletions

MaSC Mammary epithelial Stem Cell

MEC Mammary Epithelial Cell

MET Mesenchymal Epithelial Transition

MFE Mammosphere-forming efficiency

MMP-3 Matrix Metalloproteinase-3

NHEJ Non-Homologous End Joining

NIC Neu-IRES-Cre

NOX NADPH Oxidase

PCR Polymerase Chain Reaction

PFA Paraformaldehyde

PR Progesterone Receptor

PyMT Polyoma Middle T antigen

Rac1 Ras-related C3 botulinum substrate 1

ROS Reactive Oxygen Species

RT Reverse Transcription

SD Standard Deviation

SEM Standard Error of the Mean

SSC Side Scatter

TEB Terminal End Bud

TNBC Triple-Negative Breast Cancer

TKIs Tyrosine Kinase Inhibitors

ABSTRACT

Rac1b is the only known splice variant of the small GTPase Rac1 with an in-frame insertion of an additional 19 amino acids. It was previously shown that the genetic deletion of *Rac1* impairs alveolarogenesis and post-weaning tissue remodelling during pregnancy and involution stages of mammary gland development, mammary epithelial stem cell (MaSC) maintenance in nulliparous glands, and breast tumourigenesis. However, it is still unclear whether these phenotypes are caused by the loss of function of Rac1 or its splice variant Rac1b. This project aims to investigate the variant specific functions of Rac1b during mammary gland development and breast tumourigenesis by utilising a knockout mouse line that specifically lacks only the Rac1b variant and a knock-in mouse line serving as the surrogate reporter for Rac1b expression that has been generated by using CRISPR gene editing method. The data obtained in this project demonstrate that the loss of Rac1b function has no obvious effects on mammary gland development and on the self-renewal of MaSCs, suggesting that it is Rac1, but not Rac1b, that is indispensable for normal mammary gland development. In contrast, in the mouse model of HER2+ breast cancer, MMTV-Neu-IRES-Cre (NIC), Rac1b is expressed by a substantial subpopulation of breast cancer stem cells (BCSCs), which require Rac1b function for maintaining their BCSC ability. Importantly, the Rac1b-null primary breast cancer cell lines display increased chemosensitivity to doxorubicin treatment compared with Rac1b-proficient primary cell lines. Taken together, the findings of this project suggests that Rac1b is dispensable for normal mammary gland development, whereas it is required for BCSC maintenance and chemoresistance of breast tumour cells. Thus, Rac1b could be a clinically relevant molecular target for the development of BCSC-targeting therapies to improve the outcomes of currently available chemotherapies.

DECLARATION

I, Fuhui Chen, the author of this thesis declare that all the work contained within this document is original, and has not been submitted in any alternative form in support of an application for any other certificate at this, or any other institute of learning.

COPYRIGHT STATEMENT

- i. The author of this thesis (including any appendices and/or schedules to this thesis) owns certain copyright or related rights in it (the “Copyright”) and s/he has given The University of Manchester certain rights to use such Copyright, including for administrative purposes.
- ii. Copies of this thesis, either in full or in extracts and whether in hard or electronic copy, may be made only in accordance with the Copyright, Designs and Patents Act 1988 (as amended) and regulations issued under it or, where appropriate, in accordance with licensing agreements which the University has from time to time. This page must form part of any such copies made.
- iii. The ownership of certain Copyright, patents, designs, trademarks and other intellectual property (the “Intellectual Property”) and any reproductions of copyright works in the thesis, for example graphs and tables (“Reproductions”), which may be described in this thesis, may not be owned by the author and may be owned by third parties. Such Intellectual Property and Reproductions cannot and must not be made available for use without the prior written permission of the owner(s) of the relevant Intellectual Property and/or Reproductions.
- iv. Further information on the conditions under which disclosure, publication and commercialisation of this thesis, the Copyright and any Intellectual Property and/or Reproductions described in it may take place is available in the University IP Policy (see [Intellectual Property Policy \(The University of Manchester\)](#)), in any relevant Thesis restriction declarations deposited in the University Library, The University Library’s regulations (see [Regulations \(The University of Manchester Library\)](#)) and in The University’s policy on Presentation of Theses.

ACKNOWLEDGEMENTS

First, I would like to express my gratitude to my supervisor, Ahmet Ucar, for unreservedly sharing his knowledge with me and teaching me experimental techniques from the beginning (cell culture). I really appreciate all the patience and support you have given me throughout my whole PhD. I am also grateful to my two intelligent co-supervisors Charles Streuli and Keith Brennan for their constructive advice to my project.

I really appreciate my lab member Sevim Gurler, an enthusiastic and kind girl. Thank you so much for organising the activities for our lab and providing lots of supports to me and mentally physically. Your enthusiasm influences me a lot and I feel so lucky to meet you at the last year of my PhD. Also, thanks to our former lab members Secil Eroglu and Lili Dimitrova, you both are so nice and so friendly. Many thanks to all the members in Keith Brennan, Andrew Gilmore and Joe Swift's lab, who provided supports to me and managed the stuff in the lab.

To my friend Jingwei, we met each other almost 9 years from Jilin to Manchester. We overcame lots of troubles and made progress together. Thank you for your accompany and for dealing with my occasional bad mood. To my friend and roommate Zelin for providing me the accommodation, I cannot imagine how hard it will be to find a place with uncertain rental term during my last year if you did not provide me the accommodation. To my friends, Heyuan, Qiuping and Junzhe and so many other people, you helped me a lot either in life or in research. All of you made my life better in Manchester.

I want to say thanks to my old friend, Ziqiang Zhang, who has left this world since 15th Feb 2019. Thank you for staying in my life for 8 years and bringing me warmth and happiness. I hope you are doing well in another world and enjoying your current life. I will continuously miss you whenever and wherever I am.

I want to say enormous thanks to my great mother Yongshuang Cui and my great father Hongquan Chen. I am so lucky to be your daughter. Thank you for trying to understand me when we have different opinions, and respecting my every decision. I definitely cannot finish my PhD without your psychological and financial supports. We have not met each other since October 2020 due to Covid, and we still have no idea when we can meet in the future. It is a tough time for us, especially for both of you. I feel so sorry that I could not accompany with you when you needed me. I really hope we could meet each other very soon. No words are enough to thank you for all the understanding and supports.

I would like to finally wish the best for all the people I have met. I hope you have a successful career at your field. Hope you enjoy your life fulfilled with love and happiness.

CHAPTER 1. General Introduction

1.1 Ras homologous (Rho) GTPases and their functions as molecular switches

Small GTPases are a large family of hydrolases that can bind to and hydrolyse GTP (guanosine triphosphate) while regulating cellular processes, such as signal transduction, synthesis and translocation of proteins, cell division and transport of vesicles. Ras superfamily of small GTPases consists of five families of regulatory GTPases: Ras, Rho, Rab, Arf, and Ran GTPases. Ras homolog (Rho) GTPases are known to regulate cell mobility, differentiation and survival, and the organization of actin cytoskeleton (Zuo et al., 2016; Svensmark & Brakebusch, 2019). They function as molecular switches that can switch on and off their downstream signal transduction pathways (Fig. 1). The binding of GTP molecule activates the small GTPase as the Rho-GTP state that is able to interact with effectors and induce cellular changes. Due to their intrinsic GTPase activity, Rho-GTP undergoes self-hydrolysis, during which the GTP molecule loses a phosphate to transform into GDP, and thus resulting in the inactive Rho-GDP state. This hydrolysis process induces the conformational shift of the small GTPases, resulting

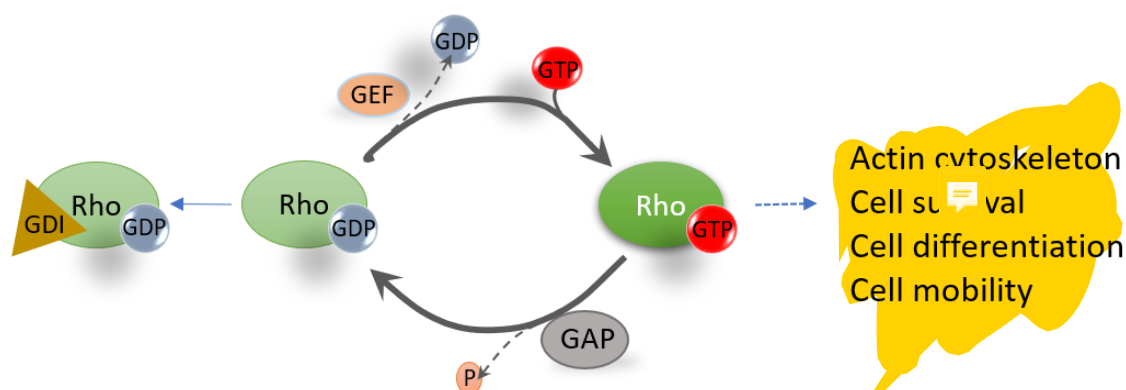


Figure 1. The regulation of Rho GTPases. GEFs are positive regulators that promote the GTP-bound active state of small GTPases. In contrast, GAPs function as inhibitory factors that accelerate the switch into the inactive GDP-bound state of all GTPases. GDIs are also inhibitory factors for small GTPases as they prevent their GEF-mediated activation.

in the disassociation of small GTPases from their effector proteins. The regulation of RhoGTPases are mediated by three functionally distinct sets of proteins downstream of various signal transduction pathways: GTPase-activating proteins (GAPs), which can accelerate and promote the hydrolysis of GTP into GDP; Guanine nucleotide exchange factors (GEFs), which induce the dissociation of GDP from small GTPases to allow the binding of a new GTP molecule; and GDP dissociation inhibitors (GDIs), which sequesters the inactive small GTPases in the cytosol and prevent their activation by GEFs (Bustelo et al., 2007; Z. Li et al., 2018; Pedersen & Brakebusch, 2012; Svensmark & Brakebusch, 2019; Zuo et al., 2016). Different cell types express different combinations of these regulatory proteins to regulate the Rho GTPase activity cycle. In humans, there are about 70 RhoGAPs, 80 RhoGEFs and 3 RhoGDIs (Zuo et al., 2016).

1.2 The functional roles of RhoGTPases in mammary gland development

There are more than 150 small GTPases identified in mammals. However, the well-characterised members of the RhoGTPase family are RhoA, Cdc42 (Cell division Cycle 42), Rac1(Ras-related C3 botulinum substrate 1), Rac2, and Rac3 (Pedersen & Brakebusch, 2012; Zuo et al., 2016). Earlier studies have revealed that some of these RhoGTPases act as signal transducers to play crucial roles in regulating mammary gland development via controlling cell proliferation, differentiation, apoptosis, mobility, cell polarity and cell adhesion.

In an *in vivo* study, Cdc42 overexpression was shown to lead to hyperbranching of the ductal tree during pubertal development due to increased mammary epithelial cell (MEC) migration and invasion rather than an alteration in cell proliferation and apoptosis. This phenotype was associated with the upregulation of mitogen-activated protein kinase (MAPK) signalling in Cdc42-overexpressed MECs (Bray et al., 2013). Using a three-dimensional (3D) cell culture

model, Akhtar and Streuli (2006) demonstrated that primary MECs with ectopic expression of dominant negative N17Cdc42 were unable to undergo normal differentiation to form functional acini due to defects in cell polarisation, which consequently impaired the milk protein production. Consistent with this observation, the genetic deletion of Cdc42 *in vivo* hampers the formation of alveolar structures, which are responsible for milk synthesis, due to dysregulated cell polarity and cell-cell contact. As a result of this, the Cdc42-null mice cannot produce enough milk to nourish their pups (Druso et al., 2016).

Another member of the RhoGTPase family, RhoA is also likely to be required for normal mammary gland development, as the genetic deletion of Neuroepithelial transforming gene 1 (Net1), a RhoA-specific GEF, results in a slower ductal outgrowth and branching during pubertal stage of mammary gland development. Furthermore, the loss of Net1 function impairs the proper organization of myoepithelial and luminal epithelial cells within the mammary epithelial ductal tree (Zuo et al., 2014). In a separate study, RhoA was shown to be required for the proper differentiation of luminal progenitors under the influence of extracellular matrix (ECM) signalling during mammary gland development (Lui et al., 2012).

The loss of Rac1 function in mammary gland was shown to have no significant effect on ductal outgrowth or lobuloalveolar structure formation during puberty and pregnancy stages respectively (Bagci et al., 2014). However, this could be due to the functional redundancy between Rac1 and Rac3, which may regulate similar downstream signalling pathways (Zuo et al., 2016). In contrast, the lack of Rac1 expression delays the involution stage via impairing Stat3 activation (Bagci et al., 2014). Consistently, another study revealed that Rac1 is critical for the post-weaning tissue remodelling process, as it regulates MEC apoptosis and clearance during the involution stage *in vivo* (Akhtar et al., 2016). However, it is still controversial whether Rac1 is also required for the lactation stage during mammary gland development (Akhtar et al., 2016; Akhtar & Streuli, 2006; Bagci et al., 2014), which I will discuss in more

detail in Chapter 3. Other studies also demonstrated that Rac3 function is important for milk secretion during lactation, and MEC apoptosis during involution stage (Leung et al., 2003; Zuo et al., 2016). These findings may suggest that there might be a functional redundancy between Rac1 and Rac3 during pubertal development and alveologenesis, but not during the lactation and involution stages of mammary gland development.

1.3 The functional roles of RhoGTPases in breast tumourigenesis and metastasis

Compared with their normal expression levels in mammary glands, some of the RhoGTPases are found to be overexpressed and/or hyperactivated during breast tumourigenesis and metastasis (Zuo et al., 2016). An earlier study using a transplacental approach showed that RhoA, Cdc42 and Rac1 GTPases contribute to the growth and migration of breast cancer cells through distinct signalling pathways (Bouzahzah et al., 2001).

Overexpression of RhoA can trigger malignant transformation of various human cell types (Fritz et al., 1999), including human mammary epithelial cells (hMECs) (Zhao et al., 2009). This study showed that ectopic RhoA overexpression induce the hMECs becoming immortal, which then have the potential to undergo malignant transformation into becoming a breast cancer cell. Furthermore, the loss of function of Net1, a RhoA-specific RhoGAP, in the MMTV-PyMT (polyoma middle T antigen) mouse model of breast cancer was shown to decrease tumour cell proliferation and tumour angiogenesis, while increasing tumour cell apoptosis, and reducing lung metastasis (Zuo et al., 2018). This indicates that Net1 is required for breast tumourigenesis and metastasis. Hence, RhoA may play an inhibitory role in the progression and metastasis of breast tumours, and thus its functions may differ from Rac1 and Cdc42 functions. Individual members of the RhoGTPase family are known to play distinct

functions in regulating actin cytoskeleton and cell mobility. For instance, Rac1, Cdc42 and RhoA functions are required for lamellipodia formation, filopodial protrusion and stress fibre formation respectively (Pennisi et al., 2002). According to a study by Keely and colleagues (1997), the activation of Rac1 and Cdc42 induces the T47D human breast cancer cells acquiring more migratory and invasive phenotypes in 3D collagen culture through regulating the PI3K signalling pathway. Consistent with this, it was also shown that the reduction of insulin-like growth factor I receptor (IGF-IR) in MCF-7 human breast cancer cell line leads to an increase of Rac1 and Cdc42 activities, with an associated decrease in RhoA activity, resulting in enhanced cell mobility and reduced stress fibre formation (Pennisi et al., 2002). Furthermore, these phenotypes are also consistent with similar observations made in EGFR-overexpressing breast tumour cells (Hirsch et al., 2006). Rac1 and Cdc42 were also shown to play a crucial role in cell migration and invasion of epidermal growth factor receptor 2 (ErbB2/HER2/Neu)-overexpressing breast cancer cells (Johnson et al., 2010). Another *in vitro* study showed that the activation of Rac1 and Rac3 is required for promoting cell migration and invasion in a highly metastatic human breast cancer cell line (Baugher et al., 2005).

Rac1 was shown to mediate BCAR3 (Breast cancer anti-estrogen resistance protein 3) signalling to regulate the proliferation of oestrogen receptor-positive (ER+) breast cancer cells (Cai et al., 2003; Xie & Haslam, 2008). Furthermore, it is demonstrated that ARGEF5/TIM, a Rho-GEF protein, regulates cancer cell proliferation through activating Rac1 and Cdc42 (Debily et al., 2004). Consistent with this, Cdc42 knockdown leads to a reduction of cell proliferation through inhibiting EGFR and ERK signalling (Hirsch et al., 2006).

In addition to cell proliferation, the RhoGTPases are also required for regulating apoptosis in breast cancer. An *in vitro* study using T47D human breast cancer cell line indicated that Cdc42 is a substrate of caspase cascade and play an anti-apoptotic role in FAS-mediated apoptosis (Tu & Cerione, 2001). Furthermore, another study has demonstrated that RhoGDIs could

prevent the apoptosis in MDA-MB-231 human breast cancer cell line through inhibiting the apoptotic cleavage of Cdc42 and Rac1 (B. Zhang et al., 2005).

In summary, the RhoGTPases have various functions during breast tumourigenesis and metastasis. The activation of RhoA contributes to the malignant transformation but inhibits tumour metastasis. Conversely, the activities of Rac1 and Cdc42 promotes cell migration and invasion during the progression of breast cancer, while also regulating cell proliferation and apoptosis.

1.4 Rac1 and Rac1b functions in various tumours

Rac1 is the only RhoGTPase that has a known alternatively spliced variant, which was discovered two decades ago and named as Rac1b. Rac1b is expressed in some epithelial tissues such as colon, liver, pancreas, spleen and skin during embryogenesis (Jordan et al., 1999). It has an additional 57- nucleotide-long exon 3b that is located between exon 3 and exon 4 of the *Rac1* gene (Fig. 2). The additional exon3b sequence results in an in-frame insertion of 19 amino acids between the 75th and 76th residues of Rac1 protein. Rac1 has two functionally important switch domains: switch I (30-38 residues) and switch II (60-76 residues). Thus, the additional 19 amino acids in Rac1b protein are located at the end of the switch II region, which may induce Rac1b acquiring novel functions (Jordan et al., 1999; Singh et al., 2004).

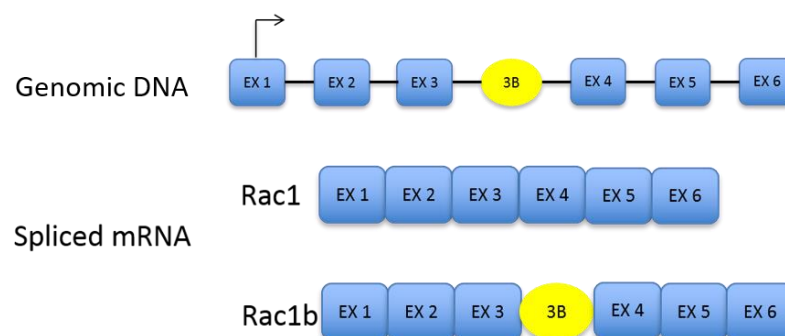


Figure 2. Genomic locus for Rac1 and its splice variant Rac1b at the genomic DNA and spliced mRNA level.

Conformational changes within the switch domains are critical for the transition between the inactive and active states of Rac1 protein, and the activation of its downstream effectors as well as its interaction with GEFs and GAPs. For the GTP-bound form, switch I and switch II domains are brought together by the existence of the GTP molecule, thus allowing its interactions with downstream effectors. After GTP is hydrolysed into GDP, the structure of the switch domains changes. This conformational change prevents a new GTP molecule binding to Rac1, and this prevents Rac1 activating its downstream targets (Beausoleil et al., 2009). Notably, it has been suggested that the inserted 19 amino acids of Rac1b leads to a conformational change of the switch domains. This change maintains Rac1b mostly in the active GTP-bound form, since Rac1b is unable to bind to GDP with high affinity, which then recruits and binds to new GTP molecules when GTP is hydrolysed into GDP (Beausoleil et al., 2009; Schnelzer et al., 2000). In addition, unlike Rac1, Rac1b is not regulated by rho-GDIs that sequester the RhoGTPases in the cytoplasm and keep them in an inactive GDP-bound state. As a consequence, Rac1b is most often found close to the plasma membrane, where GEF molecules usually are, and thus gets activated quickly. Due to these structural differences, Rac1b is often referred to as the constitutively active form of Rac1 GTPase (Beausoleil et al., 2009; Fiegen et al., 2004; Schnelzer et al., 2000). However, although Rac1b and Rac1 may regulate some overlapping downstream signalling pathways, they also have their variant specific downstream pathways.

For instance, Rac1 activate several downstream pathways such as p21-activated kinase (PAK), nuclear factor κ B (NF- κ B), Jun N-terminal kinase (JNK) and AKT serine/threonine kinase pathways. Although Rac1b is able to activate NF- κ B and AKT signalling, it does not activate JNK or PAK pathways (Matos et al., 2003). Rac1b was shown to influence the expression of Cyclin D1 that mediates G1/S progression during cell cycle and cell survival of NIH 3 mouse fibroblasts through regulating I κ B α , the suppressor of NF- κ B signalling

pathway (Matos & Jordan, 2005). Controversially, Singh and colleagues' (2004) study has shown that Rac1b may contribute to the malignant transformation of NIH 3T3 mouse fibroblasts via regulating AKT signalling pathway and Rac1b cannot promote the activation of NF- κ B, JNK and PAK signalling pathways. Furthermore, it was suggested that Rac1b protein is more stable compared with Rac1, as Rac1 can undergo ubiquitination and proteasomal degradation mediated by JNK signalling to balance Rac1 expression levels whereas Rac1b is unable to interact with JNK pathway (Visvikis et al., 2008). Taken together, Rac1 and Rac1b have overlapping and distinct effects on transducing various signals.

It has been demonstrated that Rac1 and Rac1b may play different functional roles in regulating cell proliferation, apoptosis and motility to moderate tumorigenesis and metastasis of various cancers. Rac1b was shown to be overexpressed in colorectal cancer. Both Rac1 and Rac1b can stimulate NF- κ B signalling pathway to regulate cell cycle progression through the canonical RelA-I κ B α pathway in colorectal cancer. Interestingly, Rac1 can also activate another pathway called RelB-NF- κ B2/p100, which then provides negative feedback to RelA-I κ B α signals (Matos & Jordan, 2006). In 2008, Matos and Jordan has shown that the lack of Rac1b expression leads to the reduction of NF- κ B activation, resulting in reduced cell viability through markedly upregulating cell apoptosis and slightly downregulating cell proliferation. Additionally, it is indicated that Rac1 is responsible to regulate gene expression in colorectal tumour cells through PAK1 downstream signalling pathway to inactivate Bcl-6, the transcriptional repressor for NF- κ B1/p105 and CD44 adhesion molecules (Barros et al., 2009). Interestingly, a recent study indicates that Rac1b may contribute to the chemo-resistance of tumour cells through activating NF- κ B pathway, since the Rac1b-null cells display higher sensitivity to oxaliplatin treatment (Goka et al., 2019). Apart from the NF- κ B signalling, both Rac1 and Rac1b are capable of activating Wnt signalling pathway to promote colorectal tumour progression, even though it is through regulating different mediators; β -catenin and

Dishevelled-3 (Dvl-3) respectively (Esufali et al., 2007). In turn, the increased Wnt signalling would downregulate the expression of Rac1b through regulating SRp20 splicing factor, thus forming a negative feedback loop. SRp20 induces the splicing of Rac1 by excluding exon3b, which prevents Rac1b expression. Interestingly, another splicing factor ASF/SF2, which is inhibited by PI3K pathway, promotes Rac1b expression through inducing the inclusion of exon3b into the spliced mRNA (Bordonaro, 2013; Goncalves et al., 2014). Thus, the expression of Rac1b, which is negatively regulated by Wnt and PI3K signalling, can consequently activate Wnt pathway to promote cell survival in colorectal cancers. Another study using HT-29 human colorectal cancer cell line demonstrated that Rac1b mediates cell-cell adhesion regulated by phosphoinositide 3-kinase PI3K pathway, which may indicate yet another negative feedback loop between Rac1b expression/function and PI3K signalling (Chartier et al., 2006). The knockdown of Rac1b was shown to reduce Slug expression and to increase E-cadherin expression, suggesting that Rac1b may be involved in epithelial-mesenchymal transition (EMT) process during colorectal cancer progression (Esufali et al., 2007). EMT is a key process for tumour progression, where epithelial cells acquire mesenchymal characteristics that are more migratory and invasive.

Rac1b is also overexpressed in lung cancer cells containing K-Ras mutation (Ungefroren et al., 2018; C. Zhou et al., 2013). An *in vivo* study showed that the overexpression of Rac1b in lung epithelia accelerates the tumour cell proliferation to promote K-Ras induced lung tumorigenesis. However, unlike Rac1, Rac1b isoform is not required for the initiation of lung cancer induced by mutated K-Ras, since the knockdown of Rac1b had no effect on the cell proliferation *in vitro* (Kissil et al., 2007; C. Zhou et al., 2013). Thus, the underlying mechanism of the involvement of Rac1b function in lung cancer still needs to be further studied. In another study by Stallings-Mann and colleagues (2012), Rac1b was shown to be overexpressed during

the early stages of human lung cancer, and to be activated by MMP-3 signals to promote EMT process, which consequently induces lung tumour progression *in vivo*.

Rac1b is also overexpressed in thyroid tumours (Faria et al., 2016). Recent studies on K1 PTC cell lines derived from human thyroid carcinomas demonstrated that Rac1b promotes thyroid tumour growth by regulating NF- κ B activity levels (Faria et al., 2017). NF- κ B signalling pathway is known to play various crucial roles in thyroid tumorigenesis such as inducing cell proliferation and cell migration and preventing cell apoptosis. An earlier study has also shown that Rac1b is overexpressed in a population of thyroid cancer cells (Silva et al., 2013). Although Rac1 can activate NF- κ B signalling stronger than Rac1b in normal thyroid cells, NF- κ B activity is mostly regulated by Rac1b in thyroid tumour cells. Rac1b promotes the progression of thyroid cancer via enhancing cancer cell proliferation and inhibiting cancer cell apoptosis. In thyroid tumour cells, Rac1b overexpression decreases the level of I κ B α , which is the inhibitor of NF- κ B pathway. Consequently, the increased NF- κ B signalling pathway suppresses cell apoptosis, which promotes the survival of thyroid cancer cells. Surprisingly, the process that Rac1b enhances cancer cell proliferation however does not depend on NF- κ B signalling pathway (Faria et al., 2017). The mechanism how Rac1b promotes cell proliferation in these cells has not been yet understood.

In pancreatic cancer, Rac1 is overexpressed and it promotes tumour progression. It is demonstrated that the crosstalk between Rac1 and transforming growth factor beta (TGF- β) signalling regulates tumour progression via TGF- β -mediated cell proliferation and EMT process. Rac1 was shown to regulate TGF- β pathway in pancreatic cancer via its effects on Smad2 and Smad3. TGF- β has opposite functions during distinct stages of tumour progression: in early stage tumorigenesis, it represses tumour formation through repressing cell proliferation and driving cell apoptosis; in the later stages of tumours, TGF- β induces tumour metastasis through promoting EMT, where cancer cells acquire motile and invasive abilities.

Notably, the EMT mediated by TGF- β depends on MAPK signalling pathway. Rac1 can activate NADPH oxidase (NOX), which then induces the production of reactive oxygen species (ROS). There are three downstream effectors for ROS: p38, MAPK and PAK. Thus, the combination of Rac1 and TGF- β signals accelerates tumour metastasis. Additionally, PAK signalling pathway directly activated by Rac1 can also increase the motility of cancer cells. Thus, Rac1 promotes tumour metastasis in pancreatic cancer (Ungefroren et al., 2018). In contrast, Rac1b has the opposite role in regulating cell migration induced by TGF- β signalling pathway. Rac1b-knockdown *in vitro* results in the increase of cell migration induced by TGF- β /Smad pathway, indicating that Rac1b suppresses the activation of TGF- β pathway via inhibiting the activation of Smad3 factors that are downstream effectors of TGF- β in pancreatic cancer cells (Ungefroren et al., 2014; Ungefroren et al., 2019). Thus, Rac1 and Rac1b have antagonistic functions in regulating TGF- β signalling in pancreatic adenocarcinoma. Interestingly, the expression of Rac1b increases with the pancreatic tumour progression in patient samples, which is also correlated with MMP3 expression. The pancreatic tumour cells treated with MMP3 was shown to activate Rac1b expression and to increase the motility of the cancer cells (Mehner et al., 2014), a seemingly contradictory phenotype observed in the other studies, which may depend on the KRAS status of the pancreatic cancer cell lines used.

The antagonistic relationship between Rac1 and Rac1b was also shown in breast cancer. In an *in vitro* study, Rac1 knockdown was shown to inhibit cell migration, whereas Rac1b-knockdown displayed the opposite phenotype (Melzer et al., 2017). In accordance with this result, Nimnual et al. (2010) demonstrated that the presence of Rac1b prevents Rac1 locating in the plasma membrane, leading to the inhibition of Rac1 activity in HeLa cells. Thus, Rac1b might function as an inhibitor of Rac1 activation in some tissues and tumours.

Taken together, Rac1b is the only known alternatively spliced variant of Rac1 GTPase, and is considered as a constitutively active isoform of Rac1. Notably, Rac1 and Rac1b may regulate

overlapping or variant-specific downstream signalling pathways. For instance, PAK and JNK signalling can be activated by Rac1 but not Rac1b isoform, whereas NF- κ B and TGF- β pathways can be regulated by both. Rac1 and Rac1b are able to regulate various cellular activities including cell proliferation, apoptosis, and motility, even though sometimes through distinct downstream signalling pathways. Recent studies also indicate that Rac1 and Rac1b isoforms may have antagonistic functions between each other in regulating cell activities in some tissues and tumours. Although Rac1 functions has been extensively studied for a long time in the field of tumour biology, our knowledge on the functional roles of Rac1b is just emerging in the recent years. Notably, Rac1b function could be involved in the chemoresistance response of cancer cells, suggesting that Rac1b might be a potential target for future cancer therapies. Thus, further studies are necessary to reveal the variant-specific functions of Rac1b in various normal tissues and malignant tumours, as well as to acquire a deeper understanding of the relationship between Rac1 and Rac1b in regulating their downstream signalling pathways. Here, this project aims to elucidate the Rac1b-specific functions in both normal mammary gland development and breast tumourigenesis *in vivo*.

CHAPTER 2. Materials and methods

2.1 Molecular Biology

2.1.1 PCR (Polymerase Chain Reaction) for High-fidelity cloning

For high-fidelity clonings, PCR reactions were set by mixing 1µl pGemT vector or Eph4 gDNA, 5µl 5x Buffer, 0.5µl 10mM dNTP Mix (Bioline BIO-39025), 0.2µl forward primer and 0.2µl reverse primer (Sigma), 0.2µl Q5 DNA polymerase (New England Biolabs M0491G), and supplemented with ddH₂O to a total volume of 25µl. If the fragment to be cloned is known to be GC-rich, 5µl enhancer was added to increase the reaction efficiency. The reaction was set up on Veriti Thermal Cycler. The PCR products were then purified by PCR Purification Kit (QIAGEN 28104) following the manufacturer's protocols.

The information for primer sequences and used PCR programs are listed below:

Target Fragments	Primers	PCR Program
T2A-RFP	T2A-Frw: 5'-GTTAAGGCGGCCGCAATTAAGAATTC GAGGGCAGAGGAAGTCTTCTAAC-3' T2A-Rev: 5'-CCAAACACTAGTATATATCTCGAG GACTCATGCGCCGGTGGAGTG-3'	95°C: 10 mins 66°C: 30s 72°C: 90s 94°C: 30s 72°C: 5 mins 10°C: ∞ x35
Exon3b	EXT-Frw: 5'-GATTACGCGGCCGCGATCG GAACAAGGGGTAAACCCTAGGAG-3' EXT-Rev: 5'-CAATGTACTAGTCGATCG CAAAATGGAGTTCAAGAGTTTGCTC-3'	95°C: 10 mins 66°C: 30s 72°C: 240s 94°C: 30s 72°C: 5 mins 10°C: ∞ x35

5' Homolog of Exon3b	EXT-Frw: 5'-GATTACGCGGCCGCCGATCG GAACAAGGGGTAAACCCTAGGAG-3'	95°C: 10 mins 66°C: 30s 72°C: 120s 94°C: 30s x35 72°C: 5 mins 10°C: ∞
	A5-Rev: 5'-CAGTTAGAATTC GTCTCCAACCTAGTAATGCATCAGAACTTTG-3'	
	B5-Rev: 5'-CAGTTAGAATTCGGGTCTATCTTTACCACATGT GTCTCCAACCTAGTAATGCATCAGAACTTTG-3'	
	C5-Rev: 5'-CAGTTAGAATTCCTTGTCTTTGAGACTGGA GGGTCTATCTTTACCACATGT GTCTCCAACCTAGTAATGCATCAGAACTTTG-3'	
3' Homolog of Exon3b	EXT-Rev: 5'-CAATGTACTAGTCGATCG CAAAATGGAGTTCAAGAGTTTGCTC-3'	95°C: 10 mins 66°C: 30s 72°C: 105s 94°C: 30s x35 72°C: 5 mins 10°C: ∞
	A3-Frw: 5'-GTACTACTCGAG ACATGTGGTAAAGATAGACCCTCCAGTCTCAAAGAC-3'	
	B3-Frw: 5'-GTACTACTCGAG TCCAGGGGCAAAGACAAGCCGATTG-3'	
	C3-Frw: 5'-GTACTACTCGAG CCGATTGCCGTATGTAAGACTTTGAG-3'	

2.1.2 Digestion, Purification and Ligation



50µl of purified PCR products were mixed with 8µl 10x Buffer, 0.8µl 100x BSA, 3µl restriction enzyme A, 3µl restriction enzyme B, supplemented with ddH₂O to a total volume of 80µl. 15µl pGEM-T vector (Promega, A362A), 6µl 10x Buffer, 0.6µl 100x BSA, 3µl restriction enzyme A, 3µl restriction enzyme B, supplemented with ddH₂O to a total volume of 60µl. The prepared reactions were incubated at 37°C overnight. Next day, ddH₂O was added to a final volume of 95µl to the digested solutions, then 5µl 0.5M EDTA was also added into the reactions. The mixtures were then purified by PCR Purification Kit (QIAGEN 28104) following the manufacturer's protocols. At the last step, the products were eluted with 30µl elution buffer, rather than 50µl buffer. The purified digestion products (target DNA fragments and plasmids) were ligated in proper ratio using T4 DNA ligase (New England Biolabs M0202S) at room temperature overnight.

2.1.3 Bacterial Heat-shock transformation and plasmid DNA extraction

The competent bacteria (E.coli, DH5alpha) was taken out of -80°C storage freezer and put on ice for about 30 minutes. After that, 3µl of the ligation reaction was added into the bacteria, and incubated for another 30 minutes on ice. Next, the bacteria solution was incubated at 42°C for 45 seconds, and then put on ice for 2 minutes. Then, 500µl LB broth (without antibiotics) was added on top of the bacteria, and the mixture was incubated with shaking for 45 minutes at 37°C incubator. After incubation, the transformed bacteria was spread on the pre-warmed LB-Agar plates containing Ampicillin, and cultured at 37°C for 16-18 hours. The colonies were picked and cultured in 6ml LB broth containing Ampicillin at 37°C for 16-18 hours, which was then used to extract plasmid DNA using MiniPrep kit (QIAGEN 27106) following the manufacturer's instructions. For MidiPrep (QIAGEN 12143), each colony was cultured in 50ml LB broth containing Ampicillin. For MaxiPrep (QIAGEN 12663), each colony was cultured in 100ml LB broth containing Ampicillin.

2.1.4 Sequencing

5µl of PCR products or plasmids were mixed with 5µl 1:20 diluted primers, which were sequenced by Eurofins Genomics company. The sequencing results were analyzed by Sequencher DNA Sequence Analysis Software from Gene Codes.

2.1.5 Genomic DNA isolation

Tissues or cell pellets were lysed in 500µl diluted proteinase K (Sigma P6556) at 56°C overnight. Proteinase K was diluted to 1mg/ml using lysis buffer (100mM Tris pH8, 5mM EDTA pH8, 200mM NaCl, 0.2% SDS). The genomic DNA was precipitated by mixing the lysates with 700µl isopropanol, followed by a harsh shake. The precipitated genomic DNA was further washed in 1ml 70% ethanol to get rid of excess salt, dried and resuspended using T1/10E buffer (10mM Tris pH7.2, 1mM EDTA) at 60°C.

2.1.6 RNA isolation

Cell pellets were lysed within 1ml Trizol Reagent and incubated for 5 minutes at room temperature. Afterwards, 200µl of chloroform was added and vigorously shaken and centrifuged to separate RNA, DNA and protein phases. The RNA in the upper aqueous phase was collected and then precipitated by adding 500µl isopropanol. The precipitated RNA was washed briefly with 1ml 75% ethanol, dried and resuspended using T1/10E buffer.


2.1.7 Reverse Transcription (RT) - cDNA synthesis

Isolated total RNA (1µg) was used in 20µl reverse transcription reactions using Tetro cDNA Synthesis Kit (Bioline: BIO-65043) that contains Random Hexamer Primer Mix. The program was set up as: 25°C (10mins), 45°C (40mins), 85°C (5mins), and 10°C (∞). The reaction was set up on Veriti Thermal Cycler.

2.1.8 DNA gel electrophoresis

The PCR products or constructs were run on agarose gel. Agarose (Bioline BIO-41025) was dissolved in TAE buffer (40mM Tris-acetate, 1mM EDTA), and supplemented with SYBR safe DNA Gel Stain (Invitrogen). 1kb DNA ladder (New England Biolabs G571A) was used as size marker. Gels were visualized using the Kodak Gel Logic 100 Imaging System.

2.1.9 Protein isolation

Adherent cells were lysed for 15mins with gular cell scraping in 100µl 1x RIPA buffer supplemented with protease inhibitor cocktail (Merck 539131). The lysate was collected and centrifuged at ~20,000rcf for 15mins. The supernatant containing protein was collected and then aliquoted. The protein concentration was determined using the Pierce BCA Protein Assay Kit according to the manufacturer's protocols.

2.1.10 Western blotting

50µg protein samples were mixed with 4x sample buffer (Life Technologies 1368836) supplemented with β-Mercaptoethanol (Sigma M3148), and then denatured at 95°C for 5 mins. The samples were run on a 15% polyacrylamide SDS-PAGE gel in running buffer. Samples were run at 35mA per gel for about 1 hour with 7µl Blue Prestained Protein Standard Broad Range Ladder (Biolabs P7706S). Protein was transferred to a nitrocellulose membrane (Amersham Protran 0.45 NC, GE Healthcare) in transfer buffer for 1hr at 100V. Notably, the membrane should be pre-activated by ddH₂O before transfer process. The membrane was blocked in 5% milk in PBS-T blocking buffer for 40 minutes. The blocked membrane was incubated in the primary antibodies diluted in blocking buffer overnight. The membrane was then washed 3 times in 1x PBS-T and incubated for 1hr in the secondary antibodies diluted in blocking buffer. The membrane was washed 3 times in 1x PBS-T and visualised using the Odyssey CLx Imaging System and Image Studio software (LI-COR).

Dissolve 30.2g Tris base and 144g Glycine and top up to 1L with ddH₂O to make up 10x Running buffer. 1x running buffer contains 100ml 10x Running buffer, 10ml 10% SDS and 890ml ddH₂O. Transfer buffer contains 100ml 10x Running buffer, 200ml methanol and 700ml ddH₂O.

The preparation for 15% polyacrylamide SDS-PAGE gel:

15% Resolving Gel		Stacking Gel	
Acr/bis (mLs)	12	Acr/bis (mLs)	1.33
1.88M pH8.8 Tris (mLs)	4.8	0.625M pH6.8 Tris (mLs)	1.6
0.5% SDS (mLs)	4.8	0.5% SDS (mLs)	1.6
ddH ₂ O (mLs)	2.4	ddH ₂ O (mLs)	3.48
TEMED (μLs)	20	TEMED (μLs)	8
APS (μLs)	120	10% APS (μLs)	40

The antibodies information are listed as below:

	Antibodies Information	Dilution
Primary Antibodies	Mouse anti-Rac1(#23A8, Merck)	1:1000
	Goat anti-β-actin (#8229, Abcam)	1:1000
Secondary Antibodies	IRDye 800CW donkey anti-mouse	1:10000
	IRDye 680RD donkey anti-goat	1:10000

2.2 Cellular Biology

2.2.1 Cell culture and passaging for cell line

EpH4 cells were cultured in Dulbecco Modified Eagle's medium (DMEM) with high glucose (Sigma D6429), supplemented with 10% foetal bovine serum (FBS) (Labtech) and 1% Penicillin-Streptomycin (Sigma T3924) and L-Glutamine (Sigma G7513). Cells were maintained at 37°C and 5% CO₂, with routine medium changes and passaging.

2.2.2 CRISPR/Cas9 double nickase transfection

The mouse sgRNA-mA (UGUCUCCAACCUAGUAAUGC) and sgRNA-mB (GGUAAAGAUAGACCCUCCAG) for targeting mouse *Rac1b* was cloned into pSpCas9n(BB)-2A-GFP (pX461, Addgene #48140) vector by our group member before I started PhD. HDR templates were cloned into pGEM-T vector (Promega, A362A) by myself. For each well of the 6-well plate, the transfection mixture was prepared by mixing 100µl pure DMEM, 4µl X-tremeGENE™ 9 DNA transfection reagent (Roche 06365787001), 3µg sgRNA-A construct, 3µg sgRNA-B construct and 1µg HDR template, which was then incubated for 20 minutes at room temperature. Meantime, the medium for the cells was changed into antibiotics-free DMEM medium containing FBS and L-Glutamine. Afterwards, 100µl of transfection mixture was added into each well dropwise. After 4-6 hours, the medium was changed into complete medium that contained antibiotics. Co-transfected cells (i.e. GFP⁺) were sorted 24 hours post-transfection directly into the 96 well plates as one cell per well using FACS and grown as single-cell clones.

2.2.3 Primary monolayer cell culture and passaging for mouse tumour cells

The CD24⁺CD49f⁺ primary breast cancer cells isolated from mouse tumours by FACS were cultured in DMEM/F12 (Corning 10-092-CV) medium supplemented with 10% foetal bovine serum (FBS) (Labtech), 5µg/ml Insulin (Sigma I9278), 0.02µg/ml EGF (Sigma E4127),

Penicillin-Streptomycin. Cells were maintained at 37°C and 5% CO₂, with routine medium changes and passaging at low split rate (1:2).

2.2.4 Mammospheres Assay

Sorted primary single cells were seeded in ultra-low attachment 96-well plates (Corning 3474) in mammosphere media consisting of MEBM supplemented with 5µg/ml Insulin (Sigma I9278), 4µg/ml Heparin (Sigma H3149-50KU), 5µg/ml Hydrocortisone (Sigma H0888-1G), Penicillin-Streptomycin, 0.02µg/ml Recombinant human bFGF (Gibco, PHG0021), 0.02µg/ml EGF (Sigma E4127) and 1x B27 (Gibco 17504-044). Cell samples sorted from mammary glands were seeded at a concentration of 10,000 cells/ml and 100,000 cells/ml. Primary tumor cells were plated at a concentration of 50,000 cells/ml and 100,000 cells/ml. After 7 days, the numbers of the spheres in each well were recorded and analyzed. Solid structures with a minimum diameter of 50µm are considered as mammospheres.

2.2.5 Doxorubicin treatment

Primary tumour cell lines were seeded in flat-bottom 96-well plates. Once they reach >90% confluence, they were treated with 1µM and 2.5µM doxorubicin (#BP990, Sigma) for 24 hours and then washed several times to remove the chemotherapeutic agent. For cell quantification, AlamarBlue reagent (#799771, Invitrogen) was used according to the manufacturer's protocols and absorbances of reduced versus oxidised reagents were measured at 562 nm and 630 nm wavelengths using plate reader ELx800 (BioTek). The formula for calculating the percent reduction of AlamarBlue = $[A_{562} - (A_{630} \times R_o)] \times 100\%$, the correction factor $R_o = A_{O562} / A_{O630}$, $A_{O562} = A_{562}$ (AlamarBlue in blank medium) - A_{562} (medium blank), $A_{O630} = A_{630}$ (AlamarBlue in blank medium) - A_{630} (medium blank).

2.2.6 Immunofluorescence for cytopinned cells

Sorted primary cells were fixed in 4% paraformaldehyde solution and then immobilised onto Poly-lysine slides (ThermoFisher J2800AMNZ) using cyto-spin at a concentration of 10 000 cells per slide. This step was performed using Shandon Cytospin 2 at 400rpm for 10 mins. After immobilisation, samples were permeabilised and blocked with 0.2% Triton and 5% horse serum in PBS prior to incubation with primary antibodies diluted in blocking buffer against CK14 and CK18 in room temperature for 1 hour. After a subsequent incubation with secondary antibodies diluted in blocking buffer and DAPI for 1h at room temperature in dark, they were mounted with Fluorescence mounting medium (#S3023, DAKO). Stained samples were pictured using Zeiss Imager M2 fluorescent microscope with 63x objective.

The primary antibodies used in the experiments described above were cytokeratin 14 Polyclonal Antibody (#PA5-16722, Invitrogen) and anti-Keratin K18 Mouse Monoclonal Antibody (#61028, Progen), used in 1:100 dilution. The secondary antibodies used were donkey anti-Rabbit IgG (H+L) Alexa Fluor 488 (#21206, Invitrogen) and donkey anti-Mouse IgG (H+L) Alexa Fluor 594 (#21203, Invitrogen), used in 1:500 dilution. DAPI (Sigma D8417) was used at 0.1µg/ml concentration.

2.2.7 Immunofluorescence for 3D spheres derived from mammosphere assay

The organoids formed in mammosphere culture were collected and fixed in 4% paraformaldehyde solution for 20 min. They were then blocked and permeabilized with organoid washing buffer (0.1% Triton-X100, 5% BSA in 1xPBS) for 15 min, followed by incubation with primary antibodies diluted in organoid washing buffer against CK14 and CK18 for 1 h at room temperature. After 3 rounds of washing with organoid washing buffer, the organoids were then incubated with secondary antibodies diluted in organoid washing buffer and DAPI for 1 h at room temperature in dark. Organoids were then transferred into 6 well plate containing 1xPBS and imaged by using Leica SP8 Upright dipping lens Confocal

microscope with 63x objective. The detailed information of primary and secondary antibodies and DAPI solutions used in the experiments described above were listed in Section 2.2.6.

2.3 Mice studies

2.3.1 Mouse experiments

All mouse experiments were performed under the license of the UK Home Office Animals (Scientific Procedures) Act (1986) regulations with the approval of study protocols by the Animal Welfare and Ethical Review Body (AWERB) of the University of Manchester. Rac1b-KO mouse line was provided by our collaborators in Cancer Research UK Beatson Institute (Gudiño, Pohl, et al., 2021). The mouse line were then backcrossed into C57BL/6J and FVB/J backgrounds for at least 7 generations in our lab. Rac1b^{RFP/+} mouse line in pure FVB/J background has been generated in this project using HDR-coupled CRISPR-targeting as described in Chapter 3.

2.3.2 PCR for genotyping mice

For genotyping the cell/tissue samples, the PCR reactions were prepared by mixing 1µl gDNA extracted from cell/tissues, 5µl 5x Buffer, 0.5µl 10mM dNTP Mix (Bioline BIO-39025), 0.2µl forward primer and 0.2µl reverse primer (Sigma), 0.25µl GoTaq DNA polymerase (Promega M7845) and supplemented with ddH₂O to 25µl. Reactions were carried out in the Veriti Thermal Cycler (Applied Biosystems). The primer sequences used for genotyping mice are listed below:

Mouse line	Primers	Band size	PCR Program
Rac1b-KO	AU-R1bKO-newFrw: 5'-GACACCCTTAGAAATAGCCCACAG-3' AU-R1bKO-newWTRev: 5'- CCCTGGAGGGTCTATCTTTACCAC-3' AU-R1bKO-newRev: 5'-CCAAGCATCCAAGTTGATTCCACAC-3'	WT allele: 799bp KO allele: 580bp	95°C: 10 mins 68°C: 30s 72°C: 30s 94°C: 30s 72°C: 5 mins 10°C: ∞ x35

Rac1b^{RFP}-KI	FC-mmR1b span-Frw: 5'-GGCTCTCAGCTTCCAAGGTGAC-3' FC-WT R1b-Rev: 5'-GACCCTCCACACCTGCACCTC-3' FC-KI-Rev: 5'-CGCATGAACTCCTTGATGACGTC-3'	WT allele: 484bp KI allele: 285bp	95°C: 10 mins 66°C: 30s 72°C: 30s 94°C: 30s 72°C: 5 mins 10°C: ∞
MMTV-NIC (Cre)	Cre-Frw: 5'-ATGCTTCTGTCCGTTTGCCG-3' Cre-Rev: 5'-CCTGTTTTGCACGTTACCG-3'	WT allele: No band Cre allele: ~250bp	95°C: 10 mins 57°C: 30s 72°C: 30s 94°C: 30s 72°C: 5 mins 10°C: ∞

2.3.3 Whole-mount Carmine-Alum staining

The dissected No:4 mammary glands were spread on glass slides and fixed in Carnoy's fixative (6 parts 100% EtOH, 3 parts Chloroform and 1 part glacial acetic acid) for 4 hours at room temperature. The fixed mammary glands were rehydrated in sequential incubations within 70%, 50% and 25% EtOH for 30 minutes respectively, and then rinsed in distilled water for 2 minutes. Then, the mammary glands were stained in Carmine-alum in dark overnight. The stained mammary glands were dehydrated in sequential incubations within 70%, 90%, 96% and 100% EtOH for 30 minutes respectively. Subsequently, the slides were placed in used HistoClear for 1 hour, and then transferred to fresh HistoClear to keep. The images were taken by Leica Wild MZ8 microscope with Carl Zeiss AxioCam colour microscope camera 412-312.

Carmine-alum stain preparation:

10g Alum potassium sulphate (Sigma A7167) and 4g Carmine (Sigma C1022) to 2L ddH₂O. Boil for at least 40 minutes and keep hot till the powder dissolved. Adjust final volume to 2L with ddH₂O. Filter and add a crystal of thymol for preservation. store the solution at 4°C.

2.3.4 Hematoxylin & Eosin staining

The mammary glands or breast tumours are fixed in 4% Paraformaldehyde (PFA) solution overnight at 4°C, and then washed with 1xPBS for three times. Following that, the tissues are incubated with 0.08% NaCl overnight, 50% EtOH at least 4 hours, and finally stored in 70% EtOH at 4°C to accumulate more samples. The fixed samples will be processed by Leica ASP300S fully enclosed tissue processor, which are then embedded in paraffin. The paraffin-embedded tissue blocks are sectioned by Leica RM2255 Microtomes and placed onto slides with section thickness of 5µm. The slides are heated within 60°C incubator, deparaffinised in two changes of xylene (10 minutes for each time), and rehydrated in sequential incubations within 100% EtOH for 5 minutes, followed by 96%, 90%, 70%, 50% and 25% EtOH for 2 minutes respectively. The slides are stained in Hematoxylin (Sigma HHS16-500ml) solution for 8 minutes, which is followed by a wash under running tap water for 2 minutes. After that, the slides are dipped in 70% EtOH with 0.1% HCl solution 2-5 times, and placed them back into tap water, followed by distilled water for 2 minutes. Subsequently, the slides are stained within 1:5 diluted Eosin Y (Sigma 318906-500ml) with one drop of glacial acetic acid solution. The slides are then washed with distilled water (twice), 50%, 70%, 90%, and 96% EtOH for 2 minutes respectively, and 100% EtOH for 5 minutes to dehydrate the slides. Following that, the slides were placed in two changes of Histoclear for 10 minutes each time, and mounted by Eukitt medium. The pictures were taken by Olympus BX63 Upright Colour Camera Snapshot Microscope and Single Slide Scanner.

2.3.5 Immunohistochemistry

The slides were dewaxed and rehydrated as described above in Hematoxylin & Eosin staining protocol. After rehydration, the slides were treated in 3% H₂O₂ within Methanol for 10 minutes to block endogenous peroxidase activity and subsequently washed in distilled water. The

‘antigen retrieval’ step was carried out by boiling the sections in 0.01M pH 6.0 citrate buffer (9ml 0.1M Citricacid, 41ml 0.1M Natriumcitrat and 450ml ddH₂O) for 15 minutes, followed by incubation in 0.05M pH7.6 Tris buffer (4.5g NaCl, 50ml 0.5M pH7.6 Tris and 450ml ddH₂O) twice and PBS for 5 minutes each. Afterwards, within a humidity chamber, the slides were incubated in blocking buffer in 1xPBS at room temperature for 1 hour, followed by incubation with primary antibody solutions in blocking buffer at 4°C overnight. Next day, the slides were washed in 3 changes of 1xPBS solution to wash off excess primary antibody, and then incubated in biotinylated secondary antibody diluted in blocking buffer for 30 minutes within a humidity chamber. Subsequently, the slides were washed in 1xPBS and treated with ABC reagent, which is prepared by mixing reagent A and B (1:1 ratio) 30 minutes before use, for 30 minutes within a humidity chamber. Following that, the slides are incubated in DAB reagent at room temperature within a humidity chamber. The DAB reagent is composed of 150ul 15x substrate buffer, 50ul 50x DAB chromogen and 50ul 50x peroxidase substrate and approximately 1.7ml ddH₂O. Last, the slides are counterstained with Hematoxylin and mounted with Eukitt medium. The pictures were taken by Olympus BX63 Upright Colour Camera Snapshot Microscope and Single Slide Scanner.

The primary antibodies used in the experiments described above were ER α (#sc-542, Santa Cruz Biotechnology, 1:100 dilution), PR (#sc-538, Santa Cruz Biotechnology, 1:400 dilution) and Ki67 (#sc-7846, Santa Cruz Biotechnology, 1:100 dilution). The blocking buffers, biotinylated secondary antibodies and ABC reagents are prepared from Rabbit IgG Peroxidase ABC-HRP Kit (#PK-6101, Vector Laboratories) and Goat IgG Peroxidase ABC-HRP Kit (#PK-6105, Vector Laboratories). DAB reagents are prepared from the kit ABC staining system (#sc-2018, Santa Cruz Biotechnology)

2.3.6 Primary cell isolation

The breast tumours or No. 3-4-5 mammary glands (6 glands in total per mouse) were dissected from sacrificed mice, and kept in DMEM/F12 medium on ice. The tissues were dipped into 70% ethanol 3 times and rinsed with DMEM/F12 medium twice. After that, the tissues were minced with scissors into $\sim 1\text{mm}^3$ pieces and digested in Collagenase/Hyaluronidase digestion cocktail (50ul L-Glutamine, 500ul FBS, 500ul Collagenase in 10ml DMEM/F12, and 1.5ml freshly prepared Hyaluronidase) at 37°C for about 4 hours with slow shaking. After dissociation of ducts from stroma, the tissue solutions were vortexed for 5 seconds and left for 5 minutes untouched to settle. The upper fat layer was carefully removed using a pipette. HBSS (Sigma H9394) with 2% FBS was added to stop the digestion process and centrifuged at 350rcf for 5 mins. The tissue pellets were then washed with pure HBSS. Following that, the tissue pieces were digested within 2-10ml (depending on the size of the pellet) pre-warmed Trypsin-EDTA by continuously pipetting to mechanically dissociate the organoids for 1-3 minutes till there was no visible organoid structures. Again, the reaction was stopped by adding 2% FBS in HBSS and subsequently washed within pure HBSS. Then, the cell pellets were further digested with 1-5ml (depending on the size of the pellet) pre-warmed Dispase and DNase (2ml Dispase + 400 μ l DNase in 8ml pure HBSS) for 1-3mins by pipetting up and down to dissociate the remained clumps. The digested cells were then filtered using 40 μ m cell strainer.

The preparation of the enzymes:

Collagenase A (25mg/ml, Roche 11088793001): 500mg powder was dissolved in 20ml HBSS and sterilized by passing through 0.22 μ m filter. Hyaluronidase (1mg/ml, Sigma H3506): Dissolve 10mg lyophilized Hyaluronidase in 10ml HBSS and sterilize by passing through 0.22 μ m filter. It was always freshly prepared and quickly used. Dispase II (5mg/ml, Roche 4942078001): 1g powder was dissolved in 200ml HBSS modified which contains 2ml of 1M

HEPES. Then, sterilize by passing through 0.22µm filter. DNase I (10mg/ml, Roche 11284932001): 100mg powder was dissolved in 10ml ddH₂O.

2.3.7 FACS (Fluorescence-activated cell sorting) sorting

The cells were blocked in FACS buffer (2% FBS in PBS) containing Rat Anti-Mouse CD16/CD32 (Clone 2.4G2, BD Biosciences 553142) blocking antibodies for 15 minutes. Then, the blocking solution was washed away with FACS buffer and the cells were incubated in primary antibodies diluted within FACS buffer for 15 minutes. Again, the primary antibodies were washed away with FACS buffer and the cells were incubated in secondary antibodies diluted within FACS buffer for 15 minutes. The secondary antibodies were washed away with FACS buffer, and the cells were resuspended in FACS buffer. Last, the dead/live cell markers were added into the cell suspensions. The prepared cells were analyzed and sorted into 5ml tubes using Aria Fusion sorter with 85 or 100 micron nozzle.

The primary antibodies used include Biotin Rat Anti-Mouse TER-119/Erythroid Cells (BD Biosciences 553672), Biotin Rat anti-mouse CD31 (BD Biosciences 558737), Biotin Rat Anti-Mouse CD45 (BD Biosciences 553077), APC Rat Anti-Mouse CD24 (Clone M1/69, BD Biosciences 562349), eFluor450 CD49f Monoclonal Antibody (Clone eBioGoH3 (GoH3), Invitrogen 48-0495-82), and Pacific Blue CD24 (Clone M1/69, BioLegend 101820). The secondary antibodies used in this project include PE-Cy7 Streptavidin (BD Biosciences 557598) and FITC-Streptavidin (BD Biosciences 554060). The dead cell markers include 0.1µg/ml DAPI (Sigma D8417) or 1:100 dilution of DRAQ7 (BioStatus DR71000). The antibodies were all diluted in FACS buffer (2% FBS in PBS) as 1:100 dilution, except CD45 which was 1:400 dilution.

2.4 Statistical analysis

Statistical analysis used in this project were selected depending on population distribution, data type and sample centrality/variability to meet assumptions of tests using GraphPad Prism and Microsoft Excel software. P values <0.05 were considered statistically significant. Data are expressed as mean \pm standard deviation (SD) or mean \pm standard error of the mean (SEM). The specific analysis methods for each experiment were explained in their respective figure legend.

CHAPTER 3. Results Part I - Rac1b, the splice variant of Rac1, is dispensable for normal mammary gland development

3.1 Introduction

3.1.1 Mammary Gland Development: insights from mouse models

Mammary gland is a highly organized tissue which undergoes a series of morphological changes during development. The development of mammary gland is a continuous process depending on epithelia-mesenchyme interactions, occurring embryonically and postnatally throughout an individual's life. On approximately embryonic day 18 (E18), as shown in Figure 3, the mammary gland is composed of a rudimentary ductal tree (Mikkola & Millar, 2006). Then, the mammary gland will only grow isometrically until the onset of puberty during which terminal end buds (TEBs) form and promote the complete invasion of the fat pad by the ductal tree (Fig. 4). Subsequently, alveolar buds arising from mammary epithelial ducts form the secretory alveoli during pregnancy and lactation stages. Secretory alveoli can produce milk in order to feed the offspring and help the new-born to establish an immune defence. After weaning of the pups, the alveoli undergo regression under the regulation of many factors. This process is called as involution, during which the mammary gland re-structures itself to return back to its pre-pregnancy morphology. Mammary gland is a highly regenerative organ since the process of pregnancy, lactation and involution can recur with each cycle of pregnancy during the sexually active life of the females (Paine & Lewis, 2017).

3.1.1.1 Embryonic development of mammary gland

During murine embryonic development, mouse mammary gland begins to develop on approximately E10.5 with the formation of the mammary lines (Fig. 3). There are two stripes

of ventrolateral ectoderm becoming thickened, thereby forming the mammary lines. With the migration of cells, the mammary lines disappear gradually and form 5 pairs of lens-shaped mammary placodes at the end of E11.5. Notably, these placodes pattern the position of animal nipples. Within the following 24 hours, the mammary placodes invade into the underlying mesenchyme to give rise to mammary buds (Mikkola & Millar, 2006). Meantime, the mesenchyme surrounding the mammary buds undergoes condensation to form primary mammary mesenchyme (Propper et al., 2013), leading to the expression of androgen receptor to limit the growth of mammary gland ducts. Consequently, the progression of mammary gland development pauses until E15.5. Hence, the development of mammary gland also relies on epithelia-mesenchyme interactions, which is similar to the development of skin appendages, such as hair (Mikkola & Millar, 2006). On E15.5, the mammary gland buds pass through the primary mammary mesenchyme to sink into the fat pad, caused by cell proliferation that does not depend on hormones. This process leads to the formation of mammary sprouts. Subsequently, the mammary sprouts continue invading into the fat pad and start to branch, resulting in the formation of a ductal tree with lumen by approximately E18. This ductal tree, known as rudimentary mammary gland, comprises of the primary duct and several secondary

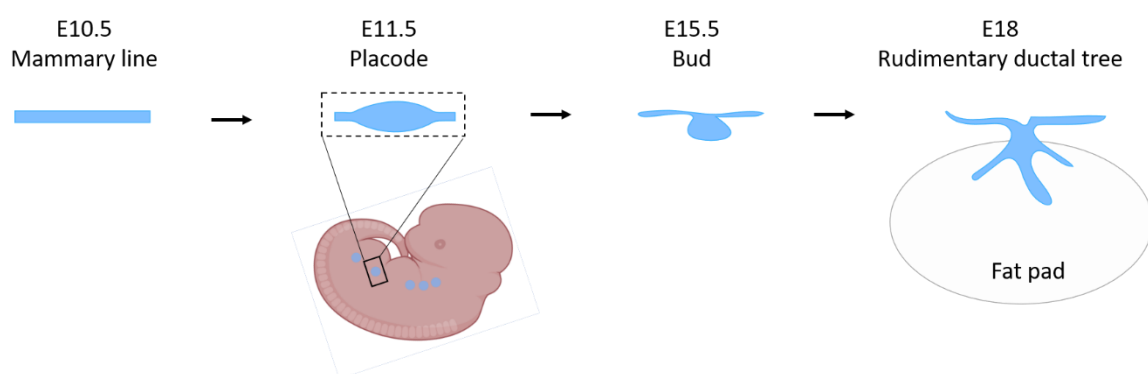


Figure 3. Mammary gland development during embryogenesis. At E10.5, mammary lines appear. At E11.5, mammary placodes form. At E15.5, mammary buds begin to invade into fat pad. By E18, the epithelial ductal tree forms.

ducts. The primary duct is composed of single-layer epithelial cells which are surrounded by stromal cells (Richert et al., 2000). Normally, the primary duct has only 15-20 secondary branches as the existence of lumen prevents duct branching. Therefore, the prenatal morphogenesis of the mammary gland stops at about E18 (Mikkola & Millar, 2006).

3.1.1.2 Puberty

With the onset of puberty, at about 3-4 weeks after birth, mammary ducts start to extend rapidly and the number of branches increases sharply (Paine & Lewis, 2017). In response to the increasing oestrogen and growth hormones, terminal end buds (TEBs), which are unique structures to the pubertal mammary morphogenesis, appear at the distal ends of the developing ducts. Due to its highly proliferative property, TEBs induce ductal elongation and bifurcates to

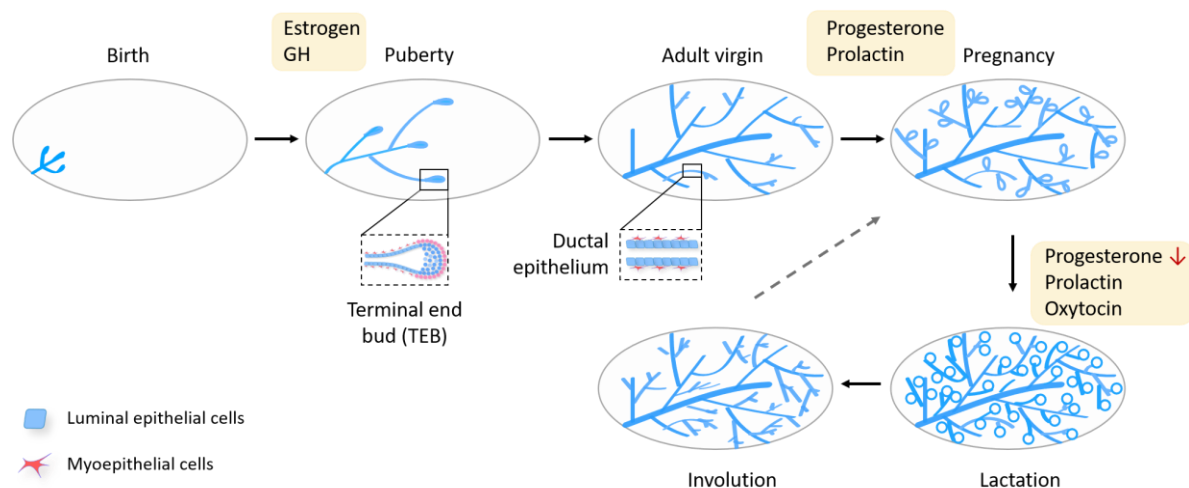


Figure 4. Overview of mammary gland development after birth. During puberty, TEBs induce the formation of epithelial ductal tree. The structure of TEB is shown below. During pregnancy, alveolar progenitors differentiate to form alveoli. Then, the fat pad is filled with alveoli during lactation. After weaning, a large scale of mammary epithelial cells undergoes apoptosis. GH, Growth Hormone.

produce secondary ducts. TEBs are composed of two compartments (Fig. 5); a single layer of cap cells are located in the outer layer of TEBs surrounding a multilayer block of body cells. With the ductal elongation, the cap cells at the neck region of TEBs differentiate into myoepithelial progenitors, while the body cells in close proximity to the cap cells can differentiate into luminal and alveolar progenitors (Paine & Lewis, 2017). Meanwhile, the body cells that are not in close contact with the cap cells undergo apoptosis resulting in the formation of lumen (Howlin et al., 2006). Subsequently, the myoepithelial progenitors differentiate into myoepithelial cells located in contact with the basement membrane and the luminal progenitors differentiate into luminal epithelial cells. As a result, the inner layer cells, which are surrounding the lumen and characterised as luminal epithelial cells, form the bi-layered mammary ducts together with the outer layer myoepithelial cells.

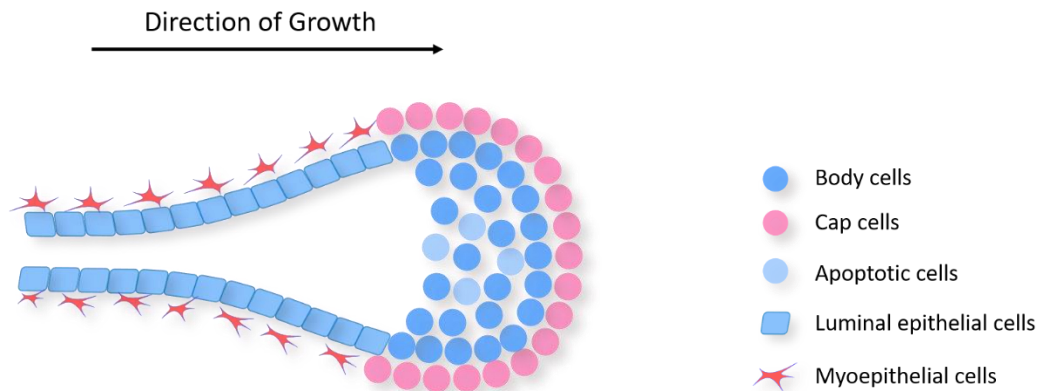


Figure 5. Structure of a Terminal End Bud (TEB). TEB is composed of two compartments, cap cell layer and body cell layers. Cap cells are responsible for the production of myoepithelial cells. Body cells contribute to luminal epithelial cells and alveolar progenitors. Apoptosis occurring in body cell layer is important for the formation of lumen.

The TEBs keep invading into the fat pad until they reach its peripheries. Consequently, TEBs regress once they arrive at the physical limitation at the edges of the fat pad. This ductal outgrowth results in the fat pad being completely infiltrated by the primary and secondary ducts that form a highly arborized and branched ductal tree (Fig. 4). Notably, the secondary ducts will further branch to form tertiary ducts under the regulation of progesterone during the oestrous cycle, whereas this lateral branching is not directed by TEBs (Paine & Lewis, 2017; Richert et al., 2000).

3.1.1.3 Pregnancy and Lactation


Upon pregnancy, the alveolar buds formed at the tertiary ducts can undergo further differentiation and extensive proliferation of the alveolar progenitors (Fig. 4). At around day 10.5 of pregnancy, the cells within alveolar buds undergo differentiation and polarization to form alveoli (Paine & Lewis, 2017) where cells are capable of producing milk proteins. This process is regulated by the production of secreted progesterone and prolactin. During the late stages of pregnancy, the majority of the fat pad is covered by alveoli structures. Post-partum, the cells within the alveoli are activated to produce and secrete milk proteins to the lumen of the mammary gland due to the increase in the levels of oxytocin and the sharp decrease of progesterone (Richert et al., 2000). This stage is referred to as lactation stage.

3.1.1.4 Involution

After weaning, the highly differentiated mammary glands undergo a unique tissue remodelling process known as involution (Richert et al., 2000). It is suggested that the involution stage is a two-step process according to its reversibility (Stein et al., 2007). The first process is caused by the milk accumulation after weaning. Notably, this phase can be reversed via re-suckling.

Morphologically, the alveoli seem to remain intact while some apoptotic bodies appear in the alveolar luminal regions during the reversible process. Subsequently, involution enters into the second phase, which is irreversible, on day 3 after weaning. During this process, a large portion of the secretory alveolar epithelial cells undergoes apoptosis, which are then cleared by macrophages or the adjacent epithelial cells (Paine & Lewis, 2017). Some alveolar epithelial cells transit from secretory to phagocytotic state to assist macrophages in clearing the neighbouring apoptotic cells. Meantime, the adipocytes are refilling the fat pad as the alveolar structure breaks down. Also, the collapsing alveoli are being surrounded by a single layer of myoepithelial cells. At the end of the second phase, all alveoli collapse, and the mammary gland structure is remodelled completely. Consequently, the structure of the mammary gland regresses to its pre-pregnancy state. The three stages, pregnancy, lactation and involution, can occur iteratively every time when the mouse becomes pregnant (Fig. 4).

3.1.2 Mammary Epithelial Cell ontogeny

During the mammary gland development, the relative quantities of different cell types of mammary epithelial cells (MECs) change gradually at distinct stages. The various cell types of MECs have distinct proliferation and differentiation potentials and contribute to forming mammary epithelial differentiation hierarchy. Mammary epithelial stem cells (MaSCs) reside at the apex of the MEC ontogeny . A single MaSC is able to form the entire mammary gland structure when it is transplanted into a cleared fat pad. First, the MaSC differentiates into mammary epithelial progenitors that are also bipotent. Secondly, the repopulating cells can differentiate into the common luminal progenitors and myoepithelial progenitors (Fig. 6). These progenitors have relatively poor self-renewal ability. The common luminal progenitors are able to give rise to both ductal luminal progenitors and alveolar progenitors (Fig. 6). Subsequently, the ductal luminal progenitors evolve into ductal luminal epithelial cells,

contributing to the inner layer formation of the ductal tree during prenatal and pubertal mammary morphogenesis (Fig. 6). Meantime, the myoepithelial progenitors develop into myoepithelial cells (Fig. 6), which form the outer layer of the ductal tree. The outer layer is also known as basal layer and is surrounded by basement membrane. Notably, it is demonstrated that the majority of the repopulating cells lie in the basal layer (Makarem et al., 2013; Shackleton et al., 2006a; Stingl et al., 2006), although this is still quite controversial. The alveolar progenitors are responsible for the formation of mature alveolar cells, contributing to the expansion of alveoli during pregnancy and lactation (Fig. 6). The cells within the alveoli can produce milk proteins and lipid droplets during lactation stage of mammary gland development. Some scientists believe that the repopulating cells can give rise to alveolar progenitors directly. Overall, these distinct cell types with different self-renewal and differentiation potentials compose the MEC ontology.

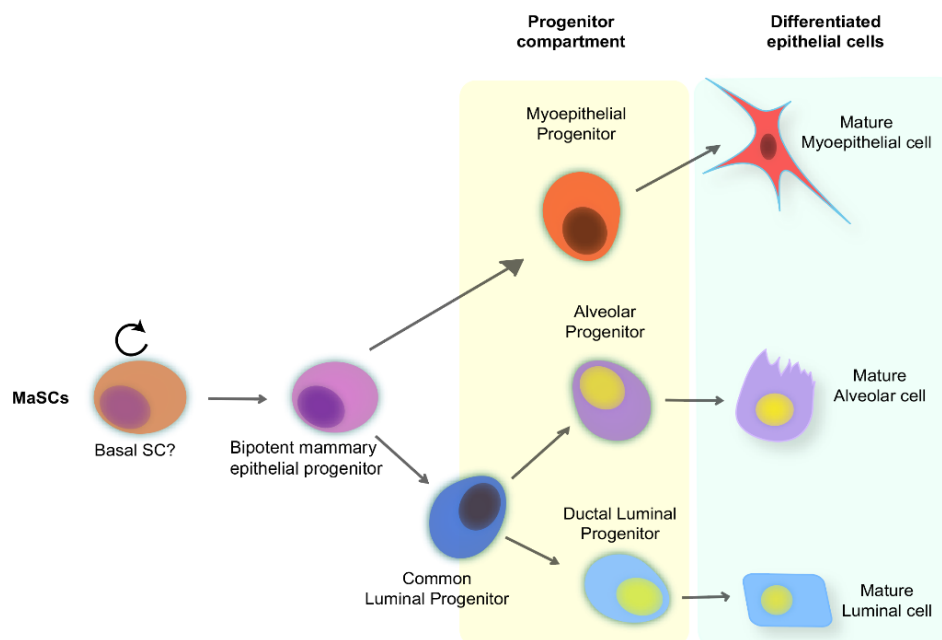


Figure 6. Proposed model of the mammary epithelial hierarchy (adapted from Visvader & Stingl, 2014).

Mammary stem cell resides at the apex of the mammary epithelial hierarchy.

3.1.3 The surface marker used for isolating distinct mammary epithelial subsets

FACS (Fluorescence-Activated Cell Sorting) technique based on flow cytometry can be used to isolate specific single-cell subsets from the mammary gland tissue for further downstream analysis. During this process, the solid tissue is digested with specific protease enzymes to achieve single-cell suspensions. Subsequently, the single cell suspensions are immunostained with antibodies that are conjugated with distinct fluorochromes. These labelled antibodies bind to their specific surface antigen markers on the cell membrane. Therefore, the surface antigen markers play a crucial role in sorting different cell subpopulations based on their expression levels. Over the past decades, several cell type-specific surface antigen markers for MECs has been identified, and commonly they are used in combinational manner for flow cytometry analysis.

Co-staining for CD24 and CD49f cell surface antigen markers is usually used to separate the luminal and basal compartments. CD24 is highly expressed in luminal populations. In contrast, CD49f is highly expressed in basal layer MECs (Sleeman et al., 2007; Stingl et al., 2006).

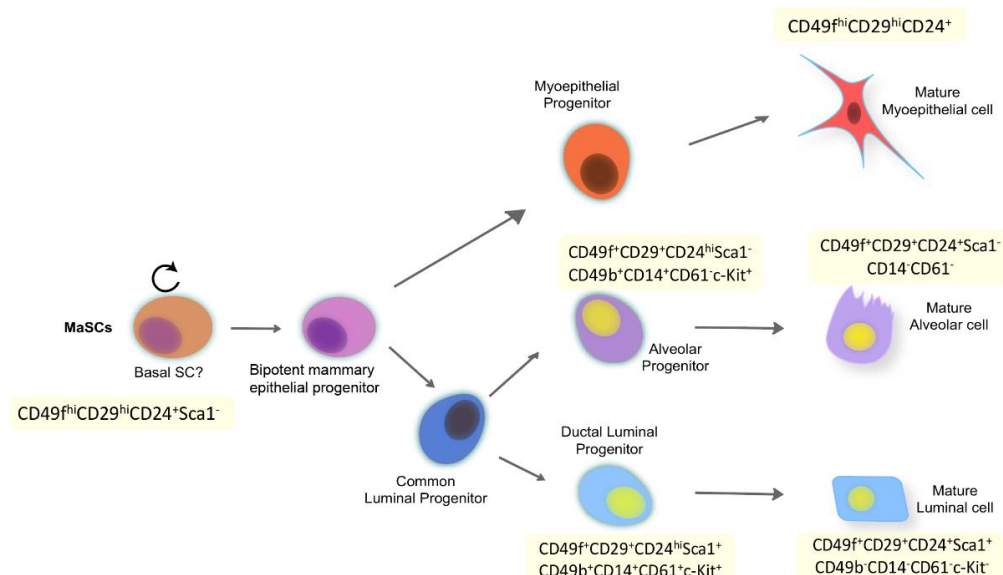



Figure 7. Surface markers of different cell subpopulations for both mice and human mammary epithelial cells (adapted from Visvader & Stingl, 2014).

Therefore, the luminal cells are defined as $CD24^{high}CD49f^{low}$, and the $CD24^{low}CD49f^{high}$ profile identifies the basal layer cells. Additionally, the molecule CD29 is able to function as the substitute for CD49f in separating luminal and basal subpopulations (Visvader, 2009). Table 1 shows different surface markers used and their features, and Figure 7 displays the surface markers expressed on distinct mammary epithelial subpopulations in mice. A subpopulation of mammary epithelial cells with the surface profile of $CD49f^{hi}CD29^{hi}CD24^{+}Scal^{-}$ are capable of regenerating entire mammary epithelial structure upon cleared fat pad transplantation. These cells are referred to as MaSCs (Visvader, 2009; Visvader & Stingl, 2014). Additionally, the ability of lobuloalveolar structure formation by these transplanted glands during pregnancy underpins the ‘stem cell’ character of these cells. As mentioned above, most of the MaSCs (>99%) have the $CD49f^{hi}CD29^{hi}CD24^{+}Scal^{-}$ phenotype. However, only approximately 5% cells within the $CD49f^{hi}CD29^{hi}CD24^{+}Scal^{-}$ subset are MaSCs. The rest of this subset consists of mature myoepithelial cells, myoepithelial progenitors and other undefined subpopulations. Thus, it is proposed that MaSCs may be located in the basal layer and share the similar expression profile as the cells of myoepithelial lineage. Given the high expression levels of CD29 and CD49f, which are $\beta 1$ integrin and $\alpha 6$ integrin proteins, respectively, it is hypothesized that the $\alpha 6/\beta 1$ integrin complex plays a critical role for MaSCs and myoepithelial cells anchoring to the basal lamina and extracellular matrix. $\beta 1$ integrin was shown to be important for the maintenance of MaSC ability with the help of Rac1 GTPase function (Asselin-Labat et al., 2008; Olabi et al., 2018). Notably, MaSCs cannot be distinguished from the myoepithelial cells by flow cytometry as they share the same surface antigen profile.

Furthermore, the various cell subpopulations within the luminal lineage can be isolated by using further surface antigen markers. There are four commonly used cell surface antigen markers for luminal progenitors including CD61 ($\beta 3$ integrin), CD49b ($\alpha 2$ integrin), CD14 and c-Kit, which are all used to distinguish luminal progenitors from the mature luminal cells.

Table 1. Surface Markers used in mammary epithelial cells in mouse and human (Adapted from Visvader, 2009)

Surface Marker	Features
Mouse	
CD49f $\alpha 6$ integrin	Receptors for laminin. Expressed on the surface of epithelial cells, T lymphocytes, monocytes and endothelial cells.
CD24 HSA	A kind of glycoprotein anchored on the cell surface via glycosyl phosphatidylinositol (GPI).
CD29 $\beta 1$ integrin	Receptors for the signals from extracellular matrix. Expressed on the surface of epithelial cells, leukocytes and endothelial cells.
CD61 $\beta 3$ integrin	Receptors for vitronectin, fibronectin, laminin and so on. Expressed on blood vessels and angiogenic vascular tissues.
CD49b $\alpha 2$ integrin	Receptors for collagen and laminin. Expressed on the surface of specific epithelial cells and hematopoietic cells.
CD14	Also a kind of GPI-anchored cell surface glycoprotein, expressed on macrophages, neutrophils, B cells and mammary cells.
c-Kit CD117	Tyrosine kinase receptor for steel factor or stem cell signal, located on the surface of specific hematopoietic cells.
Sca-1 Ly-6A/E	A member of Ly-6 family which is also GPI-anchored glycoprotein. Expressed on
Human	
CD49f $\alpha 6$ integrin	See above.
EpCAM ESA, CD326	Epithelial cell adhesion molecule, a transmembrane glycoprotein that mediates Ca^{2+} -independent cell-cell adhesion. Expressed on the surface of most epithelial cells.
c-Kit	See above.

However, the use of these markers has some relative differences to each other. CD49b and CD14 molecules are able to identify all luminal progenitors, whereas CD61 can only be expressed in ductal luminal progenitors but not alveolar progenitors. The luminal progenitors within the luminal lineage can be distinguished from mature luminal cells due to their CD49f⁺c-Kit⁺ expression (Visvader, 2009). Earlier studies found that CD61 and c-Kit markers work well to isolate luminal progenitors from mice in FVB  but not in C57Bl6/J backgrounds, indicating that the expression of these cell markers by luminal progenitors vary depending on mouse background (Asselin-Labat et al., 2007). Another surface protein, Sca1, is used to identify a subpopulation of differentiated luminal cells which are oestrogen receptor-positive (ER⁺) cells (Sleeman et al., 2007). Given the distinct surface profile (CD49b⁺CD14⁺CD61⁺c-Kit⁺) of the mature luminal cells, including ductal luminal epithelial cells and alveolar epithelial cells, they can easily be distinguished from luminal progenitors. Additionally, it is suggested that CD24 is higher expressed in luminal progenitors compared with differentiated luminal cells. Combining all these information, the specific expression profiles of each MEC subpopulation are identified as shown in Figure 7. For the isolation of human MEC subtypes, the used surface antigen profiles also remain controversial. A small fraction of MECs within CD49f^{hi}EpCAM^{low} subpopulation is supposed to be human MaSCs since they can regenerate the breast structure after transplanted into a ‘humanized’ fat pad (Kuperwasser et al., 2004). The fat pad of cleared mouse mammary gland is pre-injected with human fibroblasts to create a humanized microenvironment, which is significant for *in vivo* research on human breast. Additionally, Ginestier et al. (2007) demonstrated that the cells with high expression of ALDH1 could repopulate mammary epithelial structures upon transplantation. Therefore, the ALDH1⁺ cell subpopulation might represent the human MaSCs. However, the ALDH1⁺ cells are located in the luminal layer, which represents a contradictory difference to murine MaSCs that are presumed to be located in the basal layer.

3.1.4 The evidence supporting the existence of MaSCs

As mentioned above, MaSCs cannot be isolated as a pure subpopulation, since they share the same expression profile (CD49^{hi}CD29^{hi}CD24⁺Scal⁻) with myoepithelial cells. Nevertheless, there is some existing evidence showing that MaSCs maintain the regenerative property of the mammary gland. For this purpose, DeOme and his colleagues (1959) established the cleared fat pad transplantation approach. First, they have removed the mammary epithelium from the prepubertal mammary gland to produce a cleared fat pad, which is critical for the subsequent *in vivo* transplantation assay in mouse. Donor tissues were then transplanted into the cleared fat pads to determine their regenerative functions within the epithelia-free fat pads. The presence of MaSCs in mammary gland was initially demonstrated by using this approach upon transplanting the fragments of the mammary gland into a cleared fat pad, leading to the successful regeneration of the entire ductal tree. Further studies revealed that any mammary duct fragments or isolated single-cell suspensions from the mammary glands at different developmental stages could induce the formation of the intact epithelial ductal tree upon transplantation, indicating that the MaSCs are widely spread throughout the whole adult mammary gland during the whole lifespan (Hoshino, 1964; Smith, 1996; Smith & Medina, 1988). Furthermore, it was shown that the functional mammary gland could be repopulated from a single stem cell (Kordon & Smith, 1998). Notably, the results from the serial transplantation assays indicated that the MaSCs may have limited self-renewal capacity and are not immortal (Daniel et al., 1968). With the use of flow cytometry, different groups have isolated various epithelial cell types with distinct surface antigen profiles and transplanted them into the cleared fat pads to assess their stemness. They found that approximately 99% of the repopulating cells have the CD49^{hi}CD29^{hi}CD24⁺Scal⁻ phenotype that is specific to the basal layer of the mammary epithelium. Thus, it is presumed that MaSCs may reside in the basal layer. Furthermore, several distinct cell types were proposed to be the MaSCs due to their

functions, such as the cap cells located at the tip of TEBs during pubertal stage of mammary gland development. It is widely believed that cap cells are MaSCs, since a single isolated cap cell has the ability of developing an entire mammary ductal tree. However, it is suggested that not all MaSCs are cap cells, based on experiments using 'stem cell' specific gene analysis (Shackleton et al., 2006b; Sleeman et al., 2007; Stingl et al., 2006). Notably, it is currently not possible to determine precisely where the MaSCs are located as we cannot distinguish MaSCs from other basal layer cells due to the lack of MaSC-specific gene markers.

Lineage-tracing assay is another technique used to study the hierarchy of MECs under physiological conditions. The cells of interest are genetically labelled with a reporter gene which is permanently expressed in the original cell and its progeny so that the cell lineages could be tracked. Van Keymeulen and colleagues (2011) employed lineage-tracing approach to demonstrate that there are two types of unipotent stem cells that generate either luminal or myoepithelial lineages during mammary gland development. This result is in agreement with the more recent findings obtained by using single-cell lineage-tracing analysis, which is indicating that the ductal outgrowth and alveoli formation are induced by different types of unipotent MaSCs during pubertal and pregnancy stages of mammary gland development, respectively (Davis et al., 2016; Scheele et al., 2017). In contrast, it was demonstrated that the multipotent and unipotent MaSCs may exist at different developmental stages (van Amerongen et al., 2012). However, in(Rios et al., 2014) study, it was demonstrated that the pubertal mammary gland development is driven by the bipotent MaSCs, whereas the unipotent MaSCs might just be the lineage-committed progenitors rather than being stem cells. Consistent with this, the lineage-tracing study using protein C receptor, a novel target of Wnt signalling pathway, provides the evidence to support the existence of multipotent MaSCs (Wang et al., 2014). Taken together, although it is clear that the mammary gland development is driven by MaSCs, it is still unknown whether mammary epithelial cell expansion and differentiation are

originating from multipotent stem cells or various unipotent stem cells, which needs to be further studied.

Recently, several studies have suggested that MaSCs mainly stay in a quiescent state, which then transit into cycling stem cell state when needed for development (Lee et al., 2019). The long-lived quiescent MaSCs has high repopulating abilities that are able to give rise to the intact mammary epithelium under regenerative conditions, thereby the quiescent MaSCs may be crucial for maintaining homeostasis of mammary gland (Lloyd-Lewis et al., 2017). In 2014, Boras-Granic et al. showed that the long-lived quiescent MaSCs arise from embryonic MaSCs. Following that, Cai and colleagues (2017) demonstrated that a subpopulation of cells in basal layer ($CD49f^{hi}CD24^{+}Lin^{-}$) express high levels of Bcl11b protein as shown by single-cell gene expression analysis. The results of serial transplantation assay showed that these $Bcl11b^{hi}$ cells are able to regenerate complete mammary ductal tree. These cells are considered as quiescent cells, where Bcl11b prevents them entering into cycling phase and maintain them in quiescent state. Meantime, another research group suggested that there are three distinct types of quiescent MaSCs, which could be separated by their Lgr5 and Tspan8 expression levels, and those cells with the $Lgr5^{+}Tspan8^{hi}$ surface antigen profile represent the most quiescent MaSCs. They also showed that Foxp1, the transcription factor that represses Tspan8 transcription, induces the transition of quiescent stem cells into their cycling state (Fu et al., 2017; Fu et al., 2018). These studies provide evidence for the existence of quiescent MaSCs that could transit into cycling cells in response to the developmental signals, to promote normal mammary gland development and maintain homeostasis of the mammary tissues, although the identity and properties of quiescent MaSCs are still not fully clear.

Overall, different studies using cleared fat pad transplantation assay and/or lineage-tracing approach demonstrate together that the mammary gland development and homeostasis is dependent on the function of stem cells. However, due to the lack of exclusive markers of

MaSCs, their histological location as well as the underlying mechanisms of their regulation is still poorly characterised. Furthermore, the potential heterogeneity within the MaSC pool in terms of being multi-, bi-, or uni-potent as well as them being at quiescent versus cycling state complicates our current understanding of how MaSCs regulate development, function and homeostatic maintenance of mammary glands.

3.1.5 Rac1 function during mammary gland development

Previous studies demonstrated that Rac1 plays different functions at different developmental stages of the mammary gland development. In an *in vitro* experiment, Zhu and Nelson (2013) treated the mammary epithelial tubules with the inhibitor NSC23766 to inhibit the Rac1 function and observed an impaired branch elongation of the mammary epithelial tubules. This suggested that Rac1 might be required for the branching of mammary ducts during puberty. This result was in agreement with an earlier study by Ewald and colleagues (2008), which demonstrated that activated Rac1 was localized at the end of the extending branches. However, the mammary gland of the transgenic mice where Cre-loxP system was used to knock out *Rac1* gene in mammary epithelia could develop normally during puberty, pregnancy and lactation (Bagci et al., 2014), suggesting that Rac1 is dispensable for these stages of mammary gland development. The reason for this contradiction might be due to the functional redundancy between Rac1 and Rac3, which shares some common downstream signalling effectors (Zuo et al., 2016). However, the lack of importance of Rac1 function for the pubertal stage of mammary gland development still remains questionable. In Bagci and colleagues' (2014) study, the Cre recombinase was expressed under the control of the MMTV promoter, which may not be active in all MECs in some transgenic MMTV-Cre mouse lines. If that was the case, Rac1 was probably not deleted in all MECs.

Other studies has demonstrated that Rac1 has a functional role during the lactation stage of mammary gland development. In an *in vitro* experiment, dominant negative Rac1 (N17Rac1) was ectopically expressed in MECs in a 3D culture system, resulting in an inhibition of the synthesis of milk protein β -casein. Previous studies have demonstrated that MEC differentiation occurring during lactation stage is controlled by the combination of integrins interacting with the extracellular matrix (ECM) and the hormone receptor signalling. Rac1 was shown to be the key link between β -integrin and Prolactin receptor (Prlr) signalling, which promotes the differentiation of MECs during lactation (Akhtar & Streuli, 2006). It is suggested that Rac1 is activated downstream of β 1-integrin signalling pathway and subsequently contributes to the signalling downstream of Prlr, which then results in the activation of signal transducer and activator of transcription 5 (Stat5). Stat5 is a transcription factor that regulates the lactational differentiation of MECs, including the synthesis of milk protein β -casein. However, it is also important to note that the dominant negative N17Rac1 may not only inhibit Rac1 function, but also other RhoGTPases. Therefore, it is still controversial whether Rac1 is indeed necessary for lactational differentiation during mammary gland development.

Rac1 was shown to play a crucial role for the phagocytosis of the apoptotic MECs during the involution stage of mammary gland development (Akhtar et al., 2016). As mentioned above, the involution stage has two phases. During the reversible stage, macrophages that can engulf the apoptotic cells are too few to be able to clear the apoptotic MECs. Thus, a subset of MECs experiences the switch from alveolar epithelia to phagocytic cells, which play a similar role as macrophages (Akhtar et al., 2016). Several studies have indicated that Rac1 is crucial for this switch. The loss-of-function of Rac1 during involution stage leads to the defective phagocytosis, which then causes inflammation. Akhtar and colleagues (2016) found that Rac1 regulates the initiation of mammary gland involution in two distinct ways. First, Rac1 assists apoptotic cells in attaching to the basement membrane, thus preventing the dead cells falling

into the ductal lumen. As a result, the dead cells can be engulfed by neighbouring phagocytic MECs and macrophages. Second, Rac1 can influence phagocytotic activity, as Rac1 is capable of activating signal transducer and activator of transcription 3 (Stat3) that is important for the phagocytic transition (Chapman et al., 1999; Humphreys et al., 2002). Consistently, Bagci and colleagues (2014) also showed that the loss of Rac1 function prevents the activation of Stat3, and lead to the accumulation of apoptotic MECs and milk proteins during involution. Therefore, it is clear that Rac1 is indispensable for the clearance of the dying MECs and milk proteins during mammary gland involution.

3.2 Results - The deletion of Rac1b does not alter normal mammary gland development

3.2.1 Loss of Rac1b function does not lead to obvious defects during mammary gland development at a macroscopic level

In order to investigate the Rac1b-specific indispensable functions during normal mammary gland development *in vivo*, I have performed whole-mount Carmine-Alum staining of mammary glands of Rac1b null (Rac1^{-/-}) and wild type (Rac1b^{+/+}) littermate mice, which were of the C57BL6 background, at different developmental stages.

3.2.1.1 Rac1b-null mammary ductal tree is able to elongate and branch normally similar as in wild-type mammary glands

During the pubertal stage of mammary gland development, TEBs are formed at the distal ends of the primary ducts that are essential for ductal outgrowth. Bifurcation of TEBs can give rise

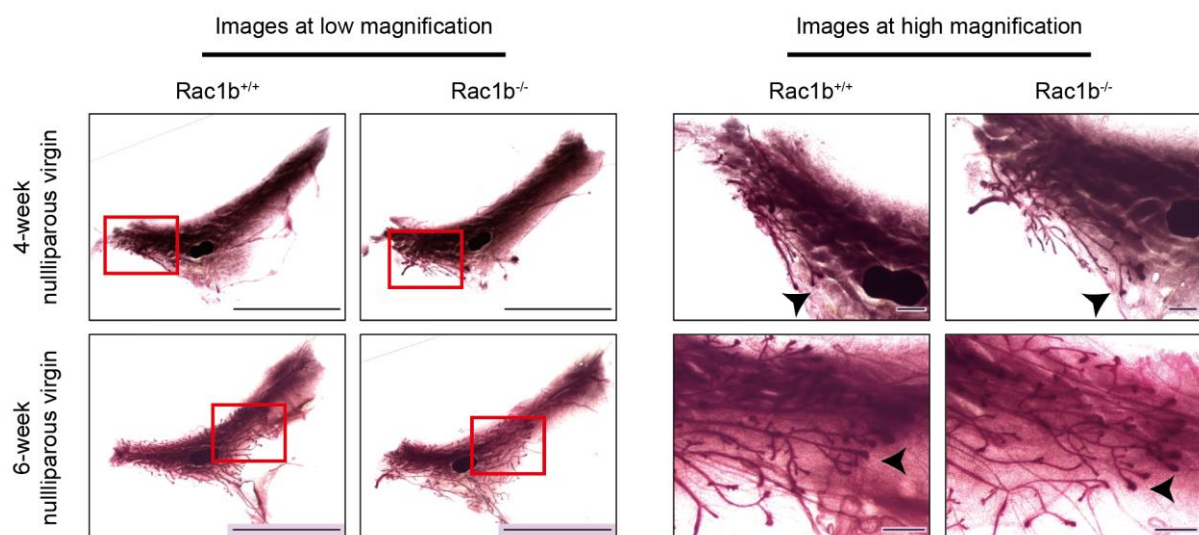


Figure 8. Mammary glands of Rac1b^{-/-} and their wild type littermate mice (N=3) were analysed by whole-mount Carmine Alum staining at 4-week and 6-week nulliparous stages. The arrowheads show the TEB structures. Scale bars represent 1 cm and 1 mm for low- and high-magnification pictures, respectively.

to secondary ducts, which then further generates tertiary ducts during oestrus cycling. The whole-mount Carmine Alum staining results has demonstrated that the *Rac1b* deficiency does not influence TEB formation as seen in both *Rac1b*-null and wild type mammary glands at 4-weeks old nulliparous stage (Figure 8). The ductal outgrowth and branching of the mammary ducts was also comparable between the *Rac1b*-deficient and wild-type mammary glands at 6-weeks old virgin stage (Figure 8).

The whole mount staining was also performed for 8- and 10-weeks old nulliparous mammary glands (Figure 9). There was no obvious difference in the structure of the mammary epithelial ductal tree between the mammary glands of 8 weeks old *Rac1b*^{-/-} and wild type littermates. Similarly, at 10-weeks old nulliparous stage, when the TEBs start to undergo regression at the distal boundaries of the fat pad, there was no genotype specific differences.

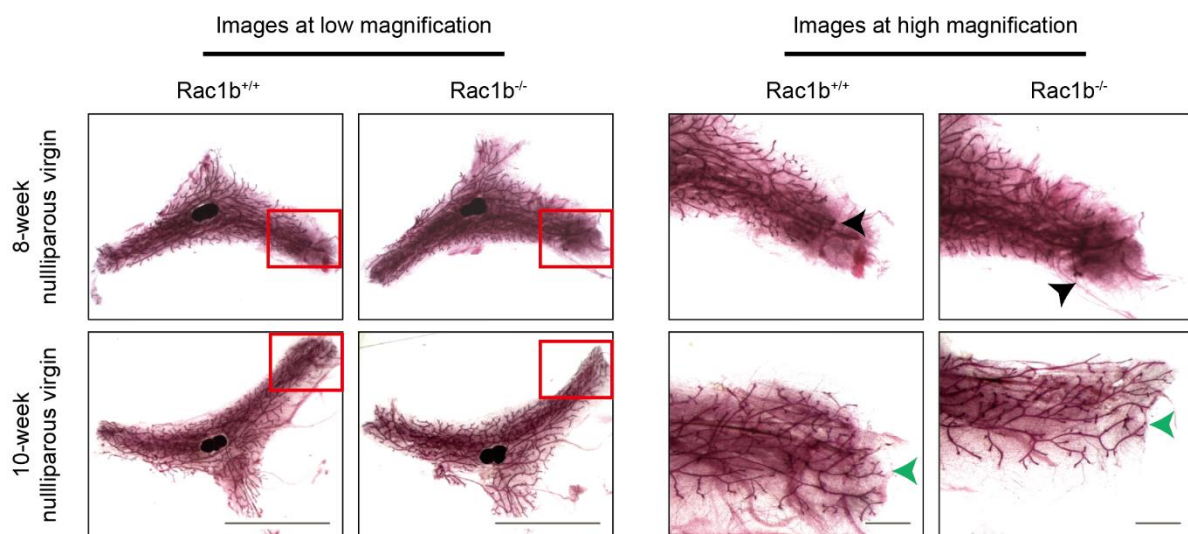


Figure 9. Representative images for mammary glands of *Rac1b*^{-/-} and *Rac1b*^{+/+} (N=3), investigated by whole-mount Carmine Alum staining at 8 week and 10 week virgin stages. The black arrowheads show the TEB structures at 8 week stages, and the green arrowheads show the regressing TEB structures at 10 week stages. Scale bars represent 1 cm and 1 mm for low- and high-magnification pictures, respectively.

Collectively, the whole-mount Carmine Alum staining data at different nulliparous pubertal stages suggested that the loss of Rac1b function does not lead to any ductal outgrowth or branching phenotypes at a macroscopic level.

3.2.1.2 Loss of Rac1b function does not alter mammary gland development during pregnancy and lactation stages

To study whether the absence of Rac1b function interferes with the normal mammary gland development during pregnancy and lactation stages, I have performed whole mount staining of mammary glands of mice at different time points of pregnancy and lactation. At the early pregnancy stage (Day 10.5), continuous high levels of progesterone results in the maturation and expansion of alveolar buds at the tertiary ducts. To generate female mice used for the analysis of this stage, 10- to 12-weeks old female mice were mated overnight and the morning when the vaginal plugs were observed were recorded as pregnancy day 0.5. After 10 days, the mammary glands were dissected and analysed by whole mount staining as the stage of early pregnancy, which has revealed that the tertiary ducts and alveolar buds in Rac1b-null glands are formed normally similar as in wild-type glands. In the next stages of pregnancy, another hormone, prolactin, induces the expansion of alveolar buds with differentiation of cells into mature alveolar cells. Whole mount staining results showed that the alveoli structures are also formed normally in the Rac1b-deficient mammary glands at the late pregnancy stage (Day 18.5) compared with their wildtype counterparts (Figure 10). Next, I have analysed the lactation stage by whole mount staining of mammary glands dissected from mice on the day after they gave birth, when they start producing and secreting milk under the control of oxytocin. My results demonstrate that there is no obvious difference on the size and structures of the lobuloalveoli in lactating mammary glands of Rac1b-null mice compared to those of their wild-type littermate mice.

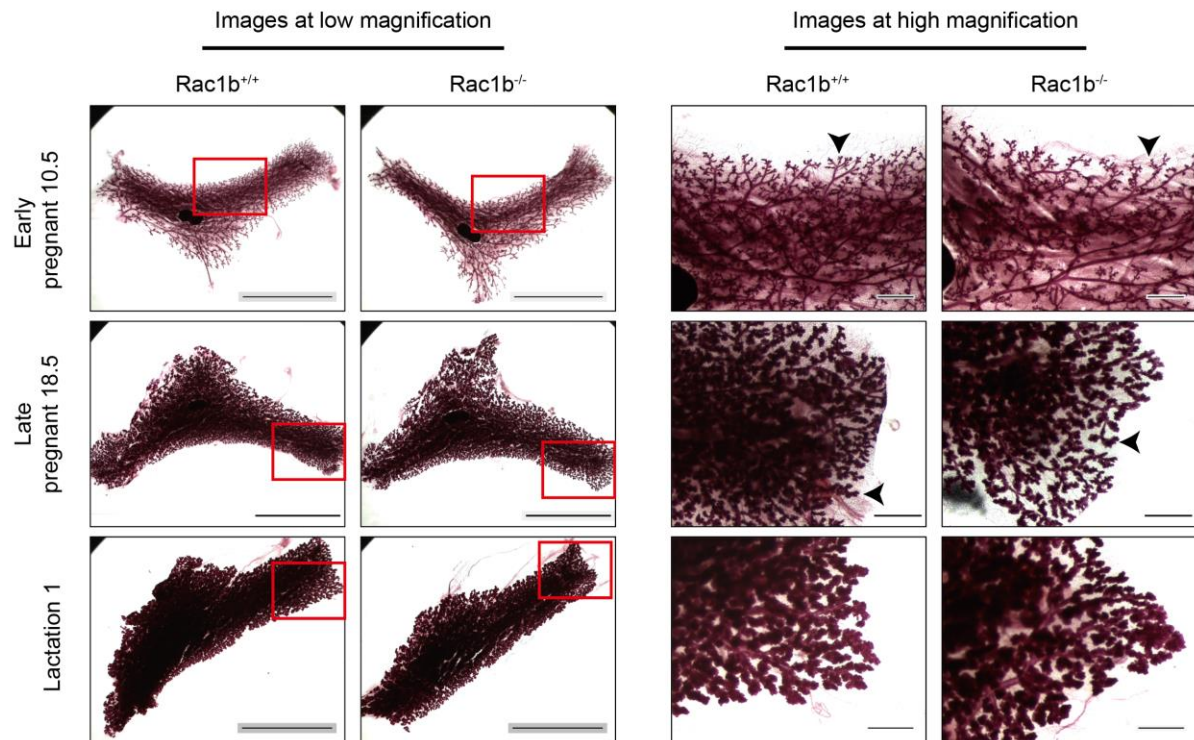


Figure 10. Mammary glands of $Rac1b^{-/-}$ and their wild type littermate mice (N=3) were analysed by whole-mount Carmine Alum staining at pregnancy (Early and Late pregnancy stages are at Day 10.5 and Day 18.5 of the pregnancy, respectively); and Lactation stage that is the 1 day after giving birth. The arrowheads show the alveolar buds at the tertiary ducts and lobuloalveolar structures at early pregnancy and late pregnancy stages, respectively. Scale bars represent 1 cm and 1 mm for low- and high-magnification pictures, respectively.

Taken together, the whole mount Carmine-Alum staining results suggest that the loss of $Rac1b$ function has no macroscopically obvious effect on the formation of tertiary ducts and lobuloalveolar structures at pregnancy or lactation stages.

3.2.1.3 The *Rac1b* deficiency has no effect on the involution stage of mammary gland development

The lactating mammary glands initiate the involution stage when pups stop suckling or are weaned. In order to reveal if *Rac1b* function is required for the proper mammary gland involution, first I have analysed the mammary glands of *Rac1b*-null mice at the end of the reversible stage, which is involution Day 5. During this first three days of involution, the alveoli starts to shrink and only few alveolar epithelial cells undergo apoptosis due to the accumulation of milk. Whole mount staining data revealed that the structure of the mammary ductal tree and the size of lobuloalveolar structures were quite similar in wildtype and *Rac1b*-null mammary glands at the end of this reversible involution stage, as seen in the low-and high-magnification images, respectively (Figure 11).

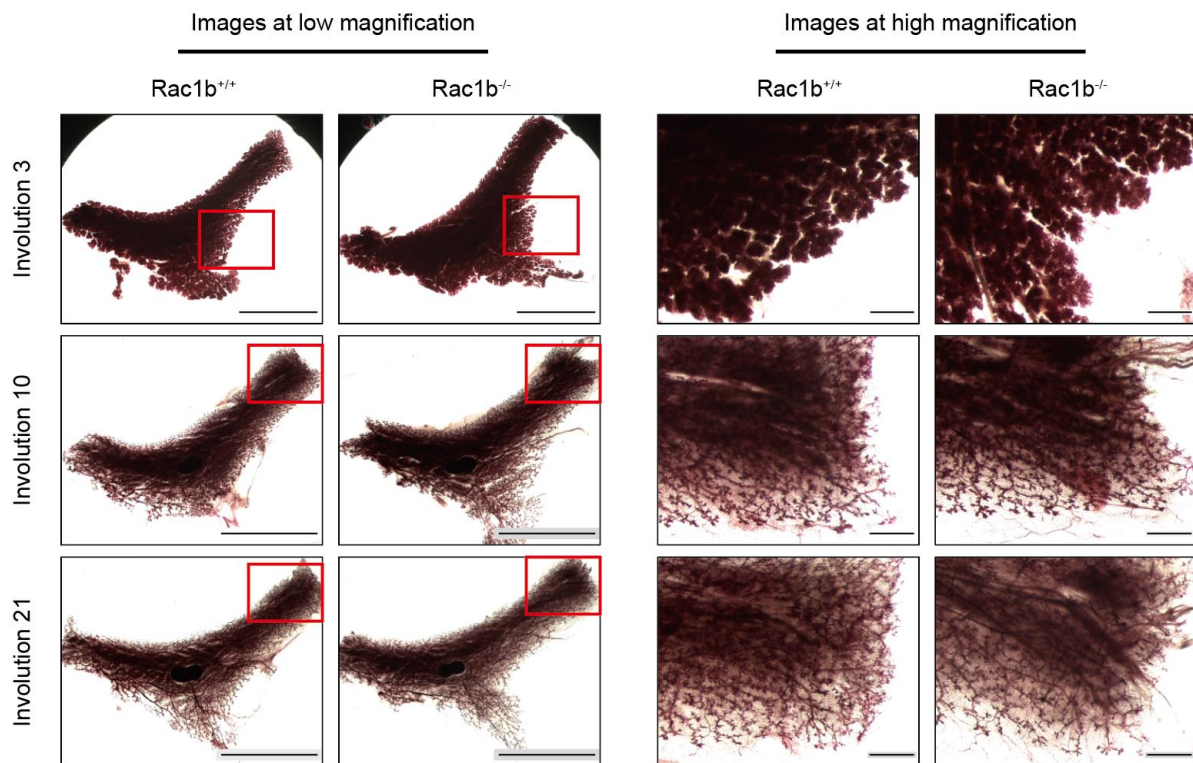


Figure 11. Mammary glands of *Rac1b*^{-/-} and their wild type littermate mice were analysed by whole-mount Carmine Alum staining at involution stages (N=3): Day 3, Day 10 and Day 21. Scale bars represent 1 cm and 1 mm for low- and high-magnification pictures, respectively.

Next, I analysed the mammary glands at Day 10 and Day 21 that represents the reversible involution stages. At Day 10 of involution, most of the alveolar cells would undergo apoptosis and shed into the lumen of the mammary ducts, and then cleared by macrophages or their neighbouring mammary epithelial cells. There was no obvious difference in alveoli structures between wildtype and Rac1b-null mammary glands at Day 10 of involution (Figure 11). Likewise, the general structure of the Rac1b-null and wild-type mammary ductal tree were similar at Day 21 of involution, as mammary glands of both genotypes have already remodelled into a virgin-like state (Figure 11). Thus, these data indicate that the involution of Rac1b-null mammary glands progresses normally as in wild-type glands at the macroscopic level, suggesting that the Rac1b function might be dispensable for cell apoptosis, cell clearance and the tissue remodelling during involution stage of mammary gland development.

3.2.1.4 Rac1 efficiency does not affect mammary glands even after multiple rounds of pregnancy

Since Rac1-null mice have structural abnormalities of mammary ductal tree, that was mostly obvious after the second pregnancy (Akhtar et al., 2016), we investigated whether Rac1b deficiency may lead to a similar phenotype. We kept the mice in breeding till the weaning of their third litter and analysed their mammary glands 3 weeks after the weaning of their last litter. Whole mount staining of their mammary glands have not displayed any phenotypic difference between Rac1b-null and wildtype mice, as shown in Figure 12 for the proximal (green) and distal (red) sides of the glands. This result suggests that the Rac1b deficiency has no effect on the mammary gland development even after undergoing several pregnancy.

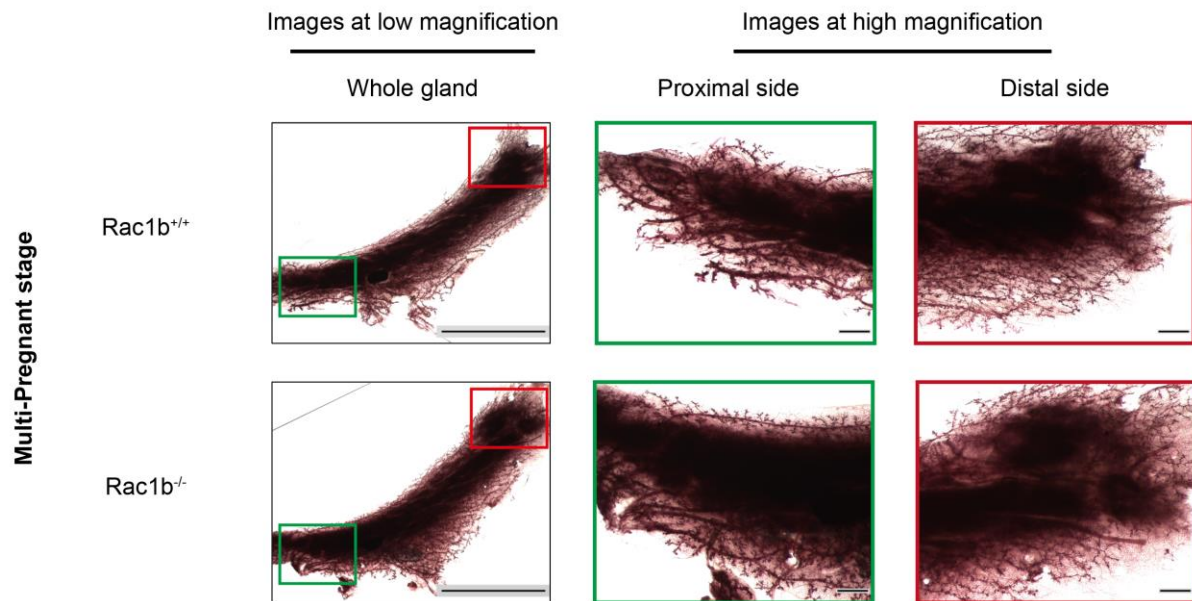



Figure 12. Mammary glands of $Rac1b^{-/-}$ and $Rac1b$ -wildtype mice were analysed by whole-mount Carmine Alum staining after 3 rounds of pregnancy (N=3). Scale bars represent 1 cm and 1 mm for low- and high-magnification pictures, respectively. The green squares label the proximal part of the mammary glands, and the red squares label the distal part.

Taken together, the whole-mount Carmine Alum staining results of mammary glands at different developmental stages indicate that compared with their wild-type littermates mammary glands of $Rac1b$ -null mice have normal TEB formation, ductal elongation and branching during pubertal stages; tertiary ducts and lobuloalveolar structure formation during pregnancy; tissue remodelling during involution stage, and also normal tissue structures after multiple pregnancies. Thus, the loss of $Rac1b$ function does not result in any macroscopically obvious phenotypes during distinct stages of mammary gland development.

3.2.2 The loss of Rac1b function does not hamper mammary gland involution

To further study the potential loss of Rac1b function phenotypes during the involution stage of mammary gland development at the histological level, I have performed Hematoxylin & Eosin (H&E)  staining on the microtome sections of Rac1b-null and wildtype mammary glands at distinct stages of involution. The Hematoxylin dye stains the nuclei in blue (darker in the images), whereas eosin dye stains proteins in pink.

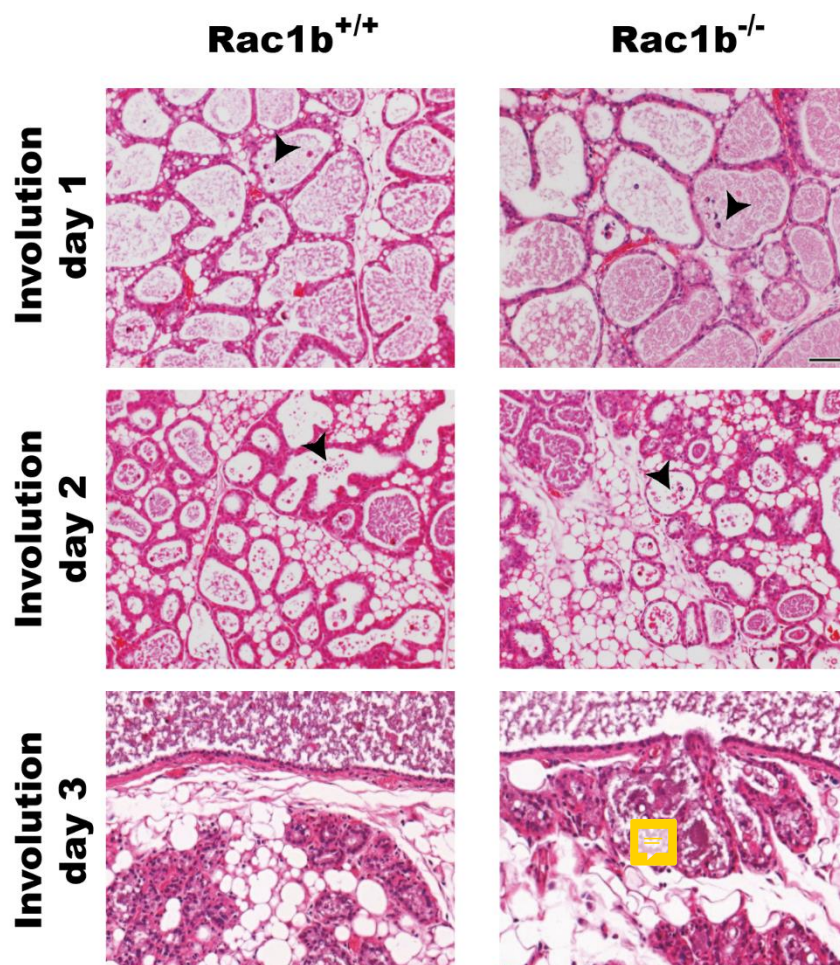



Figure 13. Hematoxylin and Eosin  Staining on microtome sections of mammary glands of Rac1b-null (Rac1b^{-/-}) mice and their wild-type (Rac1b^{+/+}) littermates at reversible involution stages (Day 1, Day 2 and Day 3 after weaning). The black arrowheads show apoptotic alveolar cells shedding into the lumen. The images were taken at 20x magnification. The scale bar represents 200µm.

As seen in Figure 13, mammary fat pads are filled by alveoli structures at involution Day 1, when only a few alveolar cells start to undergo apoptosis due to the accumulation of milk. The lobuloalveolar structures are then starting to shrink since more apoptotic alveolar cells shed into the lumen at involution Day 2 and Day 3. Compared with the wild-type mammary glands, the *Rac1b*-null glands have no obvious defects in the size or morphology of primary ducts and alveolar structures during involution Day 1, 2 and 3 (Figure 13).

Next, I have performed H&E staining on the mammary gland sections representing the irreversible involution stages, during which mammary glands undergo a complete tissue remodelling process. By Day 10 after weaning, a large number of alveolar cells have undergone apoptosis and are cleared by macrophages or their neighbouring epithelial cells. The

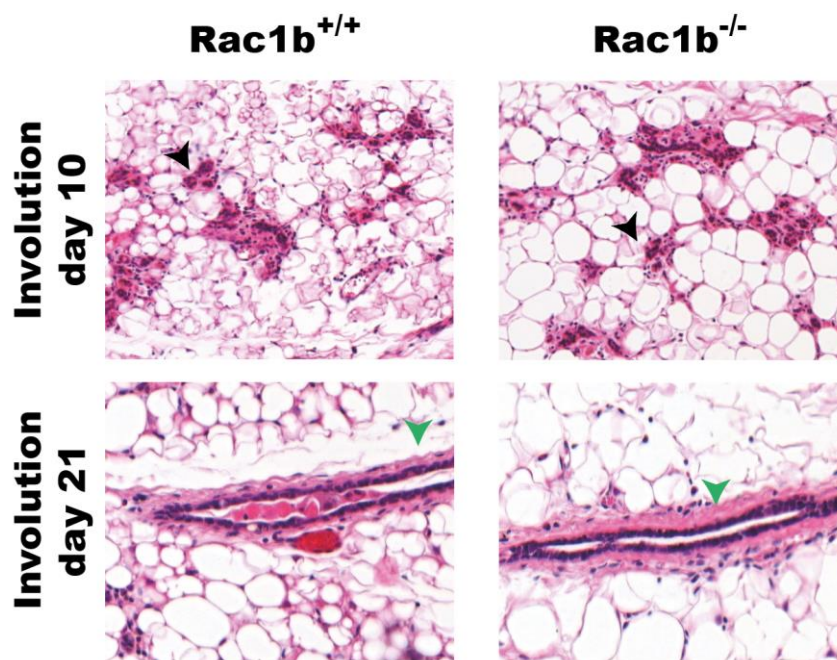


Figure 14. Hematoxylin and Eosin Staining results for mammary glands of *Rac1b*-null (*Rac1b^{-/-}*) mice and their wild-type (*Rac1b^{+/+}*) littermates at irreversible involution stages (Involution Day 10 and Day 21). The black arrowheads show the shrinking lobuloalveolar structures at involution Day 10, and the green arrows show the virgin-like primary ducts at involution Day 21. The images were taken at 20x magnification.

morphology of remaining alveoli structures were similar in wild-type and Rac1b-null glands (Figure 14). At the end of involution (Day 21), all of the alveolar structures are removed and the adipocytes refill the fat pads to reconstitute the virgin-like mammary gland structures, which similarly occurs in both Rac1b^{+/+} and Rac1b^{-/-} mammary glands (Figure 14).

Overall, the H&E staining data also confirms at the histological level that the loss of Rac1b function does not alter the mammary gland involution process, and thus Rac1b is not required for the progression of mammary gland involution.

3.2.3 The loss of Rac1b function does not alter mammary epithelial cell lineage distribution or MaSC frequency

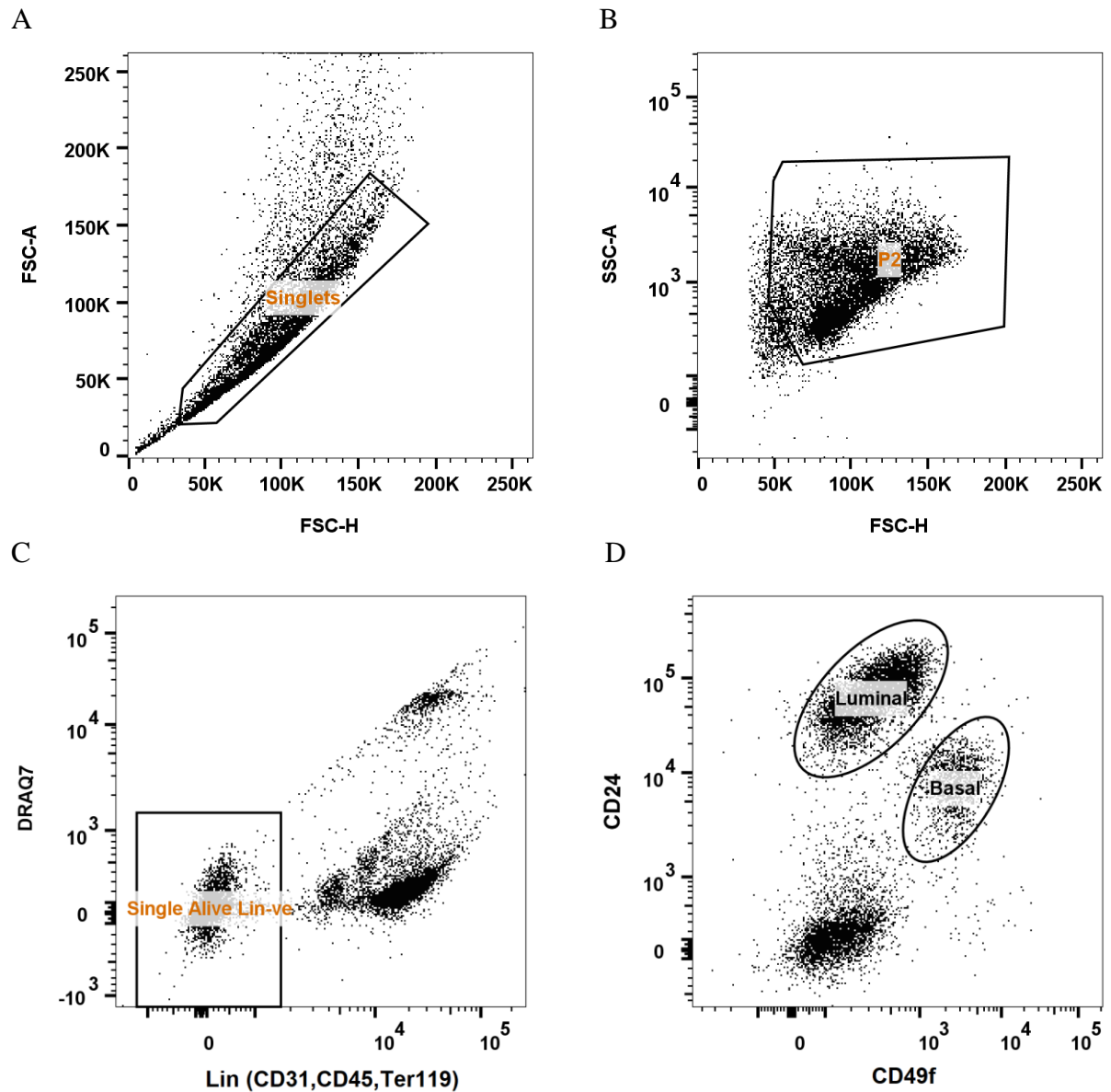


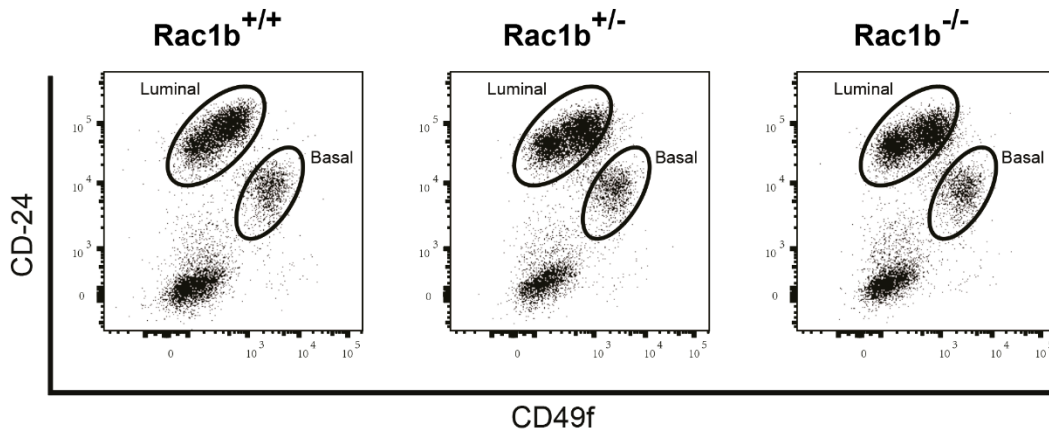
Figure 15. Representative gating strategy for analysing and sorting target cell populations from primary mammary cells. (A) Gate for single cells. The X axis is FSC-H, and the Y axis is FSC-A; (B) Gate for excluding cell debris. The X axis is FSC-H, and the Y axis is SSC-A; (C) Gate for excluding dead cells, endothelial cells, leukocytes and erythroid cells. The X axis is Lineage (CD45, CD31, TER119), and the Y axis is DRAQ7 (D) Gates for basal and luminal subpopulations. The X axis is CD49f, and the Y axis is CD24.

To determine whether loss of Rac1b function would result in a defect during lineage commitment processes, I have performed flow cytometry analysis based on a set of lineage-specific cell surface markers using Rac1b-null and littermate wildtype mice in C57BL6 and FVB backgrounds. Primary cells isolated from mammary glands of 8-10 weeks old nulliparous mice were used to compare the relative distribution of different mammary epithelial cell lineages. Single cells were identified based on FSC (forward scatter) signals (Figure 15A). Then, the cell debris were gated out by FSC versus SSC (Side scatter) signals (Figure 15B). Under 'P2 (Single cell)' population, the alive primary cells were characterised as the ones that are not stained with the dead cell marker DRAQ7. Meantime, Lineage-positive cells including the endothelial cells labelled by CD31 (which is also known as PECAM-1, Platelet endothelial cell adhesion molecule), erythroid cells targeted by Ter119 and leukocytes labelled by CD45 were excluded (Figure 15C). The remaining alive and lineage-negative cells were then separated into three compartments based on the expression levels of the lineage markers CD24 and CD49f: basal fraction ($CD24^{low}CD49f^{high}$), luminal fraction ($CD24^{high}CD49f^{low}$) (Figure 15D).

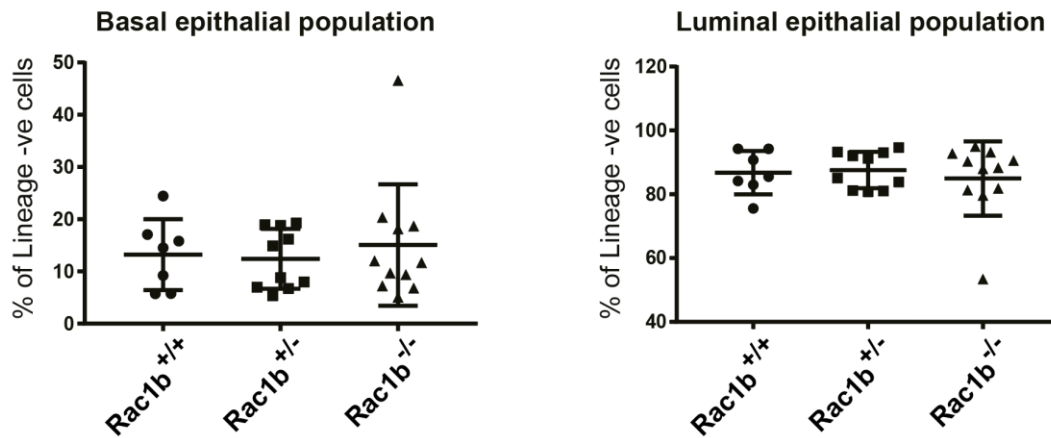
Primary cells isolated from Rac1b-null, heterozygous and wild-type mammary glands were analysed and compared by using the same gate settings (Figure 16A). The percentage distribution of basal and luminal epithelial subpopulations within the total MECs was calculated for statistical comparison. For those mice in the C57BL6 background, the basal population accounts for 13.22%, 12.4% and 15.06% of total MECs for Rac1b^{+/+}, Rac1b^{+/-} and Rac1b^{-/-} glands respectively; and the wild-type, heterozygous and Rac1b-null luminal subpopulations make up 86.78%, 87.6% and 84.94 of total MECs, respectively (Figure 16B). For the mice in the FVB background, 19.87%, 24.63% and 22.45% of MECs are basal cells in the Rac1b^{+/+}, Rac1b^{+/-} and Rac1b^{-/-} mammary glands respectively; and the luminal fractions account for 80.13%, 75.37% and 77.55% of MECs for wild-type, heterozygous and Rac1b-null

glands, respectively (Figure 16C). In both backgrounds, the obtained data shows no significant differences between the wild-type, heterozygous and *Rac1b*-null mammary glands, indicating that the loss of *Rac1b* function does not alter the lineage commitment in nulliparous mammary glands.

A



B



C

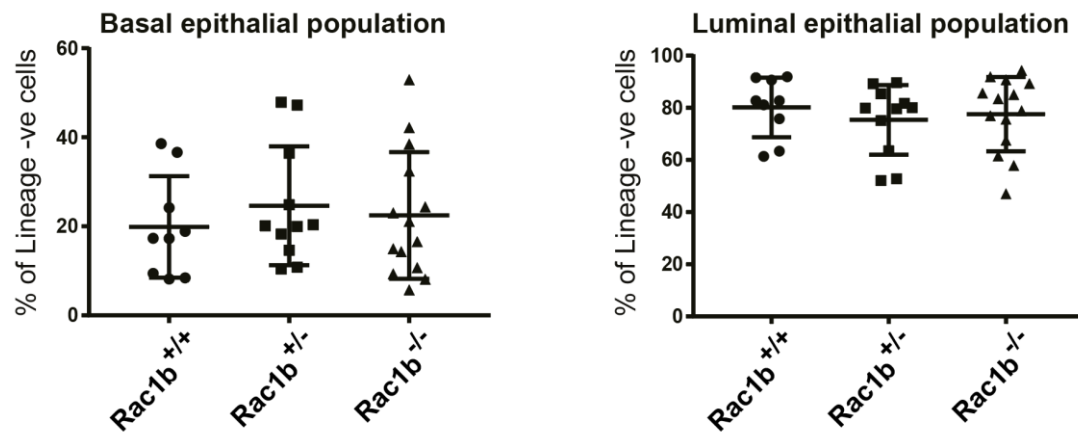
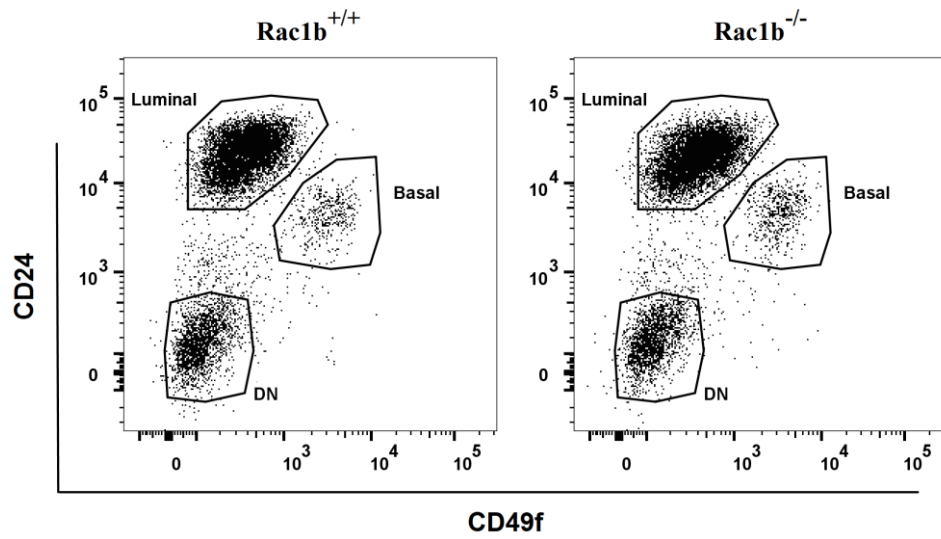


Figure 16. (A) Representative dot plots for FACS analyses of primary mammary epithelial cells obtained from mammary glands of nulliparous *Rac1b*^{+/+}, *Rac1b*^{+/-}, and *Rac1b*^{-/-} mice. The lower right compartment is basal cell population, and the upper compartment is luminal cell population. (B) (C) Statistical analysis for the percentage distribution of basal and luminal subpopulations in (B) C57BL/6 background (N=10 vs. 11) and (C) FVB background (N=11 vs. 9 vs. 14). The data for each individual mouse are represented with an individual symbol in the graphs shown.

3.2.4 *Rac1b* is dispensable for the maintenance of mammary epithelial stem cells

Rac1b function was shown to be required for the maintenance of MaSCs, but not for luminal progenitors (Olabi et al., 2018). To elucidate whether *Rac1b* may also have crucial functions for MaSCs, I performed mammosphere assay using the sorted cell subpopulations (Basal and Luminal and DN) from the mammary glands. The mammosphere assay is utilized to define the existence and the frequency of stem cells, since it is presumed that only stem cells are able to survive and form spheres in the suspension mammosphere culture.

A



B

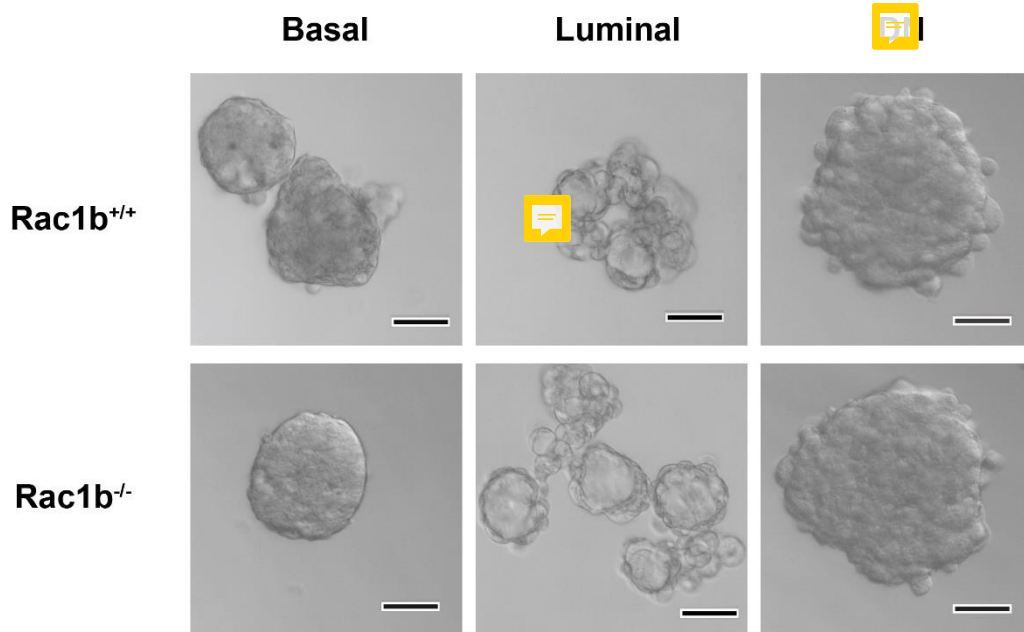


Figure 17. Mammosphere-forming assay of sorted primary mammary cells. **(A)** Representative FACS dot plots for separating three different cell subpopulations (Basal, Luminal and DN) from the single alive lineage-negative primary mammary cells. **(B)** Representative images for mammosphere assay. 100,000 cells/ml were seeded for basal fraction; 10,000 cells/ml were seeded for luminal and DN fractions respectively. Scale bars represent 50 μm.

Three cell subpopulations were sorted from primary $Rac1b^{+/+}$ and $Rac1b^{-/-}$ mammary cells based on their CD24 and CD49f expression levels: basal fraction ($CD24^{low}CD49f^{high}$), luminal fraction ($CD24^{high}CD49f^{low}$) and double-negative fraction (DN; $CD24^{-}CD49f^{-}$). Sorted cells were then plated in suspension (mammosphere) culture under low-attachment conditions. Both the wildtype and $Rac1b$ -null basal cell populations were capable of forming solid mammospheres (Fig. 17B, left panel). In contrast, cells in the luminal population mostly formed acini-like structures for both wildtype and $Rac1b$ -null cells (Fig. 17B, middle panel). Notably, the DN cells also formed solid spheres whereas the morphology of the DN spheres resembles a ‘grape-like’ structure in both genotypes (Fig. 17B, right panel).

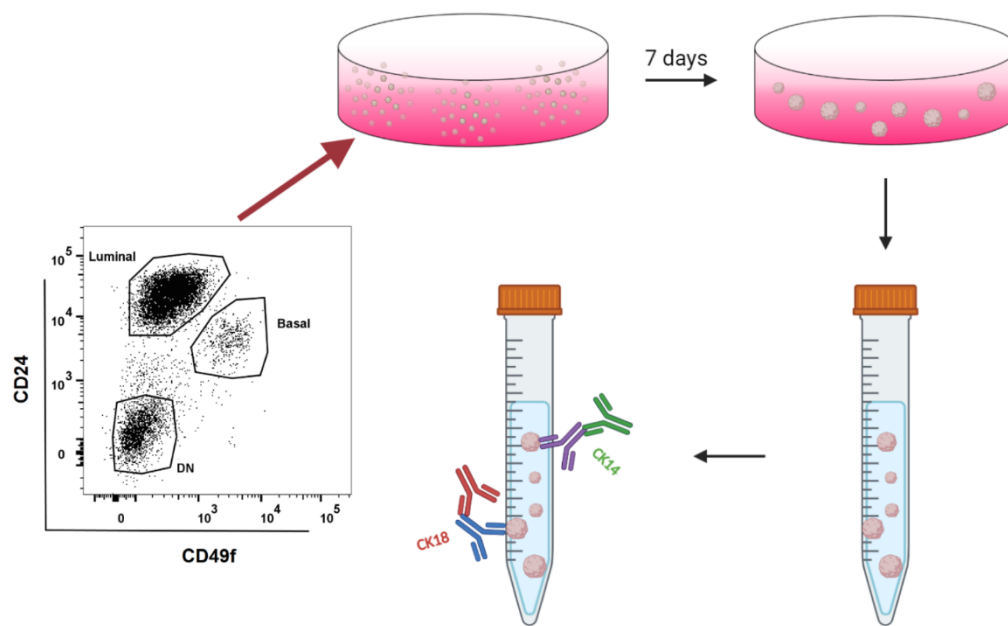
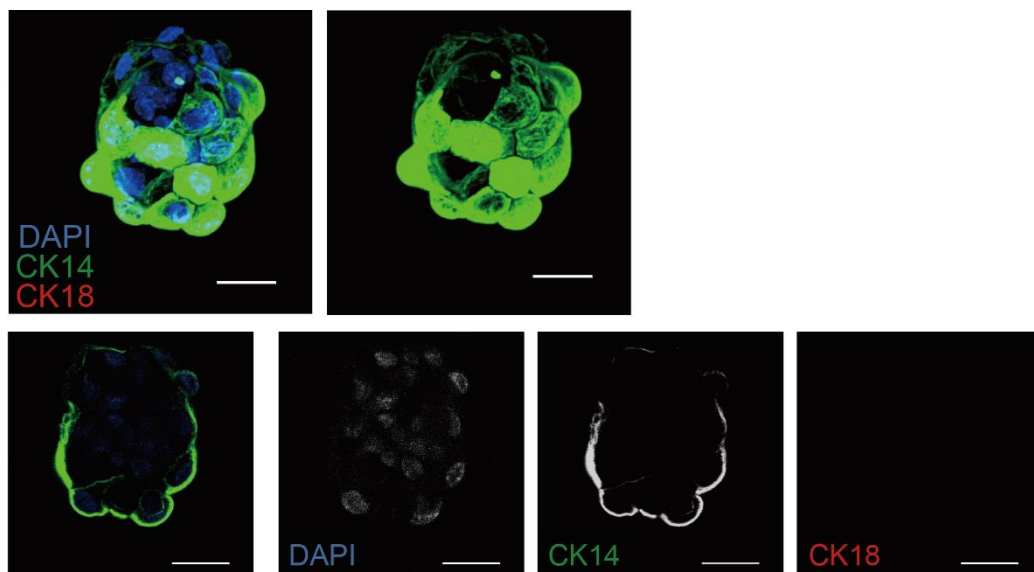


Figure 17B. The flow chart of the experiment for immunofluorescence staining of mammospheres. The basal, luminal and DN cells that were obtained from wildtype mammary glands were separately cultured in mammosphere medium in suspension culture. After 7 days of culture, formed structures were collected into 15ml Falcon tubes and fixed with 4% PFA. The primary antibodies against CK14 and CK18 (shown here in violet and blue colours, respectively) and the secondary antibodies specific to the primary antibodies (shown here in green and red colours) were used for immunostaining of intact mammospheres and acini structures.

To further investigate the characteristics of these formed structures in mammosphere culture medium, I performed the immunofluorescence staining with CK14 and CK18 antibodies. After 7 days of culture, the spheres and acini were collected and fixed, which are then incubated in primary antibody and secondary antibody solutions sequentially (Fig. 18). They were counterstained with DAPI and then transferred into 6-well plate for imaging with an upright confocal microscope.

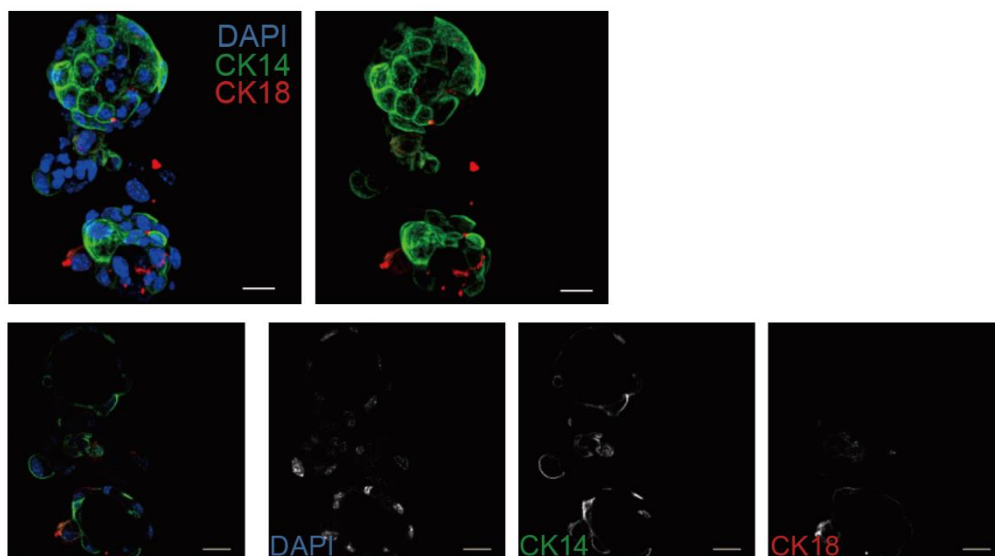
The spheres generated by the basal cells consisted of CK14-positive cells located at the outermost layer, but did not have any CK18-positive cells (Fig. 19A). The acini structure formed by the luminal cells were composed of various cell subtypes: CK14-positive, CK18-positive and double positive (Fig. 19Ba). Interestingly, the luminal cell fractions used were also capable of forming some solid spheres, which were consisted of CK14-positive, CK18-positive and double positive cells (Fig. 19Bb). The sphere structures formed by the DN cells had neither CK14- nor CK18 expression, suggesting that the DN spheres might be formed by the non-epithelial stem cells (Fig. 19C).

A

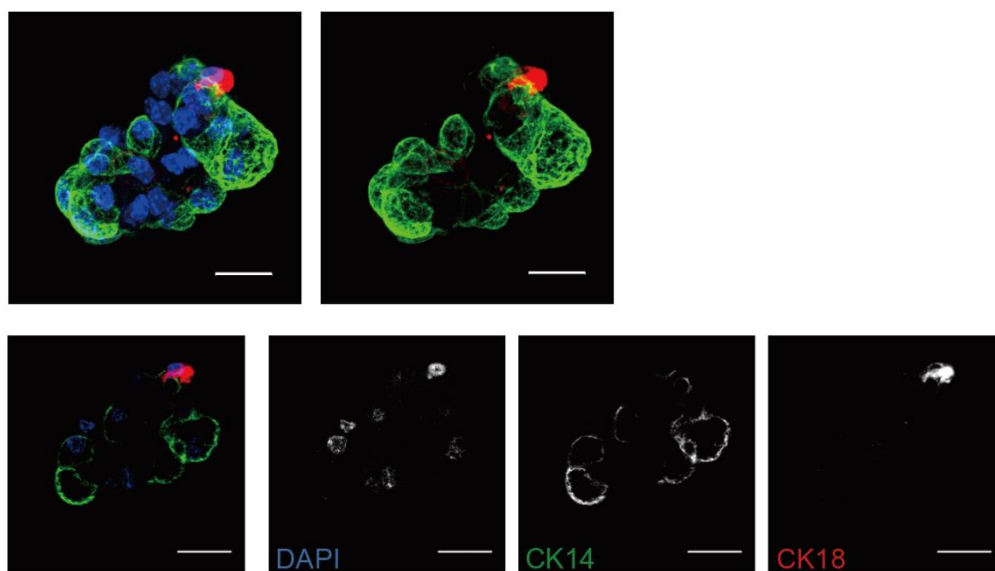


B

a.



b.



C

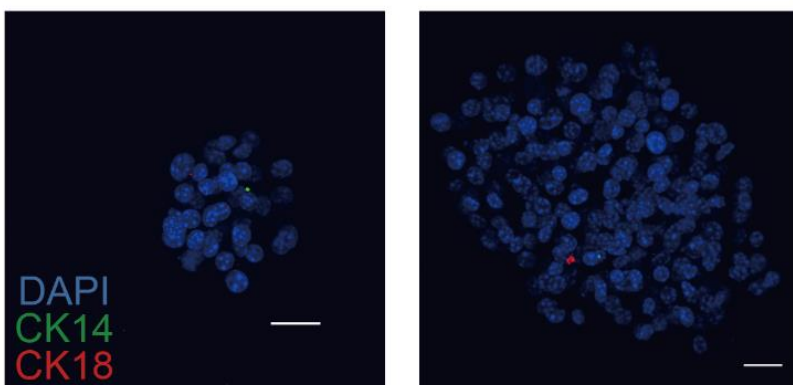


Figure 19. Representative images of CK14/CK18 immunofluorescence co-staining of spheres and acini. (A) Representative images of mammospheres formed by the basal mammary epithelia subpopulation; (B) Representative images of (a) acini and (b) solid spheres formed by the luminal epithelial fraction of cells. Upper panels: deconvoluted z-stack images with (left panel) and without (right panel) DAPI staining. Lower panels: a selected slice of the Z stack through the middle of the structures. (C) Two representative images of sphere structures formed by the cells from the DN subpopulation. All images were taken with Leica SP8 Upright dipping lens Confocal microscope with 63x objective. Blue, DAPI; Green, CK14; Red, CK18. Scale bars represent 20µm.

Interestingly, the flow cytometry analysis of the primary spheres has provided another possible explanation concerning the cell-of-origin of sphere structures formed by the DN cells. The primary spheres formed by the basal or DN subpopulation of primary mammary cells were digested into single cells after 7 days in culture and stained with CD24 and CD49f antibodies. Using flow cytometry analysis, the obtained single alive cells were separated into 4 different subpopulations (Fig. 20): $CD24^+CD49f^-$, $CD24^+CD49f^+$, $CD24^-CD49f^-$ and $CD24^-CD49f^+$. Surprisingly, the mammospheres originating from basal epithelial subpopulation were not only composed of $CD24^+$ epithelial cells, but also contained a significant population (13.9%) of DN cells (Fig. 20, lower left panel Q3 gate), which is $CD24^-CD49f^-$. On the other hand, the sphere structures formed by the DN subpopulation of primary mammary cells consisted of a large proportion of $CD24^-CD49f^-$ cells, though they have also contained approximately 9% of $CD24^+$ epithelial cells (Fig. 20, lower right panel). Approximately 30% of these $CD24^+$ cells were also expressing CD49f. Hence, it is possible that the cell of origin for the sphere structures formed by the DN subpopulation of primary mammary cells could be a previously unrecognised subset of MaSCs.

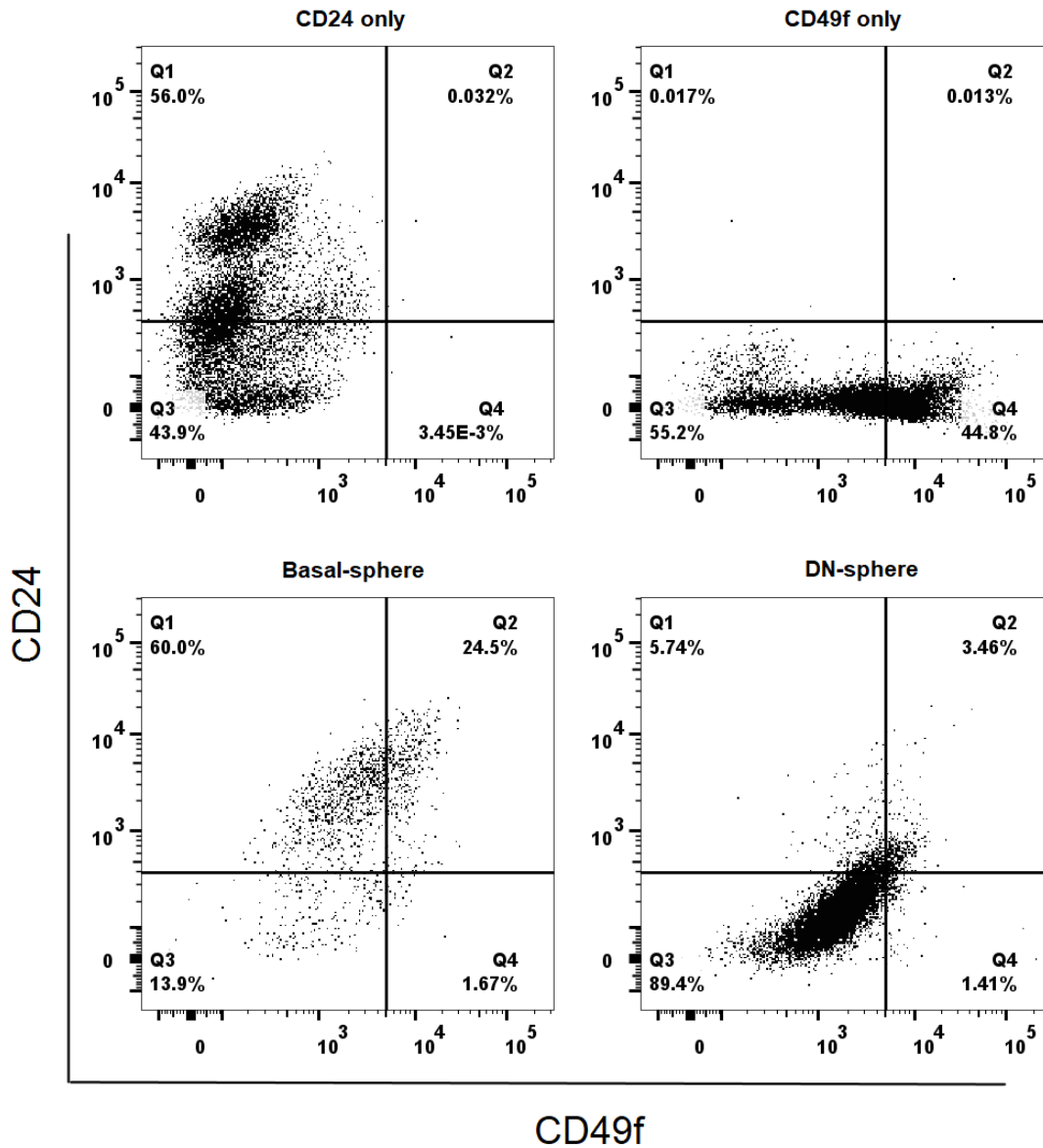


Figure 20. Flow cytometry analysis of the primary spheres originating from different cell subpopulations of wildtype mammary glands. Shown plots are representative of two independent experiments. Dead cells were excluded based on their DRAQ7staining. The single alive cells were then separated into 4 gates: Q1, CD24⁺CD49f⁻; Q2, CD24⁻CD49f⁺; Q3, CD24⁻CD49f⁻ and Q4, CD24⁺CD49f⁺. Upper left panel: CD24-only staining control; Upper right panel: CD49f-only staining control; Lower left panel: basal fraction-driven spheres; Lower right panel: DN fraction-driven spheres.

Next, to determine whether the loss of Rac1b function may alter the MaSC activities, I have quantified and compared the MFE (Mammosphere-forming efficiency) for both the basal and DN fractions of Rac1b^{+/+} versus Rac1b^{-/-} primary mammary cells. For basal epithelial fraction of primary mammary cells, the % MFE were 0.054% and 0.048% for Rac1b^{+/+} versus Rac1b^{-/-} cells, respectively (Fig. 21A). Although this has shown a slight reduction of %MFE, the P value of 0.62 indicated that there was no significant difference in the stem cell frequency within the basal subpopulations of Rac1b^{+/+} and Rac1b^{-/-} mammary glands. In DN fractions of primary

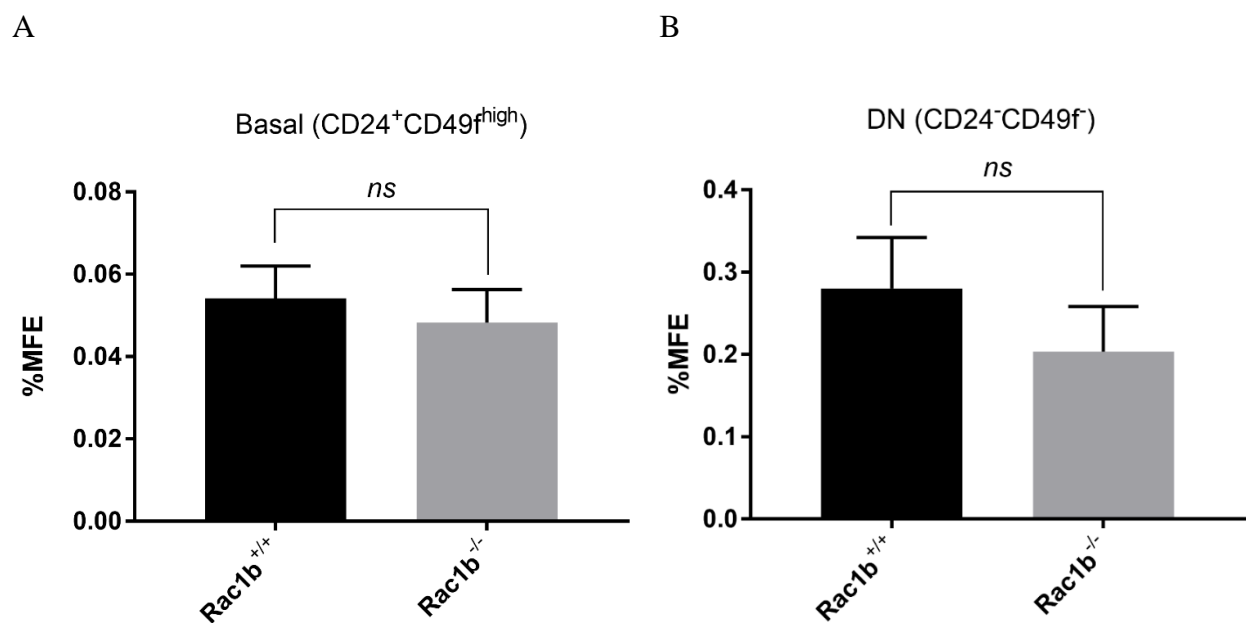



Figure 21. The loss of Rac1b function does not alter the stem cell frequency in nulliparous mammary glands. (A) Quantification results (N= 4 Rac1b^{+/+} vs. 5 Rac1b^{-/-}) for the mammosphere assay of the sorted basal mammary epithelial populations. 100,000 cells/ml were seeded for basal (CD24^{low}CD49f^{high}) fraction. (B) Quantification results (N= 5 Rac1b^{+/+} vs. 6 Rac1b^{-/-}) for the sphere-forming cell frequencies within the DN subpopulation of primary mammary cells. 10,000 cells/ml were seeded for DN fraction. Values represent the mean±SD. The statistical analysis is determined by unpaired t test. *ns*, not significant; MFE, mammosphere-forming efficiency.

mammary cells, the MFE for Rac1b-null mammary glands was 0.203%, which is slightly less than the MFE for the wildtype mammary glands (0.280%). However, the statistical analysis of the data shows that there is no significant difference ($P=0.0566$) between two genotypes (Fig. 21B). Therefore, the statistical analysis of the quantification results of the sphere forming cell frequencies in the basal and DN subpopulations of primary mammary cells indicated that there was no significant difference  between Rac1b-null and wild-type mammary glands in maintaining their stem cell abilities.

3.3 Results - The generation of Rac1^{T2A-RFP}-knockin mouse model by using CRISPR technology

3.3.1 The optimization of CRISPR/Cas9 Double Nickase strategy by using Eph4 cells

Earlier studies in our group demonstrated that Rac1b is specifically expressed in the MaSC-enriched basal compartment of the primary mammary epithelial cells obtained from nulliparous female mice. Furthermore, they have shown that Rac1b has important functions in regulating breast cancer stem cell (BCSC) populations within the human breast cancer cell line, MCF7. Therefore, we hypothesized that Rac1b might be specifically expressed by the MaSCs within the basal compartment of mammary epithelia as well as by the BCSCs *in vivo*. To test this hypothesis, it would be necessary to accurately determine the Rac1b-expressing cells in the mammary gland and breast tumours *in vivo*. Therefore, we have planned to generate a transgenic mouse line that will have an in-frame knock-in of T2A-RFP cassette within the exon3b of the *Rac1* genomic locus. This would enable us to determine the Rac1b expressing cells as RFP⁺ cells, as RFP would serve as a surrogate reporter for Rac1b splicing.

To this end, we first optimized the CRISPR/Cas9 Double Nickase strategy with HDR (Homolog-directed repair) templates using Eph4 cells. Eph4 cells are non-tumorigenic mouse mammary epithelial cell line that was originally generated from the luminal layer of the mammary tissue of a mid-pregnant mouse (Fialka et al., 1996).

To optimise the design of guide-RNA targeting, we firstly have used Eph4 cell line to generate Rac1b-specific knockout clones through CRISPR/Cas9 Double nickase approach of genome editing. To avoid the possibility of off-targeting, CRISPR/Cas9 Double nickase method was our choice of method to knock out the exon3b of *Rac1* genomic locus (Fig. 22). Compared with Cas9 endonuclease, Cas9 nickase (Cas9n) can only generate a single-strand DNA break at the genomic site complementary to the small guide RNA (sgRNA). Thus, a pair of 20-

nuclotide sgRNAs that can complement with the opposite strands of targeted genomic locus in close proximity (Fig. 22) are required in Double nickase approach to induce double strand DNA break formation, which happens as a consequence of the base excision repair (BER) of the generated two single strand DNA breaks formed by Cas9n activity. sgRNAs were designed to target the exon3b of the *Rac1* genomic locus by using Crispr design software (<http://crispr.mit.edu>): sgRNA-a: 5'-UGUCUCCAACCUAGUAAUGC-3' and sgRNA-b: 5'-GGUAAAGAUAGACCCUCCAG-3'.



Figure 22. The strategy used for targeting the exon3b of *Rac1b*. *Rac1* genomic locus is depicted with exons as rectangles or ellipse and the introns as a black line between exons. Exon3b, shown in yellow, is the exon that is differentially spliced-in for the *Rac1b* splice variant. Two red arrows on the exon3b represent the sites targeted by the Cas9n. EX, exon.

Eph4 cells were co-transfected with two constructs, each encoding one of the two sgRNAs along with the Cas9n-T2A-GFP (Fig. 23). SgRNA sequences are transcribed from the U6 promoter as a chimeric transcript with tracerRNA sequence. Expression of the Cas9n followed by T2A-GFP fragment was under the control of the CMV promoter, which provides, a strong and ubiquitous expression. Due to the nature of the T2A self-cleaving peptide, the level of GFP protein correlates with the levels of Cas9n expression in each cell. Two days after co-transfection, single cells that are GFP-positive (approximately 2%) were sorted through FACS directly into the 96-well plates containing growth medium to generate the single-cell clones.

Some of these cells gave rise to single-cell colonies approximately 2 weeks after plating. Afterwards, twenty of these single-cell colonies were expanded further and genotyped.

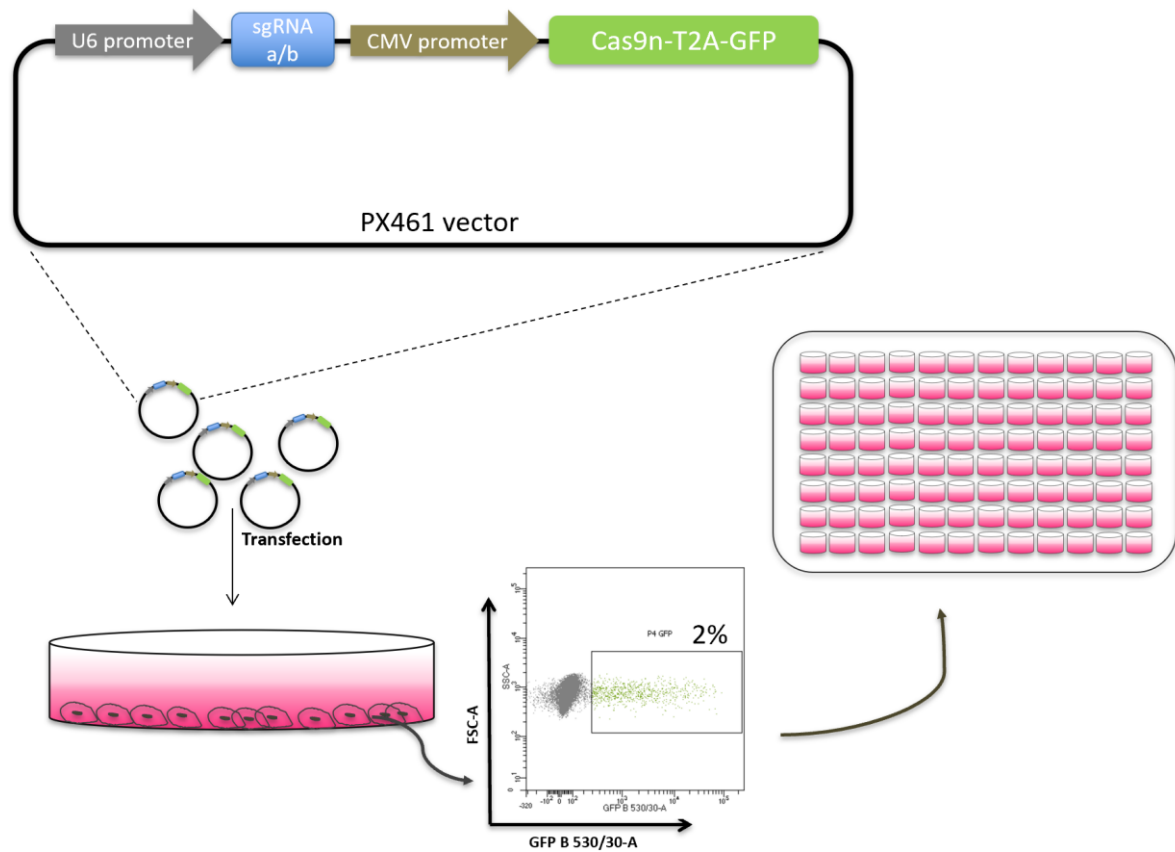


Figure 23. Flow chart of the experiment for generating single-cell Eph4 clones with CRISPR targeting. Two constructs were generated by cloning the corresponding sgRNA(a/b) coding sequences downstream of the U6 promoter within the PX461 vector. Under the control of the CMV promoter, Cas9n is expressed together with the GFP at a stoichiometric ratio. Two days after transfection, the GFP-positive cells were sorted by FACS directly into the 96-well plates containing complete growth medium.

In order to test if the obtained single-cell Eph4 clones were genetically modified at the targeted *Rac1* genomic locus, I have designed a pair of primers complementary to the introns on each side of the exon3b (Fig. 24A). The expected size for the wild-type allele was 251 bp, which was observed in parental Eph4 cells (labelled by green square in Figure 24B). The PCR results for the genomic DNA samples of the single-cell clones indicated that various clones might have acquired InDel mutations at the targeted genomic locus, as different size PCR bands were observed in these clones (Fig. 24B). Among these, I have selected the single-cell clones 7, 12 and 19 for further analyses as potential *Rac1b*-null clones.

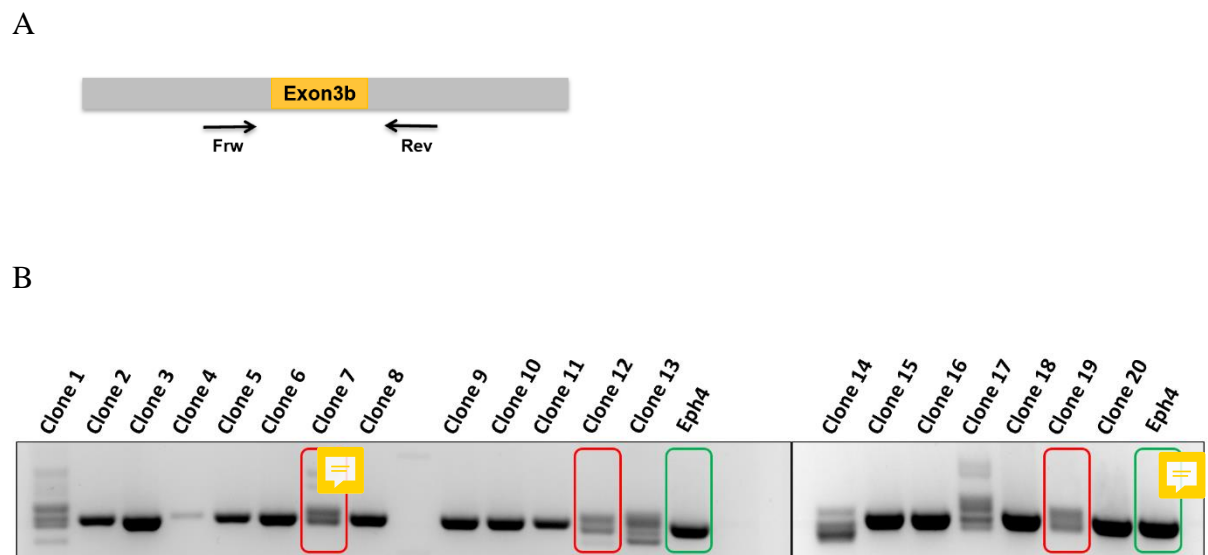
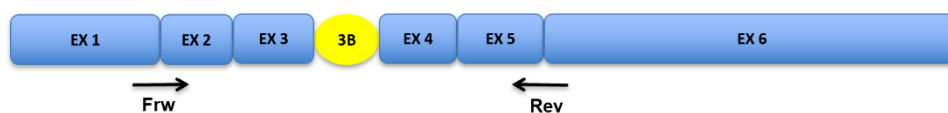


Figure 24. Genotyping of single-cell *Rac1b*-null transgenic Eph4 clones at the genomic level. (A) Primer pairs were designed for PCR to genotype the obtained single-cell clones at genomic DNA level; the grey bar represents introns on both sides of exon3b; Frw, forward primer; Rev, Reverse primer; (B) PCR results for the genomic DNA of obtained single-cell clones. Clones 7, 12 and 19 (marked by red square) were selected as potential *Rac1b*-null clones.

Next, I have designed a primer pair for RT-PCR to detect the expression of both Rac1 and Rac1b mRNA (Fig. 25A): the forward primer would align at the junction between exon 1 and 2, whereas the reverse primer is complementary to the cDNA sequence at the junction between exon 5 and 6. RT-PCR with this primer pair would amplify a 503 and 446 bp fragments corresponding to Rac1b and Rac1, respectively, as shown for wild-type Eph4 cells (Fig. 25B). In the selected clones 7, 12 and 19, no Rac1b band had been observed although they had the proper Rac1 mRNA expression. This indicates that Rac1b has been successfully knocked out in these clones.

A



B

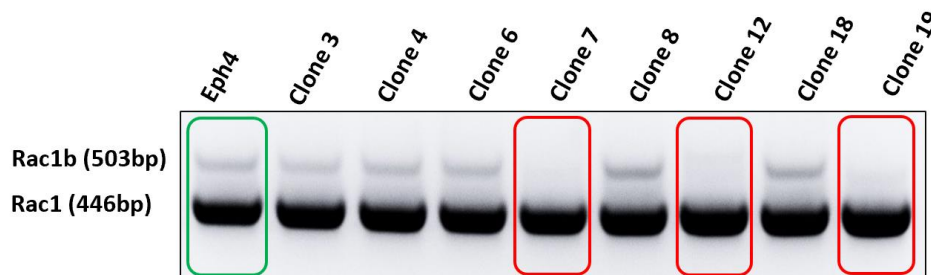


Figure 25. Genotyping of single-cell Rac1b-null transgenic Eph4 clones at the transcript level. (A) Primer pairs were designed for RT-PCR to genotype the obtained single-cell clones at the mRNA level; (B) RT-PCR results of some of the selected single-cell clones to detect the mRNA expression for both Rac1 and Rac1b. The lower band represents Rac1 cDNA (446bp), and the upper band represents Rac1b cDNA (503bp);

To better characterize the acquired mutations in these clones (Fig. 24B), I have sequenced the targeted genomic region by Sanger sequencing and generated a mutation map for both alleles of *Rac1* locus in each clone (Fig. 26). After the generation of the double strand DNA break in a cell, these are usually repaired by non-homologous end joining (NHEJ) repair pathway in the absence of available homology-directed repair templates, which would consequently result in random InDel mutations. Furthermore, I have identified that most of these InDel mutations would result in a frameshift in their coding sequence.

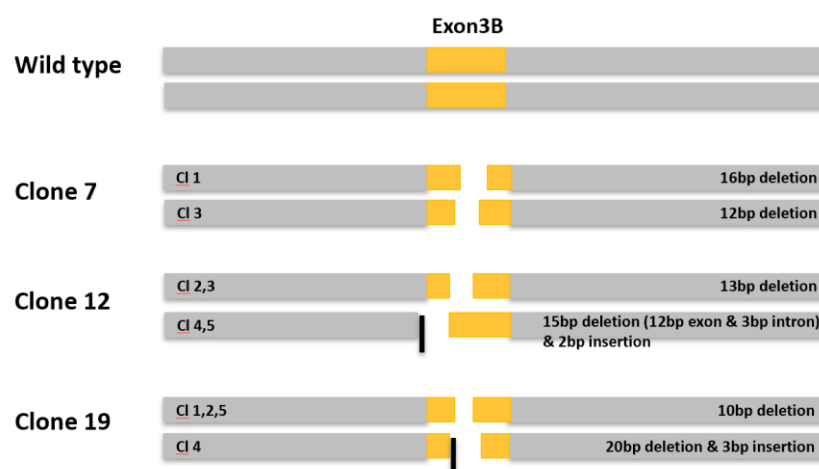


Figure 26 . Mutation map for clones 7, 12 and 19. The gray bars are the intronic region of the *Rac1* locus around exon 3b, which itself is depicted in yellow. The acquired InDel mutations for each clone were described on the right side of the grey bars and depicted as gaps within exon3b (deletions) or black boxes (insertions).

I have also confirmed that the acquired InDel mutations in these clones have not affected the Rac1 protein expression (Fig. 27), thus suggesting that these clones are lacking specifically Rac1b, but not Rac1. However, our designed sgRNA/Cas9n strategy is able to target Rac1b specifically and effectively in murine cells.

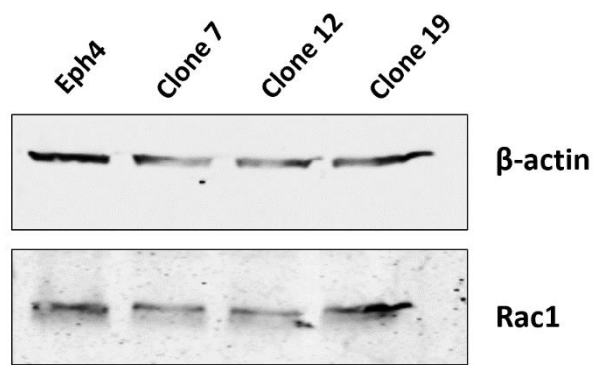


Figure 27 . Western blotting results of Rac1 expression in selected single-cell clones. Rac1 protein was detected in both parental Eph4 and Rac1b-null clones 7, 12 and 19. The molecular weight of Rac1 is 21.48KDa and β -actin (loading control) is 42KDa.

3.3.2 The optimization of HDR templates for the knock-in of ‘T2A-RFP’ cassettes into the Exon3b sequence

After verifying that the sgRNA/Cas9n constructs were able to knock out Rac1b efficiently, we decided to test three potential HDR templates inserting T2A-RFP cassettes at different locations of the Exon3b-encoding sequence for whether they may undesirably impair the proper splicing of the Rac1b transcript. To this end, I have cloned 3 different homology-directed repair (HDR) templates containing approximately 1kb long homology arms on both sides of the T2A-RFP cassette (Fig. 28). These different HDR templates would lead to in-frame knock-in of the T2A-RFP cassette into three distinct sites within the exon3b sequence without deleting any of the genomic sequences of the exon3b. Importantly, the RFP coding sequence ends with a stop codon, but the T2A-RFP cassette does not include any polyA signal, therefore our knock-in approach should not have any effect on normal expression of Rac1 isoform.

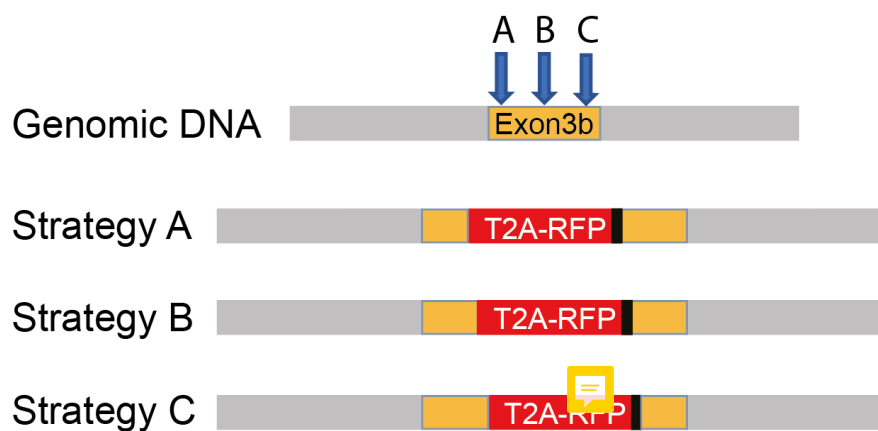


Figure 28. Optimisation of HDR templates for proper targeting strategy to generate Rac1b^{T2A-RFP} knock-in clones. Three different HDR templates were cloned aiming to knock-in the T2A-RFP cassette in-frame at one of the three distinct sites within the exon3b of the *Rac1* genomic locus. The grey bars are the intronic regions of the *Rac1* locus around exon3b, which itself is shown in yellow. ‘T2A-RFP’ cassette was shown as red bars, followed by a stop codon (black bars).

After cloning the HDR templates within the pGemT plasmid backbone and sequence verifying them, I have co-transfected Eph4 cells with either of these HDR constructs together with the two sgRNA-expression constructs that has been described above (Fig. 23). Compared with NHEJ repair, homology-directed repair is capable of generating specific mutations with the help of HDR templates, thus provide the possibility of generating knock-in transgenes.

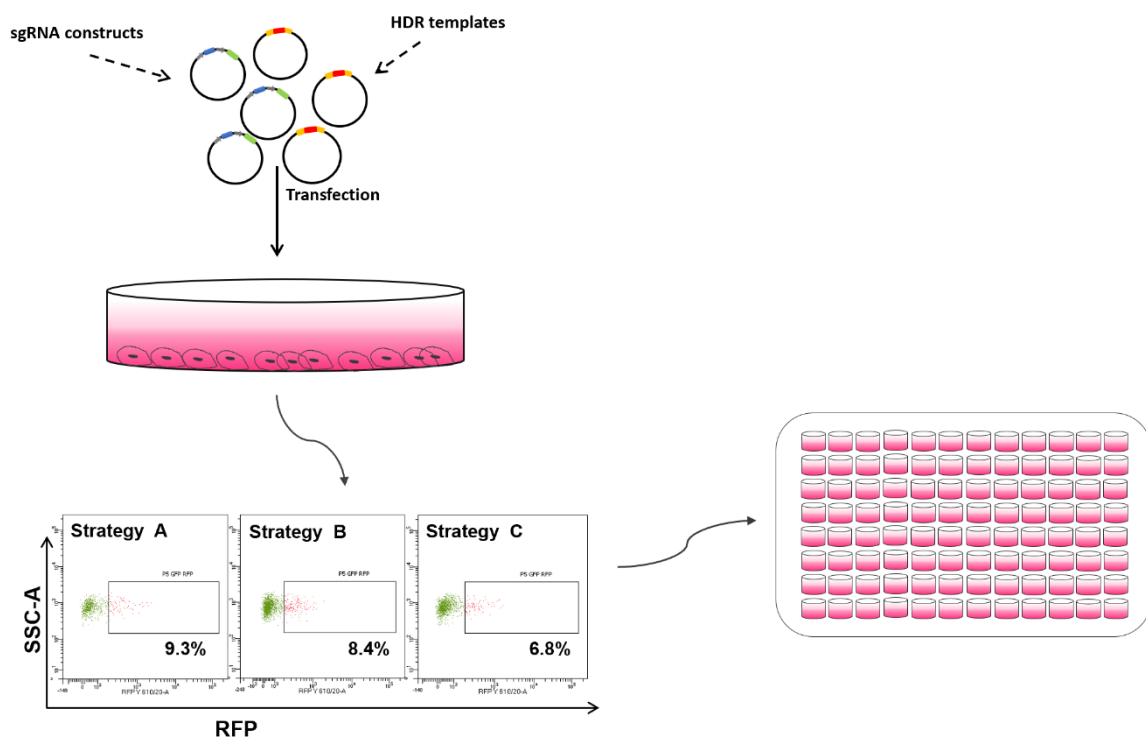


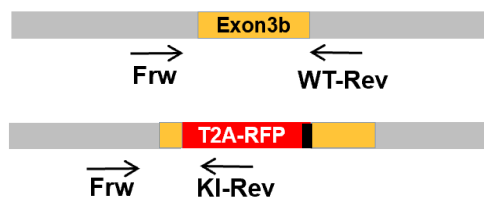
Figure 29. Flow chart for the experimental strategy used to generate Rac1b^{T2A-RFP} knock-in single-cell Eph4 clones. Eph4 cells were co-transfected with one of the three HDR templates along with the two sgRNA/Cas9n constructs that had been described in Figure 23. After 2 days of transfection, the single alive GFP⁺RFP⁺ cells were sorted by FACS directly into the 96-well plates containing complete growth medium. Within the GFP⁺ cells, there were 9.3%, 8.4% and 6.8% RFP⁺ cells for strategy A, B and C respectively as shown in the FACS dot plots.

Two days post-transfection, I have FACS sorted the GFP⁺RFP⁺ population as single cells directly into 96-well plates containing growth medium. As expected, all RFP⁺ cells were also GFP⁺, as the expression of GFP protein indicated whether Cas9n was expressed in the cells

and thus the presence of CRISPR activity, and RFP expression defined whether the ‘T2A-RFP’ cassette was correctly integrated into the targeted genomic locus. Surprisingly, the FACS plots showed that all three strategies worked successfully (Fig. 29).

To genotype the obtained single-cell clones at the genomic DNA level, I have developed a triplex PCR strategy, which would generate a 443bp fragment for the wild-type allele and 265, 286, or 304 bp fragments for the knock-in alleles depending on the used HDR templates (A, B, and C, respectively) (Fig. 30). Genotyping results suggested that the ‘T2A-RFP’ cassette had been successfully inserted into the desired sites within the Exon3b in all clones except the clone C14 (Fig. 30B). I have also verified the correctness of the in-frame insertion of the T2A-RFP cassette in these knock-in alleles by cloning the corresponding PCR fragments and Sanger sequencing.

A



B

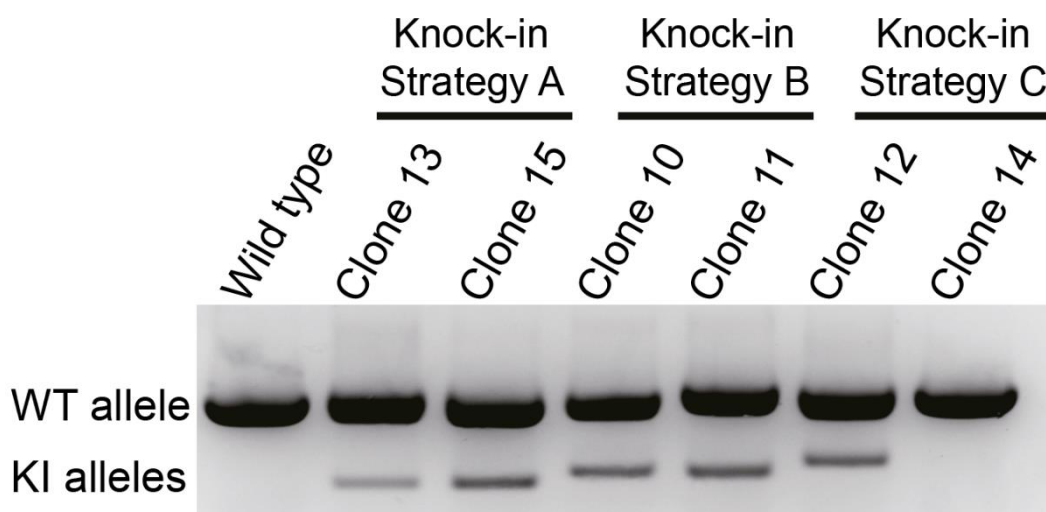


Figure 30. Genotyping of $Rac1b^{T2A-RFP}$ knock-in Eph4 single-cell clones. (A) Designed strategy for genotyping the $Rac1b^{T2A-RFP}$ knock-in Eph4 single-cell clones at the genomic DNA level. Primers for the triplex genotyping PCR are depicted as black arrows. Forward primers are common for both alleles, and reverse primers are allele-specific. (B) Genotyping PCR results show that the ‘T2A-RFP’ cassette had been correctly integrated into the exon3b coding sequence of *Rac1* genomic locus in all clones except clone C14.

Next, I have analysed some of these clones for RFP expression using flow cytometry. Interestingly, RFP^+ cells corresponded to a small population of cells within these clones (Fig. 31). The single-cell clone A15 (generated by Strategy A) had approximately 5.1% RFP^+ cells, whereas 6.0% of cells were RFP^+ in clone B11 (generated by strategy B). Surprisingly, the single-cell clone C12, which is generated by the strategy C, did not have any RFP^+ cells, although the ‘T2A-RFP’ cassette was correctly inserted into the genome based on the genotyping results at the genomic DNA level. Thus, the HDR template-C was considered as an unsuitable option for generating the $Rac1b^{T2A-RFP}$ -knockin mouse line.

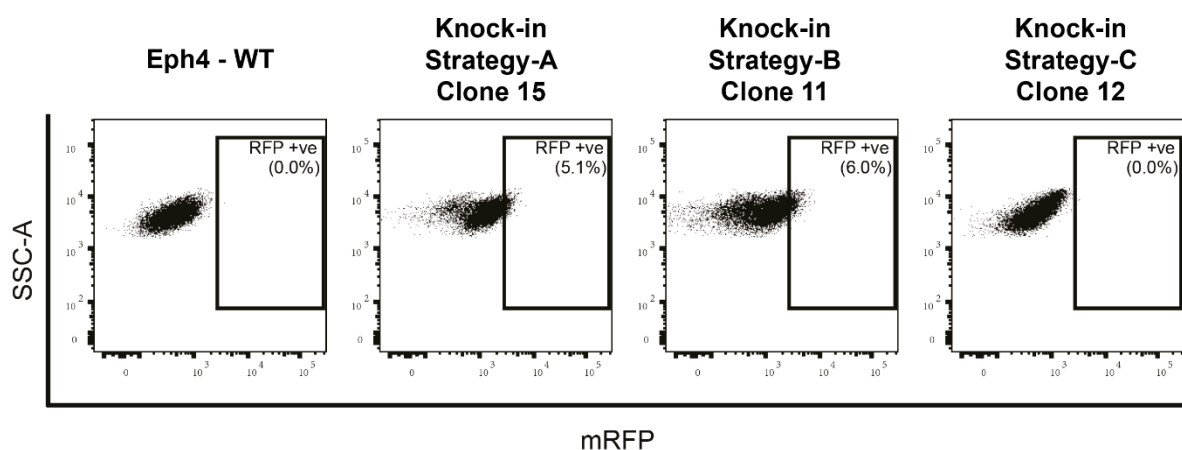


Figure 31. Flow cytometry analysis of selected single-cell clones demonstrate that RFP positive cells, indicative of $Rac1b$ expressing cells, constitute a small subpopulation of Eph4 cells.

Furthermore, to verify whether Rac1 expression was not affected due to the insertion of the 'T2A-RFP' cassette, I performed western blot analysis of the transgenic single-cell clones (Clone A15 and B11) against Rac1 and β -actin (Fig. 32). The results showed that the strategy A and B were able to successfully knock-in the 'T2A-RFP' cassette into the exon3b of Rac1b without altering Rac1 expression.

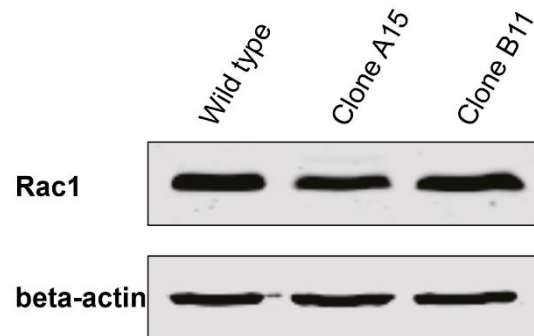


Figure 32. Western blot analysis to confirm the normal expression of Rac1 in the Rac1b^{T2A-RFP} single-cell Eph4 clones. Rac1, approximately 21.48kDa; beta-actin, 42kDa.

3.3.3 The generation of Rac1b^{T2A-RFP}-knockin mouse line

After I have successfully optimized the strategy for generating Rac1b^{T2A-RFP}-knockin transgenic cell clones, I initiated the process of generating a novel transgenic mouse line in collaboration with the transgenic facility of the University of Manchester. The single-cell zygotes obtained from the mice in pure FVB background had been injected with a shortened version of the HDR template-B and Cas9-sgRNA RNP molecules and subsequently implanted into foster mothers. Eleven founders were born and genotyped.

A

a

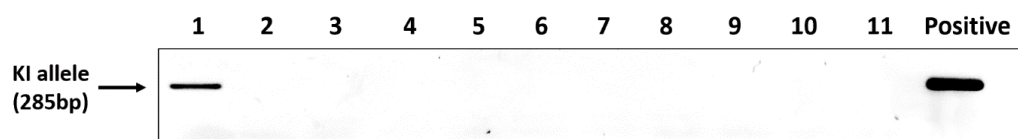


b



B

a



b

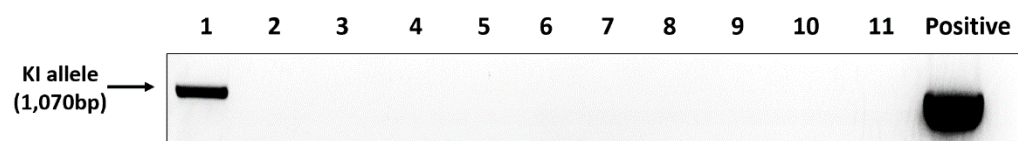


Figure 33. Genotyping of transgenic founders at the genomic level. (A) a&b. Two sets of primer pairs were designed for PCR to genotype the obtained 11 founders at genomic DNA level; the grey bar represents introns on both sides of exon3b; Frw, forward primer; Rev, Reverse primer; (B) a&b. Genotyping PCR results of the genomic DNA obtained from 11 founders (No. 1-11); Positive, positive control for PCR.

To determine if the expected knock-in mutation was acquired in those founders, I designed two sets of primers to detect the desired genetic alteration in the *Rac1* genomic locus. For the first set, the forward primer targets the upstream intronic sequence of exon 3b, and the reverse primer is complementary to a sequence within the ‘T2A-RFP’ cassette (Fig. 33Aa). The expected size of the PCR amplicon using this primer pair would be a 285bp fragment if the ‘T2A-RFP’ cassette was integrated into the correct location (Fig. 33Ba). Accordingly, only the founder No.1 had the expected transgenic modification.

To determine whether the 3’part of the HDR cassette was also correctly integrated into the genome, another set of primer pairs was designed. The forward primer targets a sequence within the ‘T2A-RFP’ cassette and the reverse primer aligns to the intronic sequence downstream of exon3b (Fig. 33Ab), which would result in the amplification of an expected fragment size of 1070 bp (Fig. 33Bb). The PCR with this primer pair has confirmed that the genomic DNA obtained from the first founder had the expected size band. Together, these PCR results suggested that this founder had the full-length T2A-RFP cassette integrated into the exon3b-coding genomic sequence.

3.4 Results - The verification of surrogate reporter ability of RFP for *Rac1b* expression

After generating a mouse colony of the novel *Rac1b*^{T2A-RFP}-knockin mouse model via breeding the founder No:1 to establish the germline transmission, I firstly confirmed whether RFP could serve as the surrogate reporter for *Rac1b* expression by analysing the heterozygous (*Rac1b*^{RFP/+}) transgenic mice. To this end, primary cells were isolated from the mammary glands of nulliparous *Rac1b*^{RFP/+} mouse to sort RFP⁺ and RFP⁻ cells within the single alive cell population via FACS.

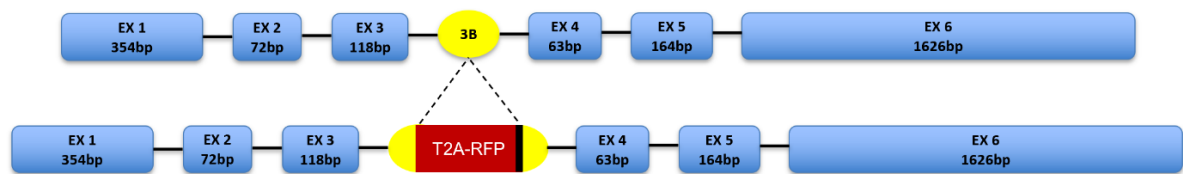


Figure 34. The genomic locus of wild-type allele (upper) and the transgenic allele (lower) for the *Rac1b*^{RFP/+} transgenic mice. The blue bars represent the exons, and the length of them are also labelled. Exon3b unique to *Rac1b* expression is labelled as yellow colour. The black lines represent the introns. The black bar represents a stop codon following ‘T2A-RFP’ cassette. EX, exon; 3B, exon3b.

The strategy used for setting up the gates were shown in Figure 35. First, the single cells were identified based on FSC (forward scatter) signal (Figure 35A). Within this population, the dying cells were excluded based on the staining of the dead cells with DAPI. Meantime, within the DAPI negative cell population, the lineage-positive cells (endothelial cells labelled by CD31, erythroid cells targeted by Ter119 and leukocytes labelled by CD45) were excluded (Figure 35B). Afterwards, the cell debris, which could not be excluded by DAPI, was also gated out based on their FSC versus SSC signals (Figure 35C). Within ‘P3’ population, the single alive lineage-negative primary cells were then separated into RFP⁺ and RFP⁻ cells by distinguishing them for their mRFP fluorescence (Figure 35D). The gate setting for

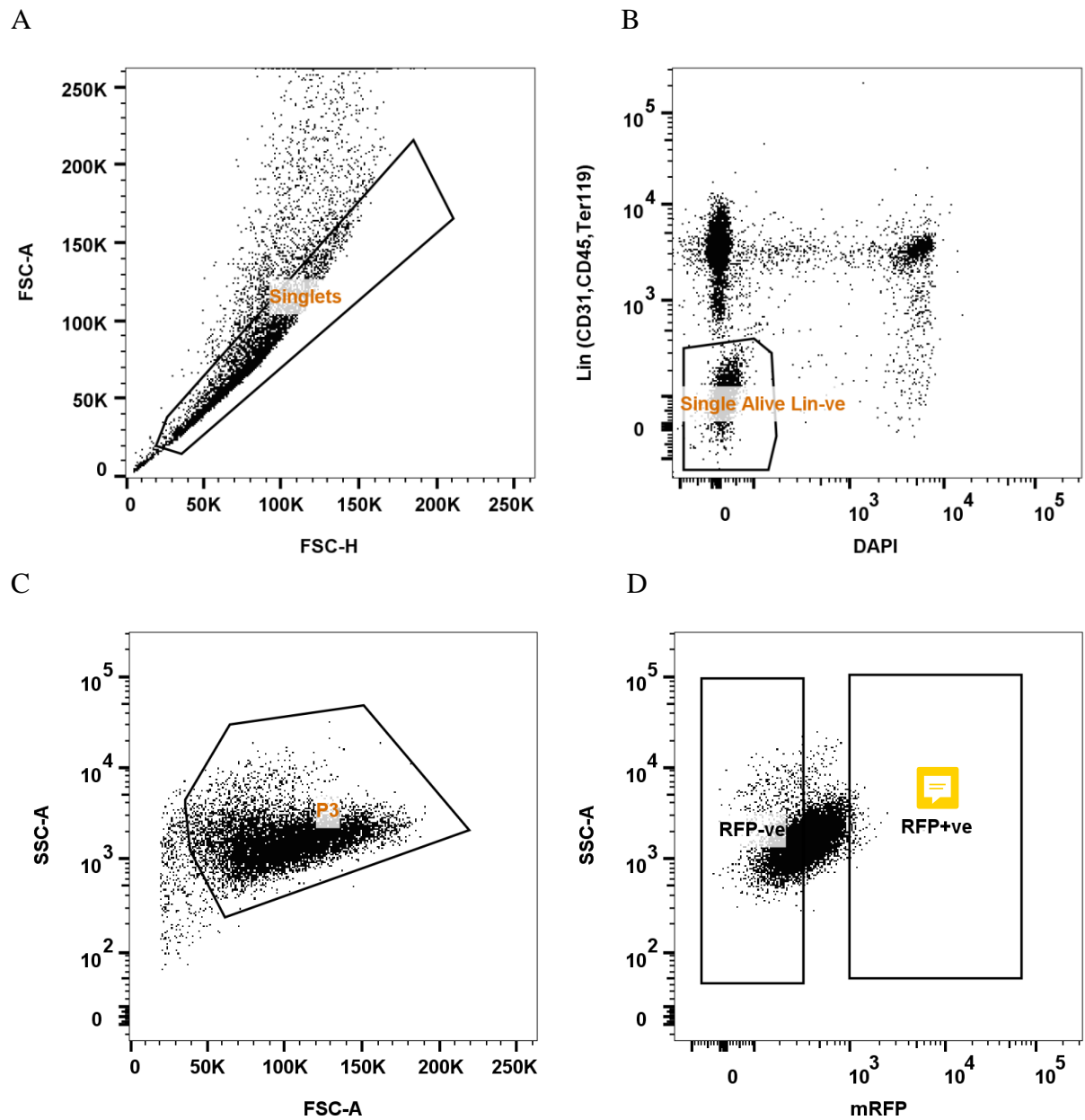


Figure 35. Representative dot plots for the FACS strategy of isolating RFP⁺ and RFP⁻ cells from Rac1b^{RFP/+} primary mammary cells. **(A)** Gate for isolating singlets from the primary cells. X axis, FSC-H; Y axis, FSC-A; **(B)** Gate for excluding dead and dying cells, and lineage-positive cells (i.e. endothelial cells, leukocytes and erythroid cells.) X axis, DAPI; Y axis, Lineage (CD31, CD45, TER119); **(C)** Gating to exclude cell debris. X axis, SSC-A; Y axis, FSC-A; **(D)** Gate for isolating RFP⁺ and RFP⁻ cell fractions, X axis, mRFP; Y axis, SSC-A.

distinguishing RFP⁺ and RFP⁻ populations was based on the wild-type cells which are considered to have 0.0% RFP⁺ cells. Notably, RFP⁺ cells accounts for only 0.4% to 1.7% of the lineage-negative primary mammary cells (Figure 36). The gate for RFP⁻ cells was placed further from the RFP⁺ gate to ensure that those two populations were sorted without cross-contamination.

After sorting RFP⁺ and RFP⁻ primary mammary cells, RNA isolation was performed, followed by reverse transcription (RT) reactions. The RT products, cDNA, were used to identify whether RFP expression does indeed act as the surrogate reporter for Rac1b expression at the transcript level.

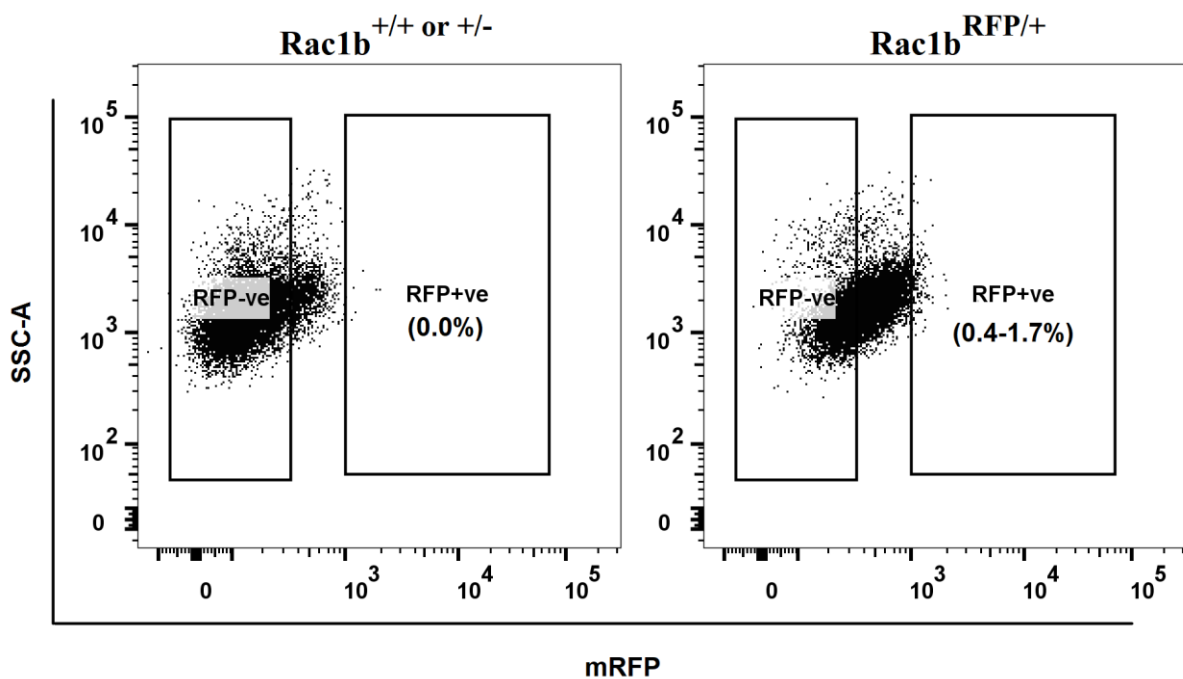
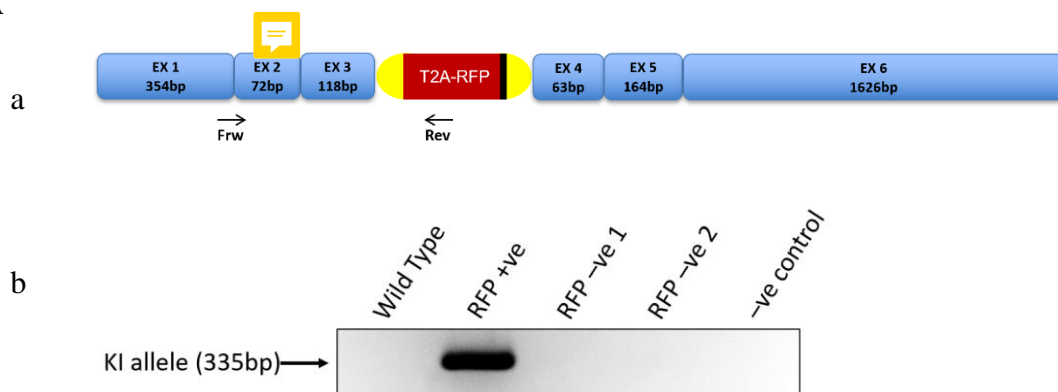


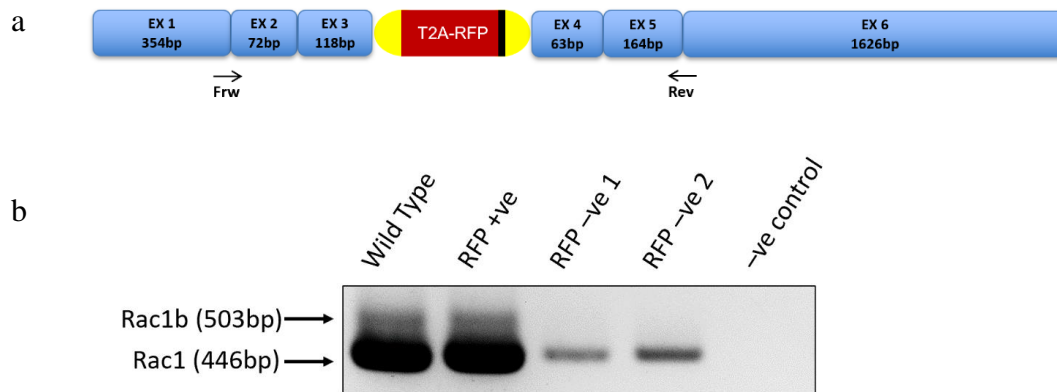
Figure 36. Representative FACS plots used for sorting RFP⁺ and RFP⁻ cells from Rac1b^{T2A-RFP} mammary glands. The left dot plot was for the wild-type (Rac1b^{+/+}) primary mammary cells, which was used as the control for setting up the RFP⁺ gate. The right plot was for the heterozygous (Rac1b^{RFP/+}) primary mammary cells. Dead cells were already excluded by the staining of DAPI in a previous gate. X axis showed mRFP fluorescence, and Y axis represented SSC-A channel.

I have designed three pairs of primers for RT-PCR to reveal the relationship between the RFP status and Rac1b mRNA expression. As shown in Figure 37A, the first PCR was designed to amplify specifically the cDNA originating from the KI allele (Fig. 37Aa). As expected, the RT-PCR of only the RFP⁺ cells produced the correct 335bp fragment (Fig. 37Ab). Primers for the second RT-PCR was designed to amplify both Rac1 and Rac1b transcripts (Fig. 37Ba) with the expected sizes of 503bp and 446bp long fragments, respectively, as confirmed for the cDNA of wild-type primary mammary cells (Fig. 37Bb). The RT-PCR results demonstrated that Rac1 mRNA is expressed in both RFP⁺ and RFP⁻ cells, whereas Rac1b mRNA was only detected in RFP⁺ cells, but not RFP⁻ cells. This result is further verified by using a third set of RT-PCR primer pair, which specifically amplifies the cDNA of the Rac1b splice variant, as the reverse primer was located at the junction between exon3b and exon4 (Fig. 37Ca). The expected 280 bp long amplicon was detected within the cDNA of both wild-type primary mammary cells and RFP⁺ cells, but not in the cDNA of RFP⁻ cells (Fig. 37Cb). Collectively, these RT-PCR results demonstrate that Rac1 is expressed in both RFP⁺ and RFP⁻ cells, whereas Rac1b is specifically expressed only in RFP⁺ cells, suggesting that RFP expression can serve as a surrogate reporter for Rac1b splicing in the Rac1b^{T2A-RFP} transgenic mouse line.

A



B



C

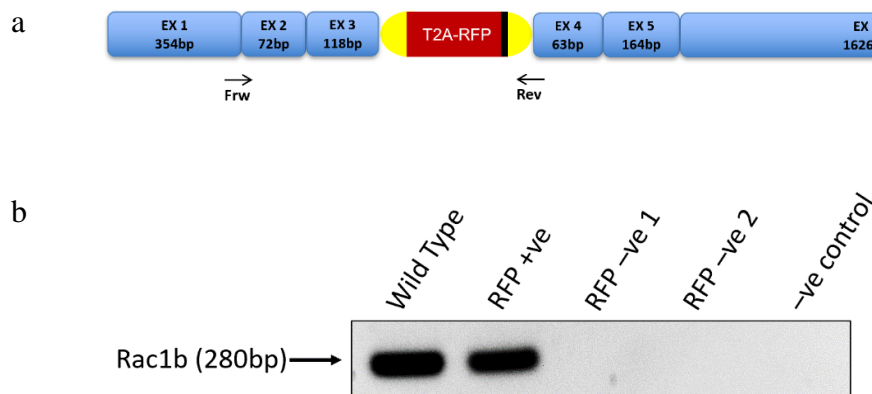


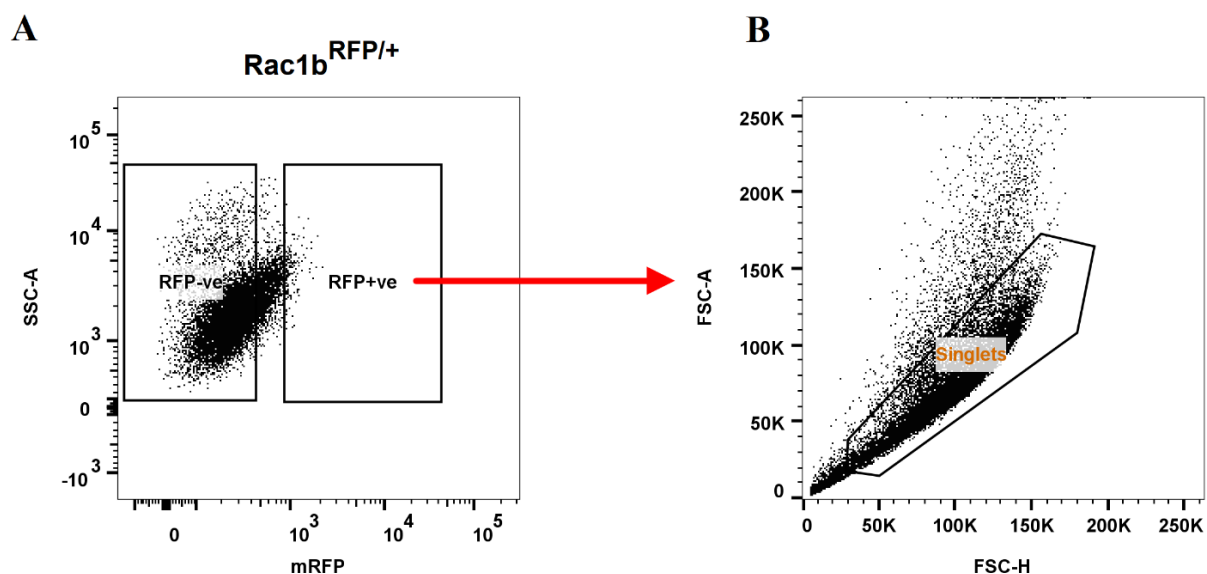
Figure 37. RT-PCR results demonstrating that RFP expression can serve as the surrogate reporter for Rac1b expression in the Rac1b^{T2A-RFP} transgenic mouse line. **(A)** (a) The RT-PCR primer design to detect the cDNA originating from the KI allele. Frw, forward primer, the junction between exon 1 and 2; Rev, reverse primer, within the ‘T2A-RFP’ cassette; (b) RT-PCR results. KI (Knock-in) amplicon, 335bp; **(B)** (a) The RT-PCR primer design to simultaneously detect both Rac1 and Rac1b cDNA. Rev, reverse primer, the junction between exon 5 and 6; (b) RT-PCR results. Rac1-specific amplicon(lower band), 446bp; Rac1b-specific amplicon (upper band), 503bp; **(C)** (a) The RT-PCR primer design to detect Rac1b-specific cDNA. Rev, reverse primer, the junction between exon 3b and 4; (b) RT-PCR results. Rac1b-specific amplicon, 280bp.



3.5 Results - Characterisation of Rac1b-expressing mammary cells

3.5.1 Rac1b-expressing cells consists of both CD24⁺ and CD24⁻ mammary cells

In order to characterise Rac1b-expressing mammary cells, I performed flow cytometry analysis for CD24 expression, which is widely considered as a marker for mammary epithelial cells. CD24 is highly expressed by luminal epithelial cells, whereas basal cells have lower CD24 levels. CD24⁻ cells are considered to be mesenchymal cells. I have sorted the Lin⁻RFP⁺ primary mammary cells isolated from Rac1b^{RFP/+} mammary glands (Fig. 38A), which were then stained with CD24 antibody and DAPI. After selecting for single cells (Fig. 38B) and excluding the cell debris (Fig. 38C) and dead cells (Fig. 38D), the remaining RFP⁺ cells were analysed for their CD24 expression (Fig. 38E). Interestingly, the RFP⁺ cell population were composed of both CD24-expressing (around %32.0) and CD24⁻ cells (around 68%).



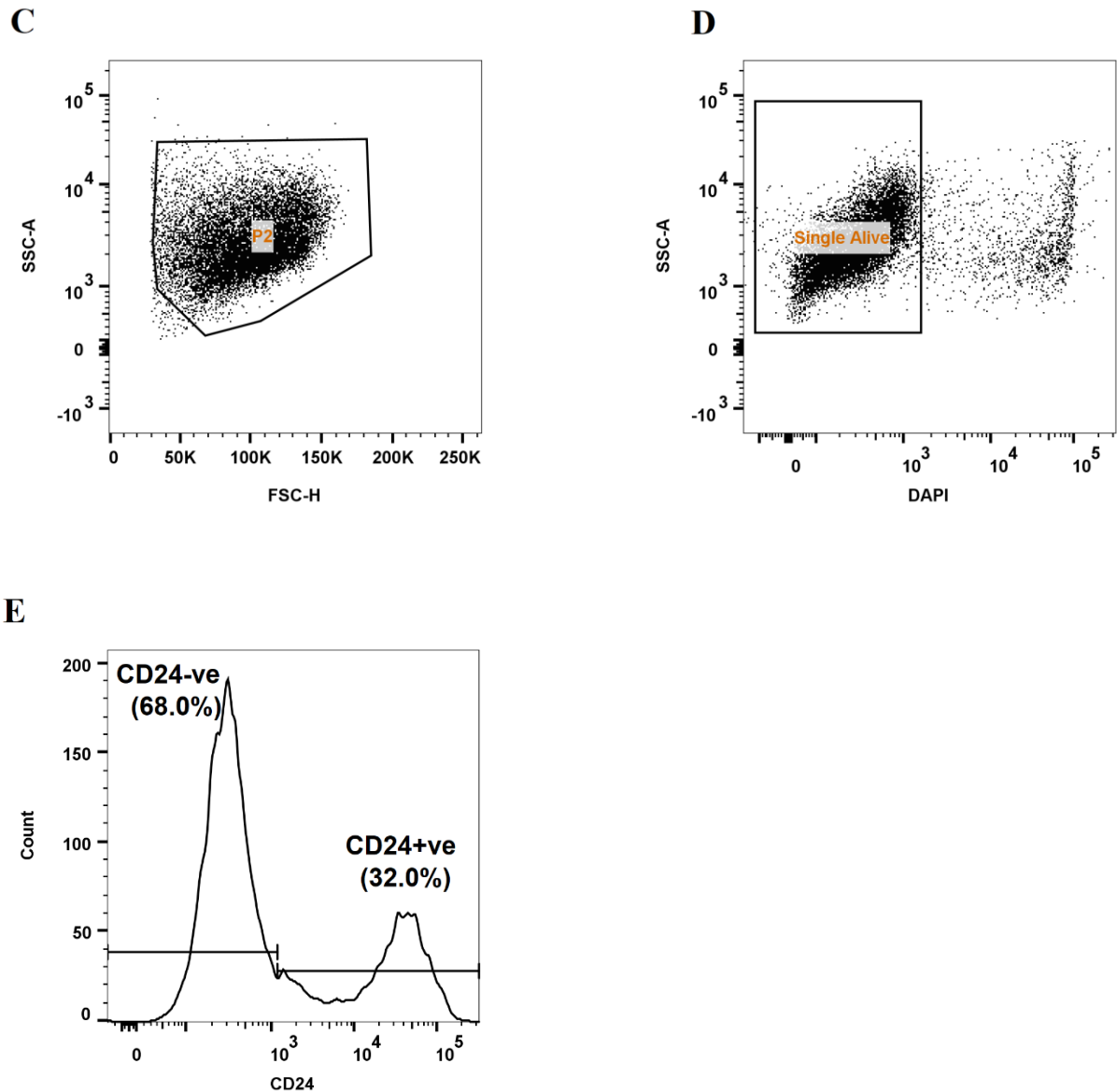


Figure 38. The flow cytometry analysis of CD24 expression of RFP⁺ primary mammary cells. (A) Dot plot used for sorting RFP⁺ cells from Rac1^{+/+} primary mammary Lineage⁻ cells. X axis, mRFP; Y axis, SSC-A; (B) Dot plot used for selecting single cells. X axis, FSC-H; Y axis, FSC-A; (C) Dot plot used for gating out cell debris. X axis, FSC-H; Y axis, SSC-A; (D) Dot plot used for gating for alive cells based on DAPI staining. X axis, DAPI; Y axis, SSC-A; (E) Representative histogram graph showing CD24 expression level distribution of the RFP⁺ cells. X axis, CD24; Y axis, Count. Data shown is representative of three independent experiments.

3.5.2 Rac1b-expressing cells consists of both epithelial and non-epithelial cells

Cytokeratin 14 (CK14) and cytokeratin 18 (CK18) are frequently used as the mammary lineage-specific markers for basal epithelial and luminal epithelial cells, respectively. Therefore, to further investigate the distinct cell types within the Rac1b-expressing subpopulation of primary mammary cells, I have performed immunofluorescence staining of Lin⁻RFP⁺ primary mammary cells for CK14 and CK18.

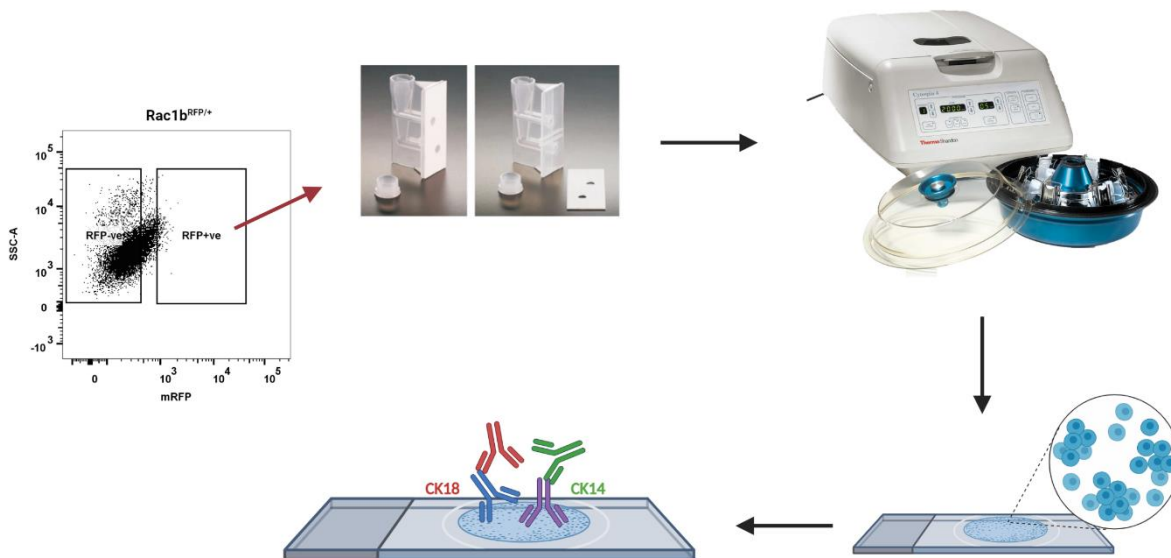


Figure 39. Schematic representation of the experimental design for the immunofluorescence staining of the cyto-spinned RFP⁺ cells sorted from $Rac1b^{RFP/+}$ mammary glands. Primary antibodies against CK14 and CK18 are shown in violet and blue, respectively; and the secondary antibodies binding to the primary antibodies are shown in green (CK14) and red (CK18), respectively.

Lin⁻RFP⁺ mammary cells were sorted by FACS from $Rac1b^{RFP/+}$ mammary glands, fixed in 4%PFA and cytopspinned onto glass slides for 10 minutes at 400 rpm (Fig. 39). Subsequently, these samples were co-stained with CK14 and CK18 (Fig. 39), and DAPI was used as a counterstain. Interestingly, a substantial fraction of these cells had either CK14 or CK18 expression, but there was only very few cells that had both CK14 and CK18 expression (the yellow cell in the merged image) (Fig. 40A).

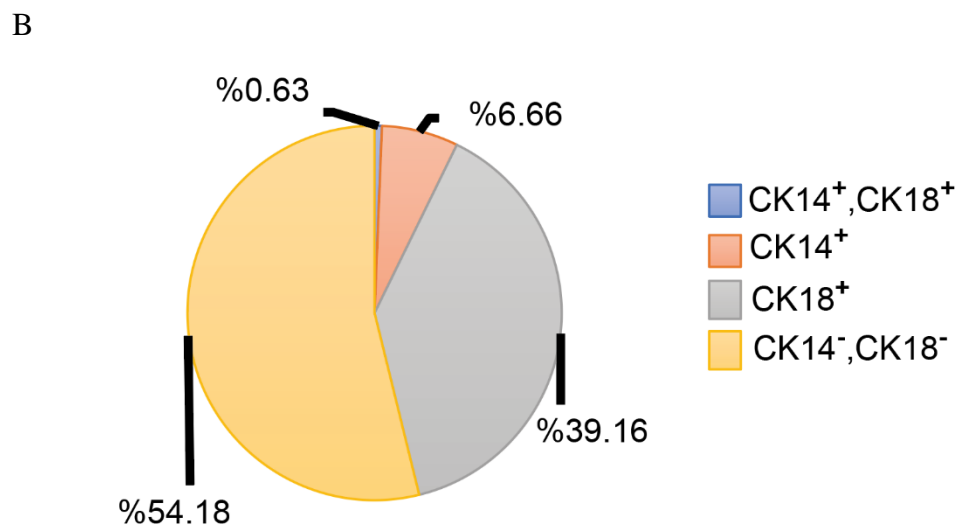
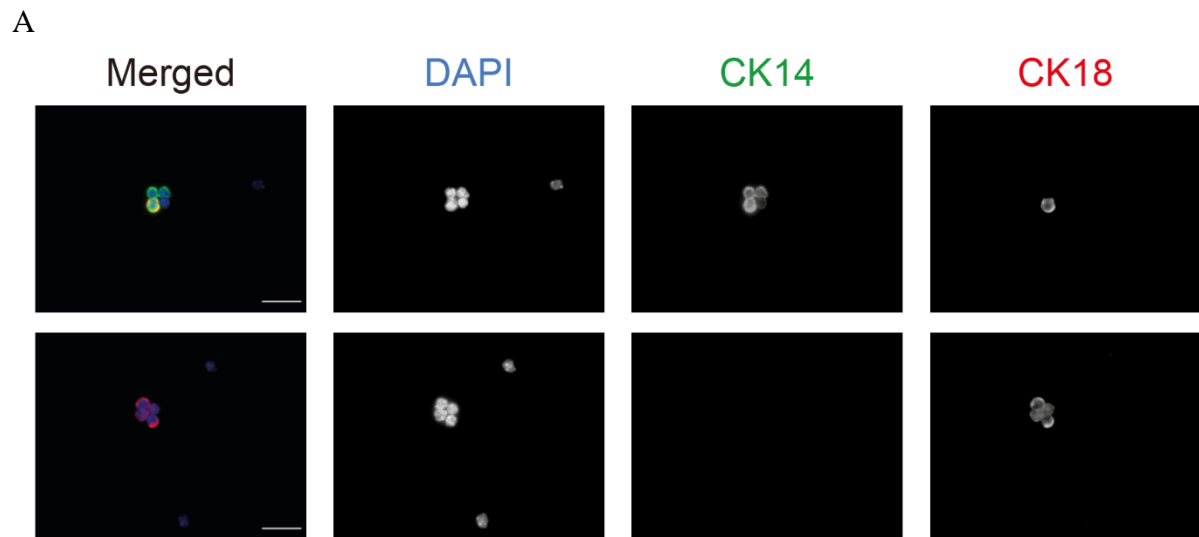


Figure 40. Immunofluorescence (IF) staining of Lin^{RFP+} cells sorted from Rac1b^{RFP/+} mammary glands for CK14 and CK18 expression. (A) Representative images for IF staining of cytopinned cells, which were imaged using the Zeiss Imager M2 fluorescent microscope under 63x objective. Blue, DAPI; Green, CK14; Red, CK18. Scale bars represent 20μm. (B) Pie chart representation of the distribution of Lin^{RFP+} cells into four groups based on their CK14 versus CK18 expression .

The quantification of cell numbers based on their CK expression pattern showed that the Lin⁻ RFP⁺ cells were composed of 4 distinct cell subtypes (Fig. 40B): basal cells (CK14-positive) representing 6.66%, luminal cells (CK18-positive) representing 39.16%, bipotent progenitors (double positive) representing 0.63% and double negative cells, which may be the non-epithelial cells, representing 54.18%.

Taken together, both the immunofluorescence staining data and the flow cytometry analysis of CD24 expression as described in the previous subsection suggest that a large proportion of the Rac1b-expressing cell populations in mammary glands does not express well-known mammary epithelial markers, and thus may include either mesenchymal cells or mesenchyme like mammary epithelial cells. Nevertheless, the Rac1b-expressing subpopulation of mammary epithelial cells also contain basal epithelial and luminal epithelial cells.

3.6 Results - Rac1b is expressed by a substantial subset of sphere-forming mammary cells

3.6.1 Rac1b expression marks a large subset of sphere-forming cells in the mammary gland

RFP expression serving as a surrogate reporter for Rac1b expression in the Rac1b^{T2A-RFP} mouse line allows us to isolate and study the Rac1b-expressing cells in the mammary glands. FACS analysis of primary mammary cells isolated from 8-weeks old nulliparous mammary glands of Rac1b^{RFP/+} mice demonstrated that the RFP⁺ (Rac1b-expressing) cells account for a small population (from 0.4 to 1.7 percent) of the single alive lineage (CD31, TER119, CD45)-negative cells (Fig. 41).

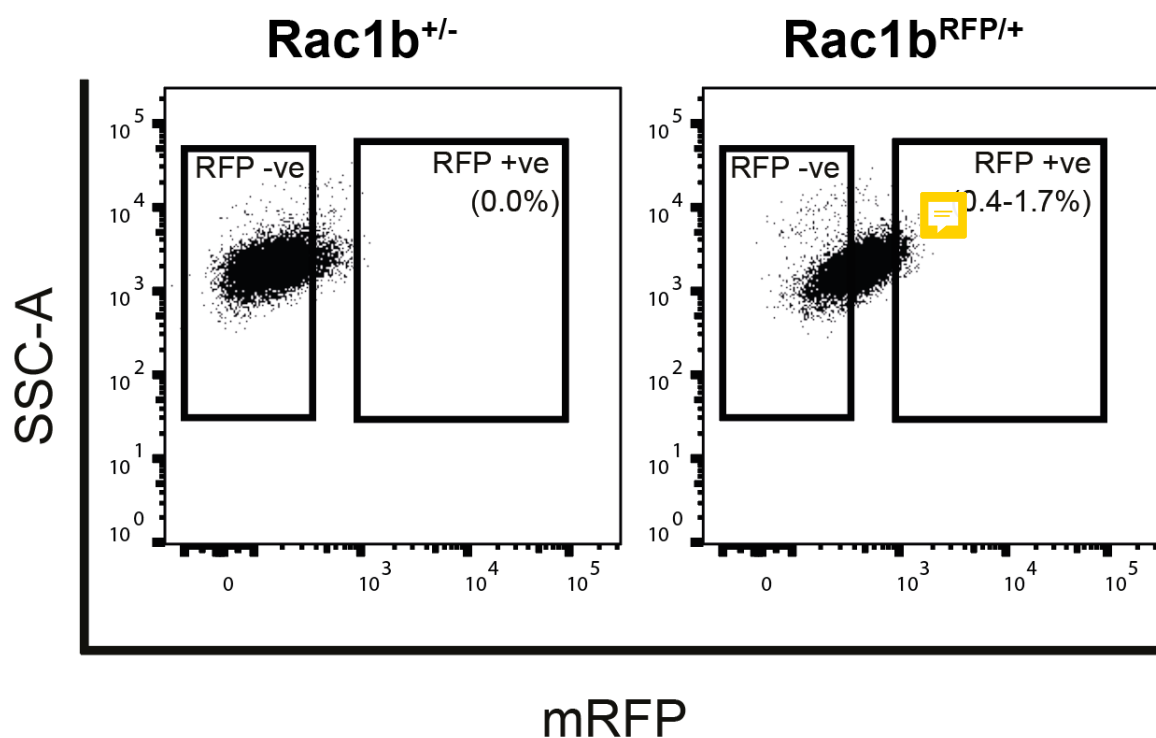


Figure 41. Representative FACS plots used for sorting RFP⁺ and RFP⁻ cells. Dead cells were excluded based on their staining with DAPI, and the lineage-positive cells labelled by CD31, CD45 and Ter119 antibodies were also excluded from the single alive cells as described in Figure 35. The gate for RFP-positive cells was set based on the fluorescence signal levels in the Rac1b^{+/+} or ^{+/-} cells (the left plot), which should not be expressing RFP protein. X axis, RFP fluorescence; Y axis, SSC-A.

Next, I have performed mammosphere assay for the sorted RFP⁺ and RFP⁻ cell populations to investigate whether Rac1b is expressed in the stem cell populations. Interestingly, the results showed that the spheres could be formed by both RFP⁺ and RFP⁻ cell fractions (Fig. 42), indicating that both populations contained stem cells. However, it is notable that the stem cell frequency for these two populations were different. The RFP⁺ cell population was able to form proper solid spheres even when 100 cells were seeded in each well of the 96-well plate (Fig.

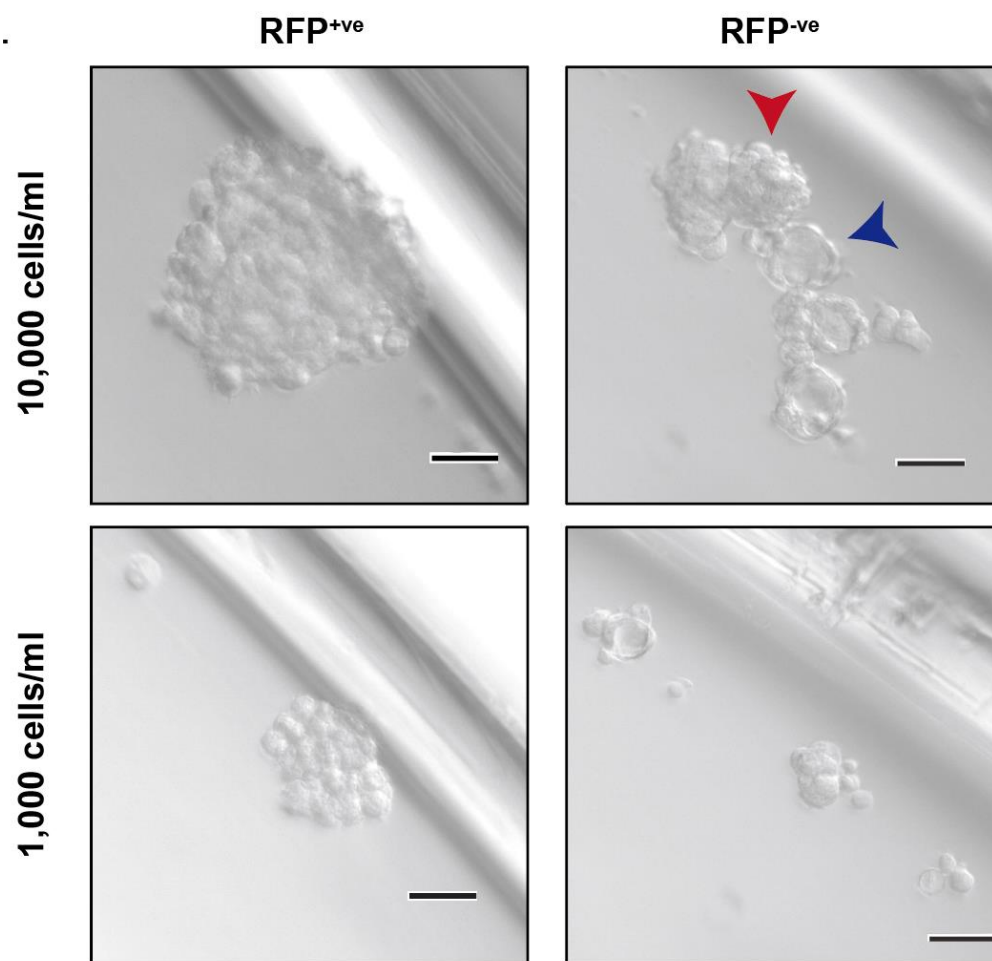


Figure 42. Representative images of mammosphere structures formed by RFP⁺ and RFP⁻ cell fractions isolated from Rac1b^{RFP/+} mammary glands. One thousand or ten thousand cells per millilitre were seeded into the 96-well plate. Images are representative of 6 independent experiments Scale bars represent 50µm.

42). The larger size spheres were formed when 1000 RFP⁺ cells were plated in each well due to the merge of several normal spheres. Comparatively, for the RFP⁻ population, cells were not able to form spheres (i.e. >50µm diameter) at the 100 cells/well concentration. However, at the concentration of 1000 cells/well RFP⁻ population of cells had also formed spheres properly. Additionally, there were some acini structures formed by the RFP⁻ cells, suggesting that the luminal progenitors reside within the RFP⁻ population, thus are not expressing Rac1b (Fig. 42). Quantification of mammosphere-forming efficiencies (MFE) revealed that RFP⁺ cells had an approximately 1.5% MFE, whereas RFP⁻ cells had 0.24 % MFE (Fig. 43). Thus, the frequency of sphere-forming cells in RFP⁺ populations are around 6 times higher than the frequency in the RFP⁻ cell populations, indicating that the Rac1b is expressed by a substantial subset of sphere-forming cell populations in the mammary gland.

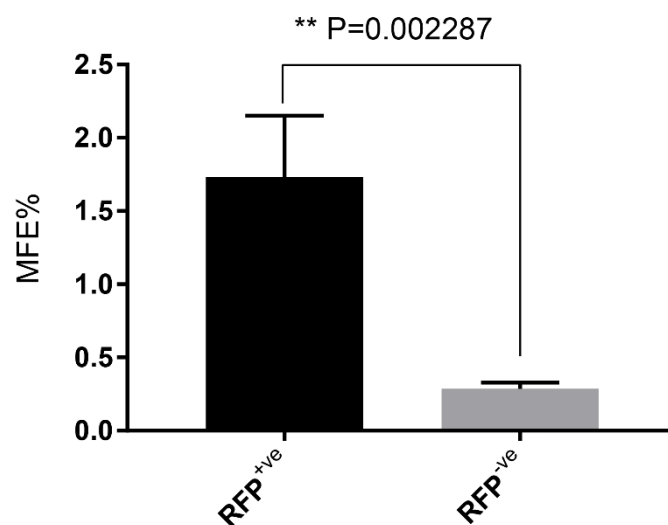
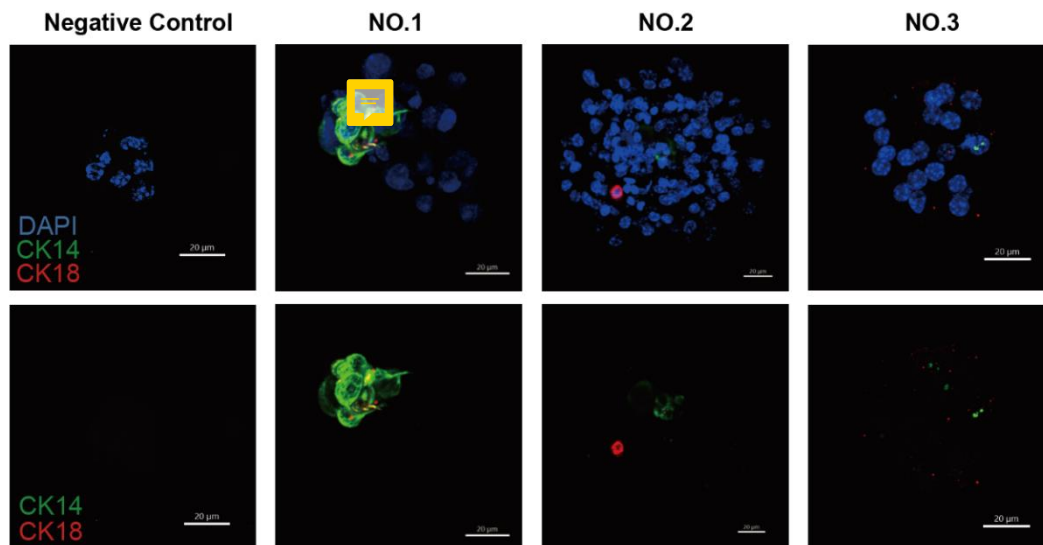


Figure 43. Quantification results for mammosphere assay of RFP⁺ versus RFP⁻ cells isolated from the Rac1b^{RFP/+} nulliparous mammary glands. The number of spheres were quantified at 100 cells/well and 1000 cells/well for RFP⁺ populations and RFP⁻ cell fractions, respectively. Values represent mean±SD of 6 animals. ** P=0.0023 < 0.05, paired t test.

3.6.2 Characterisation of the Rac1b-expressing sphere-forming cells

As described in Section 3.8.1, Rac1b-expressing cells are capable of forming solid sphere structures in mammosphere culture. I further investigated the epithelial characteristics of the RFP⁺ cell-driven spheres by performing immunofluorescence staining of those structures for the epithelial cell markers CK14 and CK18 (Fig. 44). Most of the spheres formed by the RFP⁺ cells did not have any CK14 or CK18-expressing cells (Fig. 44A). However, there were still some spheres that contained cells expressing CK14 and/or CK18 (Fig. 44A NO.1; Fig. 44B). These results indicate that there may be a heterogeneity within the Rac1b-expressing sphere-forming cell population that contains two types of sphere-forming cells resembling either the basal mammary epithelial or double-negative population of primary mammary cells as described in Section 3.2.4.

A



B

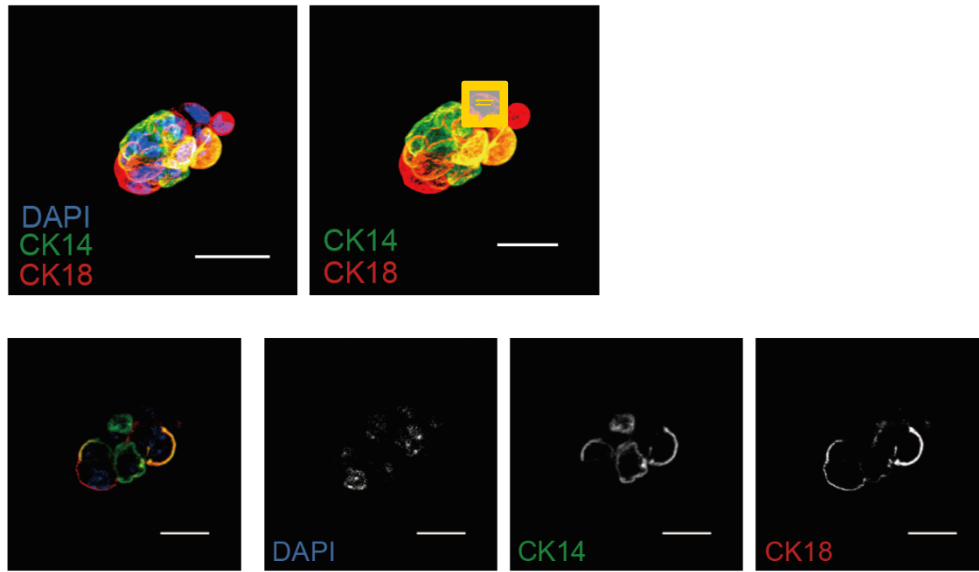


Figure 44. Representative images for immunofluorescence staining of spheres formed by the RFP⁺ cells isolated from Rac1b^{RFP/+} nulliparous mammary glands (A) Deconvoluted confocal images of the negative control (left) and three spheres with (upper) and without (lower) DAPI staining shown. (B) Confocal images of a RFP⁺ cell-driven sphere showing the cytokeratin-expressing cells. Upper panels: Deconvoluted confocal images with (left panel) and without (right panel) DAPI staining shown. Lower panels: a selected slice of the Z stack in the middle of the spheres shown as merged or single colours of DAPI, CK14 and CK18 staining. Data is representative of three independent experiments. Blue, DAPI; Green, CK14; Red, CK18. The confocal images were taken with Leica SP8 Upright dipping lens Confocal microscope with 63x objective. Scale bars represent 20μm.

3.6.3 Loss of Rac1b function does not alter the stem cell frequency in neither the RFP+ nor the RFP- cell fractions

To elucidate whether the Rac1b deficiency would alter the distribution of Rac1b-expressing cell fractions, the single alive lineage-negative cells from Rac1b^{RFP/+} and Rac1b^{RFP/-} mammary glands were compared for their RFP-expressing cell populations (Fig. 45). In the Rac1b-deficient (i.e. Rac1b^{RFP/-}) mammary glands, the frequency of RFP⁺ cells were between 0.6% to 4.0%. This is similar to the frequency of RFP⁺ cells seen in the Rac1b-proficient (i.e. Rac1b^{RFP/+}) mammary glands, which was between 0.6%-4.2%.

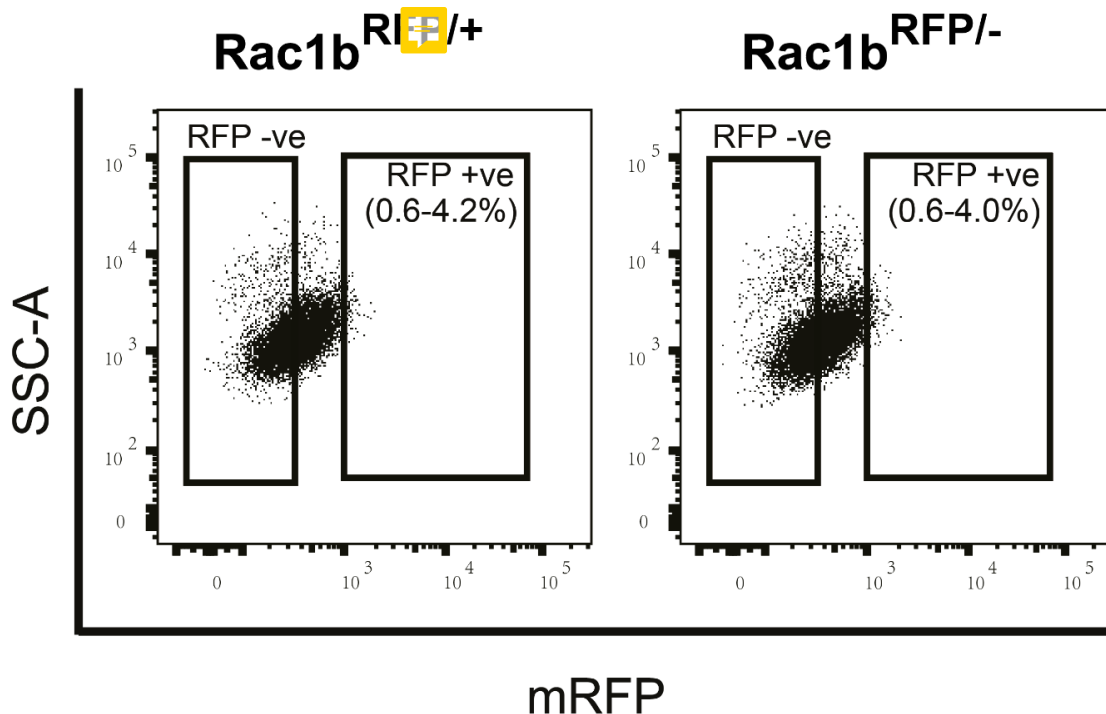


Figure 45. Representative dot plots of flow cytometry used for sorting RFP⁺ and RFP⁻ cells from 8-weeks-old nulliparous Rac1b^{RFP/+} and Rac1b^{RFP/-} mammary glands. Dead cells were excluded based on their staining with DAPI, and the lineage-positive cells, labelled with CD31, CD45 and Ter119 antibodies, were also excluded from the single alive cells as described in Figure 35. The gate for RFP-positive cells was set according to the fluorescence signal level for the Rac1b^{+/+} or ^{-/-} cells (as shown in Figure 41), which should not have RFP expression. Dot plots shown are representative of 6 mice per genotype. X axis, RFP fluorescence; Y axis, SSC-A.

Next, I investigated whether Rac1b function is essential for maintaining the stem cell frequency within either the RFP⁺ or RFP⁻ cell subpopulations. To achieve this purpose, the RFP⁺ and RFP⁻ cells were sorted from the single alive lineage-negative primary cells isolated from Rac1b^{RFP/+} and Rac1b^{RFP/-} nulliparous mammary glands (Fig. 45) and plated in the mammosphere culture. The quantification results showed that the mean value of MFE is slightly lower in both RFP⁺ and RFP⁻ cell fractions of Rac1b^{RFP/-} mammary cells compared with the same cell fractions of Rac1b^{RFP/+} mammary cells (Fig. 46). However, the statistical test results indicated that the P values for both comparisons are higher than 0.05, suggesting that there is no significant difference in the stem cell frequency within either the RFP⁺ or the RFP⁻ cell fractions between Rac1b^{RFP/+} and Rac1b^{RFP/-} mammary cells (Fig. 46).

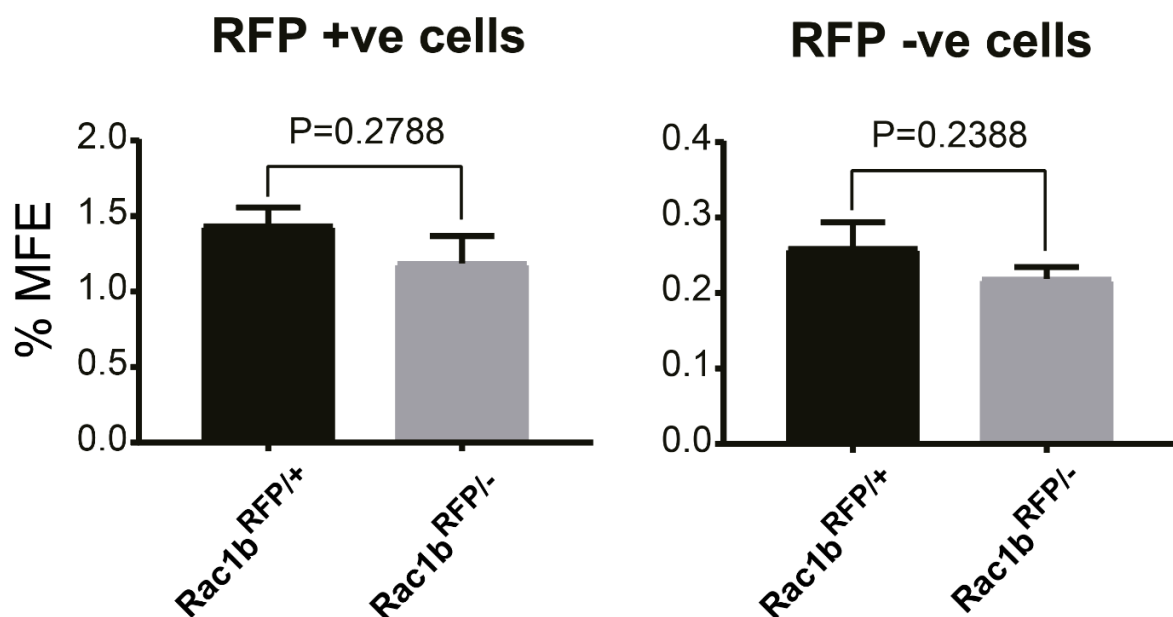


Figure 46. Mammosphere forming efficiency (%MFE) of RFP⁺ (left panel) and RFP⁻ (right panel) cell populations sorted from 8-week-old nulliparous Rac1b^{RFP/+} and Rac1b^{RFP/-} mammary glands as shown in Figure 45. One thousand or ten thousand cells from RFP⁺ and RFP⁻ cell populations, respectively, were seeded per millilitre into the 96-well plate. Values represent the mean \pm SEM of 4 animals, and the mean is 1.44% and 1.19% for RFP⁺ populations and 0.26% and 0.22% for RFP⁻ populations. P values obtained by the paired t-test are shown on the graphs.

3.7 Discussion

3.7.1 Rac1b function is dispensable for mammary gland development

According to literature, Rac1 has various crucial functions during different stages of mammary gland development. The *in vitro* experiments suggest that Rac1-deficiency impairs ductal elongation during pubertal development stage (Ewald et al., 2008; Zhu & Nelson, 2013), and the formation of alveolar structures and milk production during lactation stage (Akhtar et al., 2016). The *in vivo* experiments confirmed that genetic deletion of Rac1 prevents the apoptotic alveolar cells shedding into the lumen and inhibits the clearance of cell debris, which then delays tissue remodelling during the involution stage of mammary gland development (Akhtar et al., 2016; Bagci et al., 2014). However, in these loss of Rac1 function studies it was not only Rac1 but also Rac1b that had been knocked out simultaneously. Therefore, it is still unclear whether these observed phenotypes are due to the loss of Rac1 function and/or Rac1b function. Accordingly, one of this project's aims has been to reveal the Rac1b-specific indispensable functions during different stages of mammary gland development.

First, the Rac1b-knockout mouse model, which specifically lacks exon3b sequence and thus only the Rac1b isoform, has been used for the investigation of Rac1b functions in mammary gland development. The whole-mount Carmine-Alum staining data demonstrated that the loss of Rac1b function does not alter the ductal branching and elongation or the formation of tertiary ducts during pubertal stage; the formation of alveolar buds and lobuloalveolar structures at pregnancy; the milk production and secretion during lactation; and cell apoptosis and clearance and tissue remodelling during involution stages at a macroscopic level. Besides, the haematoxylin and eosin staining of the tissue sections at different involution stages confirmed that Rac1b function is dispensable for the tissue remodelling during involution stages of mammary gland development also at the histological level. Furthermore, the FACS analysis of the primary cells isolated from nulliparous Rac1b^{+/+}, Rac1b^{+/-} and Rac1b^{-/-}

mammary glands revealed that the loss of Rac1b function does not impair mammary epithelial cell lineage distribution in either FVB or C57BL6 backgrounds. In conclusion, unlike Rac1, its splice variant Rac1b is dispensable for normal mammary gland development *in vivo*, and thus the mammary gland phenotypes described in the literature for the genetic deletion of *Rac1* are not due to the absence of its Rac1 isoform.


Olabi and colleagues (2018) showed that Rac1 is required for the maintenance of MaSCs using an *ex vivo* 3D organoid formation assay. In this project, I performed mammosphere assay for the basal, luminal and DN cells isolated from Rac1b^{+/+} and Rac1b-null mammary glands to assess the potential loss of Rac1b function phenotypes for MaSCs. As expected, basal epithelial cell subpopulation, which is widely believed to contain MaSCs, formed solid mammospheres. The immunofluorescence staining data showed that these mammospheres contain CK14⁺ cells in their outer peripheries. Rac1b-null basal epithelial cells also gave rise to mammospheres with similar morphology to those that are formed by the wild-type basal epithelial cells. The quantification results indicated that Rac1b-null basal cells have a slightly, but not significantly, less mammosphere-forming efficiency compared with the wildtype basal cells. For both genotypes luminal epithelial cell population was capable of forming acini, the hollow structures formed by the luminal progenitors. Notably, the luminal cell population was also capable of forming some solid spheres. The immunofluorescence staining results show that both the acini and the solid spheres formed by the luminal epithelial population were composed of CK14⁺, CK18⁺ and CK14⁺CK18⁺ cells, which is different from the basal spheres. The histological location of MaSCs in the mammary gland still remains controversial. Previously, it has been believed that the MaSCs are all located at the basal layer, but not luminal layer based on the results obtained via cleared-fat pad transplantation assay of sorted cells (Shackleton et al., 2006b; Sleeman et al., 2007; Stingl et al., 2006). However, recently the results of lineage-tracing experiments suggested that there might be some bipotent MaSCs located at luminal

compartments in addition to those found at the basal compartments (Davis et al., 2016; Scheele et al., 2017; van Amerongen et al., 2012; van Keymeulen et al., 2011).

Interestingly, the DN (CD24⁻CD49f⁻) cell fractions were also able to form ‘grape-like’ spheres, morphologically resembling the sphere structures formed by basal breast cancer cell lines. However, these spheres formed by DN cells were composed of only the CK14⁻CK18⁻ cells. The DN cells are widely believed to be composed of mesenchymal cells, such as mammary fibroblasts. However, the flow cytometry analysis of the primary spheres formed by the DN cell fractions showed that some of the cells within these spheres express the epithelial marker CD24, suggesting that the sphere-forming DN cells may give rise to epithelial cells. If this is true, then it is possible that these epithelial cells may express other cytokeratins rather than CK14 or CK18, which requires further research studies. Furthermore, mammospheres formed by the basal mammary epithelial population consisted of approximately 13.9% CD24⁻CD49f⁻ cells, suggesting that the mammary epithelial cells within basal epithelial compartment may also give rise to DN cells. Collectively, this can suggest that the CD24^{low}CD49f^{high} MaSCs and the CD24⁻CD49f⁻ stem cells may be able to transit into each other, at least during the mammosphere culture environment. More research would be needed in future to address further questions, such as what these transited cells are and what triggers the transition of these cells, or whether this stem cell transition represents a stem cell plasticity of being a quiescent versus proliferative MaSC states. Recently, several studies have suggested that the MaSC pool is composed of both proliferative and quiescent stem cells, which are able to transit into each other to promote normal mammary gland development and maintain the homeostasis of mammary tissues (Boras-Granic et al., 2014; Cai et al., 2017; Fu et al., 2017; Fu et al., 2018; Lloyd-Lewis et al., 2017). Whether the quiescent MaSCs are located at the CD24⁻CD49f⁻ compartment still needs to be further verified by cleared-fat pad transplantation assay. Nevertheless, the mammosphere assay results revealed that the loss of Rac1b function does not

significantly alter the stem cell frequency of the CD24⁺CD49f⁺ population, too. Collectively, we have concluded that the Rac1b-deficiency does not alter the stem cell frequencies in either CD24^{low}CD49f^{high} or CD24⁺CD49f⁺ fractions. Therefore, the phenotypic impairment in MaSC maintenance observed previously for the genetic deletion of Rac1, is due to the loss of Rac1, but not Rac1b, function.

3.7.2 The generation of Rac1bT2ARFP knock-in transgenic mouse model



Rac1 is ubiquitously expressed in almost all cell types in the mammary gland, whereas Rac1b is  considered to have a more restricted expression. However, due to the lack of specific antibodies against mouse Rac1b protein, it has been difficult to identify exactly which cell types express the Rac1b isoform. In this project, I have generated a novel Rac1b^{T2ARFP} knock-in mouse model by using CRISPR/Cas9 method, in which the mRFP expression serves as the surrogate reporter for Rac1b expression. To our knowledge this is the first of its kind as a knock-in transgenic mouse line with a surrogate reporter activity for an internally spliced gene variant.

The CRISPR strategy was optimised using the Eph4 murine mammary epithelial cell line. I have used CRISPR/Cas9 Double nickase approach to generate three independent single-cell clones of Eph4 that specifically lack Rac1b expression without interfering with Rac1 expression. Sequencing results for the targeted genomic locus in these clones demonstrated that each allele within each clone has acquired different InDel mutations. This was expected since the NHEJ-mediated repair of introduced double strand DNA breaks would lead to random InDel mutations. Most of these InDels were identified to cause frameshift mutations, leading to the disruption of normal protein synthesis of Rac1b. Surprisingly, these InDel mutations have also interfered with the normal splicing of the exon3b, as I was not able to detect an mRNA transcript for the modified alleles of Rac1b. Interestingly, a similar observation was

previously made by our group when exon3b of *Rac1* genomic locus had been targeted by CRISPR in human breast cancer cell lines, MCF7 and T47D. These observations suggest that there may be splicing regulatory sequences present within the exon3b-coding sequence and thus the InDel mutations that are disrupting these regulatory sequences may hamper the proper splicing of exon3b. However, the western blot analysis of Rac1b-null Eph4 clones demonstrated that Rac1 expression was not affected by these introduced mutations, indicating that any effect caused in splicing of exon3b does not impair the proper Rac1 splicing.

For the knock-in of the T2A-RFP cassette into the exon3b to serve as a surrogate reporter of Rac1b expression, it is essential that this genetic modification should not alter the proper Rac1b splicing. Given the possible existence of splicing regulatory sequences within the exon3b-coding sequence, I have designed three different HDR templates aiming to insert the ‘T2A-RFP’ cassette at one of the three different locations within the exon3b of the *Rac1* genomic locus. Importantly, none of these HDR templates would replace any part of the exon3b sequence, but rather insert the T2A-RFP cassette within the existing sequence that would correctly align with the open-reading frame of the Rac1b-coding sequence. After the co-transfection of Eph4 cells with CRISPR targeting constructs and HDR templates, I have obtained several single cell clones for each individual strategy of HDR templates as confirmed by genotyping at the genomic DNA level. However, the flow cytometry analysis of these clones demonstrated that the strategy C of the HDR template, which inserts the T2A-RFP cassette close to the 3’-end of the exon3b, resulted in cells that were not expressing mRFP. This is likely to be due to the potential impairment of proper Rac1b splicing when the 3’-end of the exon3b was altered by the knock-in of the T2A-RFP cassette. In contrast the single-cell clones generated by the HDR templates that targets the insertion close to the 5’end of exon3b (strategy A) or in the middle of exon3b (strategy B) were able to express mRFP. Furthermore, the western blot results indicated that Rac1 is expressed normally in these successful Rac1b^{T2A-RFP}

knock-in transgenic Eph4 clones A15 and B11. Therefore, we have decided that either of the HDR template option A or B can be used for generating the $\text{Rac1b}^{\text{T2A-RFP}}$ knock-in transgenic mouse line.

By using the optimised sgRNA constructs and the strategy B option of HDR templates, I have then generated the $\text{Rac1b}^{\text{T2A-RFP}}$ transgenic mouse line in pure FVB background.  We have obtained 11 founder mice after the implantation of the microinjected single-cell embryos, but only one of them had acquired the correct knock-in insertion of the 'T2ARFP' cassette in the *Rac1* genomic locus. In order to verify whether RFP expression can indeed serve as the surrogate reporter for Rac1b expression in this mouse line, I have sorted RFP^+ and RFP^- cell subpopulations of primary cells isolated from the $\text{Rac1b}^{\text{RFP/+}}$ heterozygous nulliparous mammary glands. RNA samples isolated from these sorted cells were then analysed by RT-PCR, which clearly indicated that Rac1b mRNA was only detectable in the RFP^+ cells, confirming the surrogate reporter ability of RFP expression for Rac1b splicing in the $\text{Rac1b}^{\text{T2ARFP}}$ transgenic mouse model. .

3.7.3 The characterization of Rac1b-expressing RFP^+ cells in nulliparous mammary glands

FACS analyses of the $\text{Rac1b}^{\text{T2A-RFP}}$ knock-in transgenic mammary glands showed that Rac1b is expressed in a small sub-population of primary mammary cells. To further characterise the Rac1b-expressing RFP^+ cells, I have analysed these cells for the expression of CD24, a widely accepted marker of epithelial lineage in the mammary gland. The flow cytometry data showed that 2/3 of the RFP^+ cells are CD24^- cells and 1/3 of the RFP^+ cells are CD24^+ cells, indicating that the Rac1b-expressing mammary cells are predominantly DN cells rather than epithelial cells. This result is also consistent with the CK14/CK18 immunofluorescence staining result for the RFP^+ cells, which showed that more than half of the RFP^+ cells are $\text{CK14}^- \text{CK18}^-$ cells.

Taken together, these results suggested that the Rac1b-expressing cells are mostly DN cells rather than the CK14- or CK-18 expressing mammary epithelial cells.

Nevertheless, the results of the mammosphere assay has revealed that both RFP⁺ and RFP⁻ cells can form spheres, though the mammosphere-forming efficiency (MFE) of RFP⁺ cells is almost 6 times higher than the MFE of RFP⁻ cells. Unsurprisingly, the immunofluorescence staining of these spheres showed that most of the spheres formed by the RFP⁺ cells are composed of cells that does not express CK14 or CK18, and thus resemble to the spheres formed by the DN (CD24⁻CD49f⁻) subpopulation of cells within the mammary gland. However, it is important to note that there was also a small number of spheres formed by the RFP⁺ cells that has CK14- and CK18-expressing cells.

To better understand whether the Rac1b function is required by these sphere-forming cells, I have analysed the MFE of both RFP⁺ and RFP⁻ cells isolated from the Rac1b-proficient Rac1b^{RFP/+} and Rac1b-null Rac1b^{RFP/-} nulliparous mammary glands. The quantification results showed that the Rac1b-deficiency does not significantly influence the MFE in either Rac1b-expressing or non Rac1b-expressing cell subpopulations.

In conclusion, unlike Rac1, the functions of Rac1b in normal mammary gland development is dispensable. An interesting finding in this part is the potential transition between CD24^{low}CD49f^{high} and CD24⁻CD49f⁻ cells, both of which can form spheres in the mammosphere culture. Interestingly, Rac1b-expressing cells contain sphere-forming cells that can form both types of spheres, though it is predominantly the type that is formed by the CD24⁻CD49f⁻ cells. Therefore, it would be necessary to further study in future the potential roles of Rac1b in the transition between these two distinct subsets of sphere forming mammary cells.

CHAPTER 4. Results Part II Rac1b is required for maintaining BCSCs and chemoresistance of breast tumour cells

4.1 Introduction

4.1.1 The subtypes of breast cancer and their conventional treatments

Breast cancer is the most common disease in women all around the world. There are 2.1 million new cases of breast cancer diagnosed in 2018 worldwide. In the UK, ~55,200 women are diagnosed with breast cancer every year, and approximately 1 in 7 women would be developing breast cancer during their lifetime. Breast cancer is a heterogeneous disease. There are four major subtypes of breast cancer based on the expression of hormone receptors (ER or PR, oestrogen or progesterone receptor), and human epidermal growth factor receptor 2 (HER2). The hormone receptor-positive subtypes (Luminal-A and Luminal-B) express ER with or without PR and HER2. Another subtype is known as HER2-positive (HER2+) breast cancer, which has a gene amplification and/or overexpression of HER2 and do not express ER or PR. The subtype that is negative for ER, PR and HER2 is referred to as triple negative breast cancer (TNBC). For different types of breast cancer, various therapeutic approaches are being developed including radiotherapy, chemotherapy, immunotherapy, and hormonal therapies.

Approximately 60% of diagnosed cases of breast cancer belongs to the hormone receptor-positive subtypes. Based on the expression levels of Ki67, the hormone receptor-positive breast cancer can be further categorised as luminal A (low Ki67) or luminal B (high Ki67). Some of the luminal breast cancers also overexpress HER2. Hormonal therapy is the most common treatment strategy used for hormone receptor-positive breast cancers aiming to interfere with the ER signalling pathway to prevent tumour cell growth (Patel & Bihani, 2018). There are different options to inhibit ER signalling pathway: 1) aromatase inhibitors (AIs) are able to prevent the production of oestrogen hormone; 2) the selective oestrogen receptor modulators

(SERM) bind to ER molecules to form an inactive complex; 3) the selective oestrogen receptor degraders (SERD) bind to ER to trigger its degradation. Tamoxifen, a SERM, is a gold standard for the treatment of hormone receptor-positive breast cancer, which dramatically decreases the mortality rate approximately for 30% (Day et al., 2020). It is documented that the use of Tamoxifen as an adjuvant therapy in ER-positive breast cancer patients improves the 10-year survival rate at about 50% (Day et al., 2020). Nevertheless, the number of deaths caused by ER-positive breast cancer is still higher than HER2-positive or triple negative breast cancer-induced deaths due to the tumour recurrence and therapy resistance (Clarke et al., 2015). The molecular mechanisms of how ER-positive cancer cells can escape from the effects of hormonal treatment is still not well understood.

HER2+ subtype accounts for approximately 20% of all breast cancers. HER2, encoded by *ErbB2*, is a member of human epidermal growth factor receptor family that also contains HER1 (EGFR), HER3 and HER4. HER2 regulates cell proliferation, apoptosis and migration mainly through PI3K/AKT and MAPK pathways in breast cancer. The EGFR/HER family members are transmembrane receptor tyrosine kinases, which contain similar intracellular tyrosine kinase domains, but distinct extracellular ligand-binding domains. HER1 can be activated by binding to epidermal growth factor and transforming growth factor α . In contrast, there is no known ligand that can bind to HER2 and thus it is activated via forming heterodimers with other activated EGFR members.

Trastuzumab (Herceptin) is the most commonly used therapeutic agent for HER2-overexpressed breast cancer, which is a humanized monoclonal antibody specifically recognising the extracellular domain of HER2 receptor (Ahmed et al., 2015). Trastuzumab may exert its effects on cancer cells through multiple mechanisms, though they are probably not fully understood. Trastuzumab treatment can prevent the HER2 cleavage, leading to the failure of the extracellular domain being released, which consequently suppresses HER2-related



pathways (Molina et al., 2001). It is also shown that trastuzumab treatment prevents the ligand-independent dimerization between HER2 and HER3, which consequently downregulates the activation of PI3K signalling pathway (Junttila et al., 2009). Additionally, there are some evidence showing that trastuzumab treatment may induce antibody-dependent cellular cytotoxicity (ADCC) to trigger immune responses (Arnould et al., 2006). Trastuzumab is often used as an agent in combo treatments together with other drugs such as chemotherapy or other targeted therapies (Arnould et al., 2006). The combination of trastuzumab with chemotherapy has been a standard of care for HER2-overexpressing breast cancers (Junttila et al., 2009).



Another humanized monoclonal antibody used in clinics is pertuzumab, which targets the extracellular domain II of HER2 protein. Compared with trastuzumab, pertuzumab treatment can inhibit the ligand-dependent interaction between HER2 and HER3 (Ahmed et al., 2015). In addition to these monoclonal antibody treatments, Ado-trastuzumab emtansine (T-DM1), an antibody-drug conjugate, is also used for the treatment of metastatic HER2+ breast cancers as a secondary line. T-DM1 is composed of trastuzumab linked to the cytotoxic agent DM1 that induces mitotic arrest and apoptosis (Ahmed et al., 2015; Barok et al., 2014).

Furthermore, the orally-administered tyrosine kinase inhibitors (TKIs) are also effective therapeutic approaches for HER2+ breast cancer as a targeted therapy. Bearing a similar structure to ATP molecules, the TKIs can bind to the intracellular tyrosine kinase domain of the EGFR family members in a competitive fashion. This binding prevents the autophosphorylation of EGFR family of receptor proteins, resulting in the blockade of their downstream signalling especially MAPK and PI3K/AKT pathways (Xuhong et al., 2019). Lapatinib functions as a TKI to reversibly inhibit both HER1 and HER2 by preventing the ATP molecules binding to their intracellular kinase domains. Lapatinib treatment was shown to affect the cell proliferation, apoptosis and migration. On the other hand, neratinib and pyrotinib are irreversible inhibitors that target the ATP-binding domains of HER1, HER2 and HER4.

These TKIs have been currently tested in a combo-treatment setting with trastuzumab to improve the therapeutic outcomes for HER2-overexpressing breast cancer patients (Ahmed et al., 2015; Xuhong et al., 2019).

TNBCs represent 10-20% of all diagnosed breast cancers and are highly aggressive with high levels of recurrence (Yin et al., 2020). Approximately 46% of TNBC patients will develop metastasis. Moreover, the TNBCs can develop metastases faster, which occurs within 19-40 months after diagnosis, compared with the other subtypes of breast cancers that require 35-67 months post-diagnosis. Unlike the hormone receptor-positive and HER2-positive breast cancers, there are still no targeted therapies for TNBC. Therefore, the adjuvant and neoadjuvant chemotherapy are commonly used as treatment options for TNBC patients. However, a large fraction of TNBCs are known to quickly acquire resistance to the chemotherapy, leading to a high recurrence rate 1 year after treatment (Barzaman et al., 2020).

Over the past decade, some studies provided a further understanding of TNBCs to better classify them based on their gene expression profiles. Lehmann and colleagues (2011) subdivided TNBCs into 6 subtypes, including basal-like 1 (BL1), basal-like 2 (BL2), mesenchymal (M), mesenchymal stem-like (MSL), immunomodulatory (IM), and luminal androgen-receptor (LAR) breast cancers, through analysing gene expression profile of 587 TNBCs. They also demonstrated that these 6 subtypes had their own unique gene expression profiles, which provided the basis of developing more precise therapies for TNBCs. BL1 and BL2 subtypes have higher expression levels of cell cycle and DNA repair-related genes, indicating that taxanes (antimitotic agents) could be the choice of treatment for these TNBC subtypes. Additionally, several signalling pathways (e.g. EGFR, and Wnt) were shown to be abnormally activated in BL2 breast cancer, suggesting that growth factor inhibitors could probably be useful as a novel therapy. The signalling pathways regulating cell motility are highly activated in the M and MSL subtypes, suggesting the need of a potential therapeutic

approach targeting the EMT (Epithelial Mesenchymal Transition)-related genes. Interestingly, the MSL tumours also express high levels of mesenchymal stem cell markers. In the IM subtype of TNBCs, genes related to immune responses were shown to be highly expressed, thus suggesting that immune checkpoint inhibitors might potentially be a useful therapy. The LAR subtype is the most distinct subtype of TNBCs, which has high levels of androgen receptor expression. Similar to the hormone receptor-positive breast cancers, the hormone therapy can probably be used to treat patients with LAR subtype of breast cancer in the future. In a more recent study, Burstein et al. (2015) performed an analysis of 198 TNBC samples and consequently identified 4 TNBC subtypes: LAR, M, BLIS (Basal-like immunosuppressed), BLIA (Basal-like immune-activated). It is likely that further ongoing studies will shed more light on different subtypes of TNBCs, which may help to develop more precise future therapies for patients with TNBC.

Although various therapies have been discovered in the last decades that improves the prognosis for patients with breast cancer, the therapy resistance and tumour metastasis still remain as big challenges in clinics. Systemic chemotherapy is used for the treatment of almost all subtypes of breast cancers either alone or together with other targeted therapies. Thus, there is still an unmet need to identify new therapies that may improve the treatment outcomes of chemotherapies, as well as other targeted treatment options. To this end, understanding the cellular and molecular mechanisms involved in therapy resistance and tumour recurrence is of an utmost importance.



4.1.2 BCSC plasticity

Cancer stem cells (CSCs), also known as ‘tumour-initiating cells’, were first identified in leukaemia by Bonnet and Dick (1997) as tumour cells that are capable of undergoing self-renewal and giving rise to committed progenitors and thus capable of forming tumours upon transplantation. CSCs were also reported to exist in other solid tumours, including breast cancer (Al-Hajj et al., 2003; Al-Hajj & Clarke, 2004). In 2003, Al-Hajj and colleagues demonstrated that as low as 100 breast cancer cells isolated from patient samples with the surface antigen profile of $CD44^{+}CD24^{-/low}$ were able to regenerate tumours upon transplantation into the immunocompromised mice. These tumours that are reconstituted from $CD44^{+}CD24^{-/low}$ populations could be passaged several times, and the grown tumours still contained a $CD44^{+}CD24^{-/low}$ population as well as other tumour cell populations at a similar level to the original patient sample used. Hence, it is suggested that the $CD44^{+}CD24^{-/low}$ population of breast tumour cells possess the self-renewal and multipotent properties. This study provided a powerful evidence for the existence of BCSC populations, which possess $CD44^{+}CD24^{-/low}$ surface antigen profile.

Another study revealed that breast tumour cells with high expression levels of aldehyde dehydrogenase 1 ($ALDH1^{high}$) were also able to undergo self-renewal, generate other tumour cell types and thus formed tumours in xenograft model (Ginestier et al., 2007) s. However, the $CD44^{+}CD24^{-/low}$ and the $ALDH1^{high}$ populations of BCSCs had a very small overlap with approximately 1% of the total primary xenograft tumour cells. Notably, this small population had the highest efficiency for tumour regeneration, although the cells that belong to either of the BCSC population were also able to form tumour upon further xenograft transplantations (Ginestier et al., 2007).

To further understand whether $CD44^{+}CD24^{-/low}$ and $ALDH1^{high}$ surface profiles identify distinct subsets of BCSC populations, tumours from 45 patients were analysed at both

histological and molecular level through performing immunofluorescence and microarray gene expression analysis (Liu et al., 2014). This study demonstrated that $CD44^+CD24^{-/low}$ cells are mostly located at the leading edge of primary breast tumours staying in a quiescent state, whereas most of the $ALDH1^{high}$ populations are proliferative and positioned at the core of these tumours. Importantly, this study also demonstrated that $CD44^+CD24^{-/low}$ populations were mesenchymal-like BCSCs due to their transcriptome resembling a mesenchymal cell, whereas $ALDH1^{high}$ populations were referred to as epithelial-like BCSCs.

Taken together, as shown in figure 47, $CD44^+CD24^{-/low}$ and $ALDH1^{high}$ surface antigen profiles identify two distinct subtypes of BCSCs in human breast cancer. The $CD44^+CD24^{-/low}$ subtype displays quiescent and mesenchymal-like characteristics, whereas the $ALDH1^{high}$ cell subtypes are more proliferative and in epithelial-like state. Importantly, the epithelial-like and mesenchymal-like states of BCSCs are able to transit into each other, suggesting an important concept of stem cell plasticity in breast tumours.

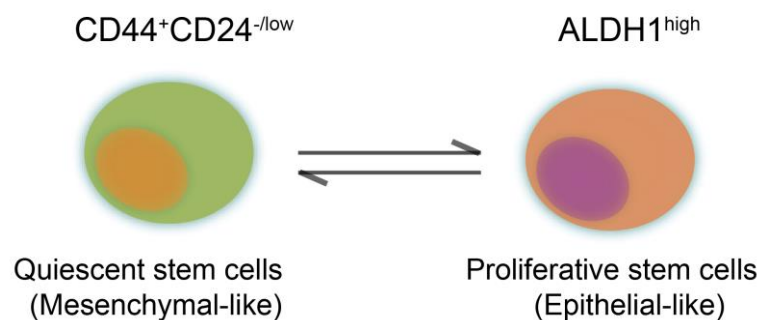


Figure 47. The schematic representation for two states of BCSCs.

4.1.3 The BCSC plasticity is presumed to play crucial roles in tumour metastasis, tumour recurrence and therapeutic resistance in breast cancer

Tumour metastasis is a complex multi-step process that requires a high degree of plasticity of tumour cells (Kong et al., 2020). Some of the epithelial tumour cells at the primary site initially undergoes epithelial-mesenchymal transition (EMT) to acquire mesenchymal properties, which improves their cell migration and invasion abilities and survival chances in the bloodstream. Importantly, it is suggested that the EMT process can increase the stemness properties of the mesenchymal-like cells with self-renewal and multipotent characteristics (Mani et al., 2008; Morel et al., 2008). The mesenchymal-like stem cells then intravasate into the blood vessels and may exist in the bloodstream either as single circulating tumour cells (CTCs) or CTC clusters. These mesenchymal-like tumour cells can then extravasate into the tissue space of the distant organs and undergo mesenchymal-epithelial transition (MET) to return back into the epithelial state, which allows these cells locating at the secondary sites to acquire epithelial-like cancer stem cell features. Consequently, these CSCs with self-renewal ability will drive the proliferation and differentiation into epithelial tumour cell types to expand the tumours at the secondary metastatic sites (Kong et al., 2020). As BCSCs are the only cells in breast tumours with the tumour-initiating abilities, it is likely that the cell-of-origin of the metastatic tumour is a mesenchyme-like BCSC of the primary tumour and the BCSC plasticity is required for tumour metastasis. Furthermore, due to their unique tumour-initiating abilities, Br-CSCs are also considered to be responsible for the post-treatment tumour recurrence. Several studies also indicated that the conventional therapies can induce breast tumour cells acquiring therapy resistance by promoting tumour cells to acquire stem cell properties through YAP/TAZ mechanotransduction or ZEB promoter activity (Chaffer et al., 2013; Cordenonsi et al., 2011; Totaro et al., 2019). Moreover, when primary breast tumour samples from patients

were analysed before and after chemotherapy, it was revealed that chemotherapy can enlarge the CD44⁺CD24^{-low}, the quiescent mesenchymal-like BCSC subpopulations (Li et al., 2008).

Currently, the most important clinical challenges in the treatment of breast cancer are therapy resistance, tumour recurrence and metastasis, all of which relies or is dependent on the Br-CSC plasticity and activity (Bai et al., 2018; de Angelis et al., 2019; Palomeras et al., 2018). Tumours are highly heterogenous as they are composed of various cell subtypes including CSCs. However, currently available anti-cancer treatments are often able to kill only the non-CSC tumour cells. Thus, CSCs surviving the treatment will still be able to induce tumour metastasis and recurrence that is observed in clinics (Wicha et al., 2006). Therefore, it is essential to develop novel cancer therapies that can target and eliminate CSC populations. The idea is that once the CSCs would be eliminated successfully, the remaining tumour cells, which lacks the self-renewal and tumour-initiating abilities, cannot proliferate extensively or invade into other sites, and eventually will undergo apoptosis and be cleared. Alternatively, a combination treatment option of conventional therapies together with a potential CSC-targeting therapy may successfully eradicate the tumour and provide a ‘true cure’ for patients. However, the current lack of our knowledge in identifying and isolating CSCs hamper the progress of discovering novel CSC-targeted therapies (Wicha et al., 2006).

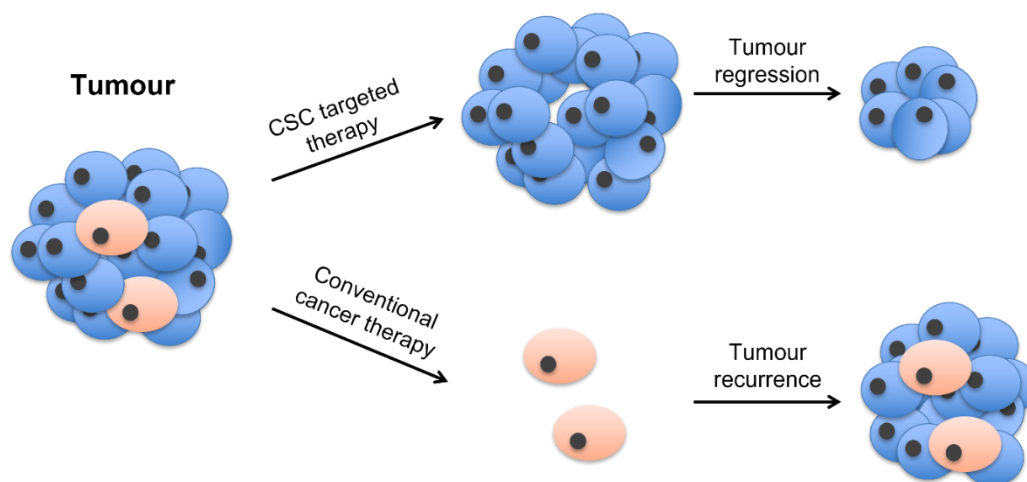



Figure 48. The hypothetical schematic model for conventional and CSC-targeted therapies. Pink cells, cancer stem cells; blue cells, differentiated tumour cells.

4.1.4 Comparison of Rac1 and Rac1b functions in various cancers

The small GTPase Rac1 is upregulated in various cancers including breast cancer and regulates numerous cellular processes including cell proliferation, survival, and invasion (Barros et al., 2009; D. Cai et al., 2003; De et al., 2019; Johnson et al., 2010).  High expression levels of Rac1 correlates with poor survival in breast cancer patients (Butera et al., 2020). It was demonstrated that Rac1 is overexpressed in all stages of breast cancer including hyperplasia, DCIS, and IBC in comparison with normal breast tissue (Schnelzer et al., 2000). It was suggested that Rac1 and Cdc42, another member of RhoGTPase family, are involved in the transformation of mammary epithelial cells into tumour cells via activating the PI3K signalling pathway to disrupt cell polarity and promote cell mobility and invasiveness (Keely et al., 1997). Another study revealed that Rac1 activity can mediate cell cycle induced by FGF2 in MCF7 cell line (Liu et al., 1999). In the metastatic breast tumour cell line SP1, the interaction between CD44 and Tiam1 (a member of RhoGEF family) promotes Rac1 activity to regulate tumour cell migration (Bourguignon et al., 2000). ZNF750, a human zinc finger protein that functions as a tumour suppressor, was shown to suppress Rac1 expression through binding to its promoter in breast cancer cell lines (Butera et al., 2020). Numerous studies revealed that Rac1 is essential for maintaining CSC activity in different types of cancers. For instance, Rac1 is essential for promoting the proliferation of colorectal CSCs driven by Wnt pathway through activating ROS production and NF- κ B pathway (Myant, Cammareri, et al., 2013; Myant, Scopelliti, et al., 2013). Another study using colorectal cancer cell lines also suggests that Rac1 regulates the cell-cell interaction of stem cells via mediating Lgr5 in Wnt signalling (Carmon et al., 2017). Rac1, a target of miR-365, is responsible for the expansion of CSCs caused by the downregulation of miR-365 in liver cancer (Jiang et al., 2019). In lung cancer, the overexpression of Rac1 promotes cancer cell invasion *in vitro* and tumour initiation *in vivo*, whereas the inhibition of Rac1 attenuates stem cell activities (Akunuru et al., 2011).

Furthermore, in gastric adenocarcinoma, Rac1 was shown to be essential for tumour cells undergoing EMT process and acquiring CSC features (Yoon et al., 2017). Notably, the loss of Rac1 activity was shown to reverse the chemoresistance of tumour cells (Yoon et al., 2017). Consistently, several studies have also indicated that Rac1 plays critical roles in anti-cancer drug resistance. For instance, Rac1 induces the melanocytes acquiring mesenchymal features via activating AKT, PAK and SRF/MRTF transcriptional pathway and thus drives the resistance of tumours to BRAF inhibitor treatment (Lionarons et al., 2019). In breast cancer, Li et al. (2020) demonstrated that the overexpression of Rac1 upregulates nucleotide metabolism, which helps tumour cells to survive the DNA damage induced by chemotherapies. Moreover, Rac1 is indispensable for the therapy resistance of the tumour cells in lung, liver and thyroid cancers (Bagheri-Yarmand et al., 2021; T. Zhang & Wang, 2018; Y. Zhou et al., 2019).



Although Rac1 has numerous indispensable functions at almost all stages of breast tumourigenesis, targeting Rac1 as a potential novel anti-cancer treatment is not a viable option. This is due to the fact that Rac1 is almost ubiquitously expressed in all organ systems and has vital roles for various organ functions. Interestingly, Rac1b was shown to be overexpressed in some cancers, including breast cancer and colorectal cancer. However, unlike Rac1, the expression pattern of Rac1b is more restricted in normal organ systems. Furthermore, loss-of-Rac1b function does not lead to any obvious health problems *in vivo*, as I have observed for the Rac1b^{-/-} mice in Chapter 3. Therefore, variant-specific targeting of Rac1b could be a clinically relevant option, if Rac1b function were shown to be essential for breast tumourigenesis or in other cancer types.

Rac1b was shown to be expressed at a higher level in colorectal cancer compared with normal colorectal tissues (Alonso-Espinaco et al., 2014). A recent study demonstrated that the loss of Rac1b function delays colorectal tumourigenesis in mice and that Rac1b function is required

for the oncogenic functions of EGFR signalling (Gudiño, Pohl, et al., 2021). Furthermore, genetic deletion of Rac1b was shown to improve the sensitivity of colorectal tumour cells to the EGFR inhibitor, cetuximab, treatment (Gudiño, Pohl, et al., 2021). Rac1b plays an important role in mediating Wnt signalling in colorectal cancer (Gudiño, Pohl, et al., 2021; Kotelevets et al., 2018), and can prevent colorectal cancer cell apoptosis via inhibiting TGF- β pathway (Gudiño, Cammareri, et al., 2021). Another study demonstrated that Rac1b overexpression confers chemoresistance of colorectal cancer cells through NF- κ B signalling pathway (Goka et al., 2019). Hence, Rac1b could be a potential molecular target for developing novel therapies to improve the treatment outcome for patients with colorectal cancer.

Although Rac1b is known to be overexpressed in breast cancer, there are only a few *in vitro* studies that has addressed the role of Rac1b in breast cancer. In SCp2 mouse mammary epithelial cell line, matrix metalloproteinase-3 (MMP-3) expression was shown to upregulate Rac1b expression, which then increases ROS that promotes EMT process through increasing Snail, vimentin and α -Smooth muscle actin (α SMA) expression (Radisky et al., 2005). MMP-3 is known to be overexpressed in various breast cancers and it was shown that it can regulate EMT, cell spreading and malignant transformation in a Rac1b-dependent manner (Cichon et al., 2015; Nelson et al., 2008; Radisky et al., 2005). Thus, Rac1b function was associated with the EMT process and cell motility induced by MMP-3. Further studies demonstrated that α 6-integrin can prevent Rac1b localizing to the plasma membrane to inhibit MMP-3 induced EMT process, whereas β 5-integrin has an opposite function to α 6-integrin (Chen et al., 2013)). Interestingly, the subcellular localisation and function of Rac1b was shown to be influenced by the stiffness of the microenvironment. Rac1b predominantly localizes on the plasma membrane in a stiff microenvironment and forms a complex with NADPH oxidase to promote the ROS production and EMT process (Lee et al., 2012). As explained earlier, EMT process is associated with increased stemness in tumours , conferring tumour therapy resistance, tumour recurrence

and metastasis. Therefore, it would be important to reveal whether Rac1b plays crucial roles during breast tumorigenesis *in vivo*, in particular for BCSC activities and chemoresistance. In this regard, I aimed in this project to characterize the functional roles of Rac1b in a mouse model of breast cancer using the MMTV-Neu transgenic mouse line with a particular focus on BCSCs and chemoresistance.

4.2 Results

4.2.1 Rac1b-expressing cells consists of various cell subtypes in Her2+ tumours

In order to identify and characterise the Rac1b-expressing cell types within breast tumours *in vivo*, I have crossed the Rac1b^{T2A-RFP}-knockin transgenic mouse line with the MMTV-Neu-IRES-Cre (NIC) mouse line, which are able to spontaneously develop Her2+ breast cancer. Tumours that are grown by the double transgenic mice were dissected to isolate primary tumour cells for FACS analysis. After gating out the dead cells and lineage-positive cells (including endothelial cells, leukocytes and erythroid cells), remaining tumour cells were assessed for their RFP expression (Fig. 49). The gate for RFP⁺ cells was set comparatively by using Rac1b^{+/+ or +/-}; NIC/+ tumour samples that should not have any RFP⁺ cells. Similar to my observations made

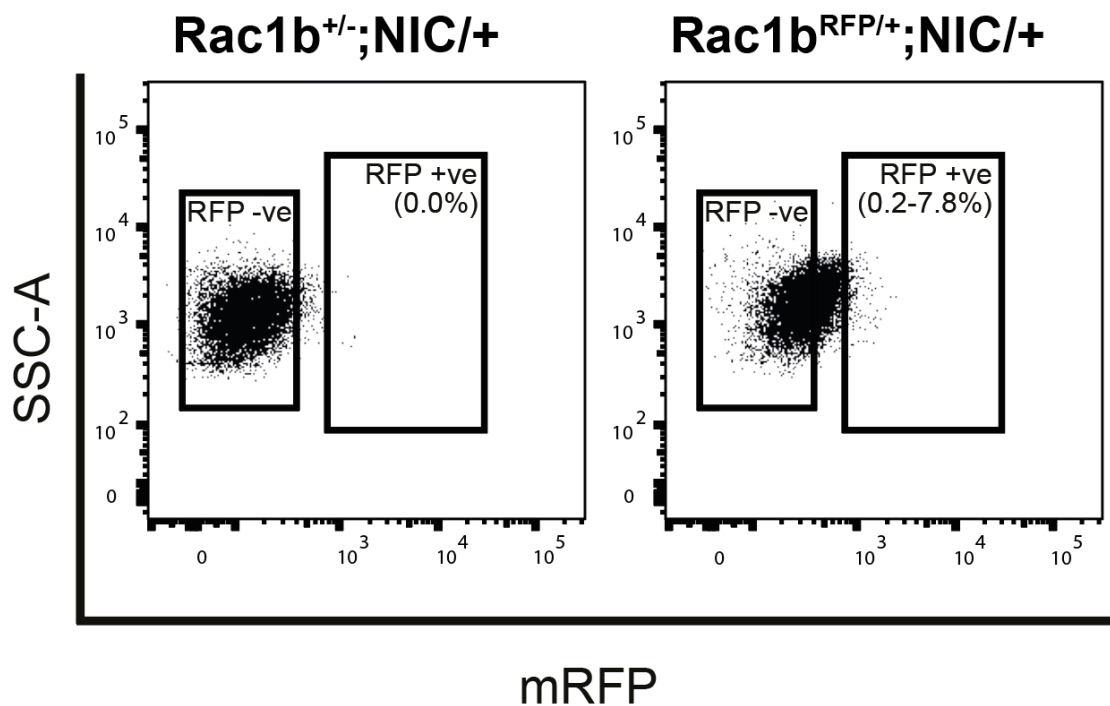


Figure 49. Representative dot plots used for sorting RFP⁺ and RFP⁻ tumour cells from the Rac1b^{RFP/+}; NIC/+ tumours. The gate for RFP-positive cells was set based on the Rac1b^{+/+ or +/-}; NIC/+ cells (the left plot), which should not express RFP proteins. X axis, RFP fluorescence; Y axis, SSC-A.

for normal mammary glands that are presented in Chapter 3, tumour cells also consisted of a small population of Rac1b-expressing cells (0.2%-7.8%). To further characterise the Rac1b-expressing tumour cells, the RFP⁺ cells were then analysed for their CD24 expression. Approximately 92.4% of the RFP⁺ cells were CD24⁺ (Fig. 50A), suggesting that the Rac1b-expressing cell population predominantly consists of tumour epithelial cells .

Next, the IF staining of the sorted RFP⁺ cells were performed to determine CK14 and CK18 expression using the same methodology as described in Section 3.8. My results have suggested that RFP⁺ breast tumour cells were consisted of 4 different cell subpopulations (Fig. 50B&C). The largest population (79.3%) of the RFP⁺ cancer cells were luminal epithelial-like cells (CK18-positive), while CK14-expressing basal-like tumour cells accounted for only 0.7% of the RFP⁺ cancer cells. On the other hand, 2.7% of the RFP⁺ cancer cells were expressing both CK14 and CK18, suggesting that they may be the bipotent progenitors. Finally, the CK14⁻CK18⁻ cells (double negative) represented 17.3% of the RFP⁺ cancer cells, which may represent the mesenchymal-like cells.

Taken together, both the flow cytometry analysis of CD24 expression and immunostaining for CK14 and CK18 expression indicated that the Rac1b-expressing tumour cell population include different cell subpopulations, although majority of the Rac1b-expressing cells are also expressing widely accepted epithelial lineage markers.

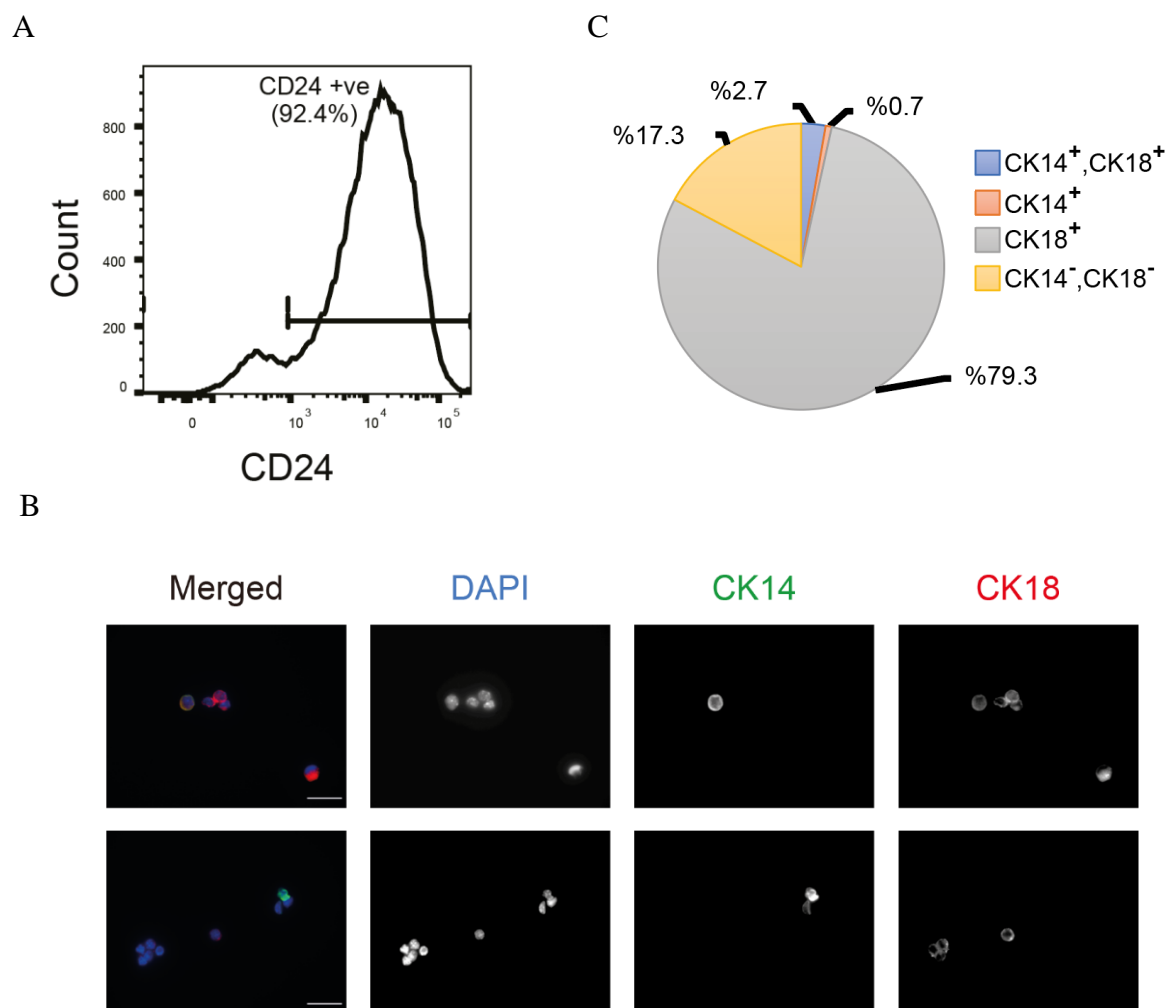


Figure 50. Characterisation of RFP⁺ cells isolated from Rac1b^{RFP/+}; NIC/+ breast tumours. **(A)** Representative histogram graph of flow cytometry analysis showing CD24 expression within the RFP⁺ cell population isolated from Rac1b^{RFP/+}; NIC/+ breast tumour cells (N=3). The gating strategy was similar as described in Section 3.8. X axis, CD24; Y axis, Count. **(B)** Representative images for IF staining of RFP⁺ cells isolated from Rac1b^{RFP/+}; NIC/+ breast tumour cells for CK14 and CK18 expression (N=3). Images were taken by using Zeiss Imager. M2 fluorescent microscope under 63x objective. Blue, DAPI; Green, CK14; Red, CK18. Scale bars represent 20μm. **(C)** Pie chart representation of the quantification results of IF staining shown in **B**. The percentage proportions of each cell subtype was shown on the graph. CK14⁺ (CK14-positive), orange; CK18⁺ (CK18-positive), grey; CK14⁺ CK18⁺ (CK14 and CK18 double positive), blue; CK14⁻ CK18⁻ (CK14 and CK18 double negative), yellow.

4.2.2 Rac1b is expressed by a substantial fraction of mammosphere-forming BCSCs

To determine whether BCSCs are expressing Rac1b, I performed Mammosphere assay using the RFP⁺ and RFP⁻ cell populations sorted from the Rac1b^{RFP/+}; NIC/+ tumours. Interestingly, both RFP⁺ and RFP⁻ populations were capable of forming solid spheres and acini structures, indicative of the existence of BCSCs and luminal progenitors, respectively (Fig. 51). At both 50,000 cells/ml and 10,000 cells/ml dilutions of plating, the RFP⁺ cell populations formed a higher number of solid spheres with a fewer number of acini compared to the RFP⁻ cell populations. This suggests that sorting for RFP⁺ tumour cell population enriches for sphere-forming BCSCs and that a **large subset of BCSCs express Rac1b**.

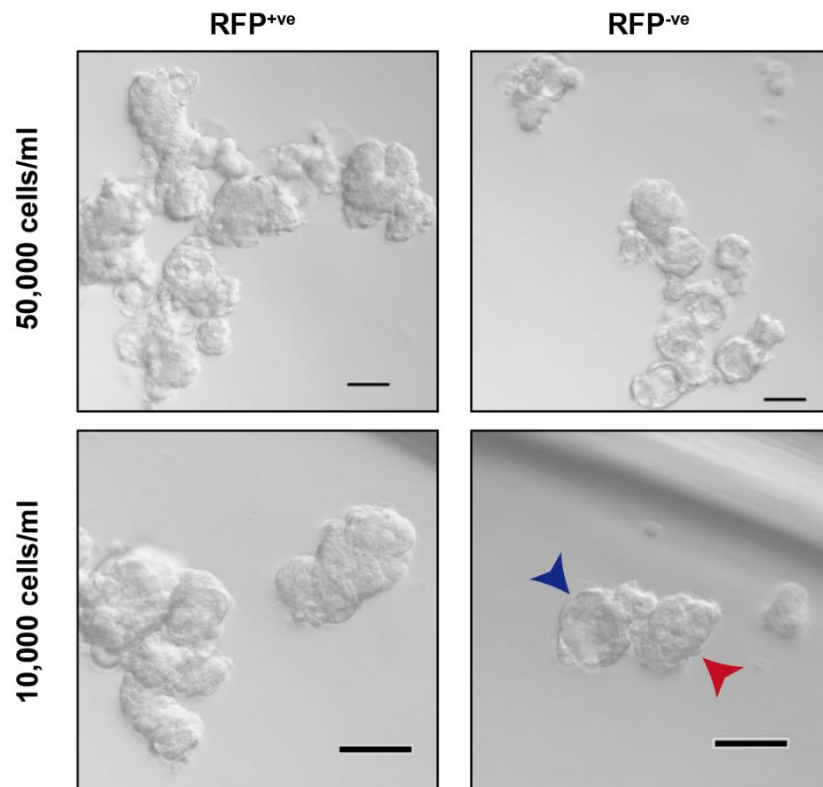


Figure 51. Representative images of structures formed in the mammosphere culture of the RFP⁺ and RFP⁻ cell fractions sorted from the Rac1b^{RFP/+}; NIC/+ tumour cells (N=6). Ten thousand and fifty thousand cells per millilitre were seeded onto the low-attachment 96-well plate for each cell populations. Blue arrowhead shows an acini structure, whereas the red arrowhead points to a solid sphere structure. Scale bars represent 50µm.

The quantification results has demonstrated that RFP⁺ tumour cell population had an average mammosphere-forming efficiency (MFE) of 0.36%, which was 4 times higher than the average MFE of 0.09% for RFP⁻ tumour cell population (Fig. 52). The statistical analysis of these results has also confirmed that the RFP⁺ tumour cell population contains a significantly higher frequency of sphere-forming BCSCs compared with the RFP⁻ tumour cell population.

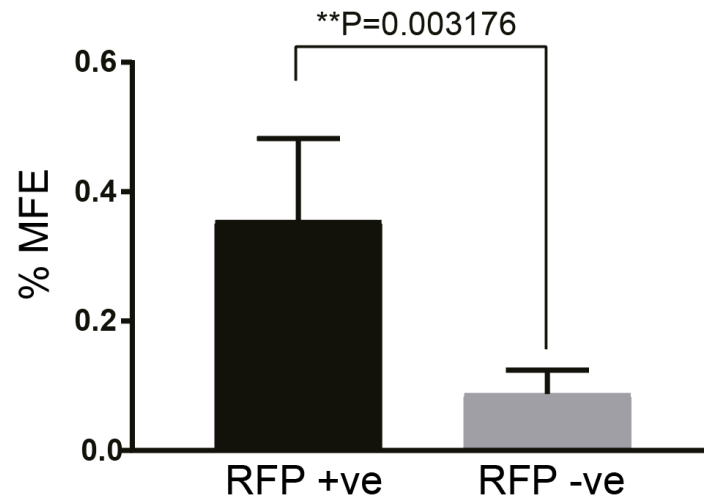


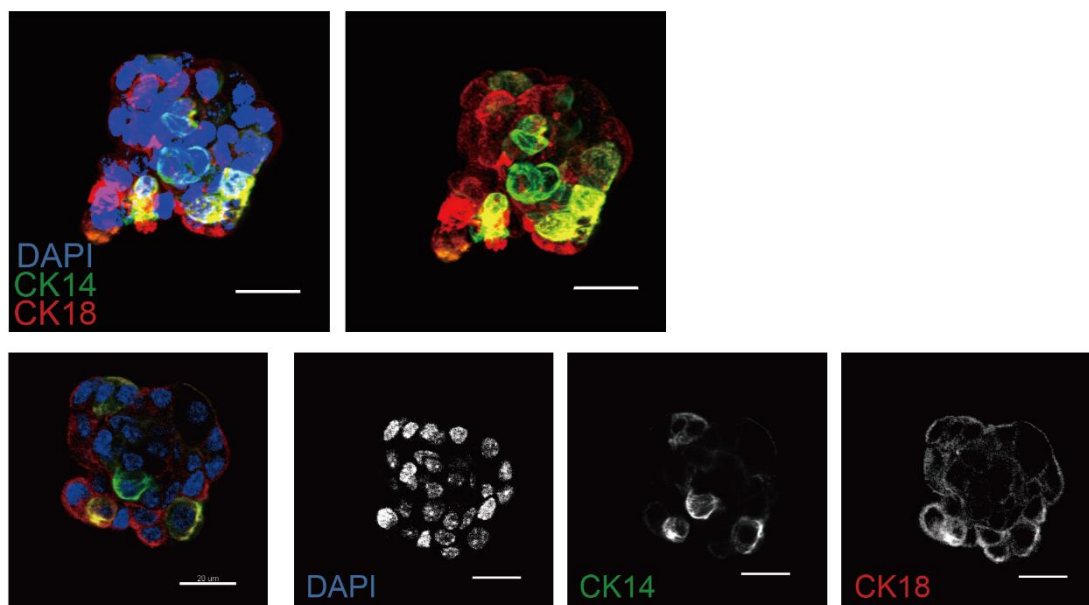
Figure 52. Mammosphere-forming efficiency of RFP⁺ and RFP⁻ tumour cell populations isolated from the Rac1b^{RFP/+}; NIC/+ tumour cells (N=6). The number of spheres was quantified from 50,000 cells/ml and 10,000 cells/ml conditions for RFP⁺ and RFP⁻ cell populations, respectively. The mean %MFE values for RFP⁺ versus RFP⁻ cell populations were 0.36 and 0.09, respectively. The statistical analysis is determined by ratio paired t test. ** P=0.0032 < 0.05.

4.2.3 Characterisation of RFP+ tumour cell driven spheres

As described in Section 3.5.2, most of the spheres formed by the RFP⁺ cell population isolated from the Rac1b^{RFP/+} mammary glands were composed of cells that are expressing neither CK14 nor CK18. Therefore, I have decided to verify whether the sphere structures formed by the RFP⁺ tumour cell population isolated from the Rac1b^{RFP/+};NIC/+ tumours would contain CK14- and/or CK18-expressing cells. Accordingly, the immunostaining results revealed that most of the tumour-spheres formed by the RFP⁺ tumour cell population were predominantly composed of CK14- and/or CK18-expressing cells (Fig. 53A&B). However, approximately 10% of those spheres were again consisted of cells expressing neither CK14 nor CK18, which resembles to the majority of the mammospheres formed by the RFP⁺ cell population of the Rac1b^{RFP/+} mammary glands (Fig. 53C).

Taken together, these results clearly indicate that Rac1b is expressed in a substantial subset of BCSCs within the MMTV-Neu tumours that can give rise to mammospheres that are predominantly composed of epithelial cells.

A



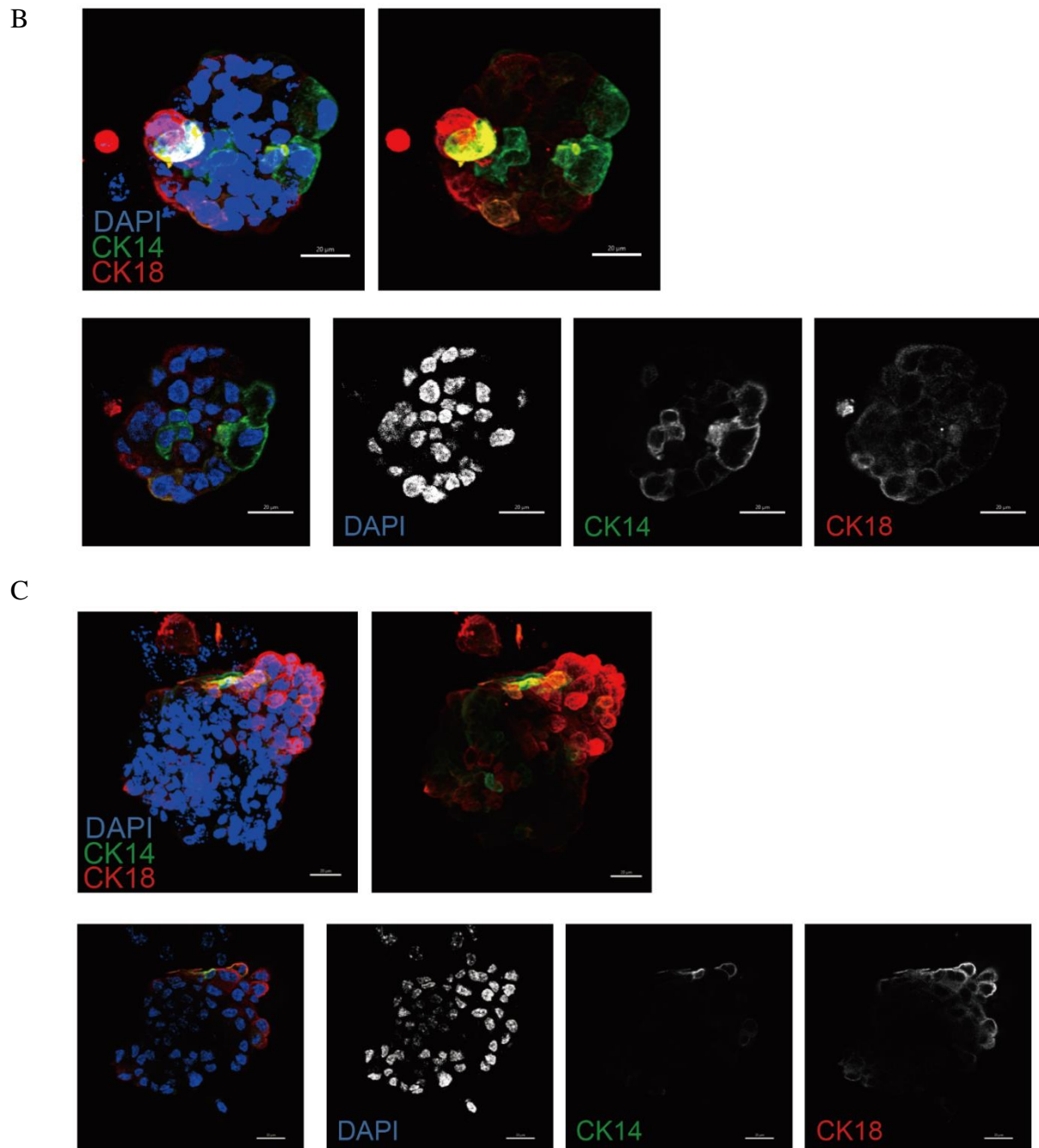
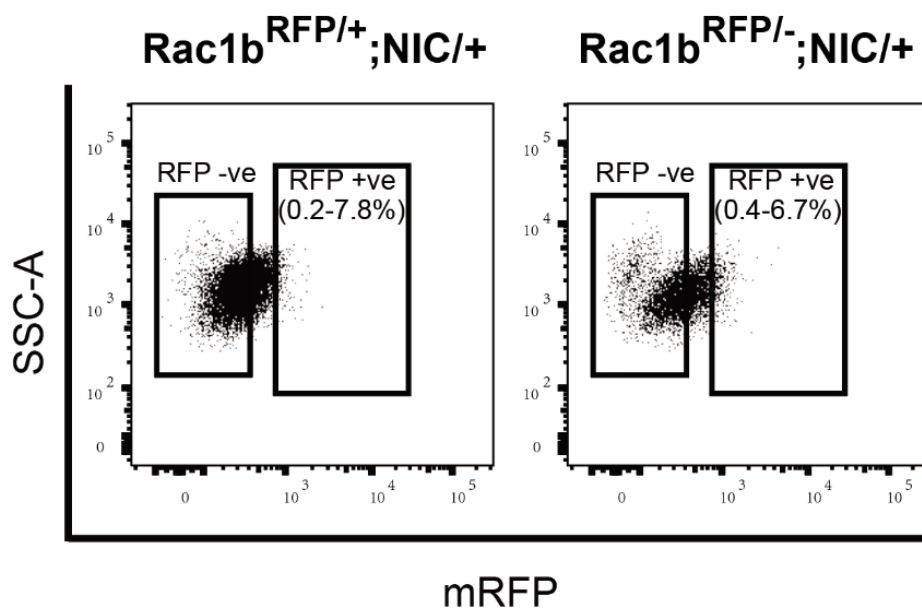


Figure 53. Representative confocal images for immunofluorescence staining of tumour spheres formed by the RFP⁺ tumour cells. Three different tumour spheres were shown in (A), (B) and (C). Upper panels: Deconvoluted confocal images with (left image) and without (right image) DAPI staining shown. Lower panels: A selected slice of the Z stack through the middle of the spheres with DAPI, CK14 and CK18 staining shown as the merged image on the leftmost picture and the individual channels are shown next to the merged image. Confocal images were taken by using Leica SP8 Upright dipping lens Confocal microscope with 63x objective. Blue, DAPI; Green, CK14; Red, CK18. Scale bars represent 20μm.

4.2.4 Rac1b is required for the maintainance of Rac1b-expressing BCSCs

Since I have shown that Rac1b is expressed by a substantial subpopulation of BCSCs, I have then investigated whether Rac1b function is required in those BCSCs. To this end, I isolated RFP⁺ cells from Rac1b-proficient (i.e. Rac1b^{RFP/+};NIC/+) and Rac1b-deficient (Rac1b^{RFP/-};NIC/+) breast tumours for performing mammosphere assay. The frequency of RFP⁺ cells in Rac1b^{RFP/-};NIC/+ tumours was between 0.4% and 6.7%, which is similar to the RFP⁺ cell frequency in Rac1b^{RFP/+}; MMTV-NIC tumours (0.2% and 7.8%) (Fig. 54). Sorted RFP⁺ and RFP⁻ cells from these tumours were then cultured for assessing their mammosphere formation efficiencies. For the RFP⁺ cell populations, Rac1b-null cells had a significant 42% reduction in their MFE compared with the same cell population of Rac1b-proficient tumours (Fig. 54). In contrast, RFP⁻ Rac1b-proficient and RFP⁻ Rac1b-null tumour cells did not significantly differ in their MFEs (Fig. 54). These results indicate that the loss of Rac1b function results in a drastic reduction of only the Rac1b-expressing BCSCs. Taken together, my results demonstrated that Rac1b is expressed by a substantial subset of BCSCs, which require Rac1b function for their maintenance.

A



B

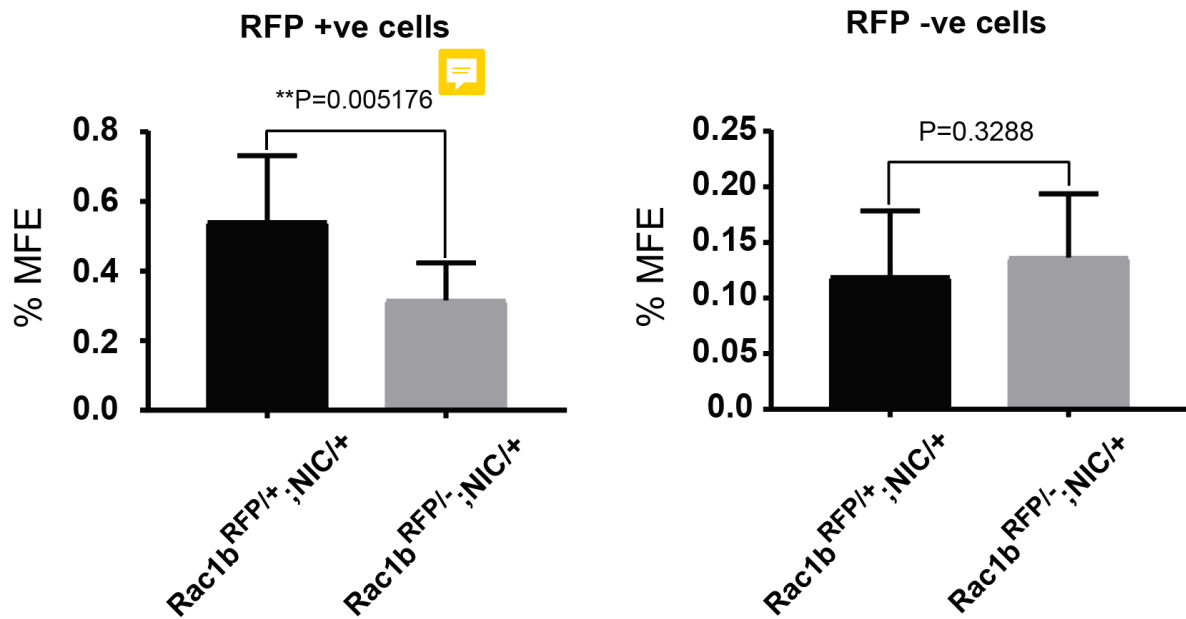


Figure 54. Rac1b function is required for the maintenance of BCSCs that express Rac1b. (A) Representative dot plots for flow cytometry analysis of primary tumour cells of Rac1b^{RFP/+}; MMTV-NIC and Rac1b^{RFP/-}; MMTV-NIC mice. Dead cells were excluded based on their staining with DAPI, and the lineage-positive cells labelled by CD31, CD45 and Ter119 antibodies were also excluded from the single alive cells as described in Figure 35. The percentages of RFP⁺ cell frequency in each genotype are shown within the RFP⁺ gate (N=9).

(B) Quantification results for mammosphere forming efficiency (%MFE) of RFP⁺ and RFP⁻ cell populations isolated from Rac1b^{RFP/+};NIC/+ and Rac1b^{RFP/-};NIC/+ breast tumours. The number of spheres was quantified from the cultures with 50,000 cells/ml and 100,000 cells/ml plating cell concentrations for RFP⁺ populations (left panel) and RFP⁻ cell compartments (right panel), respectively. For their RFP⁺ cell populations, the average MFE values for Rac1b^{RFP/+};NIC/+ and Rac1b^{RFP/-};NIC/+ tumours were 0.54% and 0.32%, respectively; whereas for their RFP⁻ fractions, the average MFE values for Rac1b^{RFP/+};NIC/+ and Rac1b^{RFP/-};NIC/+ were 0.12% and 0.14%, respectively. Statistical significance was tested by using paired t test (N=3). Bars represent average values \pm SEM. ns, not significant, $p > 0.05$; $**P < 0.01$.

4.2.5 Loss-of Rac1b function does not alter MMTV-Neu tumour latency

BCSCs are presumed to be important for the growth of tumours as well as for their aggressiveness. Given the findings presented above demonstrating a drastic effect of Rac1b-deficiency on BCSCs, I have then investigated whether the loss-of Rac1b function would alter the tumour latency in the MMTV-Neu model of breast cancer. To achieve this goal, I have crossed the Rac1b-KO and the MMTV-NIC mouse lines and have analysed the latency of palpable tumour formation.

The obtained data did not reveal any significant difference in the palpable tumour formation latency for the Rac1b^{+/+};NIC/+, Rac1b^{+/-};NIC/+ and Rac1b^{-/-};NIC/+ mice, which has developed palpable tumours with a median age of 125, 117, and 113.5 days of postnatal life, respectively (Fig. 55B).

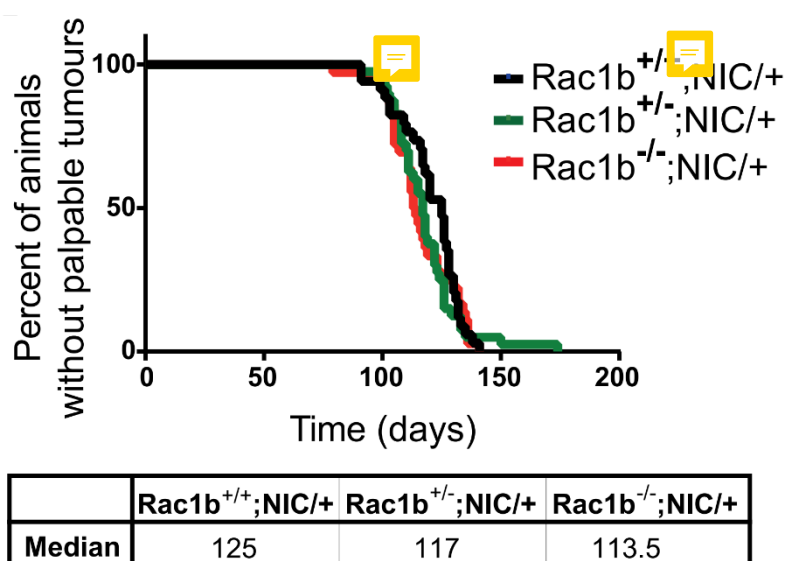
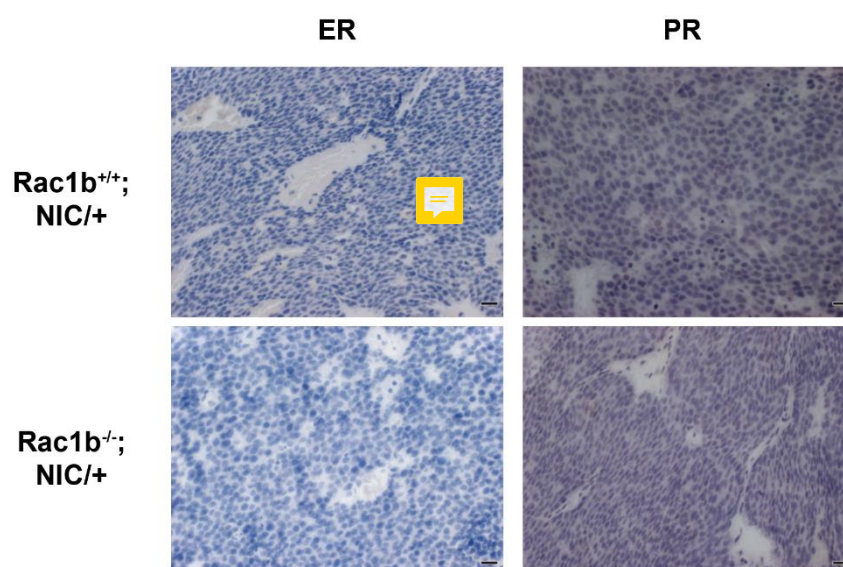


Figure 55. Tumour latency analysis for Rac1b^{+/+}; NIC/+, Rac1b^{+/-}; NIC/+ and Rac1b^{-/-}; NIC/+ mice (N=34 vs. 40 vs. 36). The median values are 125 days, 117 days and 113.5 days, respectively.

Next, I have performed immunohistochemistry staining on sections of $Rac1b^{+/+};NIC/+$, and $Rac1b^{-/-};NIC/+$ tumours for oestrogen receptor (ER) and progesterone receptor (PR) in order to determine whether the loss-of $Rac1b$ function could alter the tumour characteristics of the MMTV-Neu mouse model, which is known to generate $ER^{-}PR^{-}$ tumours. My results showed that ER and PR are expressed in neither $Rac1b$ -null nor $Rac1b$ -proficient tumours (Fig 56A), suggesting that the $Rac1b$ -deficiency does not alter the tumour morphology or characteristics of Neu-driven tumourigenesis *in vivo*. To investigate whether loss-of $Rac1b$ function may change the proliferative features of MMTV-Neu tumours, I have also performed immunohistochemistry analysis for Ki67 expression, a cellular marker for cell proliferation. Interestingly, most of the proliferative cancer cells (i.e Ki67-positive) were located at the boundaries of the $Rac1b^{+/+};NIC/+$ tumours (Fig. 56B, left panel), and the Ki67 positive cell distribution in the tumour core or boundaries did not alter in $Rac1b^{-/-};NIC/+$ tumours (Fig. 56B, middle and right panels). Taken together these results indicate that $Rac1b$ deficiency does not alter the latency, epithelial characteristics and proliferative capacities of MMTV-Neu tumours *in vivo*.

A



B

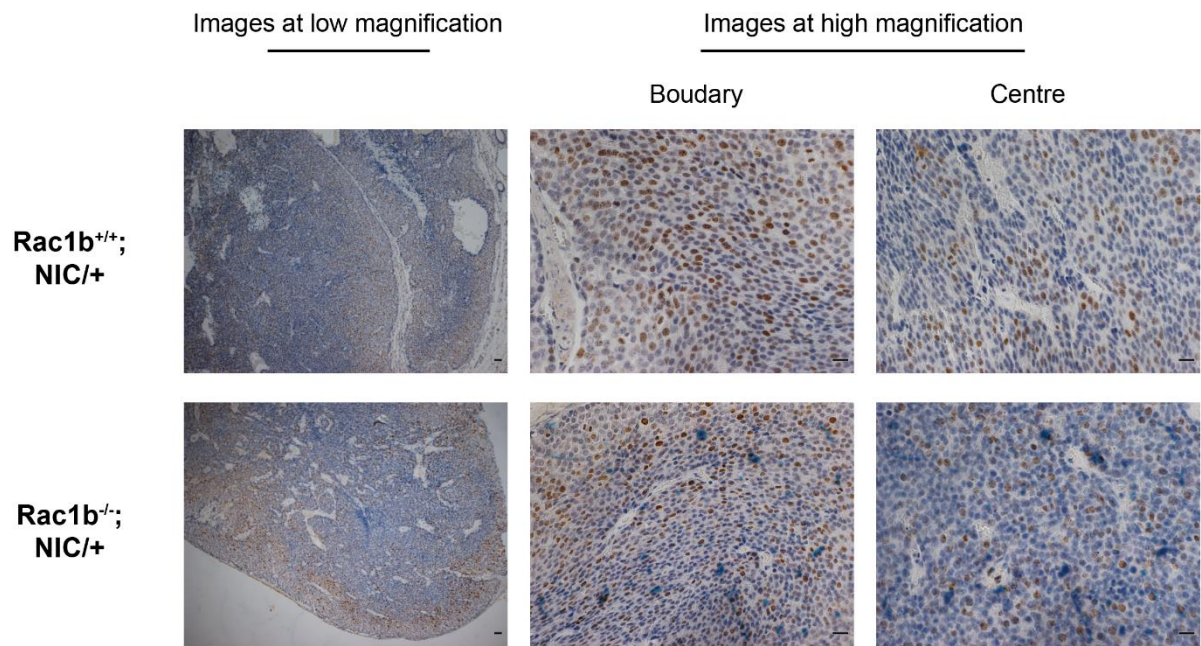


Figure 56. Representative images of ER, PR, and Ki67 immunohistochemistry staining on microtome sections of Rac1b^{+/+};NIC^{+/+} and Rac1b^{-/-}; NIC^{+/+} breast tumours. **(A)** Immunohistochemistry staining with ER or PR antibodies. **(B)** Immunohistochemistry staining with Ki67 antibody. Cells positively stained with the corresponding antibodies are seen in brown colour, whereas nuclei, which are counterstained with haematoxylin, are in blue colour. The stained sections were imaged with the Olympus BX63 Upright microscope using 10x and 40x magnifications. Scale bars represent 100µm and 50µm for low (10x) magnification and high (40x) magnification images, respectively.

4.2.6 Rac1b deficiency results in decreased BCSC frequency in MMTV-Neu tumours

I have shown earlier (Figure 54) that Rac1b deficiency in Rac1b^{RFP/-};NIC/+ tumours results in an approximately 42% decrease in sphere-forming RFP⁺ BCSCs compared to the same cell population in the Rac1b^{RFP/+};NIC/+ tumours. However, as I have not observed any obvious change in the latency, morphology or proliferative capacity of Rac1b^{-/-};NIC/+ tumours compared to Rac1b^{+/+};NIC/+ tumours, I have investigated whether the loss-of Rac1b function in Rac1b^{-/-};NIC/+ tumours would also affect the total BCSC population. To this end, I have analysed primary breast tumour cells from Rac1b^{-/-};NIC/+ and Rac1b^{+/+};NIC/+ mice by flow cytometry and mammosphere assay. After the exclusion of dead cells (identified via DRAQ7 staining) and the lineage-positive cells (CD31, CD45 and Ter119) from the single cell population, remaining cells were separated into two populations based on their CD24 and CD49f expression. Tumour epithelial cells were identified as CD24⁺CD49f⁺ (DP) cells, whereas the remaining CD24⁻CD49f⁻ (DN) cells are likely to contain the mesenchymal cells and potentially the mesenchymal-like tumour cells (Fig. 57A). The distribution of single Lin⁻ cells between the DP versus DN populations were observed to be similar in the Rac1b^{-/-};NIC/+ and the Rac1b^{+/+};NIC/+ tumours. The sorted DN and DP cell populations from the tumours of both genotypes were then plated for mammosphere assay. The quantification results demonstrated that for the CD24⁺CD49f⁺ tumour cell populations Rac1b^{-/-};NIC/+ tumours have a significant 65% decrease in their MFE compared with the Rac1b^{+/+};NIC/+ tumours (Fig. 57B). In contrast, for the MFE of the CD24⁻CD49f⁻ cell population there was no significant difference between genotypes (Fig. 57B). These results confirm and further extend my findings observed in the RFP⁺ population sorted from the Rac1b^{RFP/-};NIC/+ tumours, suggesting that Rac1b is indeed required for the BCSC maintenance within the MMTV-Neu tumours.

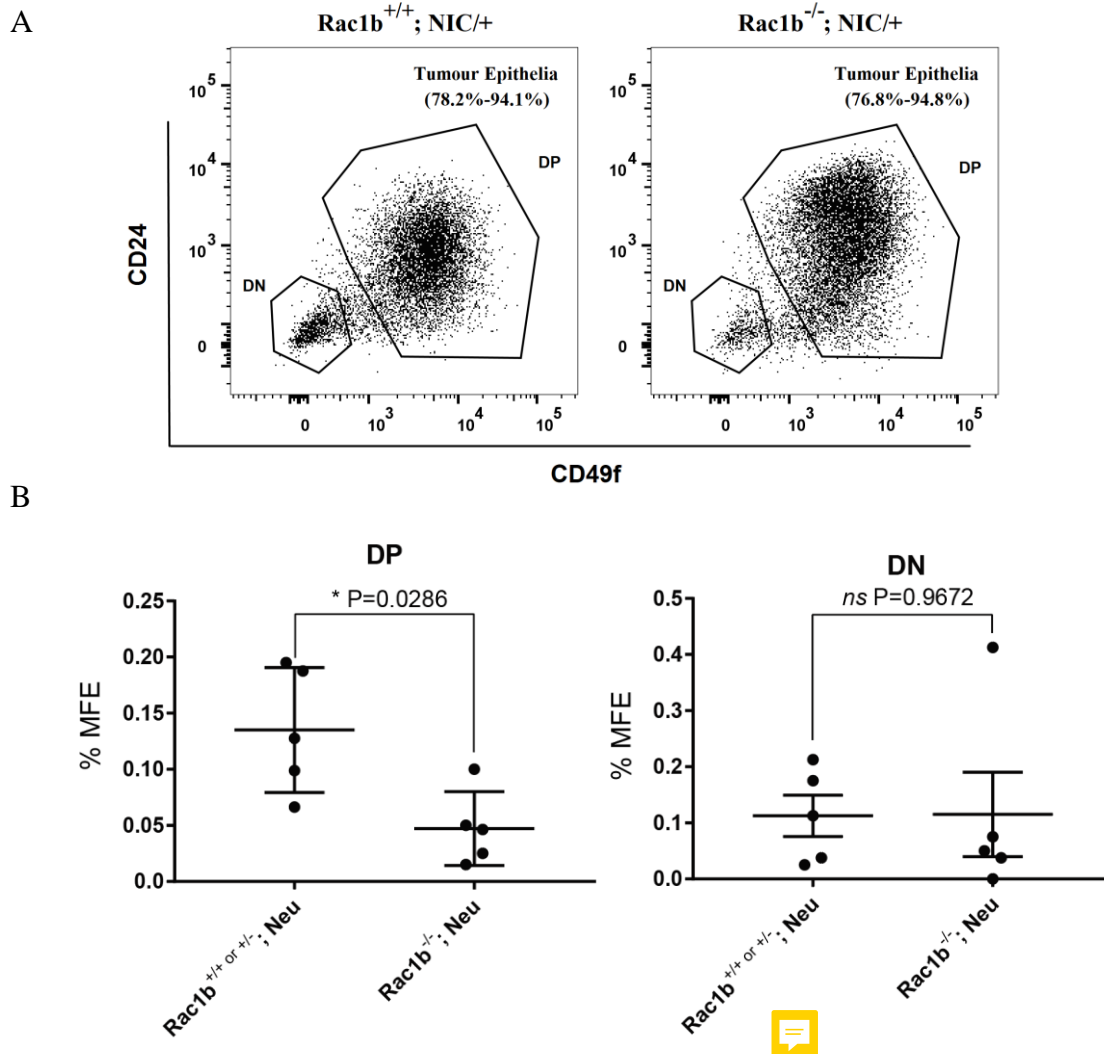
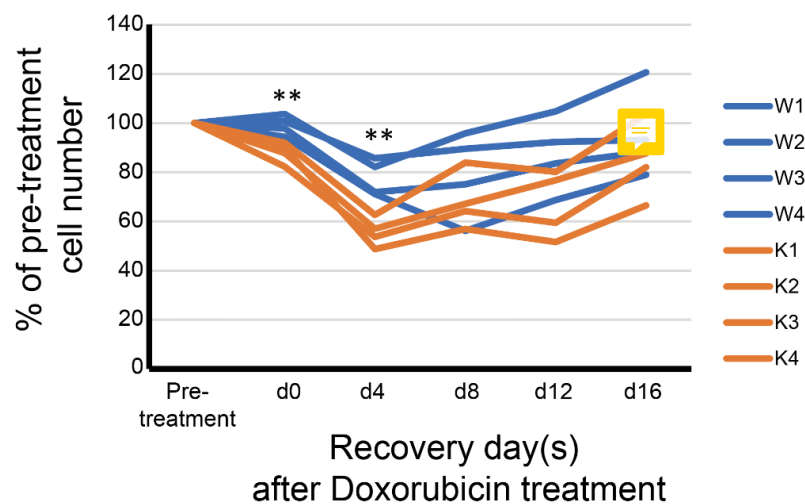


Figure 57. Rac1b is required for the BCSC maintenance within the MMTV-Neu tumours. **(A)** Representative FACS dot plots for sorting CD24⁺CD49f⁺ (DP) and CD24⁻CD49f⁻ (DN) primary cells from Rac1b^{+/+} or ^{+/-}; NIC/+ and Rac1b^{-/-}; NIC/+ breast tumours (N=9). Dead cells were excluded based on their staining with DRAQ7, and the lineage-positive cells labelled by CD31, CD45 and Ter119 antibodies were also excluded from the single alive cells as described in Figure 15. DP, double positive; DN, double negative. **(B)** Scatter plots for statistical analysis of %MFE data for comparing Rac1b^{+/+} (or ^{+/-}); NIC/+ and Rac1b^{-/-}; NIC/+ tumours (N=5). Left panel shows the comparison of DP populations, where the average values of %MFE for Rac1b^{+/+} (or ^{+/-}); NIC/+ and Rac1b^{-/-}; NIC/+ were 0.14% and 0.05%, respectively. Right panel shows the comparison of DN population, where the average values of %MFE for Rac1b^{+/+} (or ^{+/-}); NIC/+ and Rac1b^{-/-}; NIC/+ were 0.11% and 0.12%, respectively. The number of spheres was quantified at 100,000 cells/ml. Lines represent the means \pm SEM of 5 animals. Statistical analysis was determined using ratio paired t test. *P< 0.05; *ns*, not significant.

4.2.7 Rac1b deficiency sensitises primary breast tumour cells to chemotherapy

A previous study of our research group (manuscript under revision) has demonstrated that Rac1b function is essential for the chemoresistance of the MCF7 cell line to Doxorubicin treatment. As I have shown above, Rac1b deficiency leads to a drastic decrease of BCSCs in MMTV-Neu tumours. Since BCSCs are presumed to be responsible for the therapy resistance and tumour recurrence, I have investigated whether Rac1b-null MMTV-Neu breast tumour cells would also have an increased sensitivity to the effects of Doxorubicin treatment. To this end, I have generated Rac1b^{+/+};NIC/+ and Rac1b^{-/-};NIC/+ primary tumour cell lines by plating CD24⁺CD49f⁺ tumour epithelial cells sorted by FACS (as shown in previous section) as monolayer culture cell lines. After establishing these primary cell lines, I have treated them with 1 μ M Doxorubicin for 24 hours and subsequently let them to recover from the effects of chemotherapy. Relative cell numbers were measured by using AlamarBlue assay at different time points (pre-treatment, and Day 0, Day 4, Day 8, Day 12 and Day 16 after removing doxorubicin) to quantitate the cytotoxic effects of doxorubicin treatment and the efficiency of post-treatment recovery. As shown in Fig. 58, the immediate (Day 0) and sustained (Day 4) cytotoxic effects of Doxorubicin treatment was higher for the Rac1b-null primary tumour cells, as their relative cell numbers (i.e. normalised to the pre-treatment cell numbers) were significantly lower compared with the corresponding samples of Rac1b-proficient primary tumour cells. At 8-, 12- and 16- days post-treatment, the mean value for the relative cell numbers of Rac1b-null tumour cell lines were still slightly, though not significantly, lower than the corresponding mean values for Rac1b-proficient primary tumour cell lines. The lack of any significant difference between genotypes at these time points was due to the heterogeneity of post-treatment recovery levels of the individual cell lines belonging to the same genotype groups.

A



B

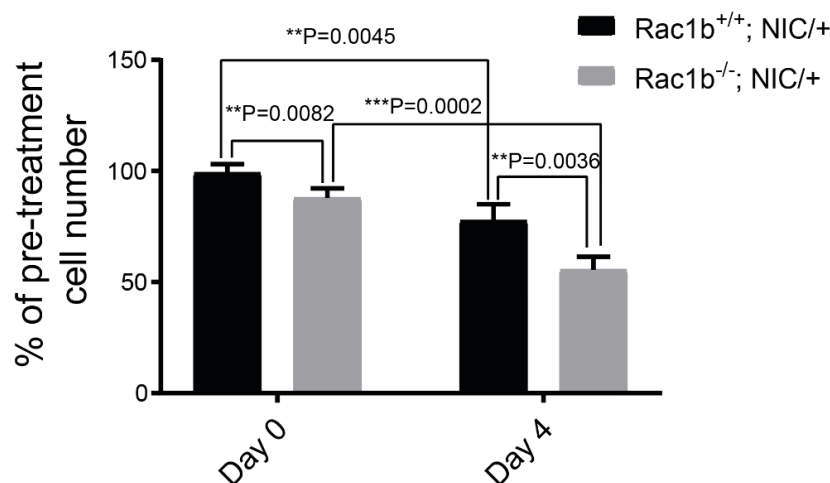


Figure 58. Loss of Rac1b function increases the chemosensitivity of primary breast tumour cells to 1µM doxorubicin treatment. (A) Cell growth curve of primary breast tumour cell lines after removing 1µM Doxorubicin treatment for 24 hours. This analysis compared Rac1b^{+/+}; NIC/+ with Rac1b^{-/-}; NIC/+ primary tumour cells isolated from their corresponding mice (N=4), which are labelled as blue lines (W1-W4) and orange lines (K1-K4), respectively. Cell numbers are normalized to the pre-treatment cell number in each sample and represented as percentage. (B) Bar graphs providing statistical comparison of the relative cell numbers at Day 0 and Day 4 shown in (A) after removing 1µM Doxorubicin treatment to compare the data between genotypes and recovery time points. Bars represent mean values \pm SD of 4 independent primary cell lines. Statistical analysis was determined by two-tailed unpaired t-test. *: P< 0.05; **: P< 0.01; ***: P< 0.001.. ns: not significant.

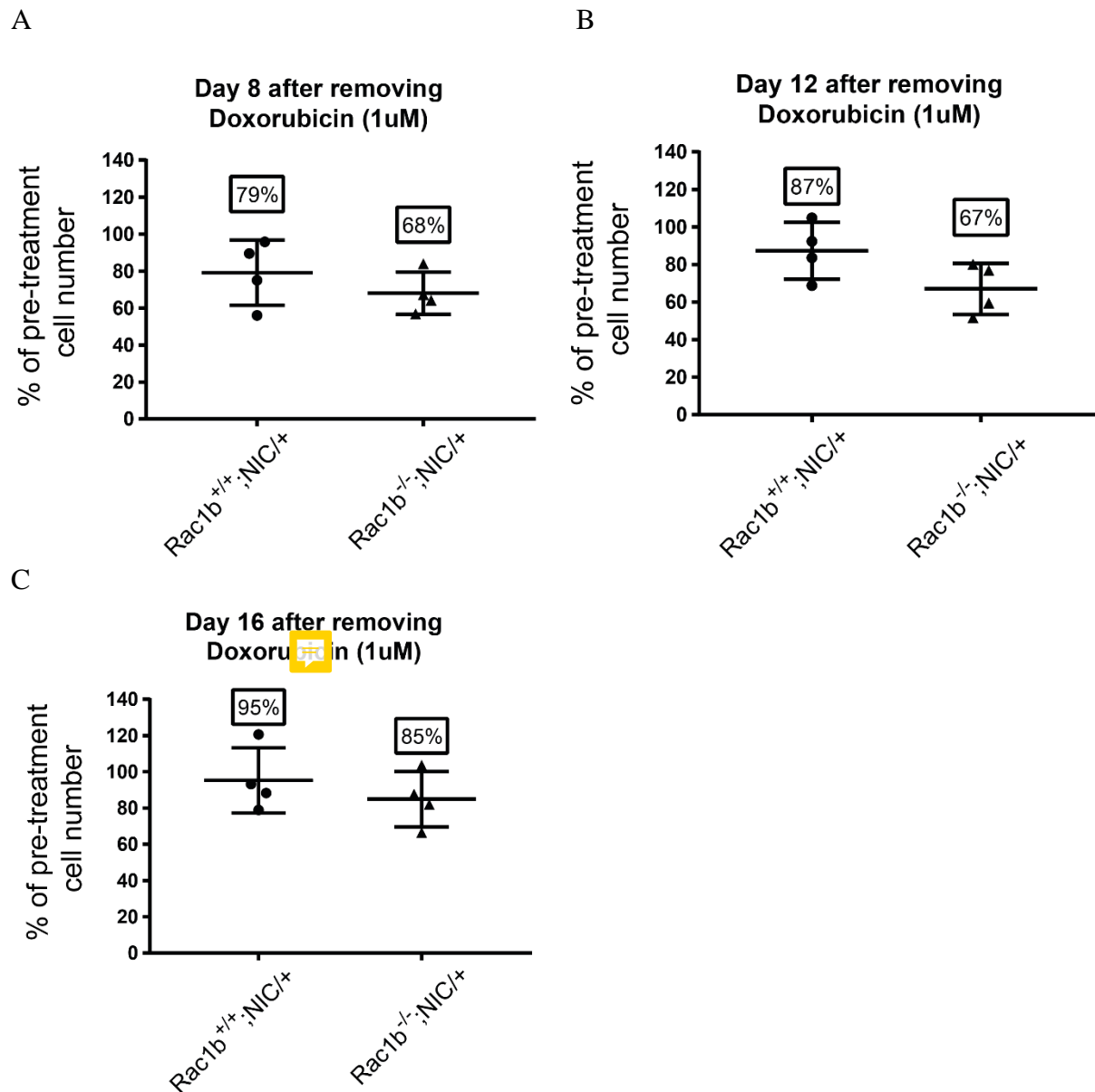


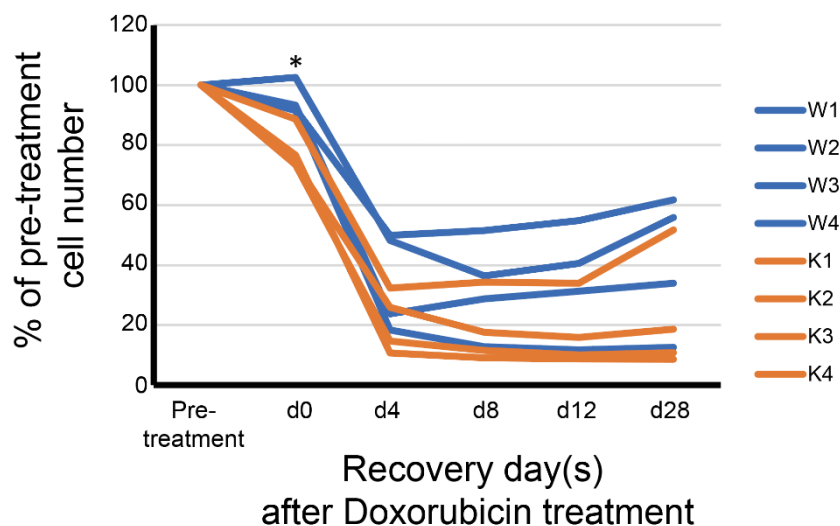
Figure 59. Comparison of cell growth recovery after 1uM Doxorubicin treatment of primary cell lines. Scatter plots represent the relative cell numbers at Day 8 (**A**), Day 12 (**B**), and Day 16 (**C**) to compare cell growth at later stages shown in Figure 58(A) between genotypes of Rac1b^{+/+}; NIC and Rac1b^{-/-}; NIC primary tumour cell lines. Each dot represents one independent primary cell line. The lines represent mean values \pm SD of 4 independent primary cell lines, and the mean values are shown in the rectangles in percentage values. Despite the statistical analysis using two-tailed unpaired t-test reveals $p>0.05$ between two genotypes at all later stages, the mean values for the Rac1b^{-/-}; NIC primary lines are consistently lower than Rac1b^{+/+}; NIC primary lines.



To achieve a higher level of initial cytotoxicity and thus a better resolution of post-treatment cell recovery, the same experiment as above was also performed by treating these primary cells with 2.5uM doxorubicin. However, at this higher concentration of doxorubicin a significant difference between genotypes was observed only at Day 0, but not Day 4, Day 8, Day 12 and Day 28 (Fig. 60A). At Day 0, 2.5uM doxorubicin treatment led to a significantly higher cell loss in Rac1b-null cell lines compared with Rac1b-proficient cell lines (Fig. 60B), demonstrating that Rac1b-deficiency increases the sensitivity to the immediate effects of doxorubicin treatment. At day 4 post-treatment, there is no significant difference between the relative cell numbers between two genotypes, though Rac1b-null cells still have slightly less relative cell numbers. Although the relative cell numbers of Rac1b^{+/+}; NIC/+ and Rac1b^{-/-}; NIC/+ cell lines do not show significant differences during the recovery stage (Day 8, Day 12 and Day 28) (Fig. 60A), the mean values of relative cell numbers for Rac1b-null primary cell lines are consistently lower than the Rac1b-proficient primary cell lines at different recovery time points (Fig. 61). Notably, 3 out of 4 Rac1b-proficient primary cell lines showed an obvious recovery between days 8 and 28 post-treatment (Fig. 60A). In contrast, 3 out of 4 Rac1b-null cell lines did not show any signs of recovery during the same time period. Thus, this may suggest that the loss-of Rac1b function in breast tumour cells makes it less likely to recover from the cytotoxic effects of Doxorubicin treatment.

Overall, my data shows that compared to Rac1b-proficient primary tumour cells, the Rac1b-null cells undergo a significantly higher level of cell loss when treated with a lower dose of doxorubicin (1uM), and have a reduced likelihood of recovery from the effects of treatment when treated with higher doses of doxorubicin (2.5uM).

A



B

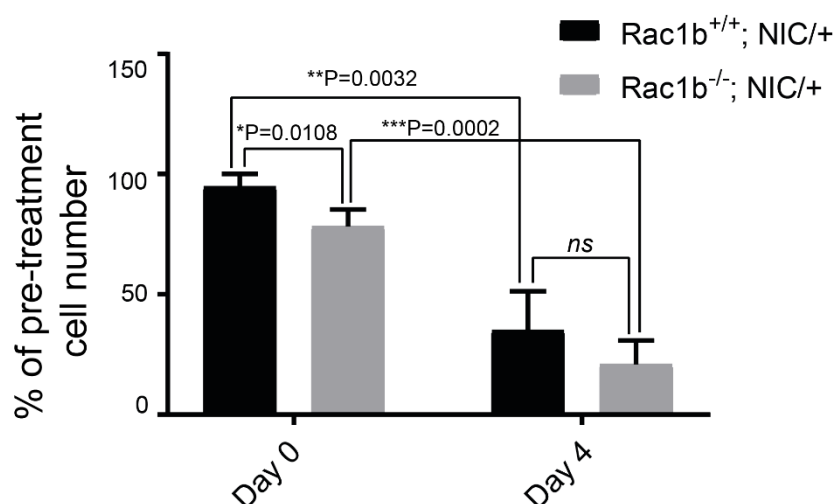


Figure 60. Loss of Rac1b function increases the chemosensitivity of primary breast tumour cells to 2.5uM doxorubicin treatment. (A) Cell growth curve of primary breast tumour cell lines after removing 2.5uM Doxorubicin treatment for 24 hours. This analysis compared Rac1b^{+/+}; NIC/+ with Rac1b^{-/-}; NIC/+ primary tumour cells isolated from their corresponding mice (N=4), which are labelled as blue lines (W1-W4) and orange lines (K1-K4), respectively. Cell numbers are normalized to the pre-treatment cell number in each sample and represented as percentage. (B) Bar graphs providing statistical comparison of the relative cell numbers at Day 0 and Day 4 shown in (A) after removing 2.5uM Doxorubicin treatment to compare the data between genotypes and recovery time points. Bars represent mean values \pm SD of 4 independent primary cell lines. Statistical analysis was determined by two-tailed unpaired t-test. *: P< 0.05; **: P< 0.01; ***: P< 0.001.. ns: not significant.

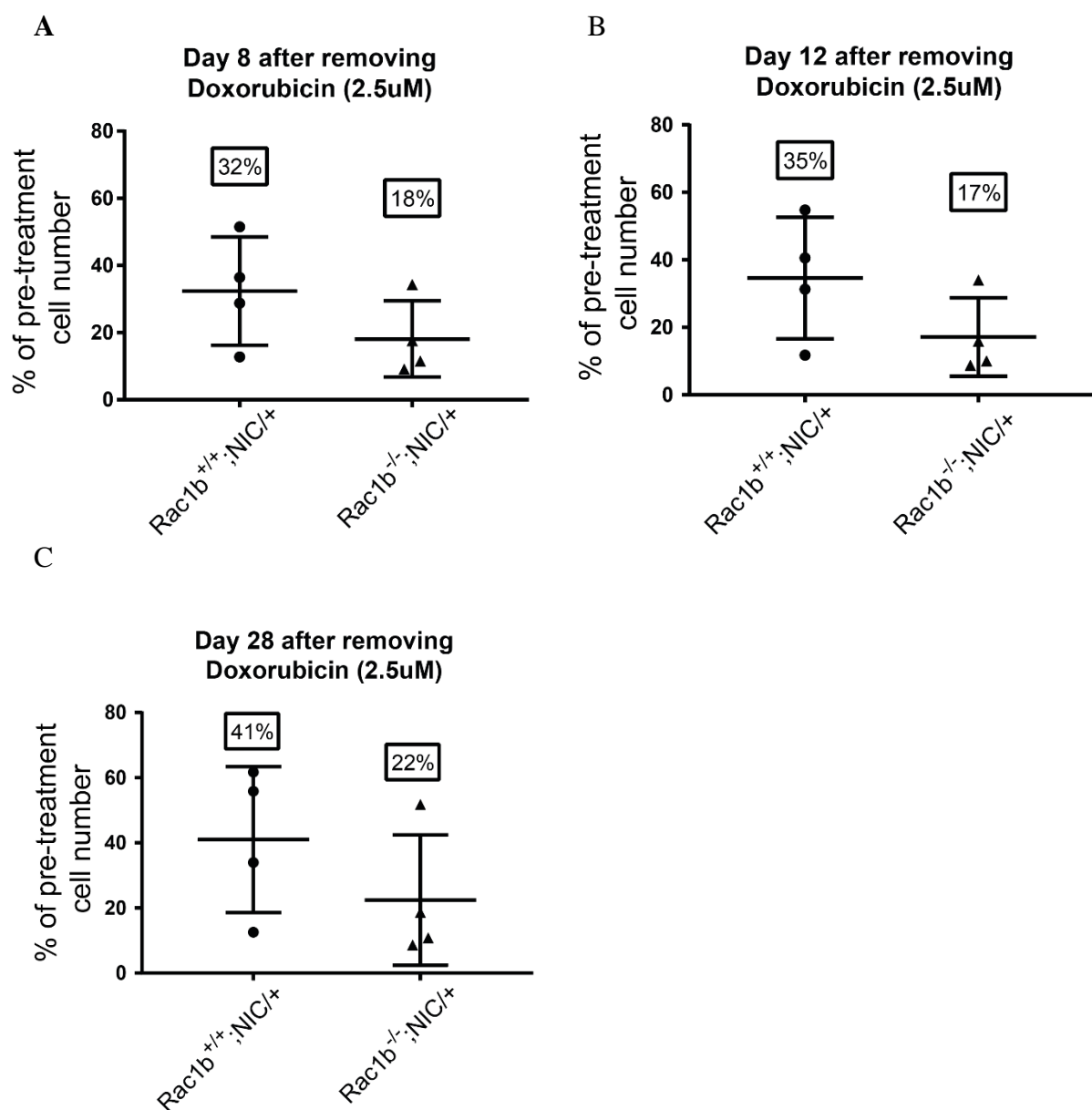


Figure 61. Comparison of cell growth recovery after 2.5uM Doxorubicin treatment of primary cell lines. Scatter plots represent the relative cell numbers at Day 8 (A), Day 12 (B), and Day 28 (C) to compare cell growth at later stages shown in Figure 60(A) between genotypes of Rac1b^{+/+}; NIC and Rac1b^{-/-}; NIC primary tumour cell lines. Each dot represents one independent primary cell line. The lines represent mean values \pm SD of 4 independent primary cell lines, and the mean values are shown in the rectangles in percentage values. Despite the statistical analysis using two-tailed unpaired t-test reveals $p > 0.05$ between two genotypes at all later stages, the mean values for the Rac1b^{-/-}; NIC primary lines are consistently lower than Rac1b^{+/+}; NIC primary lines.

4.3 Discussion

4.4.1 Characterization of Rac1b-expressing cells in breast tumour

In order to investigate which cell types express Rac1b in an *in vivo* model of breast cancer, the RFP⁺ Rac1b-expressing cells obtained from the tumours of the Rac1b^{T2ARFP/+}; MMTV-NIC double transgenic mouse model were analysed. These RFP⁺ tumour cell population was consisted of approximately 92.4% of CD24^{+ve} cells and 7.6% of CD24^{-ve} cells, indicating that Rac1b is predominantly expressed by the tumour epithelial cells. This is seemingly different from the Rac1b-expressing cell population in Rac1b^{T2ARFP} mammary glands, which were predominantly CD24^{-ve}. Consistent with this finding, around 83% of RFP⁺ tumour cells were found to be expressing CK18 and/or CK14, whereas only around 45% of RFP⁺ mammary cells express at least one of these cytokeratins. However, in both mammary glands and tumours, CK-18 expressing RFP⁺ epithelial cells were at a higher level than CK-14 expressing RFP⁺ cells, suggesting that Rac1b could be preferentially expressed by mammary luminal or luminal-like tumour epithelial cells.

4.4.2 Rac1b is expressed by a substantial subpopulation of BCSCs

By using mammosphere assay, I have demonstrated in this study that sorting for RFP⁺ population of Rac1b^{RFP/+};NIC tumour cells significantly enriches for the sphere-forming BCSCs compared to the RFP⁻ population of same primary tumour cells. This indicates that Rac1b is expressed by a substantial subpopulation of BCSCs. Unlike the spheres formed by the RFP⁺ mammary cells isolated from Rac1b^{RFP/+} glands, the immunostaining data has revealed that the spheres formed by RFP⁺ tumour cells are predominantly composed of epithelial cells expressing CK14 and/or CK18. These results together may suggest that the

Rac1b-expressing MaSCs may present a mesenchymal-like fraction of stem cells, whereas in breast tumours most BCSC are epithelial-like and are expressing Rac1b.

Furthermore, the comparison of MFE of RFP⁺ and RFP⁻ BCSCs isolated from Rac1b-proficient (Rac1b^{RFP/+};NIC) and Rac1b-deficient (Rac1b^{RFP/-};NIC) breast tumours has demonstrated that Rac1b function is specifically required for maintaining the stem cell ability of Rac1b-expressing BCSCs, but not of the BCSCs that does not express Rac1b. Consistent with this finding, the MFE of the CD24⁺CD49f⁺ tumour cells were also drastically reduced in Rac1b^{-/-};NIC tumours compared with the same cell population of the Rac1b^{+/+};NIC tumours. Therefore, the results presented in this study clearly suggest that the loss-of Rac1b function results in a significant decrease of BCSC frequency in tumours of the MMTV-neu model of breast cancer, but not in the normal mammary gland. In this regard, it can be considered that the indispensable Rac1b functions are tumour-specific and thus Rac1b might be a clinically-relevant molecular target for developing BCSC-targeting therapies.

4.4.3 Loss of Rac1b function does not alter tumour latency and morphology in the MMTV-Neu model of breast cancer

A previous study in our research group (manuscript under revision) demonstrated that the genetic deletion of *Rac1*, which results in the loss-of both Rac1 and Rac1b functions, significantly delays the latency of palpable tumour formation in the MMTV-Neu mouse model. However, I have determined in this study that the variant-specific knockout of Rac1b in the MMTV-Neu model does not delay the tumour latency, suggesting that it is the loss of Rac1, but not Rac1b, function that results in the delayed tumour latency phenotype in the Rac1^{flox/flox};MMTV-NIC mouse line. Given our observations that the Rac1b-null tumours had a drastically reduced BCSC frequency, it was surprising not to observe a tumour latency

phenotype for the loss-of Rac1b function. However, clinical observations may suggest that there may not be any correlation between the tumour size and the BCSC content of tumours, as the increased BCSC frequency is rather associated with the aggressiveness and poor prognosis, but not the size of breast tumours.

Apart from the tumour latency, I have also shown that the loss-of-Rac1b function does not alter the ER⁺PR⁺ status or the histological distribution of proliferative tumour cells within the MMTV-Neu tumours. However, for future studies it may be necessary to determine the expression of Ki67 and other genes/proteins known to be involved in BCSC functions or EMT specifically in the Rac1b-expressing tumour cells in order to determine the cell-autonomous functions of Rac1b.

It would also be important to further investigate in future studies whether Rac1b regulates the plasticity of BCSCs in the MMTV-Neu model, as a previous study in our research group has already demonstrated that Rac1b function is required for the BCSC plasticity in MCF7 cells by favouring the transition of the proliferative BCSCs into a quiescent mesenchyme-like BCSC state. However, these BCSC states have only been characterised in human breast cancer cell lines and primary human tumour samples (as described in the Introduction section) and the current knowledge does not provide appropriate cell surface markers to study similar BCSC states in a mouse model. Given that the mesenchyme-like quiescent BCSCs were characterised in human breast cancer cell lines as CD44⁺CD24^{-/low} (Liu et al., 2014), the question remains whether CD24⁻ sphere-forming cells in the murine mammary gland and breast tumours, which I have documented in this study, may represent a mesenchyme-like quiescent state of MaSCs and BCSCs, respectively. It was demonstrated that the quiescent BCSCs are mesenchymal-like (EMT) stem cells, which are presumed to drive drug resistance and tumour recurrence (Li et al., 2008; Liu et al., 2014). Previous studies also suggested that EMT process increases the

stemness properties of the mesenchymal-like cells with self-renewal and multipotent features (Mani et al., 2008; Morel et al., 2008). Furthermore, it was shown by others that Rac1b is related to EMT process via regulating the signalling downstream of MMP-3 and ROS production. Taken together, it may be possible that Rac1b can regulate an EMT-like process also in the MaSC and BCSC populations and thus its function would be required for the stem cell plasticity. It is presumed that a defect in the BCSC plasticity that would render them continuously in a proliferative state may cause exhaustion of BCSCs, and thus may explain the drastic reduction of BCSCs within the Rac1b-null MMTV-Neu tumours.

4.4.4 Loss of Rac1b function increases the chemosensitivity of breast tumour cells

BCSCs are considered to be responsible for the therapy resistance and tumour recurrence. Since Rac1b function is required for the maintenance of BCSC population of MMTV-Neu tumours, I have investigated the effects of loss-of Rac1b function on the chemoresistance to doxorubicin treatment using primary tumour cell lines generated from Rac1b^{-/-};NIC/+ and Rac1b^{+/+};NIC/+ tumours. The results obtained demonstrated that Rac1b function is required for the chemoresistance of primary MMTV-Neu tumour cell lines as well as for the post-treatment recovery of tumour cell growth. More specifically, the Rac1b-null primary tumour cells displayed a higher level of 'immediate' cytotoxicity when treated either with a low (1uM) or high (2.5uM) dose of doxorubicin. On the other hand, the 'sustained' cytotoxic effect of doxorubicin treatment was correlated with Rac1b status of the cells only when they were treated with 1uM doxorubicin. These results may suggest that it would be possible to kill a higher proportion of tumour cells at lower doses of chemotherapy, if Rac1b function can be inhibited therapeutically. Furthermore, the likelihood of post-treatment recovery from 2.5 uM doxorubicin treatment was lower in Rac1b^{-/-} primary tumour cell lines compared with Rac1b-proficient cell lines. The heterogeneity of response seen among the 4 Rac1b-null primary tumour cell lines could reflect the differences of their clonal tumour evolution, which

is known to depend on acquiring random mutations during tumourigenesis. Nevertheless, these results may suggest that the therapeutical inhibition of Rac1b may improve the outcome of chemotherapy for patients with breast cancer. However, a future study could be performed to analyse the mutation spectrum and transcriptome of Rac1b-null primary tumour cell lines and compare the 3 good-responders versus the one worse-responder in order to identify a prognostic marker for predicting which tumours would benefit from therapeutic Rac1b-inhibition.

Furthermore, the results I have obtained for the MMTV-Neu primary breast tumour cell lines is consistent with the findings of an earlier study of our research group, which has demonstrated that loss-of-Rac1b function in MCF7 cells abrogates the post-treatment recovery of tumour cell growth upon doxorubicin treatment. Taken together, the loss-of Rac1b function can increase the chemosensitivity of both murine and human breast cancer cells to the effects of doxorubicin treatment and thus we propose a novel strategy to improve the outcome of chemotherapy by therapeutic Rac1b inhibition, which still needs to be developed in future studies.

CHAPTER 5. General Discussion

Over the past two decades, accumulating evidence has convincingly revealed the existence of CSCs within various tumours. It is believed that CSCs contribute to therapy resistance, tumour recurrence and metastasis in various cancers. Thus, it is essential to discover molecular targets to be able to develop CSC-targeted therapies to improve the effectiveness of conventional therapeutics. The small GTPase Rac1, which is often hyperactivated in breast cancer, is essential for maintaining CSCs (Ali et al., 2021; Lin et al., 2020; Rose et al., 2017) and inducing chemoresistance of tumour cells (Li et al., 2020). However, Rac1 may not be a clinically relevant molecular target due to its ubiquitous expression and vital functions in various tissues and organ systems. Previous studies have also demonstrated that Rac1 plays critical roles at different stages of normal mammary gland development (Akhtar et al., 2016; Akhtar & Streuli, 2006; Ewald et al., 2008; Zhu & Nelson, 2013). Moreover, the Rac1 deficiency decreases stem cell frequency in mammary glands (Olabi et al., 2018). Notably, Rac1b, the constitutively active isoform of Rac1, is found to be overexpressed in many breast cancers. Therefore, the hyperactivation of Rac1 signalling in breast tumours might be in part due to the increased Rac1b expression.

To validate the clinical relevance of potential Rac1b-targeting therapies, it is essential to elucidate the functional roles of Rac1b during the development and homeostasis of normal mammary gland as well as at the whole organismal level. I have shown in this study that unlike Rac1, its splice variant Rac1b is dispensable for normal mammary gland development. Furthermore, different from the critical roles of Rac1 in maintaining MaSC abilities (Olabi et al., 2018), the loss of Rac1b function does not impair MaSC frequency. Importantly, the Rac1b-null mice were born in the expected Mendelian ratio and had a normal healthy lifespan without

any obvious health problems, indicating that a therapeutic inhibition of Rac1b would be well-tolerated and thus represents a clinically relevant molecular target for therapeutic intervention.

An earlier study in our group (manuscript under revision) used MCF7 cells to identify Rac1b as a potential molecular target for developing novel BCSC-targeting therapies for the treatment of breast cancer. In that study, Rac1b function was shown to be required for the BCSC plasticity, chemoresistance and the *in vivo* tumour-initiating abilities of the MCF7 cells. In the current study, I have further extended those findings using an *in vivo* animal model of breast cancer. Despite the fact that MCF7 and MMTV-Neu models differ in the breast cancer subtype they represent, Rac1b was required for the chemoresistance and post-treatment recovery of tumour growth in both models.

However, unlike the data obtained in the study with MCF7 cells, the loss-of Rac1b function has not affected the *in vivo* tumour growth in the MMTV-Neu model. This could be explained based on various differences between these two models. First, Rac1b function might be required for the tumour growth of Luminal, but not Her2+ breast cancers. A second potential explanation could be due to the fact that the cell-of-origin for MCF7 cell line was a pleural effusion sample, thus it is not originated from a primary breast tumour in the absence of Rac1b function. In contrast, Rac1b protein was absent during normal mammary gland development and tumour initiation in our MMTV-Neu model, which consequently may enforce some tumour clones that are less dependent on Rac1b function to selectively grow in Rac1b-null MMTV-Neu mice.

In sum, the data presented in this study suggests that potential Rac1b-specific inhibitors could be used in a combo-treatment setting with doxorubicin, which could provide two advantages: First, the use of Rac1b-specific inhibitors could provide the possibility of using a lower dose of doxorubicin to decrease the side effects of chemotherapy without hampering the required

cytotoxicity levels for treatment purposes. Second, the patients with breast cancer could be treated with a normal dose of chemotherapy together with Rac1b inhibitors to improve the treatment outcome by reducing the likelihood of tumour recurrence. Thus, therapeutic Rac1b inhibition might be a potential CSC-targeted therapy, although a Rac1b-specific inhibitor is yet to be developed in future research. Furthermore, future research should also aim to assess the beneficial effects of doxorubicin treatment *in vivo* by comparing the response in Rac1b^{-/-};NIC/+ mice compared with Rac1b^{-/-};NIC/+ mice.

CHAPTER 6 Conclusion

Collectively, this project has demonstrated that Rac1 and Rac1b variants of the small GTPase play distinct roles during normal mammary gland development and breast tumorigenesis. During mammary gland development, the loss of Rac1 function hampers ductal outgrowth, lobuloalveolar structure maturation and post-weaning tissue remodelling. In contrast, Rac1b is dispensable for normal mammary gland development at all stages. Clinical studies have shown that Rac1b is overexpressed in breast cancer. Herein it is suggested that Rac1b is a marker for a subpopulation of BCSCs. The loss of Rac1b function decreases stem cell frequency in breast tumours and sensitises tumour cells to chemotherapy. Therefore, the data presented here proposes Rac1b as a potential molecular target to develop a clinically relevant CSC-targeted therapy that can be used in combination with existing chemotherapy options for breast cancer treatment.



REFERENCES

- Ahmed, S., Sami, A., & Xiang, J. (2015). HER2-directed therapy: current treatment options for HER2-positive breast cancer. *Breast Cancer (Tokyo, Japan)*, 22(2), 101–116.
<https://doi.org/10.1007/S12282-015-0587-X>
- Akhtar, N., Li, W., Mironov, A., & Streuli, C. H. (2016). Rac1 Controls Both the Secretory Function of the Mammary Gland and Its Remodeling for Successive Gestations. *Developmental Cell*, 38(5), 522–535. <https://doi.org/10.1016/J.DEVCEL.2016.08.005>
- Akhtar, N., & Streuli, C. H. (2006). Rac1 links integrin-mediated adhesion to the control of lactational differentiation in mammary epithelia. *The Journal of Cell Biology*, 173(5), 781–793.
<https://doi.org/10.1083/JCB.200601059>
- Akunuru, S., Palumbo, J., Zhai, Q. J., & Zheng, Y. (2011). Rac1 targeting suppresses human non-small cell lung adenocarcinoma cancer stem cell activity. *PloS One*, 6(2).
<https://doi.org/10.1371/JOURNAL.PONE.0016951>
- Al-Hajj, M., & Clarke, M. F. (2004). Self-renewal and solid tumor stem cells. *Oncogene* 2004 23:43, 23(43), 7274–7282. <https://doi.org/10.1038/sj.onc.1207947>
- Al-Hajj, M., Wicha, M. S., Benito-Hernandez, A., Morrison, S. J., & Clarke, M. F. (2003). Prospective identification of tumorigenic breast cancer cells. *Proceedings of the National Academy of Sciences of the United States of America*, 100(7), 3983–3988.
<https://doi.org/10.1073/PNAS.0530291100>
- Ali, A., Shafarin, J., Unnikannan, H., Al-Jabi, N., Jabal, R. A., Bajbouj, K., Muhammad, J. S., & Hamad, M. (2021). Co-targeting BET bromodomain BRD4 and RAC1 suppresses growth, stemness and tumorigenesis by disrupting the c-MYC-G9a-FTH1axis and downregulating HDAC1 in molecular subtypes of breast cancer. *International Journal of Biological Sciences*, 17(15), 4474. <https://doi.org/10.7150/IJBS.62236>
- Alonso-Espinaco, V., Cuatrecasas, M., Alonso, V., Escudero, P., Marmol, M., Horndler, C., Ortego, J., Gallego, R., Codony-Servat, J., Garcia-Albeniz, X., Jares, P., Castells, A., Lozano, J. J., Rosell, R., & Maurel, J. (2014). RAC1b overexpression correlates with poor prognosis in KRAS/BRAF WT metastatic colorectal cancer patients treated with first-line FOLFOX/XELOX chemotherapy. *European Journal of Cancer*, 50(11), 1973–1981.
<https://doi.org/10.1016/J.EJCA.2014.04.019>
- Arnould, L., Gelly, M., Penault-Llorca, F., Benoit, L., Bonnetain, F., Migeon, C., Cabaret, V., Fermeaux, V., Bertheau, P., Garnier, J., Jeannin, J. F., & Coudert, B. (2006). Trastuzumab-based

- treatment of HER2-positive breast cancer: an antibody-dependent cellular cytotoxicity mechanism? *British Journal of Cancer* 2006 94:2, 94(2), 259–267.
<https://doi.org/10.1038/sj.bjc.6602930>
- Asselin-Labat, M. L., Vaillant, F., Shackleton, M., Bouras, T., Lindeman, G. J., & Visvader, J. E. (2008). Delineating the epithelial hierarchy in the mouse mammary gland. *Cold Spring Harbor Symposia on Quantitative Biology*, 73, 469–478. <https://doi.org/10.1101/SQB.2008.73.020>
- Asselin-Labat, M.-L., Sutherland, K. D., Barker, H., Thomas, R., Shackleton, M., Forrest, N. C., Hartley, L., Robb, L., Grosveld, F. G., van der Wees, J., Lindeman, G. J., & Visvader, J. E. (2007). Gata-3 is an essential regulator of mammary-gland morphogenesis and luminal-cell differentiation. *NATURE CELL BIOLOGY*, 9. <https://doi.org/10.1038/ncb1530>
- Bagci, H., Laurin, M., Huber, J., Muller, W. J., & Côté, J. F. (2014). Impaired cell death and mammary gland involution in the absence of Dock1 and Rac1 signaling. *Cell Death & Disease*, 5(8). <https://doi.org/10.1038/CDDIS.2014.338>
- Bagheri-Yarmand, R., Busaidy, N. L., McBeath, E., Danysh, B. P., Evans, K. W., Moss, T. J., Akcakanat, A., Ng, P. K. S., Knippler, C. M., Golden, J. A., Williams, M. D., Multani, A. S., Cabanillas, M. E., Shaw, K. R., Meric-Bernstam, F., Shah, M. H., Ringel, M. D., & Hofmann, M. C. (2021). RAC1 Alterations Induce Acquired Dabrafenib Resistance in Association with Anaplastic Transformation in a Papillary Thyroid Cancer Patient. *Cancers* 2021, Vol. 13, Page 4950, 13(19), 4950. <https://doi.org/10.3390/CANCERS13194950>
- Bai, X., Ni, J., Beretov, J., Graham, P., & Li, Y. (2018). Cancer stem cell in breast cancer therapeutic resistance. *Cancer Treatment Reviews*, 69, 152–163.
<https://doi.org/10.1016/J.CTRV.2018.07.004>
- Barok, M., Joensuu, H., & Isola, J. (2014). Trastuzumab emtansine: mechanisms of action and drug resistance. *Breast Cancer Research : BCR*, 16(2). <https://doi.org/10.1186/BCR3621>
- Barros, P., Jordan, P., & Matos, P. (2009). Rac1 signaling modulates BCL-6-mediated repression of gene transcription. *Molecular and Cellular Biology*, 29(15), 4156–4166.
<https://doi.org/10.1128/MCB.01813-08>
- Barzaman, K., Karami, J., Zarei, Z., Hosseinzadeh, A., Kazemi, M. H., Moradi-Kalbolandi, S., Safari, E., & Farahmand, L. (2020). Breast cancer: Biology, biomarkers, and treatments. *International Immunopharmacology*, 84, 106535. <https://doi.org/10.1016/J.INTIMP.2020.106535>
- Baugher, P. J., Krishnamoorthy, L., Price, J. E., & Dharmawardhane, S. F. (2005). Rac1 and Rac3 isoform activation is involved in the invasive and metastatic phenotype of human breast cancer cells. *Breast Cancer Research : BCR*, 7(6), R965–R974. <https://doi.org/10.1186/BCR1329>

- Beausoleil, E., Chauvignac, C., Taverne, T., Lacombe, S., Pognante, L., Leblond, B., Pallares, D., Oliveira, C. de, Bachelot, F., Carton, R., Peillon, H., Coutadeur, S., Picard, V., Lambeng, N., Désiré, L., & Schweighoffer, F. (2009). Structure-activity relationship of isoform selective inhibitors of Rac1/1b GTPase nucleotide binding. *Bioorganic & Medicinal Chemistry Letters*, 19(19), 5594–5598. <https://doi.org/10.1016/J.BMCL.2009.08.037>
- Bonnet, D., & Dick, J. E. (1997). Human acute myeloid leukemia is organized as a hierarchy that originates from a primitive hematopoietic cell. *Nature Medicine*, 3(7), 730–737. <https://doi.org/10.1038/NM0797-730>
- Boras-Granic, K., Dann, P., & Wysolmerski, J. J. (2014). Embryonic cells contribute directly to the quiescent stem cell population in the adult mouse mammary gland. *Breast Cancer Research*, 16(1), 1–14. <https://doi.org/10.1186/S13058-014-0487-6/FIGURES/6>
- Bordonaro, M. (2013). Crosstalk between Wnt Signaling and RNA Processing in Colorectal Cancer. *Journal of Cancer*, 4(2), 96–103. <https://doi.org/10.7150/JCA.5470>
- Bourguignon, L. Y. W., Hongbo, Z., Shao, L., & Chen, Y. W. (2000). CD44 Interaction with Tiam1 Promotes Rac1 Signaling and Hyaluronic Acid-mediated Breast Tumor Cell Migration *. *Journal of Biological Chemistry*, 275(3), 1829–1838. <https://doi.org/10.1074/JBC.275.3.1829>
- Bouzahzah, B., Albanese, C., Ahmed, F., Pixley, F., Lisanti, M. P., Segall, J. D., Condeelis, J., Joyce, D., Minden, A., Der, C. J., Chan, A., Symons, M., & Pestell, R. G. (2001). Rho family GTPases regulate mammary epithelium cell growth and metastasis through distinguishable pathways. *Molecular Medicine*, 7(12), 816. <https://doi.org/10.1007/bf03401974>
- Bray, K., Gillette, M., Young, J., Loughran, E., Hwang, M., Sears, J. C., & Vargo-Gogola, T. (2013). Cdc42 overexpression induces hyperbranching in the developing mammary gland by enhancing cell migration. *Breast Cancer Research : BCR*, 15(5). <https://doi.org/10.1186/BCR3487>
- Burstein, M. D., Tsimelzon, A., Poage, G. M., Covington, K. R., Contreras, A., Fuqua, S. A. W., Savage, M. I., Osborne, C. K., Hilsenbeck, S. G., Chang, J. C., Mills, G. B., Lau, C. C., & Brown, P. H. (2015). Comprehensive genomic analysis identifies novel subtypes and targets of triple-negative breast cancer. *Clinical Cancer Research : An Official Journal of the American Association for Cancer Research*, 21(7), 1688–1698. <https://doi.org/10.1158/1078-0432.CCR-14-0432>
- Bustelo, X. R., Sauzeau, V., & Berenjano, I. M. (2007). GTP-binding proteins of the Rho/Rac family: regulation, effectors and functions in vivo. *BioEssays : News and Reviews in Molecular, Cellular and Developmental Biology*, 29(4), 356–370. <https://doi.org/10.1002/BIES.20558>

- Butera, A., Cassandri, M., Rugolo, F., Agostini, M., & Melino, G. (2020). The ZNF750-RAC1 axis as potential prognostic factor for breast cancer. *Cell Death Discovery*, 6(1).
<https://doi.org/10.1038/S41420-020-00371-2>
- Cai, D., Iyer, A., Felekakis, K. N., Near, R. I., Luo, Z., Chernoff, J., Albanese, C., Pestell, R. G., & Lerner, A. (2003). AND-34/BCAR3, a GDP Exchange Factor Whose Overexpression Confers Antiestrogen Resistance, Activates Rac, PAK1, and the Cyclin D1 Promoter 1. *CANCER RESEARCH*, 63, 6802–6808. <http://aacrjournals.org/cancerres/article-pdf/63/20/6802/2508946/ch2003006802.pdf>
- Cai, S., Kalisky, T., Sahoo, D., Dalerba, P., Feng, W., Lin, Y., Qian, D., Kong, A., Yu, J., Wang, F., Chen, E. Y., Scheeren, F. A., Kuo, A. H., Sikandar, S. S., Hisamori, S., van Weele, L. J., Heiser, D., Sim, S., Lam, J., ... Clarke, M. F. (2017). A Quiescent Bcl11b High Stem Cell Population Is Required for Maintenance of the Mammary Gland. *Cell Stem Cell*, 20(2), 247-260.e5.
<https://doi.org/10.1016/J.STEM.2016.11.007>
- Carmon, K. S., Gong, X., Yi, J., Wu, L., Thomas, A., Moore, C. M., Masuho, I., Timson, D. J., Martemyanov, K. A., & Liu, Q. J. (2017). LGR5 receptor promotes cell-cell adhesion in stem cells and colon cancer cells via the IQGAP1-Rac1 pathway. *Journal of Biological Chemistry*, 292(36), 14989–15001.
<https://doi.org/10.1074/JBC.M117.786798/ATTACHMENT/650FED74-87FF-4FB7-99D6-AECBF34AC284/MMC1.ZIP>
- Chaffer, C. L., Marjanovic, N. D., Lee, T., Bell, G., Kleer, C. G., Reinhardt, F., D'Alessio, A. C., Young, R. A., & Weinberg, R. A. (2013). Poised Chromatin at the ZEB1 Promoter Enables Breast Cancer Cell Plasticity and Enhances Tumorigenicity. *Cell*, 154(1), 61–74.
<https://doi.org/10.1016/J.CELL.2013.06.005>
- Chapman, R. S., Lourenco, P. C., Tonner, E., Flint, D. J., Selbert, S., Takeda, K., Akira, S., Clarke, A. R., & Watson, C. J. (1999). *Suppression of epithelial apoptosis and delayed mammary gland involution in mice with a conditional knockout of Stat3*. www.genesdev.org
- Chartier, N. T., Lainé, M., Gout, S., Pawlak, G., Marie, C. A., Matos, P., Block, M. R., & Jacquier-Sarlin, M. R. (2006). Laminin-5-integrin interaction signals through PI 3-kinase and Rac1b to promote assembly of adherens junctions in HT-29 cells. *Journal of Cell Science*, 119(Pt 1), 31–46. <https://doi.org/10.1242/JCS.02698>
- Chen, Q. K., Lee, K. A., Radisky, D. C., & Nelson, C. M. (2013). Extracellular matrix proteins regulate epithelial–mesenchymal transition in mammary epithelial cells. *Differentiation*, 86(3), 126–132. <https://doi.org/10.1016/J.DIFF.2013.03.003>

- Cichon, M. A., Nelson, C. M., & Radisky, D. C. (2015). Regulation of epithelial-mesenchymal transition in breast cancer cells by cell contact and adhesion. *Cancer Informatics*, 14(Suppl 3), 1–13. <https://doi.org/10.4137/CIN.S18965>
- Clarke, R., Tyson, J. J., & Dixon, J. M. (2015). Endocrine resistance in breast cancer--An overview and update. *Molecular and Cellular Endocrinology*, 418 Pt 3(0 3), 220–234. <https://doi.org/10.1016/J.MCE.2015.09.035>
- Cordenonsi, M., Zanconato, F., Azzolin, L., Forcato, M., Rosato, A., Frasson, C., Inui, M., Montagner, M., Parenti, A. R., Poletti, A., Daidone, M. G., Dupont, S., Basso, G., Biciato, S., & Piccolo, S. (2011). The Hippo transducer TAZ confers cancer stem cell-related traits on breast cancer cells. *Cell*, 147(4), 759–772. <https://doi.org/10.1016/J.CELL.2011.09.048>
- Daniel, C. W., de Ome, K. B., Young, J. T., Blair, P. B., & Faulkin, L. J. (1968). The in vivo life span of normal and preneoplastic mouse mammary glands: a serial transplantation study. *Proceedings of the National Academy of Sciences of the United States of America*, 61(1), 53. <https://doi.org/10.1073/PNAS.61.1.53>
- Davis, F. M., Lloyd-Lewis, B., Harris, O. B., Kozar, S., Winton, D. J., Muresan, L., & Watson, C. J. (2016). Single-cell lineage tracing in the mammary gland reveals stochastic clonal dispersion of stem/progenitor cell progeny. *Nature Communications* 2016 7:1, 7(1), 1–13. <https://doi.org/10.1038/ncomms13053>
- Day, C. M., Hickey, S. M., Song, Y., Plush, S. E., & Garg, S. (2020). Novel Tamoxifen Nanoformulations for Improving Breast Cancer Treatment: Old Wine in New Bottles. *Molecules (Basel, Switzerland)*, 25(5). <https://doi.org/10.3390/MOLECULES25051182>
- de Angelis, M. L., Francescangeli, F., & Zeuner, A. (2019). Breast Cancer Stem Cells as Drivers of Tumor Chemoresistance, Dormancy and Relapse: New Challenges and Therapeutic Opportunities. *Cancers*, 11(10). <https://doi.org/10.3390/CANCERS11101569>
- De, P., Carlson Aske, J., Dey, N., De@avera, P., Org (, P. D., Aske@avera, J., & Org, J. C. A. (2019). RAC1 Takes the Lead in Solid Tumors. *Cells* 2019, Vol. 8, Page 382, 8(5), 382. <https://doi.org/10.3390/CELLS8050382>
- Debily, M. A., Camarca, A., Ciullo, M., Mayer, C., el Marhomy, S., Ba, I., Jalil, A., Anzisi, A., Guardiola, J., & Piatier-Tonneau, D. (2004). Expression and molecular characterization of alternative transcripts of the ARHGEF5/TIM oncogene specific for human breast cancer. *Human Molecular Genetics*, 13(3), 323–334. <https://doi.org/10.1093/HMG/DDH024>

- DEOME, K. B., FAULKIN, L. J., BERN, H. A., & BLAIR, P. B. (1959). Development of mammary tumors from hyperplastic alveolar nodules transplanted into gland-free mammary fat pads of female C3H mice. *Cancer Research*, 19(5), 515–520.
- Druso, J. E., Endo, M., Joy Lin, M. C., Peng, X., Antonyak, M. A., Meller, S., & Cerione, R. A. (2016). An Essential Role for Cdc42 in the Functioning of the Adult Mammary Gland. *The Journal of Biological Chemistry*, 291(17), 8886–8895.
<https://doi.org/10.1074/JBC.M115.694349>
- Esufali, S., Charames, G. S., Pethe, V. v., Buongiorno, P., & Bapat, B. (2007). Activation of tumor-specific splice variant Rac1b by dishevelled promotes canonical Wnt signaling and decreased adhesion of colorectal cancer cells. *Cancer Research*, 67(6), 2469–2479.
<https://doi.org/10.1158/0008-5472.CAN-06-2843>
- Ewald, A. J., Brenot, A., Duong, M., Chan, B. S., & Werb, Z. (2008). Collective epithelial migration and cell rearrangements drive mammary branching morphogenesis. *Developmental Cell*, 14(4), 570–581. <https://doi.org/10.1016/J.DEVCEL.2008.03.003>
- Faria, M., Capinha, L., Simões-Pereira, J., Bugalho, M. J., & Silva, A. L. (2016). Extending the Impact of RAC1b Overexpression to Follicular Thyroid Carcinomas. *International Journal of Endocrinology*, 2016. <https://doi.org/10.1155/2016/1972367>
- Faria, M., Matos, P., Pereira, T., Cabrera, R., Cardoso, B. A., Bugalho, M. J., & Silva, A. L. (2017). RAC1b overexpression stimulates proliferation and NF-kB-mediated anti-apoptotic signaling in thyroid cancer cells. *PloS One*, 12(2). <https://doi.org/10.1371/JOURNAL.PONE.0172689>
- Fialka, I., Schwarz, H., Reichmann, E., Oft, M., Busslinger, M., & Beug, H. (1996). The estrogen-dependent c-JunER protein causes a reversible loss of mammary epithelial cell polarity involving a destabilization of adherens junctions. *The Journal of Cell Biology*, 132(6), 1115–1132. <https://doi.org/10.1083/JCB.132.6.1115>
- Fiegen, D., Haeusler, L. C., Blumenstein, L., Herbrand, U., Dvorsky, R., Vetter, I. R., & Ahmadian, M. R. (2004). Alternative splicing of Rac1 generates Rac1b, a self-activating GTPase. *The Journal of Biological Chemistry*, 279(6), 4743–4749. <https://doi.org/10.1074/JBC.M310281200>
- Fritz, G., Just, I., & Kaina, B. (1999). Rho GTPases ARE OVER-EXPRESSED IN HUMAN TUMORS. *J. Cancer*, 81, 682–687. [https://doi.org/10.1002/\(SICI\)1097-0215\(19990531\)81:5](https://doi.org/10.1002/(SICI)1097-0215(19990531)81:5)
- Fu, N. Y., Pal, B., Chen, Y., Jackling, F. C., Milevskiy, M., Vaillant, F., Capaldo, B. D., Guo, F., Liu, K. H., Rios, A. C., Lim, N., Kueh, A. J., Virshup, D. M., Herold, M. J., Tucker, H. O., Smyth, G. K., Lindeman, G. J., & Visvader, J. E. (2018). Foxp1 Is Indispensable for Ductal Morphogenesis

- and Controls the Exit of Mammary Stem Cells from Quiescence. *Developmental Cell*, 47(5), 629–644.e8. <https://doi.org/10.1016/J.DEVCEL.2018.10.001>
- Fu, N. Y., Rios, A. C., Pal, B., Law, C. W., Jamieson, P., Liu, R., Vaillant, F., Jackling, F., Liu, K. H., Smyth, G. K., Lindeman, G. J., Ritchie, M. E., & Visvader, J. E. (2017). Identification of quiescent and spatially restricted mammary stem cells that are hormone responsive. *Nature Cell Biology*, 19(3), 164–176. <https://doi.org/10.1038/NCB3471>
- Ginestier, C., Hur, M. H., Charafe-Jauffret, E., Monville, F., Dutcher, J., Brown, M., Jacquemier, J., Viens, P., Kleer, C. G., Liu, S., Schott, A., Hayes, D., Birnbaum, D., Wicha, M. S., & Dontu, G. (2007). ALDH1 Is a Marker of Normal and Malignant Human Mammary Stem Cells and a Predictor of Poor Clinical Outcome. *Cell Stem Cell*, 1(5), 555–567. <https://doi.org/10.1016/J.STEM.2007.08.014>
- Goka, E. T., Chaturvedi, P., Lopez, D. T. M., de La Garza, A., & Lippman, M. E. (2019). RAC1b Overexpression Confers Resistance to Chemotherapy Treatment in Colorectal Cancer. *Molecular Cancer Therapeutics*, 18(5), 957–968. <https://doi.org/10.1158/1535-7163.MCT-18-0955>
- Goncalves, V., Henriques, A., Pereira, J., Costa, A. N., Moyer, M. P., Moita, L. F., Gama-Carvalho, M., Matos, P., & Jordan, P. (2014). Phosphorylation of SRSF1 by SRPK1 regulates alternative splicing of tumor-related Rac1b in colorectal cells. *RNA (New York, N.Y.)*, 20(4), 474–482. <https://doi.org/10.1261/RNA.041376.113>
- Gudiño, V., Cammareri, P., Billard, C. v., & Myant, K. B. (2021). Negative regulation of TGFβ-induced apoptosis by RAC1B enhances intestinal tumourigenesis. *Cell Death & Disease* 2021 12:10, 12(10), 1–12. <https://doi.org/10.1038/s41419-021-04177-7>
- Gudiño, V., Pohl, S. Ö. G., Billard, C. v., Cammareri, P., Bolado, A., Aitken, S., Stevenson, D., Hall, A. E., Agostino, M., Cassidy, J., Nixon, C., von Kriegsheim, A., Freile, P., Popplewell, L., Dickson, G., Murphy, L., Wheeler, A., Dunlop, M., Din, F., ... Myant, K. B. (2021). RAC1B modulates intestinal tumourigenesis via modulation of WNT and EGFR signalling pathways. *Nature Communications*, 12(1). <https://doi.org/10.1038/S41467-021-22531-3>
- Hirsch, D. S., Shen, Y., & Wu, W. J. (2006). Growth and motility inhibition of breast cancer cells by epidermal growth factor receptor degradation is correlated with inactivation of Cdc42. *Cancer Research*, 66(7), 3523–3530. <https://doi.org/10.1158/0008-5472.CAN-05-1547>
- Hoshino, K. (1964). Regeneration and growth of quantitatively transplanted mammary glands of normal female mice. *The Anatomical Record*, 150(3), 221–235. <https://doi.org/10.1002/AR.1091500303>

- Howlin, J., McBryan, J., & Martin, F. (2006). Pubertal mammary gland development: insights from mouse models. *Journal of Mammary Gland Biology and Neoplasia*, 11(3–4), 283–297.
<https://doi.org/10.1007/S10911-006-9024-2>
- Humphreys, R. C., Bierie, B., Zhao, L., Regina, R., Levy, D., & Hennighausen, L. (2002). Deletion of Stat3 Blocks Mammary Gland Involution and Extends Functional Competence of the Secretory Epithelium in the Absence of Lactogenic Stimuli. *Endocrinology*, 143(9), 3641–3650.
<https://doi.org/10.1210/EN.2002-220224>
- Jiang, Z. bin, Ma, B. Q., Liu, S. G., Li, J., Yang, G. M., Hou, Y. B., Si, R. H., Gao, P., & Yan, H. T. (2019). miR-365 regulates liver cancer stem cells via RAC1 pathway. *Molecular Carcinogenesis*, 58(1), 55–65. <https://doi.org/10.1002/MC.22906>
- Johnson, E., Seachrist, D. D., DeLeon-Rodriguez, C. M., Lozada, K. L., Miedler, J., Abdul-Karim, F. W., & Keri, R. A. (2010). HER2/ErbB2-induced breast cancer cell migration and invasion require p120 catenin activation of Rac1 and Cdc42. *The Journal of Biological Chemistry*, 285(38), 29491–29501. <https://doi.org/10.1074/JBC.M110.136770>
- Jordan, P., Brazão, R., Boavida, M. G., Gespach, C., & Chastre, E. (1999). Cloning of a novel human Rac1b splice variant with increased expression in colorectal tumors. *Oncogene*, 18(48), 6835–6839. <https://doi.org/10.1038/SJ.ONC.1203233>
- Junttila, T. T., Akita, R. W., Parsons, K., Fields, C., Lewis Phillips, G. D., Friedman, L. S., Sampath, D., & Sliwkowski, M. X. (2009). Ligand-independent HER2/HER3/PI3K complex is disrupted by trastuzumab and is effectively inhibited by the PI3K inhibitor GDC-0941. *Cancer Cell*, 15(5), 429–440. <https://doi.org/10.1016/J.CCR.2009.03.020>
- Keely, P. J., Westwick, J. K., Whitehead, I. P., Der, C. J., & Parise, L. v. (1997). Cdc42 and Rac1 induce integrin-mediated cell motility and invasiveness through PI(3)K. *Nature*, 390(6660), 632–636. <https://doi.org/10.1038/37656>
- Kissil, J. L., Walmsley, M. J., Hanlon, L., Haigis, K. M., Kim, C. F. B., Sweet-Cordero, A., Eckman, M. S., Tuveson, D. A., Capobianco, A. J., Tybulewicz, V. L. J., & Jacks, T. (2007). Requirement for Rac1 in a K-ras-Induced Lung Cancer in the Mouse. *Cancer Research*, 67(17), 8089–8094. <https://doi.org/10.1158/0008-5472.CAN-07-2300>
- Kong, D., Hughes, C. J., & Ford, H. L. (2020). Cellular Plasticity in Breast Cancer Progression and Therapy. *Frontiers in Molecular Biosciences*, 7, 72.
<https://doi.org/10.3389/FMOLB.2020.00072/BIBTEX>

- Kordon, E. C., & Smith, G. H. (1998). An entire functional mammary gland may comprise the progeny from a single cell. *Development*, 125(10), 1921–1930.
<https://doi.org/10.1242/DEV.125.10.1921>
- Kotelevets, L., Walker, F., Mamadou, G., Lehy, T., Jordan, P., & Chastre, E. (2018). The Rac1 splice form Rac1b favors mouse colonic mucosa regeneration and contributes to intestinal cancer progression. *Oncogene* 2018 37:46, 37(46), 6054–6068. <https://doi.org/10.1038/s41388-018-0389-7>
- Kuperwasser, C., Chavarria, T., Wu, M., Magrane, G., Gray, J. W., Carey, L., Richardson, A., & Weinberg, R. A. (2004). Reconstruction of functionally normal and malignant human breast tissues in mice. *Proceedings of the National Academy of Sciences of the United States of America*, 101(14), 4966–4971. <https://doi.org/10.1073/PNAS.0401064101>
- Lee, E., Piranlioglu, R., Wicha, M. S., & Korkaya, H. (2019). Plasticity and Potency of Mammary Stem Cell Subsets During Mammary Gland Development. *International Journal of Molecular Sciences*, 20(9). <https://doi.org/10.3390/IJMS20092357>
- Lee, K. A., Chen, Q. K., Lui, C., Cichon, M. A., Radisky, D. C., & Nelson, C. M. (2012). Matrix compliance regulates Rac1b localization, NADPH oxidase assembly, and epithelial-mesenchymal transition. *Molecular Biology of the Cell*, 23(20), 4097–4108.
<https://doi.org/10.1091/MBC.E12-02-0166/ASSET/IMAGES/LARGE/4097FIG8.JPEG>
- Lehmann, B. D., Bauer, J. A., Chen, X., Sanders, M. E., Chakravarthy, A. B., Shyr, Y., & Pietenpol, J. A. (2011). Identification of human triple-negative breast cancer subtypes and preclinical models for selection of targeted therapies. *The Journal of Clinical Investigation*, 121(7), 2750–2767. <https://doi.org/10.1172/JCI45014>
- Leung, K., Nagy, A., Gonzalez-Gomez, I., Groffen, J., Heisterkamp, N., & Kaartinen, V. (2003). Targeted expression of activated Rac3 in mammary epithelium leads to defective postlactational involution and benign mammary gland lesions. *Cells, Tissues, Organs*, 175(2), 72–83.
<https://doi.org/10.1159/000073751>
- Li, H. Z., Yi, T. B., & Wu, Z. Y. (2008). Suspension culture combined with chemotherapeutic agents for sorting of breast cancer stem cells. *BMC Cancer*, 8. <https://doi.org/10.1186/1471-2407-8-135>
- Li, Q., Qin, T., Bi, Z., Hong, H., Ding, L., Chen, J., Wu, W., Lin, X., Fu, W., Zheng, F., Yao, Y., Luo, M. L., Saw, P. E., Wulf, G. M., Xu, X., Song, E., Yao, H., & Hu, H. (2020). Rac1 activates non-oxidative pentose phosphate pathway to induce chemoresistance of breast cancer. *Nature Communications* 2020 11:1, 11(1), 1–18. <https://doi.org/10.1038/s41467-020-15308-7>

- Li, Z., Fang, R., Fang, J., He, S., & Liu, T. (2018). Functional implications of Rab27 GTPases in Cancer. *Cell Communication and Signaling : CCS*, 16(1). <https://doi.org/10.1186/S12964-018-0255-9>
- Lin, Y. Y., Wang, C. Y., Phan, N. N., Chiao, C. C., Li, C. Y., Sun, Z., Hung, J. H., Chen, Y. L., Yen, M. C., Weng, T. Y., Hsu, H. P., & Lai, M. D. (2020). PODXL2 maintains cellular stemness and promotes breast cancer development through the Rac1/Akt pathway. *International Journal of Medical Sciences*, 17(11), 1639. <https://doi.org/10.7150/IJMS.46125>
- Lionarons, D. A., Hancock, D. C., Rana, S., East, P., Moore, C., Murillo, M. M., Carvalho, J., Spencer-Dene, B., Herbert, E., Stamp, G., Damry, D., Calado, D. P., Rosewell, I., Fritsch, R., Neubig, R. R., Molina-Arcas, M., & Downward, J. (2019). RAC1 P29S Induces a Mesenchymal Phenotypic Switch via Serum Response Factor to Promote Melanoma Development and Therapy Resistance. *Cancer Cell*, 36(1), 68-83.e9. <https://doi.org/10.1016/J.CCELL.2019.05.015>
- Liu, J. F., Chevet, E., Kebache, S., Lemaitre, G., Barritault, D., Larose, L., & Crépin, M. (1999). Functional Rac-1 and Nck signaling networks are required for FGF-2-induced DNA synthesis in MCF-7 cells. *Oncogene*, 18(47), 6425–6433. <https://doi.org/10.1038/SJ.ONC.1203027>
- Liu, S., Cong, Y., Wang, D., Sun, Y., Deng, L., Liu, Y., Martin-Trevino, R., Shang, L., McDermott, S. P., Landis, M. D., Hong, S., Adams, A., D'Angelo, R., Ginestier, C., Charafe-Jauffret, E., Clouthier, S. G., Birnbaum, D., Wong, S. T., Zhan, M., ... Wicha, M. S. (2014). Breast Cancer Stem Cells Transition between Epithelial and Mesenchymal States Reflective of their Normal Counterparts. *Stem Cell Reports*, 2(1), 78–91. <https://doi.org/10.1016/J.STEMCR.2013.11.009>
- Lloyd-Lewis, B., Harris, O. B., Watson, C. J., & Davis, F. M. (2017). Mammary Stem Cells: Premise, Properties, and Perspectives. *Trends in Cell Biology*, 27(8), 556–567. <https://doi.org/10.1016/J.TCB.2017.04.001>
- Lui, C., Lee, K., & Nelson, C. M. (2012). Matrix compliance and RhoA direct the differentiation of mammary progenitor cells. *Biomechanics and Modeling in Mechanobiology*, 11(8), 1241–1249. <https://doi.org/10.1007/S10237-011-0362-7>
- Makarem, M., Spike, B. T., Dravis, C., Kannan, N., Wahl, G. M., & Eaves, C. J. (2013). Stem cells and the developing mammary gland. *Journal of Mammary Gland Biology and Neoplasia*, 18(2), 209–219. <https://doi.org/10.1007/S10911-013-9284-6>
- Mani, S. A., Guo, W., Liao, M. J., Eaton, E. N., Ayyanan, A., Zhou, A. Y., Brooks, M., Reinhard, F., Zhang, C. C., Shipitsin, M., Campbell, L. L., Polyak, K., Briskin, C., Yang, J., & Weinberg, R.

- A. (2008). The Epithelial-Mesenchymal Transition Generates Cells with Properties of Stem Cells. *Cell*, 133(4), 704–715. <https://doi.org/10.1016/J.CELL.2008.03.027>
- Matos, P., Collard, J. G., & Jordan, P. (2003). Tumor-related alternatively spliced Rac1b is not regulated by Rho-GDP dissociation inhibitors and exhibits selective downstream signaling. *The Journal of Biological Chemistry*, 278(50), 50442–50448. <https://doi.org/10.1074/JBC.M308215200>
- Matos, P., & Jordan, P. (2005). Expression of Rac1b stimulates NF-kappaB-mediated cell survival and G1/S progression. *Experimental Cell Research*, 305(2), 292–299. <https://doi.org/10.1016/J.YEXCR.2004.12.029>
- Matos, P., & Jordan, P. (2006). Rac1, but not Rac1B, stimulates RelB-mediated gene transcription in colorectal cancer cells. *The Journal of Biological Chemistry*, 281(19), 13724–13732. <https://doi.org/10.1074/JBC.M513243200>
- Matos, P., & Jordan, P. (2008). Increased Rac1b Expression Sustains Colorectal Tumor Cell Survival. *Molecular Cancer Research*, 6(7), 1178–1184. <https://doi.org/10.1158/1541-7786.MCR-08-0008>
- Mehner, C., Miller, E., Khauv, D., Nassar, A., Oberg, A. L., Bamlet, W. R., Zhang, L., Waldmann, J., Radisky, E. S., Crawford, H. C., & Radisky, D. C. (2014). Tumor cell-derived MMP3 orchestrates Rac1b and tissue alterations that promote pancreatic adenocarcinoma. *Molecular Cancer Research : MCR*, 12(10), 1430–1439. <https://doi.org/10.1158/1541-7786.MCR-13-0557-T>
- Melzer, C., Hass, R., von der Ohe, J., Lehnert, H., & Ungefroren, H. (2017). The role of TGF- β and its crosstalk with RAC1/RAC1b signaling in breast and pancreas carcinoma. *Cell Communication and Signaling : CCS*, 15(1), 19. <https://doi.org/10.1186/S12964-017-0175-0>
- Mikkola, M. L., & Millar, S. E. (2006). The mammary bud as a skin appendage: unique and shared aspects of development. *Journal of Mammary Gland Biology and Neoplasia*, 11(3–4), 187–203. <https://doi.org/10.1007/S10911-006-9029-X>
- Molina, M. A., Codony-Servat, J., Albanell, J., Rojo, F., Arribas, J., & Baselga, J. (2001). Laboratory of Oncology Research. *Medical Oncology Service*, 61, 4744–4749. <http://aacrjournals.org/cancerres/article-pdf/61/12/4744/2485678/4744.pdf>
- Morel, A. P., Lièvre, M., Thomas, C., Hinkal, G., Ansieau, S., & Puisieux, A. (2008). Generation of Breast Cancer Stem Cells through Epithelial-Mesenchymal Transition. *PLOS ONE*, 3(8), e2888. <https://doi.org/10.1371/JOURNAL.PONE.0002888>

- Myant, K. B., Cammareri, P., McGhee, E. J., Ridgway, R. A., Huels, D. J., Cordero, J. B., Schwitalla, S., Kalna, G., Ogg, E. L., Athineos, D., Timpson, P., Vidal, M., Murray, G. I., Greten, F. R., Anderson, K. I., & Sansom, O. J. (2013). ROS production and NF- κ B activation triggered by RAC1 facilitate WNT-driven intestinal stem cell proliferation and colorectal cancer initiation. *Cell Stem Cell*, 12(6), 761–773. <https://doi.org/10.1016/J.STEM.2013.04.006>
- Myant, K. B., Scopelliti, A., Haque, S., Vidal, M., Sansom, O. J., & Cordero, J. B. (2013). Rac1 drives intestinal stem cell proliferation and regeneration. *Cell Cycle (Georgetown, Tex.)*, 12(18), 2973–2977. <https://doi.org/10.4161/CC.26031>
- Nelson, C. M., Khauv, D., Bissell, M. J., & Radisky, D. C. (2008). Change in cell shape is required for matrix metalloproteinase-induced epithelial-mesenchymal transition of mammary epithelial cells. *Journal of Cellular Biochemistry*, 105(1), 25–33. <https://doi.org/10.1002/JCB.21821>
- Nimnual, A. S., Taylor, L. J., Nyako, M., Jeng, H. H., & Bar-Sagi, D. (2010). Perturbation of cytoskeleton dynamics by the opposing effects of Rac1 and Rac1b. *Small GTPases*, 1(2), 89–97. <https://doi.org/10.4161/SGTP.1.2.14427>
- Olabi, S., Ucar, A., Brennan, K., & Streuli, C. H. (2018). Integrin-Rac signalling for mammary epithelial stem cell self-renewal. *Breast Cancer Research : BCR*, 20(1). <https://doi.org/10.1186/S13058-018-1048-1>
- Paine, I. S., & Lewis, M. T. (2017). The Terminal End Bud: the Little Engine that Could. *Journal of Mammary Gland Biology and Neoplasia* 22:2, 22(2), 93–108. <https://doi.org/10.1007/S10911-017-9372-0>
- Palomeras, S., Ruiz-Martínez, S., & Puig, T. (2018). Targeting Breast Cancer Stem Cells to Overcome Treatment Resistance. *Molecules (Basel, Switzerland)*, 23(9). <https://doi.org/10.3390/MOLECULES23092193>
- Patel, H. K., & Bihani, T. (2018). Selective estrogen receptor modulators (SERMs) and selective estrogen receptor degraders (SERDs) in cancer treatment. *Pharmacology & Therapeutics*, 186, 1–24. <https://doi.org/10.1016/J.PHARMTHERA.2017.12.012>
- Pedersen, E., & Brakebusch, C. (2012). Rho GTPase function in development: How in vivo models change our view. *Experimental Cell Research*, 318(14), 1779–1787. <https://doi.org/10.1016/J.YEXCR.2012.05.004>
- Pennisi, P. A., Barr, V., Nunez, N. P., Stannard, B., & Roith, D. le. (n.d.). *Reduced Expression of Insulin-like Growth Factor I Receptors in MCF-7 Breast Cancer Cells Leads to a More Metastatic Phenotype*. Retrieved March 24, 2022, from <http://aacrjournals.org/cancerres/article-pdf/62/22/6529/2500080/ch2202006529.pdf>

- Propper, A. Y., Howard, B. A., & Veltmaat, J. M. (2013). Prenatal morphogenesis of mammary glands in mouse and rabbit. *Journal of Mammary Gland Biology and Neoplasia*, 18(2), 93–104. <https://doi.org/10.1007/S10911-013-9298-0>
- Radisky, D. C., Levy, D. D., Littlepage, L. E., Liu, H., Nelson, C. M., Fata, J. E., Leake, D., Godden, E. L., Albertson, D. G., Nieto, M. A., Werb, Z., & Bissell, M. J. (2005). Rac1b and reactive oxygen species mediate MMP-3-induced EMT and genomic instability. *Nature* 2005 436:7047, 436(7047), 123–127. <https://doi.org/10.1038/nature03688>
- Richert, M. M., Schwertfeger, K. L., Ryder, J. W., & Anderson, S. M. (2000). An atlas of mouse mammary gland development. *Journal of Mammary Gland Biology and Neoplasia*, 5(2), 227–241. <https://doi.org/10.1023/A:1026499523505>
- Rios, A. C., Fu, N. Y., Lindeman, G. J., & Visvader, J. E. (2014). In situ identification of bipotent stem cells in the mammary gland. *Nature* 2014 506:7488, 506(7488), 322–327. <https://doi.org/10.1038/nature12948>
- Rose, M., Kloten, V., Noetzel, E., Gola, L., Ehling, J., Heide, T., Meurer, S. K., Gaiko-Shcherbak, A., Sechi, A. S., Huth, S., Weiskirchen, R., Klaas, O., Antonopoulos, W., Lin, Q., Wagner, W., Veeck, J., Gremse, F., Steitz, J., Knüchel, R., & Dahl, E. (2017). ITIH5 mediates epigenetic reprogramming of breast cancer cells. *Molecular Cancer*, 16(1), 1–22. <https://doi.org/10.1186/S12943-017-0610-2/TABLES/3>
- Scheele, C. L. G. J., Hannezo, E., Muraro, M. J., Zomer, A., Langedijk, N. S. M., van Oudenaarden, A., Simons, B. D., & van Rheenen, J. (2017). Identity and dynamics of mammary stem cells during branching morphogenesis. *Nature* 2017 542:7641, 542(7641), 313–317. <https://doi.org/10.1038/nature21046>
- Schnelzer, A., Prechtel, D., Knaus, U., Dehne, K., Gerhard, M., Graeff, H., Harbeck, N., Schmitt, M., & Lengyel, E. (2000). Rac1 in human breast cancer: overexpression, mutation analysis, and characterization of a new isoform, Rac1b. *Oncogene*, 19(26), 3013–3020. <https://doi.org/10.1038/SJ.ONC.1203621>
- Shackleton, M., Vaillant, F., Simpson, K. J., Stingl, J., Smyth, G. K., Asselin-Labat, M. L., Wu, L., Lindeman, G. J., & Visvader, J. E. (2006a). Generation of a functional mammary gland from a single stem cell. *Nature* 2006 439:7072, 439(7072), 84–88. <https://doi.org/10.1038/nature04372>
- Shackleton, M., Vaillant, F., Simpson, K. J., Stingl, J., Smyth, G. K., Asselin-Labat, M. L., Wu, L., Lindeman, G. J., & Visvader, J. E. (2006b). Generation of a functional mammary gland from a single stem cell. *Nature* 2006 439:7072, 439(7072), 84–88. <https://doi.org/10.1038/nature04372>

- Silva, A. L., Carmo, F., & Bugalho, M. J. (2013). RAC1b overexpression in papillary thyroid carcinoma: a role to unravel. *European Journal of Endocrinology*, 168(6), 795–804. <https://doi.org/10.1530/EJE-12-0960>
- Singh, A., Karnoub, A. E., Palmby, T. R., Lengyel, E., Sondek, J., & Der, C. J. (2004). Rac1b, a tumor associated, constitutively active Rac1 splice variant, promotes cellular transformation. *Oncogene*, 23(58), 9369–9380. <https://doi.org/10.1038/SJ.ONC.1208182>
- Sleeman, K. E., Kendrick, H., Robertson, D., Isacke, C. M., Ashworth, A., & Smalley, M. J. (2007). Dissociation of estrogen receptor expression and in vivo stem cell activity in the mammary gland. *Journal of Cell Biology*, 176(1), 19–26. <https://doi.org/10.1083/JCB.200604065>
- Smith, G. H. (1996). Experimental mammary epithelial morphogenesis in an in vivo model: Evidence for distinct cellular progenitors of the ductal and lobular phenotype. *Breast Cancer Research and Treatment* 39:1, 39(1), 21–31. <https://doi.org/10.1007/BF01806075>
- Smith, G. H., & Medina, D. (1988). A morphologically distinct candidate for an epithelial stem cell in mouse mammary gland. *Journal of Cell Science*, 90(1), 173–183. <https://doi.org/10.1242/JCS.90.1.173>
- Stallings-Mann, M. L., Waldmann, J., Zhang, Y., Miller, E., Gauthier, M. L., Visscher, D. W., Downey, G. P., Radisky, E. S., Fields, A. P., & Radisky, D. C. (2012). Matrix metalloproteinase induction of Rac1b, a key effector of lung cancer progression. *Science Translational Medicine*, 4(142). <https://doi.org/10.1126/SCITRANSLMED.3004062>
- Stein, T., Salomonis, N., & Gusterson, B. A. (2007). Mammary gland involution as a multi-step process. *Journal of Mammary Gland Biology and Neoplasia*, 12(1), 25–35. <https://doi.org/10.1007/S10911-007-9035-7>
- Stingl, J., Raouf, A., Eirew, P., & Eaves, C. J. (2006). Deciphering the mammary epithelial cell hierarchy. *Cell Cycle (Georgetown, Tex.)*, 5(14), 1519–1522. <https://doi.org/10.4161/CC.5.14.2983>
- Svensmark, J. H., & Brakebusch, C. (2019). Rho GTPases in cancer: friend or foe? *Oncogene*, 38(50), 7447–7456. <https://doi.org/10.1038/S41388-019-0963-7>
- Totaro, A., Zhuang, Q., Panciera, T., Battilana, G., Azzolin, L., Brumana, G., Gandin, A., Brusatin, G., Cordenonsi, M., & Piccolo, S. (2019). Cell phenotypic plasticity requires autophagic flux driven by YAP/TAZ mechanotransduction. *Proceedings of the National Academy of Sciences of the United States of America*, 116(36), 17848–17857. <https://doi.org/10.1073/PNAS.1908228116>

- Tu, S., & Cerione, R. A. (2001). Cdc42 is a substrate for caspases and influences Fas-induced apoptosis. *The Journal of Biological Chemistry*, 276(22), 19656–19663.
<https://doi.org/10.1074/JBC.M009838200>
- Ungefroren, H., Otterbein, H., Fiedler, C., Mihara, K., Hollenberg, M. D., Gieseler, F., Lehnert, H., & Witte, D. (2019). RAC1B Suppresses TGF- β 1-Dependent Cell Migration in Pancreatic Carcinoma Cells through Inhibition of the TGF- β Type I Receptor ALK5. *Cancers*, 11(5).
<https://doi.org/10.3390/CANCERS11050691>
- Ungefroren, H., Sebens, S., Giehl, K., Helm, O., Groth, S., Fändrich, F., Röcken, C., Sipos, B., Lehnert, H., & Gieseler, F. (2014). Rac1b negatively regulates TGF- β 1-induced cell motility in pancreatic ductal epithelial cells by suppressing Smad signalling. *Oncotarget*, 5(1), 277–290.
<https://doi.org/10.18632/ONCOTARGET.1696>
- Ungefroren, H., Witte, D., & Lehnert, H. (2018). The role of small GTPases of the Rho/Rac family in TGF- β -induced EMT and cell motility in cancer. *Developmental Dynamics*, 247(3), 451–461.
<https://doi.org/10.1002/DVDY.24505>
- van Amerongen, R., Bowman, A. N., & Nusse, R. (2012). Developmental Stage and Time Dictate the Fate of Wnt/ β -Catenin-Responsive Stem Cells in the Mammary Gland. *Cell Stem Cell*, 11(3), 387–400. <https://doi.org/10.1016/J.STEM.2012.05.023>
- van Keymeulen, A., Rocha, A. S., Ousset, M., Beck, B., Bouvencourt, G., Rock, J., Sharma, N., Dekoninck, S., & Blanpain, C. (2011). Distinct stem cells contribute to mammary gland development and maintenance. *Nature* 2011 479:7372, 479(7372), 189–193.
<https://doi.org/10.1038/nature10573>
- Visvader, J. E. (2009). Keeping abreast of the mammary epithelial hierarchy and breast tumorigenesis. *Genes & Development*, 23(22), 2563–2577.
<https://doi.org/10.1101/GAD.1849509>
- Visvader, J. E., & Stingl, J. (2014). Mammary stem cells and the differentiation hierarchy: current status and perspectives. *Genes & Development*, 28(11), 1143–1158.
<https://doi.org/10.1101/GAD.242511.114>
- Visvikis, O., Lorès, P., Boyer, L., Chardin, P., Lemichez, E., & Gacon, G. (2008). Activated Rac1, but not the tumorigenic variant Rac1b, is ubiquitinated on Lys 147 through a JNK-regulated process. *The FEBS Journal*, 275(2), 386–396. <https://doi.org/10.1111/J.1742-4658.2007.06209.X>
- Wang, D., Cai, C., Dong, X., Yu, Q. C., Zhang, X. O., Yang, L., & Zeng, Y. A. (2014). Identification of multipotent mammary stem cells by protein C receptor expression. *Nature* 2014 517:7532, 517(7532), 81–84. <https://doi.org/10.1038/nature13851>

- Wicha, M. S., Liu, S., & Dontu, G. (2006). Cancer Stem Cells: An Old Idea—A Paradigm Shift. *Cancer Research*, 66(4), 1883–1890. <https://doi.org/10.1158/0008-5472.CAN-05-3153>
- Xie, J. W., & Haslam, S. Z. (2008). Extracellular matrix, Rac1 signaling, and estrogen-induced proliferation in MCF-7 breast cancer cells. *Breast Cancer Research and Treatment*, 110(2), 257–268. <https://doi.org/10.1007/S10549-007-9719-0>
- Xuhong, J.-C., Qi, X.-W., Zhang, Y., & Jiang, J. (2019). Mechanism, safety and efficacy of three tyrosine kinase inhibitors lapatinib, neratinib and pyrotinib in HER2-positive breast cancer. *American Journal of Cancer Research*, 9(10), 2103. [/pmc/articles/PMC6834479/](https://pubmed.ncbi.nlm.nih.gov/31000000/)
- Yin, L., Duan, J. J., Bian, X. W., & Yu, S. C. (2020). Triple-negative breast cancer molecular subtyping and treatment progress. *Breast Cancer Research*, 22(1), 1–13. <https://doi.org/10.1186/S13058-020-01296-5/TABLES/3>
- Yoon, C., Cho, S. J., Chang, K. K., Park, D. J., Ryeom, S. W., & Yoon, S. S. (2017). Role of Rac1 Pathway in Epithelial-to-Mesenchymal Transition and Cancer Stem-like Cell Phenotypes in Gastric Adenocarcinoma. *Molecular Cancer Research : MCR*, 15(8), 1106–1116. <https://doi.org/10.1158/1541-7786.MCR-17-0053>
- Zhang, B., Zhang, Y., Dagher, M. C., & Shacter, E. (2005). Rho GDP Dissociation Inhibitor Protects Cancer Cells against Drug-Induced Apoptosis. *Cancer Research*, 65(14), 6054–6062. <https://doi.org/10.1158/0008-5472.CAN-05-0175>
- Zhang, T., & Wang, N. (2018). miR-135a Confers Resistance to Gefitinib in Non-Small Cell Lung Cancer Cells by Upregulation of RAC1. *Oncology Research*, 26(8), 1191–1200. <https://doi.org/10.3727/096504018X15166204902353>
- Zhao, X., Lu, L., Pokhriyal, N., Ma, H., Duan, L., Lin, S., Jafari, N., Band, H., & Band, V. (2009). Overexpression of RhoA induces preneoplastic transformation of primary mammary epithelial cells. *Cancer Research*, 69(2), 483–491. <https://doi.org/10.1158/0008-5472.CAN-08-2907>
- Zhou, C., Licciulli, S., Avila, J. L., Cho, M., Troutman, S., Jiang, P., Kossenkova, A. V., Showe, L. C., Liu, Q., Vachani, A., Albelda, S. M., & Kissil, J. L. (2013). The Rac1 splice form Rac1b promotes K-ras-induced lung tumorigenesis. *Oncogene*, 32(7), 903–909. <https://doi.org/10.1038/ONC.2012.99>
- Zhou, Y., Wang, Y., Zhou, W., Chen, T., Wu, Q., Chutturghoon, V. K., Lin, B., Geng, L., Yang, Z., Zhou, L., & Zheng, S. (2019). YAP promotes multi-drug resistance and inhibits autophagy-related cell death in hepatocellular carcinoma via the RAC1-ROS-mTOR pathway. *Cancer Cell International*, 19(1), 1–15. <https://doi.org/10.1186/S12935-019-0898-7/FIGURES/7>

- Zhu, W., & Nelson, C. M. (2013). PI3K regulates branch initiation and extension of cultured mammary epithelia via Akt and Rac1 respectively. *Developmental Biology*, 379(2), 235–245. <https://doi.org/10.1016/J.YDBIO.2013.04.029>
- Zuo, Y., Berdeaux, R., & Frost, J. A. (2014). The RhoGEF Net1 is required for normal mammary gland development. *Molecular Endocrinology (Baltimore, Md.)*, 28(12), 1948–1960. <https://doi.org/10.1210/ME.2014-1128>
- Zuo, Y., Oh, W., Ulu, A., & Frost, J. A. (2016). Minireview: Mouse Models of Rho GTPase Function in Mammary Gland Development, Tumorigenesis, and Metastasis. *Molecular Endocrinology (Baltimore, Md.)*, 30(3), 278–289. <https://doi.org/10.1210/ME.2015-1294>
- Zuo, Y., Ulu, A., Chang, J. T., & Frost, J. A. (2018). Contributions of the RhoA guanine nucleotide exchange factor Net1 to polyoma middle T antigen-mediated mammary gland tumorigenesis and metastasis. *Breast Cancer Research : BCR*, 20(1). <https://doi.org/10.1186/S13058-018-0966-2>